Supersonic Post-combustion Inertial CO$_2$ Extraction System

Final Report
DOE-OA-13122

Project/Grant Period: 1 October 2013 to 31 March 2017

Reporting Period Start Date: 1 October 2013

Reporting Period End Date: 31 March 2017

Report Submission Date: 5 April 2017

Principal Investigator:

Vladimir Balepin, Ph.D

Vladimir.Balepin@OrbitalATK.com

Phone: 631 676 8922

DOE National Energy Technology Laboratory Award **#DE-FE0013122**

Recipient Organization:

Alliant Techsystems Operations LLC

77 Raynor Ave, Ronkonkoma, NY 11779

DUNS Number: 788102833

Submitting Official

Laura Hansen, Contracts Manager

Laura.Hansen@Orbitalatk.com

Phone number: (561)515-1176

Signature of Submitting Official : _____

Table of Contents

1. Executive Summary

This report summarizes the effort carried out under NETL contract DE- FE0013122 from 1 October 2013 to 31 March 2017. As described in this document, technical challenges realized during the performance of this project resulted in completion of only the first two of three planned budget periods. Despite this outcome, substantial progress was made toward understanding and maturing the CO_2 capture technology under consideration and considerable future promise remains for applications requiring lower CO_2 capture and/or lower CO_2 concentrations.

2. Summary of Accomplishments

Major goals and objectives of the project

The objective of the effort reported herein was to further the development of a novel Inertial CO_2 Extraction System (ICES) for carbon dioxide (CO_2) capture at the bench scale. ICES converts vapor-phase CO_2 contained in flue gas to solid (dry ice) using a supersonic expansion followed by inertial separation. The project was designed to advance the key technology to a technology readiness level (TRL) of 4 while demonstrating a viable path to meeting NETL efficiency requirements. The primary technical objectives of the project were consistent with the DOE Carbon Capture Program performance goals of 90% CO_2 capture rate with 95% CO_2 purity at a cost of $40/tonne of CO_2 captured by 2025. The original technical objectives of the project include:

- Budget Period 1: Demonstration of solid CO_2 particle growth methods at lab-scale. Demonstration of the separation and capture of migrated particles at bench scale using surrogate controlled CO_2 particle injection. Demonstration of the diffusion of the CO_2-depleted flue gas flow to atmospheric pressure with losses consistent with projected system economics.

- Budget Period 2: Bench-scale demonstration of CO_2 particle growth methods supporting particle sizes required for effective migration and separation.

- Budget Period 3: Demonstration of the ICES process including condensation, migration, CO_2 removal and diffusion of the CO_2-depleted flue gas flow to atmospheric pressure. Updating the ICES techno-economic analysis showing a path to meeting the DOE carbon capture goals.

A Final Milestone Summary Chart is provided in Table 1.

Table 1 Milestone Status Report

Milestone Title/Description	Planned Completion Date	Actual Completion Date	Verification Method	Comments (progress toward achieving milestone, explanation of deviation from plan, etc.)
MS 1. Updated Project Management Plan	10/31/2013	10/28/2013	Document delivery	Completed on schedule
MS 2. Kickoff Meeting	12/31/2013	11/14/2013	Presentation + electronic copy of material	Completed on schedule
MS 3. Capture duct/diffuser demonstration complete	12/22/2014	12/22/2014	Test data and results	Capture duct/diffuser demonstration complete. Bench scale test article subjected to >40 test runs. Significant CO$_2$ capture efficiency has been obtained along with low efficiency points. Overall results support DP1 success criteria of at least 50% CO$_2$ capture
MS 4. Updated Project Management Plan	1/29/2015	1/29/2015	Document delivery	Document delivered to NETL Program Manager.
MS 5. Bench scale condensation/growth testing complete	08/31/2016	12/31/2016	Test data and results	Sonic condensation of the particles complete. Significant amounts of the 30-40 micron particles observed in the surrogate flue gas.
MS 6. Updated Project Management Plan	10/31/2016	N/A	Document delivery	BP3 not executed
MS 7. Techno-economic analysis (TEA) and EH&S Assessment complete	08/29/2017	3/31/17 (TEA)	Document delivery	TEA update carried out in BP2.
MS 8. Integrated system testing complete	08/29/2017	N/A	Test data and results	BP3 not executed
MS 9. Final report complete	11/28/2017	3/31/2017	Document delivery	Closed with the present document

3. Detailed Discussion of Activity and Accomplishments

The following sections provide a chronological summary of activities and accomplishments on the project

3.1.1 Lab-scale testing at Ohio State University (OSU)

At the start of the effort lab-scale testing efforts at OSU were planned to directly support the objective of developing methodologies to increase the size of CO_2 particles in condensing supersonic flow. During an initial visit, OSU lead investigator Dr. Barbara Wyslouzil provided a detailed tour of her aerosol laboratory and supersonic nozzle test facility (see Figure 1) and supporting discussions relating to system capabilities and interfaces. Several detailed discussions followed relating to optical diagnostics near-term baseline test planning to assess water and CO_2 condensation in nitrogen.
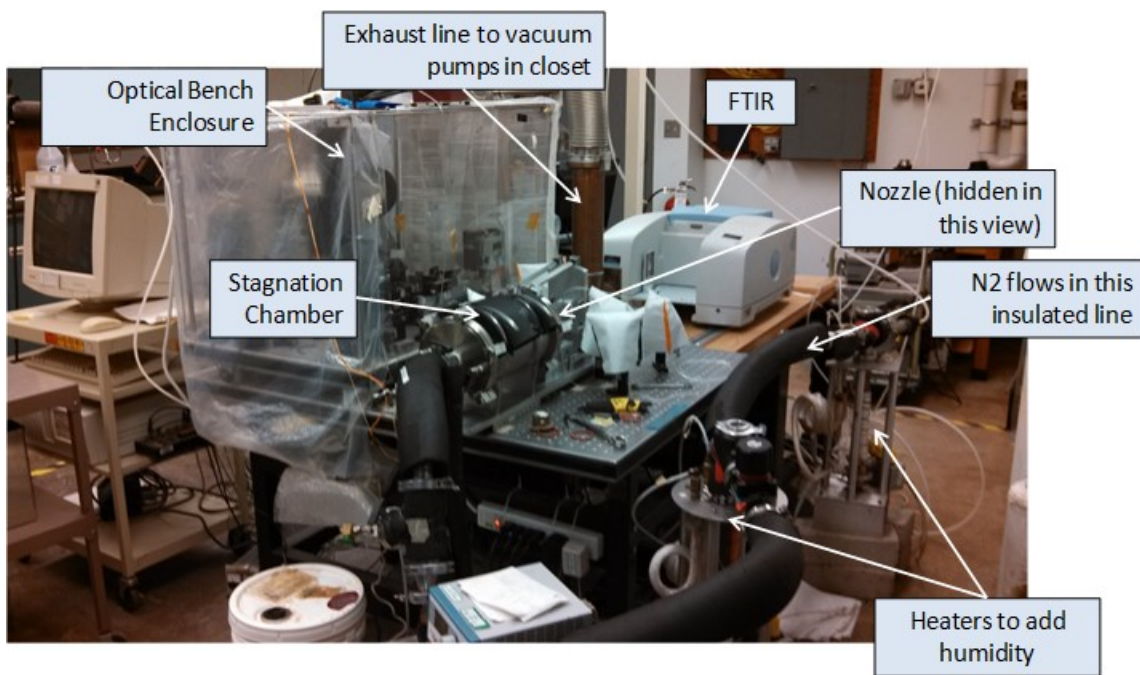
Figure 1 OSU Supersonic Aerosol Test Laboratory

Several concepts for increasing turbulent particle collisions to promote CO_2 coagulation and agglomeration were then developed. At the small scale of the OSU test facility, 3D printing was investigated as the most-promising approach to manufacture the "grating nozzles" initially considered. These are arrays of small supersonic nozzle contours designed to accelerate the flow from subsonic to a velocity near the point of initial CO_2 condensation. The downstream edges of the nozzle array were intended to shed turbulent vortices that are anticipated to promote condensate agglomeration in the downstream duct, which will continue expanding (as a single duct) to a higher Mach number. An initial example of a nine-cell grating nozzle manufactured using Orbital ATK's in-house 3D printer is shown in Figure 2. Concepts for a single-centerbody nozzle to create a single wake are shown in Figure 2 and Figure 3. CFD analysis would later show that

these configurations resulted in a local temperature increase in the wake flow due to the temperature of the surfaces and had the effect of arresting condensation rather than promoting agglomeration. A single wake-producing wire across the flow was tested instead in the configuration referred to as T3R2 to minimize the temperature increase effect.
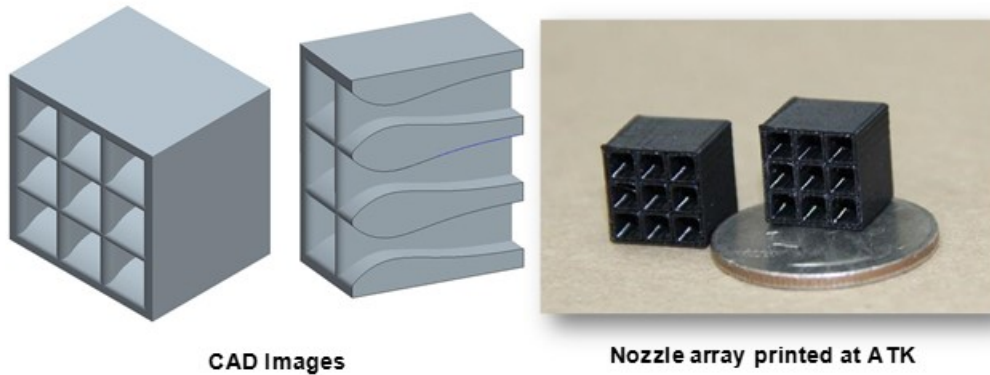

CAD Images   Nozzle array printed at ATK

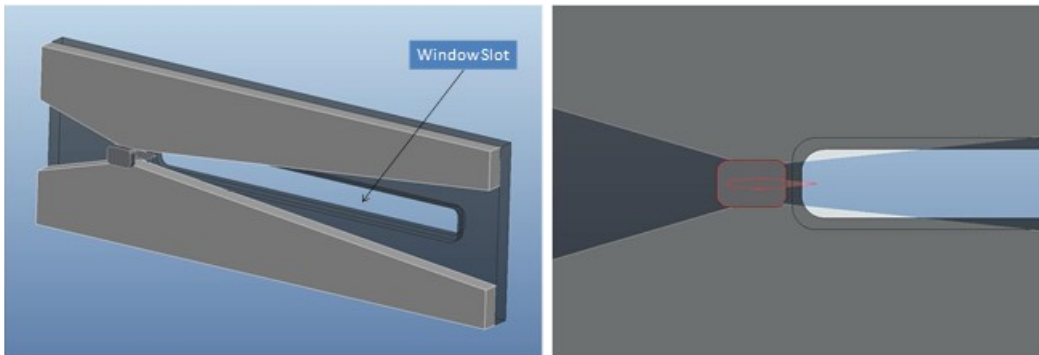**Figure 2 CAD model and photo of nine-cell grating nozzle concept**

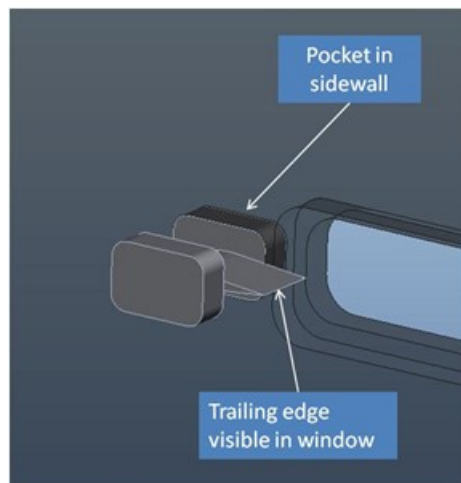**Figure 3 CAD model of single centerbody nozzle for OSU**

Figure 4: Centerbody wake generator

Table 2 summarizes 24 tests conducted at OSU.   Six nozzle configurations referred to as T1, T1_R1, T2, and T3, C3, and T3R2 were utilized to explore variations in expansion ratio and other parameters as indicated in the table.

Table 2 Summary of OSU Tests

Nozzle	Date	Details	Number of tests
B-SLAC	1/27/2014	Modified existing experiment to meet target pressures (2 atm)	2
T1	2/3/2014 2/17/2014	Used new nozzle with a higher expansion rate to reach higher Mach number (2.5) and lower temperature (132 K).	3
T1R1	2/20/2014 2/24/2014 3/7/2014 3/10/2014	Reassembled nozzle T1 to get higher expansion rate and inlet temperature was decreased to 15 degree C so that Mach number and temperature reached 2.6 and 120 K, respectively. The linear stage for moving the pressure probe was replaced by a longer one so that the pressure could be measured at wider range of position.	9
T2	3/14/2014 3/17/2014 3/18/2014	Used new nozzle with a higher expansion rate to reach higher Mach number (3.0) and lower temperature (102 K). An experiment at an inlet pressure of 1 atm was also done to confirm that the heat of condensation is effectively removed from the growing droplets.	6
T3	3/28/2014 3/31/2014	Used new nozzle with a higher expansion rate to reach higher Mach number (3.1) and lower temperature (91 K).	4
C3	5/7/2014	Conducted preliminary light scattering measurement of water droplets in nozzle C3, which has CaF_2 windows for spectroscopic measurement.	1
C3	5/10/2014	Conducted preliminary light scattering measurement of water droplets in nozzle C3 - the method improved based on the result on 5/7/2014	1
C3	5/21/2014 6/4/2014	Conducted preliminary light scattering measurements of water droplets in nozzle C3 using a much more sensitive light detector for sufficiently accurate measurement.	2
C3	6/19/2014	Conducted preliminary light scattering measurement (LSM) of n-nonane droplets in nozzle C3, and this result was compared with the result of H_2O droplets on 6/4/2014 to confirm the applicability of LSM to the determination of the size and number density of the droplets in supersonic nozzle.	1
T3R2	6/26/2014	Conducted light scattering measurement (LSM) of CO_2/H_2O droplets in nozzle T3R2, which has almost the same profile of flow area as nozzle T3, and has CaF_2 windows for LSM measurement. The size and number density of the droplets were determined.	1
T3R2	7/2/2014	The dependence of the size of CO_2/H_2O droplets on the disturbance of the supersonic flow caused by a wake-producing wire in the nozzle was investigated by LSM.	1
T3R2	7/10/2014	Conducted similar LSM as that on 6/26/2014 at different concentration of CO_2 to investigate the dependences of the size and number density of the droplets on the flow conditions.	1

As seen in Figure 5, a "dry" (N_2 only) test was initially used to obtain a baseline pressure

profile along the axis of the nozzle flow for comparison with later "wet" tests including combinations of water and CO_2. Differences in pressure measured between these tests are related to the enthalpy change in the compressible flow due to phase change heat release and are therefore directly correlated to condensation rate.
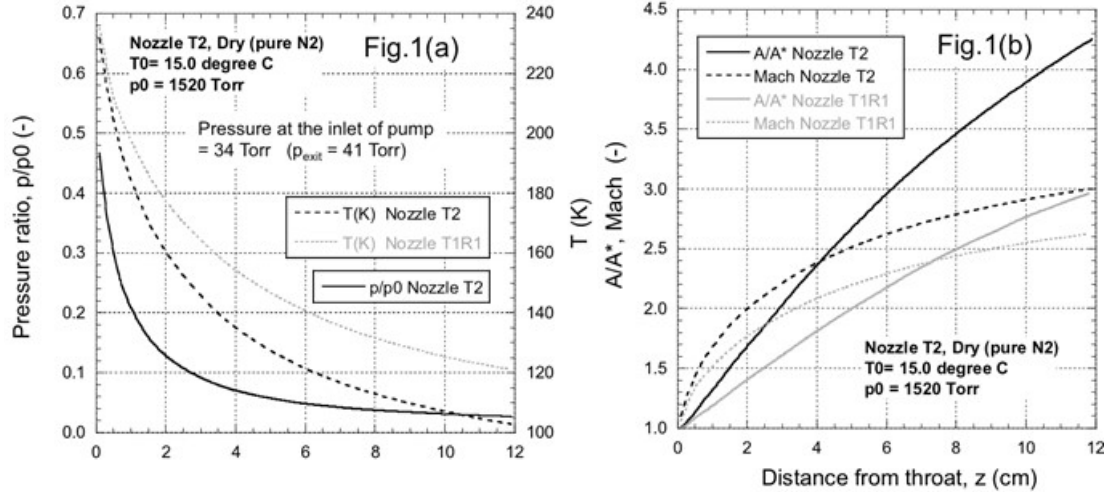
Figure 5 (a) The measured pressure profile for T2 and the derived temperature profiles for T2 and T1R1 as N2 flows through the nozzle from T0 =15 C. The stagnation pressure p0 = 1520 Torr and the exit pressure is 41 Torr. The exit temperature reaches ~102 K. (b) In nozzle T2 the effective area ratio at the nozzle exit is ~4.3, and the Mach number approaches 3. The data for nozzle T1R1 is also shown.
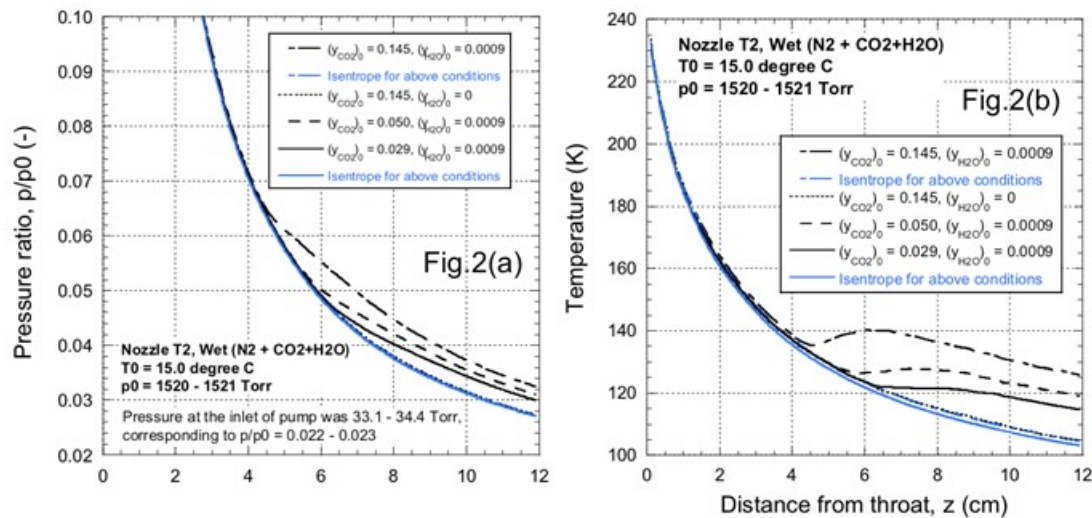
Figure 6 The (a) pressure profiles and (b) temperature profiles as mixtures of N_2 + 0.09 mol% H_2O and 3 different CO_2 concentrations flow through nozzle T2. CO_2 condensation occurs for all cases in which water is present. In contrast, when a mixture of N2 + 14.5 mol% CO_2 flows through the nozzle there is no condensation even at temperatures approaching 100 K.

Initial tests run with N_2 + CO_2 in nozzle T2 resulted in no measured condensation up to a nozzle area ratio of 4.25 (corresponding to approximately Mach 3.0). As seen in Figure

6, with trace amounts of water added to the flow, CO_2 condensation was observed to occur at an axial station of 4.5cm which corresponds (from Figure 5b) to a nozzle area ratio of 2.5 (~Mach 2.4). This is a somewhat higher area ratio than the previously expected Mach number of ~2.2 based on the sublimation line of CO_2. Condensation is evident in these plots as a departure from the (blue solid line) isentropic performance.

This initial data reinforced our understanding that CO_2 condensation in our area of interest requires heterogeneous vs. homogeneous nucleation. This was not unexpected and is not problematic since all prior tests included trace amounts of water and the eventual ICES system will include some level of trace water. The delayed condensation was, on the other hand, not expected since heterogeneous nucleation was thought to occur as soon as the temperature and partial pressure of CO_2 reached the solid-vapor equilibrium line (a.k.a. sublimation line). In-depth review of the technical literature revealed that at pressures and temperatures significantly below the triple point, non-equilibrium condensation requires that transition through a virtual liquid state must occur first. Our experimental data (and that of a limited number of others that have worked in this specialized area) shows that condensation begins when the temperature and partial pressure of the condensable vapor arrive at an extrapolation of the liquid-vapor saturation line.

This phenomenon is illustrated in Figure 7 where the onset of CO_2 condensation is revealed by the change in curvature in the black (closer to horizontal) lines. Condensation begins close to the extrapolated liquid CO_2 vapor pressure curve and, thus, is consistent with CO_2 condensation being initiated by the condensation of liquid CO_2 onto the pre-existing water particles. Our expectation was that the condensation of CO_2 would proceed as a (near equilibrium) phase transition from vapor to the super-cooled liquid, and that further condensation would follow the vapor-liquid equilibrium line. This is evidently not the case in these tests where the return of the lines to near horizontal provided the appearance that CO_2 condensation had slowed. We believe the relatively thick boundary layers relative to the small flow cross section in the OSU nozzle is resulting in a reduction in the condensable CO_2.

Figure from plot:

Legend:
- --- $(y_{CO2})_0 = 0.145$
- --- $(y_{CO2})_0 = 0.050$
- --- $(y_{CO2})_0 = 0.029$
- Vapor_Liquid equilibrium, Ref1
- Vapor_Solid equilibrium, Ref2

Fig.3

Y-axis: Partial pressure of CO2 (Torr)
X-axis: Temperature, T (K)

Nozzle T2, Wet (N2 + CO2+H2O)
T0 = 15.0 degree C
p0 = 1520 - 1521 Torr
$(y_{H2O})_0 = 0.0009$
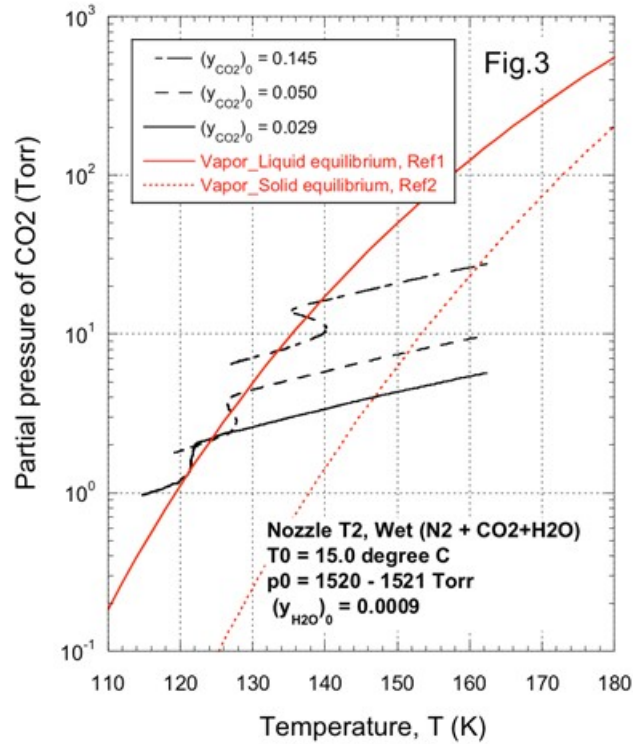
Ref1 CO2 liquid for $217 \leq T/K \leq 276$
A. Michels, T. Wassenaar, TH. Zwietering, and P. Smits
Physica 16 (5), 501-504 (1950)
Log(P/atm) = A/T + B*Log(T) + CT + D
A= -1.353202E+3
B= -8.142537
C= 6.259156E-3
D= 2.461930E+1
1atm= 1.01325E+5 Pa

Ref2 CO2 solid for $154 \leq T/K \leq 196$
NIST Web fitted to the data in
W.F.Giauque, C.J.Egan, J. Chem. Phys. 5, 45-54 (1937).

Log(p/bar) = A - B/(T + C)
A= 6.81228
B= 1301.679
C= -3.494
1bar= 1E+5 Pa

This equation can be extrapolated down to 65 K
M.A.A(i)nou, Monatshefte f(u)r chemie 136,
2017-2027 (2005)

Figure 7: The pressure temperature data for the 3 $N_2+H_2O+CO_2$ experiments are plotted on the phase diagram for CO_2. In each case, the onset of CO_2 condensation lies very close to the extrapolated vapor pressure line for liquid CO_2.
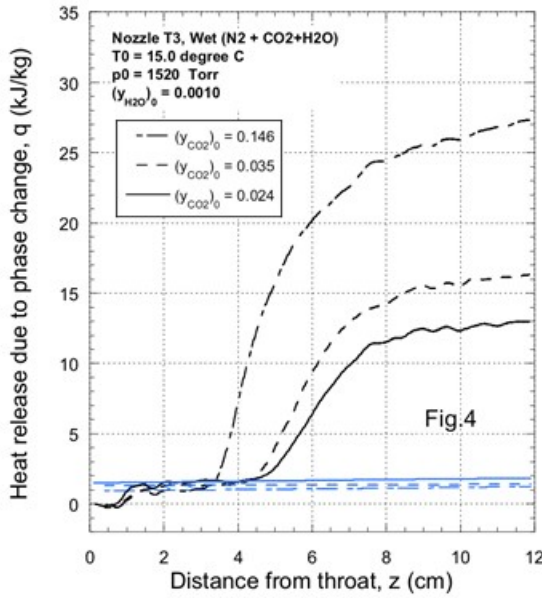
Blue straight lines show the baselines used for estimating the amount of condensed CO2
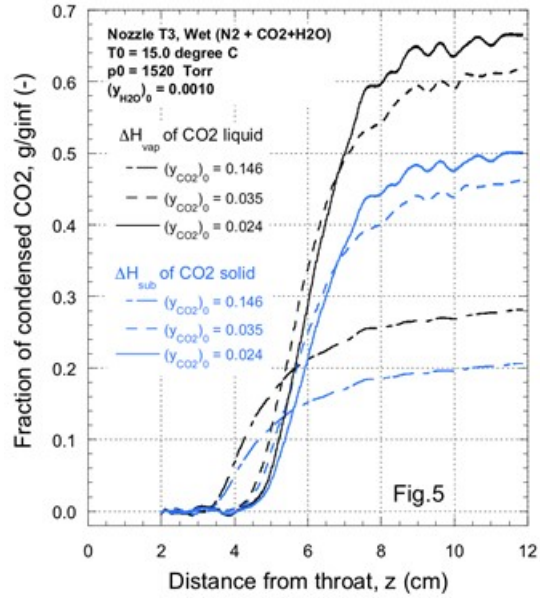
ΔHvap and ΔHsub are shown in PTM_NozzleT2_Wet03.ppt.

Figure 8: The measured heat release as a function of the experimental conditions.

Figure 9 The fraction of the incoming CO_2 that is condensed depends on the operating conditions and whether we assume the condensed phase is liquid or solid. The highest fraction corresponds to the lowest $[CO_2]_0$.

Using a new nozzle with higher expansion ratio (T3), Figure 8 summarizes the estimated heat release q. The increase around $z = 0.5$ cm is due to the condensation of H_2O. The second increase, when $3 < z < 5$ cm corresponds to the condensation of CO_2. The straight blue lines are an extrapolation of q_{H2O} in the region downstream of CO_2 condensation. The amount of CO_2 condensed is then estimated from $q_{H2O+CO2} - q_{H2O}$ and the heat of sublimation or vaporization of CO_2.

The fraction of entering CO_2 that is condensed, $g/g_{\infty,CO2}$ is summarized in Figure 9. The difference between the black and blue curves reflects the difference between using the heat of sublimation and the heat of vaporization to determine g from the heat release profiles. As expected $g/g_{\infty,CO2}$ is higher at lower $[CO_2]_0$. For the lowest $[CO_2]_0$ at least 50% of the incoming CO_2 condensed. Even at the highest $[CO_2]_0$ at least 20% of the CO_2 has condensed. Condensation does not appear to have "stopped" as previously thought using nozzle T2. The Mach number and velocities corresponding to these tests are summarized in Figure 10.
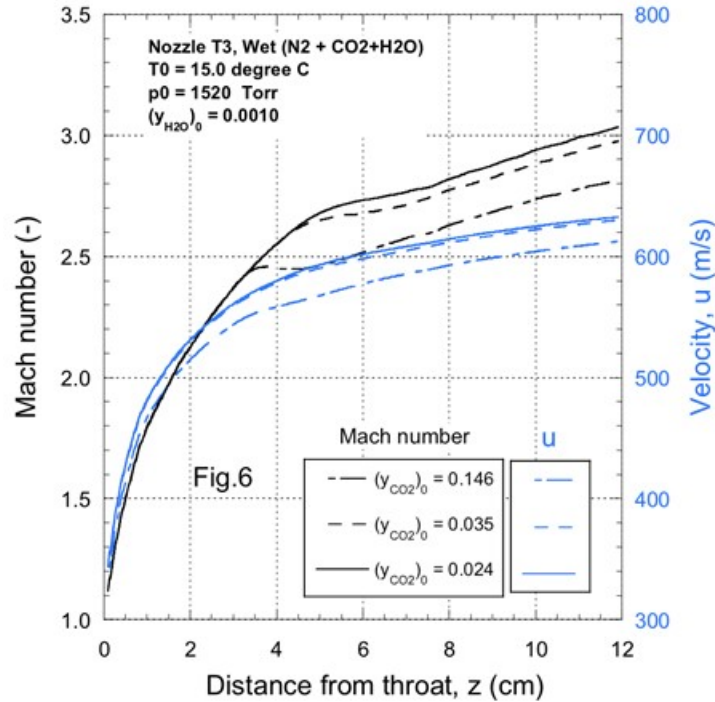
Figure 10: Mach number and velocity (u) for the heterogeneous condensation experiments.

It is important to note that the very small nozzles used at OSU are characterized by a large ratio of boundary layer flow to core (inviscid) flow and it is expected that we will require a higher physical expansion ratio at this scale compared to the scale tested at Orbital ATK. The situation is made even better at full (power plant) scale since the boundary layer thickness will be relatively small compared to the core. Since the purpose of testing at OSU was principally to understand particle size and growth dynamics, we set a target of approximately 50% condensation at a mol fraction of 14.6% to ensure adequate condensed phase exists before transitioning to particle growth testing. Approximately 30% of the CO_2 condensed for the relevant condition in nozzle T3 (Figure 9).

Figure 11 illustrates the light scattering measurement (LSM) setup used at OSU. An axially-oriented cylindrical He-Ne laser beam illuminates the flow through a window downstream of the test section. An optical detector is used to measure light intensity at various axial stations along the test section through a calcium fluoride (CaF_2) window. As an example of the type of results obtained, the differences in the output voltage of the detector for scattering light between the condensing flow and dry flow are shown in Figure 12.
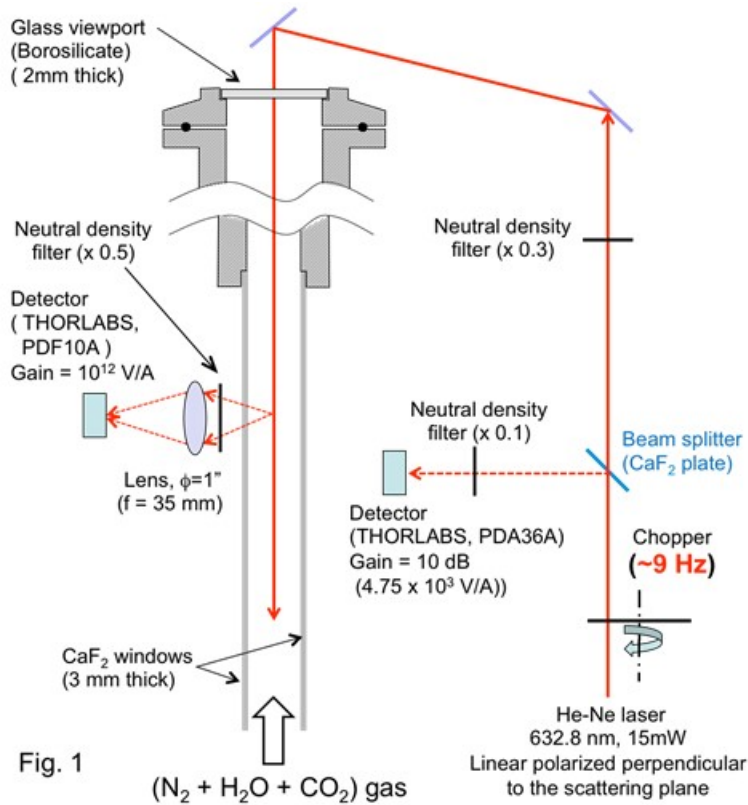
Figure 11 In the light scattering setup, the beam travels along the nozzle axis entering from the downstream end of the nozzle. Scattered light is detected at 90 degrees.
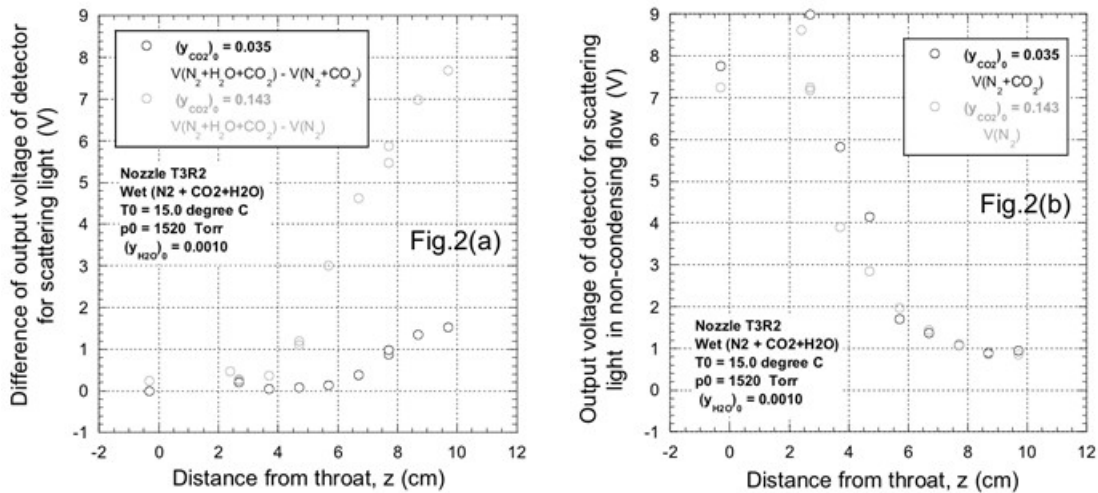
Figure 12 (a) The difference in voltage between the experiments in which CO_2 + H_2O (open circles) are condensing and the dry trace – either N_2 or N_2+CO_2 - for the current experiments (dark) and those conducted at higher CO_2 partial pressure (light). (b) The light scattering increases near the nozzle throat as the concentration of CO_2 in the "dry trace" increases.

The fraction of condensed CO_2, g/g_{inf} from LSM is compared with those from pressure trace measurements (PTM) and model calculations in Figure 13. For both levels of initial CO_2 mol fraction $(y_{CO2})_0$ the value of g/g_{inf} from LSM, $(g/g_{inf})_{LSM}$ starts to deviate from $(g/g_{inf})_{PTM}$ near z = 6 cm. At the exit of nozzle, $(g/g_{inf})_{LSM}$ is about 70 % higher than $(g/g_{inf})_{PTM}$ at $(y_{CO2})_0 = 0.143 - 0.146$, and about 80 % higher at $(y_{CO2})_0 = 0.035$. At the lower CO_2 concentration these experiments suggest that close to 80% of the CO_2 has condensed by the nozzle exit. This data confirms that boundary layer effects in the nozzle cause the PTM approach to be less valid as condensation progresses since portions of the relatively thick boundary layer cannot sustain condensation.
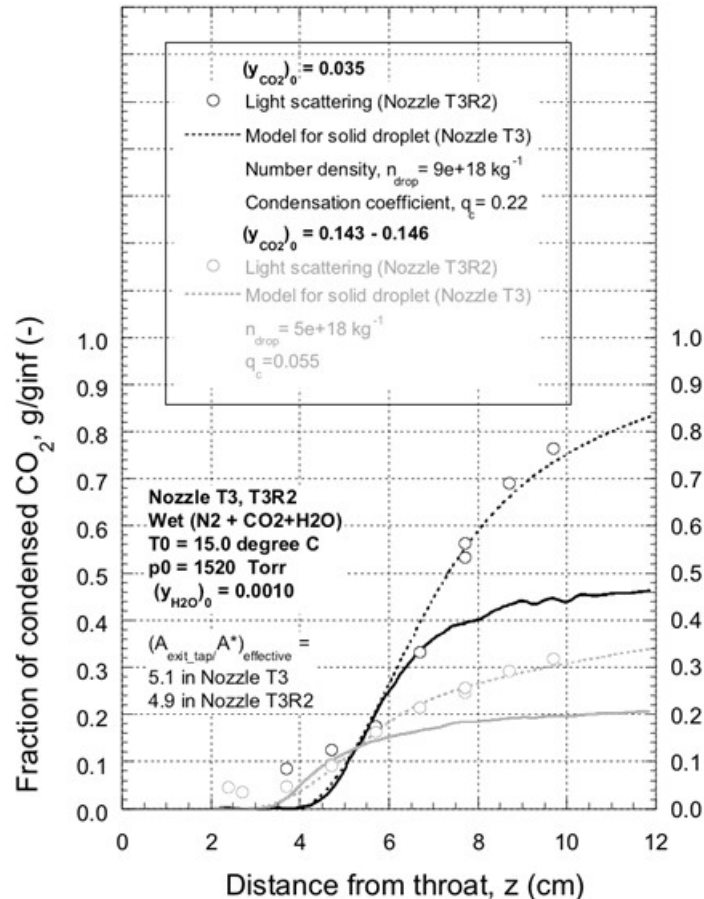
Figure 13 The fraction of CO_2 condensed that was derived from pressure trace measurement (PTM, solid black line), light scattering measurement (LSM, open circles), and model calculations (dashed line)

Figure 14 shows the predicted radius of the H_2O/CO_2 particles, which are estimated to reach about 14 nm at the exit of nozzle for $(y_{CO2})_0 = 0.143 - 0.146$, or about 10 nm for $(y_{CO2})_0 = 0.035$. Note that the relatively small scale of the OSU nozzle is not expected to produce micron-scale particles. Our goal with this testing was to demonstrate growth and/or agglomeration relative to the baseline particle sizes.
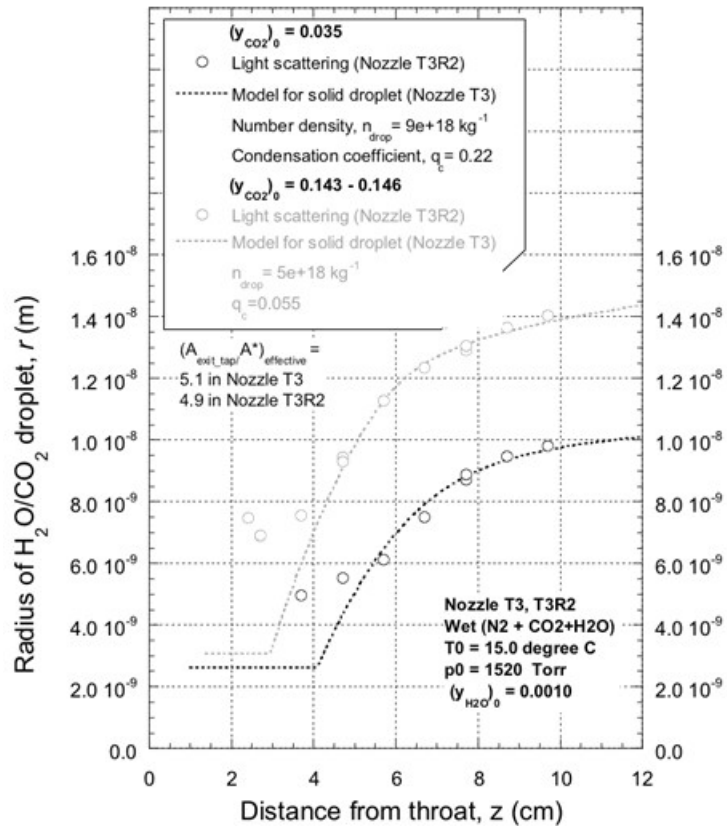
Figure 14: The size of the CO_2 particles derived LSM (circles) and model calculations (dashed lines).

The OSU test article was then modified, as illustrated in Figure 15, so that micron size CO_2 particles could be injected into the flow in a manner similar to that used at Orbital ATK's larger scale facility.
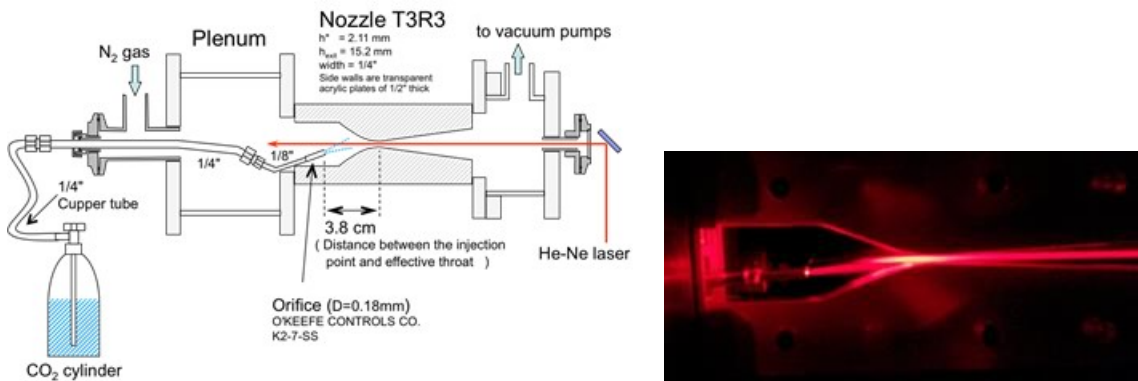
Figure 15 (left) The modified flow system includes an orifice to introduce CO2 particles into the flow. (right) The HeNe laser illuminates the stream of particles exiting the orifice and flowing through the nozzle.

Figure 15 (right) illustrates the nozzle arrangement operating with CO_2 particle injection where the strong scattering of the laser light from the micron size particles is clearly observed. Experiments conducted at OSU provided data to better understand the evolution of the injected particles in the flow and were used to validate a droplet growth model for the micron sized droplets. The model was then applied to the Orbital ATK bench-scale nozzle profile and variations of that profile that included a longer expansion region, as well as an extension at constant area ratio. As illustrated in Figure 16, modeling results suggest that CO_2 recovery is enhanced by injecting the particles as close to the throat as possible, decreasing the particle size to as small a value possible that is still consistent with inertial separation, increasing the expansion ratio modestly, and decreasing the inlet temperature of the injected CO_2. The results of the validated model appear to be consistent with the results of the bench scale CO_2 injection experiments.
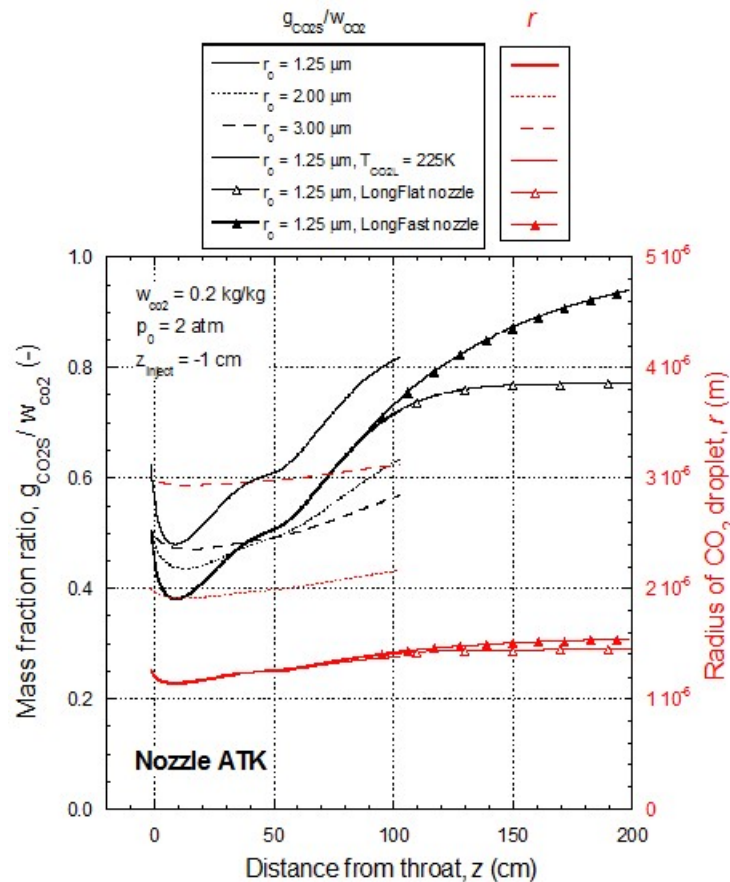
Figure 16 The mass fraction condensate and particle size predicted by the droplet growth model in the ATK nozzle.

In summary, the effort carried out at OSU confirmed that separation of condensable species via condensation in a supersonic flow apparatus is an attractive approach from the standpoint of process simplification and intensification. The challenges inherent in developing a full scale device with the goal of separating 90% of the CO_2 from flue gas are, however, not negligible. The extensive set of experimental and modeling studies

conducted at OSU provided insight into this process and led to the following conclusions. Items 1-5 below pertain to the tests with trace water and vapor phase CO_2 only.

1. CO_2 condensation from flue gas undergoing supersonic flow will be driven by heterogeneous nucleation and condensation. In the absence of injected liquid or solid media, the most likely scenario is CO_2 condensation onto homogeneously nucleated water droplets. The role that native solid particulate matter in the flue gas (e.g. fly ash) could play in this scenario was not considered in these studies because there was no information regarding this parameter and it may not be a variable that is easily controlled in the full scale process.

2. Heterogeneous nucleation appears to start near the extrapolated CO_2 vapor-liquid equilibrium line, and the supersaturation required to initiate heterogeneous nucleation increases as the water/ice particle size decreases.

3. The high number density of water droplets ($\sim 10^{12}$/cm^{-3}) results in CO_2 particles with diameters less than ~30 nm making inertial separation extremely challenging.

4. For the water/CO_2 cases, the maximum CO_2 recovery observed in lab scale experiments was about 80% for an inlet CO_2 concentration of 3.5 mol%. The maximum recovery was ~30% for an inlet concentration of 14.5 mol% that is typical of flue gas. All experiments started from a stagnation pressure of 2 atm.

5. A 1-D model considering Browning coagulation showed that this effect is unlikely to increase particle size on the timescale available in the supersonic flow. Furthermore, since particles are solid, they are likely to form fractal-like objects thereby changing their drag and their ability to be separated.

6. Limited flow perturbation experiments (turbulent wakes) suggested that the heat introduced into the flow by the relatively warm surfaces was detrimental to CO_2 recovery and did not increase particle size significantly. Modeling by Orbital ATK confirmed this observation.

7. Light scattering experiments validated a model developed to explore throttled CO_2 liquid injection as a means to provide micron size particles with which to remove CO_2 from the gas phase.

8. Models of the experiments showed that small CO_2 particles initially shrink at the high temperatures upstream of the throat. Thus, injection close to the throat is critical.

9. For a fixed CO_2 injection rate, particles should be as small as possible to ensure a large surface area for CO_2 condensation, but not so small that they evaporate completely.

10. In experiments, the addition of water vapor to the flow led to ice formation on the nozzle surfaces near the throat and unstable operating conditions. This may be a consequence of the geometry of the experiments and the small size of the test nozzle, but could also be an issue at full scale.

11. Modeling of the Orbital ATK nozzle, and variants thereof (longer, faster, and scaled up nozzles), confirmed that CO_2 droplet injection close to the throat was critical, that for a fixed CO_2 injection rate recovery is maximized when particles are as small as possible given that they should be recovered by inertial separation and not evaporate fully, and that increasing the scale of the device was helpful. When CO_2 was present both in the incoming flow and injected in the flow as a liquid to produce particles, some net CO_2 recovery was observed.

The very small scale of the OSU test facility was acknowledged to result in very short residence time so the absolute size of condensate particles was not expected to be directly relevant to the bench scale or full scale ICES systems – the essential physics of condensation and particle growth/agglomeration were, however, obtained in order to gain a better understanding of some of the key drivers underlying the particle growth challenge.

Additional details may be found in the OSU final report included herein as Appendix A.

3.1.2 Bench-scale System Design and Analysis

In support of the objective to demonstrate a bench scale diffuser and capture duct, design and analysis work relating to the addition of these hardware elements to the existing ICES test hardware was initially carried out. The goal of this task was to develop a geometry that will efficiently diffuse the supersonic flow (post-CO_2 capture) to subsonic velocities with minimal loss of total pressure. A preliminary design for capture duct and diffuser is shown in Figure 17.
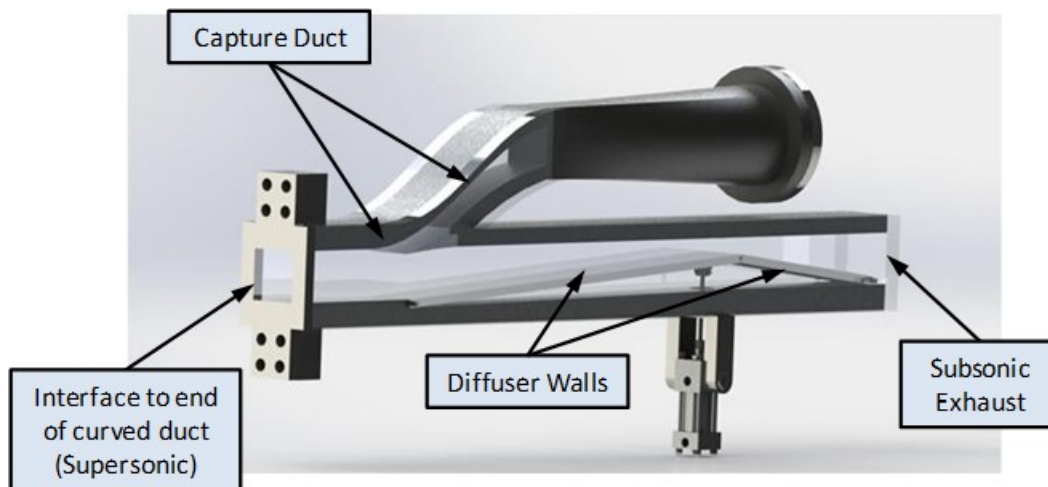
Figure 17 Preliminary capture duct and variable geometry diffuser

Initially, two-dimensional wave-diagram based analysis was used to develop preliminary flow contours. The initial configuration (see Figure 18) was comprised of a 3.5degree compression ramp followed by a 10 degree expansion after the minimum area (or throat). Based on a uniform inflow at Mach 3.0 (into the left side of duct as shown in the figure), the flow arrives at close to Mach 1.0 after 10 oblique shock waves, resulting in high predicted pressure recovery (85%) as defined by the total (or stagnation) pressure at the exit divided by that at the entrance. This contour was then analyzed using CFD.
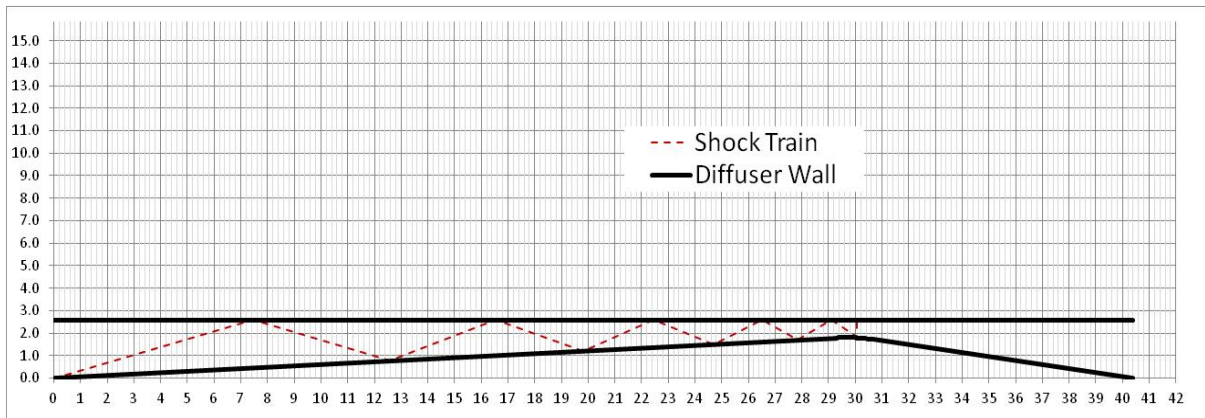
Figure 18 Initial diffuser design based on 2D supersonic wave analysis

Initial CFD results revealed that the non-uniform flow profile entering the diffuser caused a significant reduction in performance and will result in an updated geometry. This is largely due to the aspect ratio of the existing curved "migration" duct which (at near 1.0) results in lateral flow in the boundary layer from the corners adjacent to the outer wall to flow inward toward the centerline. This is evident in Figure 19 and Figure 20 below. Figure 19
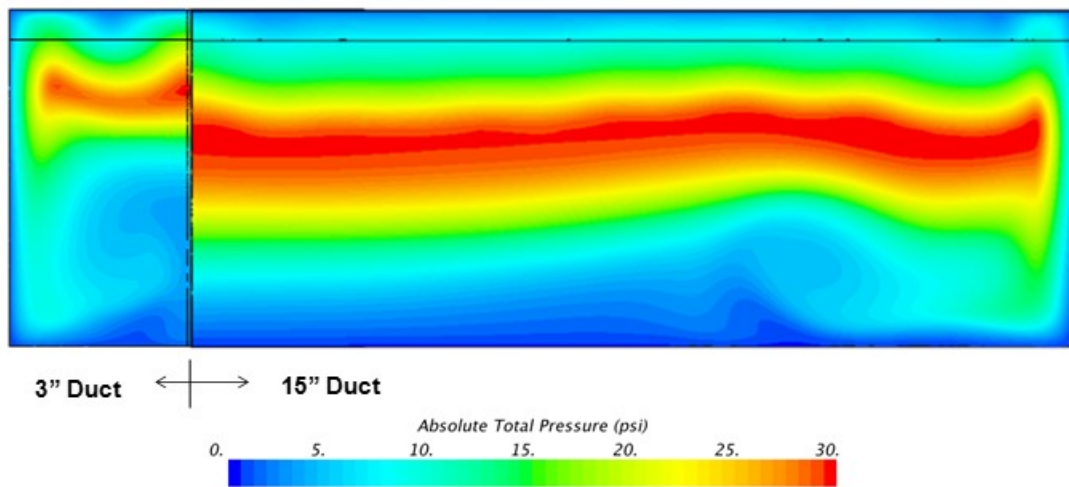
Figure 21 shows stream wise cross-section of the ICES duct with Mach number contours for 2D simulation along with 3D simulation of the existing 3" wide duct and a 15" wide

duct approximating 2D.
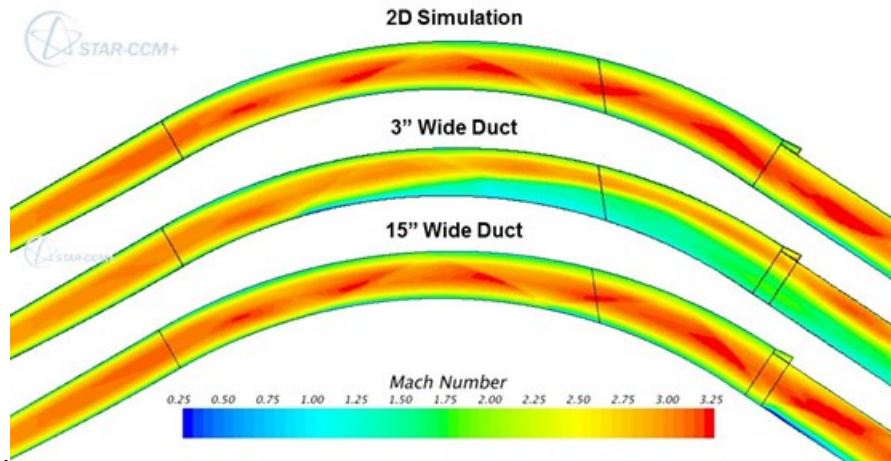
Figure 19 Comparison of centerline Mach number contours through supersonic turn for 2D (upper) and 3D 3" duct (middle) and 3D 15" duct (lower) configurations.
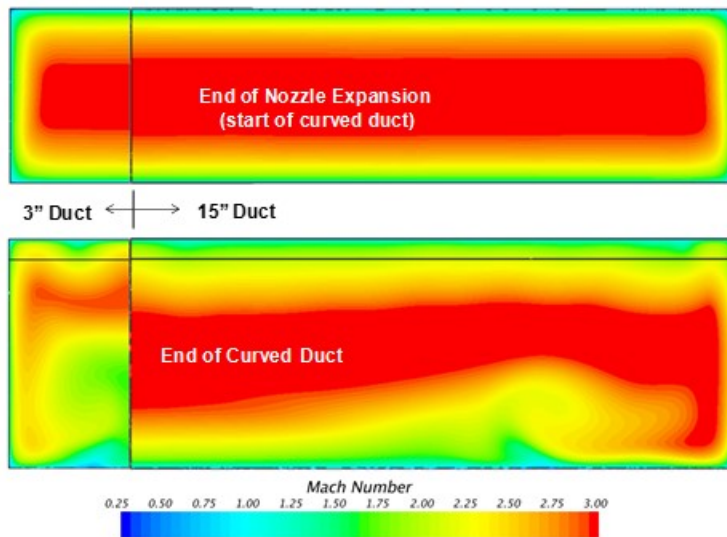
Figure 20 Comparison of Mach number contours at start and end of curved duct for current 3" wide rig (left) and 15" wide rig (right).

Figure 20 depicts cross stream section of the 3" and 15" ducts at two different stations. In the above results, it is desirable to have the highest and most uniform distribution of Mach number which is consistent with a large red-colored region. The uneven distribution of relatively low Mach numbers evident in the 3" wide duct case result in similar results for total pressure as seen in
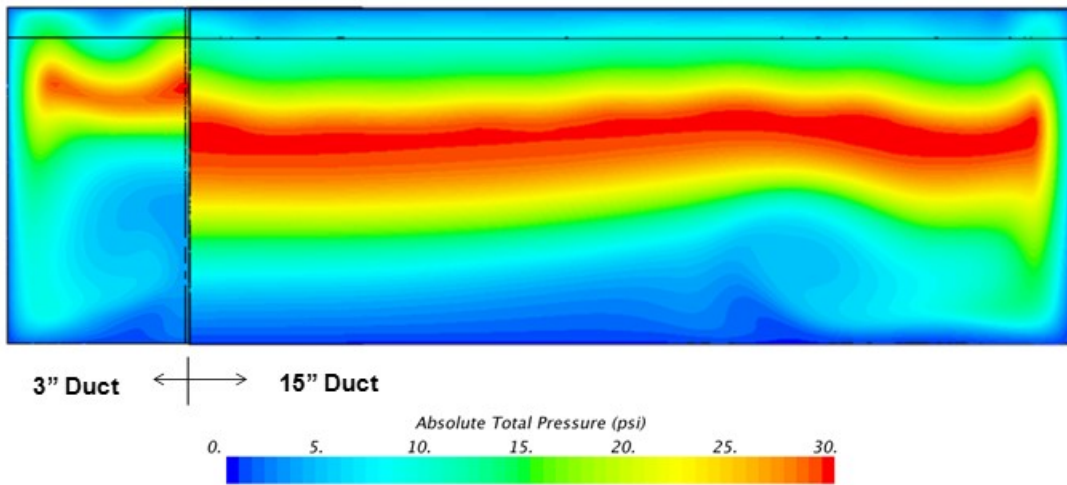
Figure 21 and reveals that full-scale ICES should have a duct aspect ratio >5:1 to produce results that are closer to the desired 2-dimensional case.
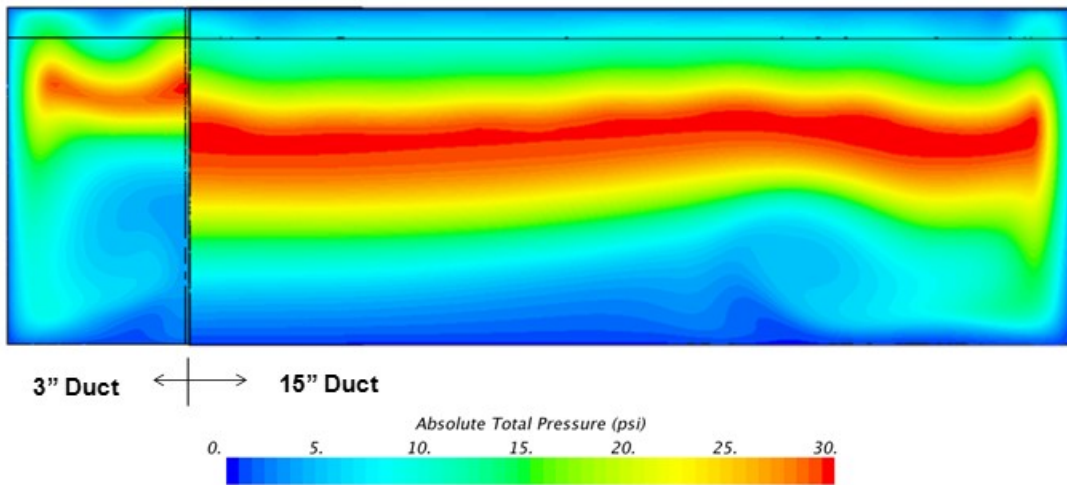
Figure 21 Comparison of total pressure contours at end of curved duct for current 3" wide rig (left) and 15" wide rig (right).

This CFD analysis was then used to provide a comparison between pressure recovery performance at the Orbital ATK test article scale and predicted performance at projected full scale. Table 3 summarizes pressure recovery by major system component/section for the current scale ICES and full scale ICES respectively. As a reminder, on overall pressure recovery of 50% is desirable (techno-economic analysis (TEA) previously carried out by WorleyParsons assumed 40% overall pressure recovery).

Table 3 Composition of Pressure Recovery by Component

Component	Total Pressure Recovery		Supporting Rationale
	Current Scale ICES at ATK	Full Scale ICES	
Nozzle expansion	69%	85%	Current nozzle is very long due to prior experimental objectives that are no longer relevant
Turning Duct	66%	85%	Can achieve 82% at current scale with 5X width based on 3D CFD
Capture Duct	95%	95%	Not an area of concern
Diffuser	33%	75%	Impact of distorted entry flow field in the current scale aspect ratio
OVERALL	**14%**	**51%**	

The key problem at the current experimental scale is due to the distorted flow profile at the exit of the turning duct as described previously.   The earlier CFD analysis showed that significant improvement in turning duct pressure recovery performance can be obtained simply by increasing the duct width from 3 inches to 15 inches since the flow leaving the duct is considerably more uniform.   At full scale, we can leverage this aspect ratio benefit in combination with the inherent benefit of larger scale to get even better pressure recovery and more uniform flow.   This has a compounding effect on diffuser performance since distorted supersonic flows have considerable difficulty in compression scenarios. In order to maximize pressure recovery given the constraint of using existing ICES hardware (nozzle + turning duct), fixed-ramp diffusers were examined using CFD as shown in Figure 22.
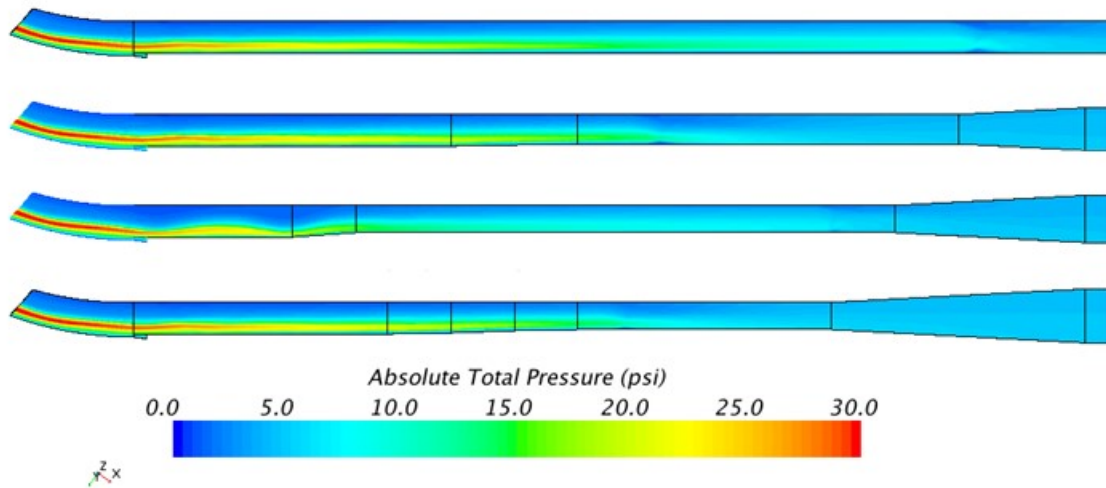
Figure 22: Total Pressure profiles for fixed geometry diffusers analyzed

.
A summary of the geometric characteristics of these diffusers along with the maximum achieved backpressure is presented in Figure 23. The highest backpressure obtainable at this scale is approximately 4.5 psia, though these results are somewhat conservative. A 2-degree segmented diffuser was selected for detailed design and fabrication as the best performing configuration.

Straight Pipe

1° Simple

1°   -3°

2° Simple

2°

-3°

2° Segmented

1°   1°   -1°   -3°

Design	Turn Start (L/D)	Max Turn (°)	Contraction Ratio	Throat Length (L/D)	Expansion Ratio	Max Back Pressure (psi)
Straight Pipe	-	0	1.0	30.9	1.0	3
1° Simple	10	1	1.08	12.9	1.14	4.1
2° Simple	5	2	1.16	17.4	1.17	4.0
2° Segmented	8	2	1.16	9.3	1.28	4.5
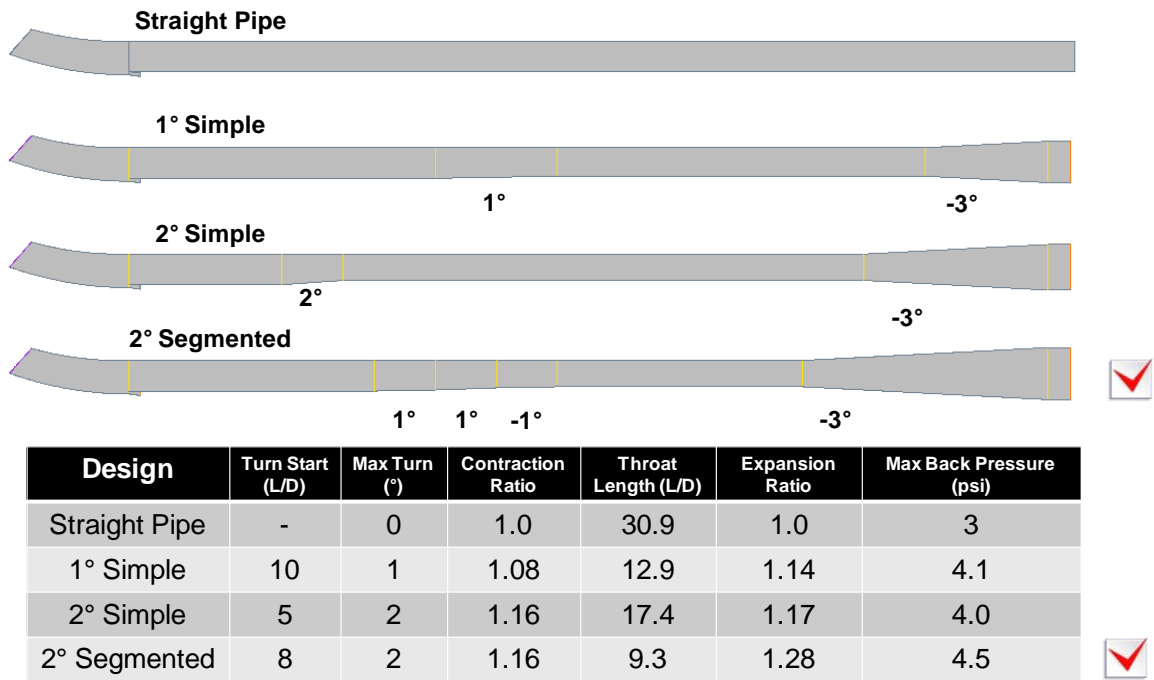
Figure 23: Fixed geometry diffuser and backpressure summary

Flow exits the as-built test rig via two paths. The main flow path dumps into a large 18"
diameter duct, which then transitions to a 12" duct connected to the facility vacuum
system. The capture duct flow path is through a much smaller duct which is connected to
the facility vacuum system with an 8" diameter flexible duct. Both paths have been sized
to keep the flow subsonic and to minimize pressure drop.

A three dimensional analysis of a straight pipe diffuser exiting into the 18"duct was
performed to assess back pressured behavior of this large volume. A portion of the 12"
duct was included as well. This analysis showed no adverse effect on the test rig both
with and without back pressure as shown in Figure 24.
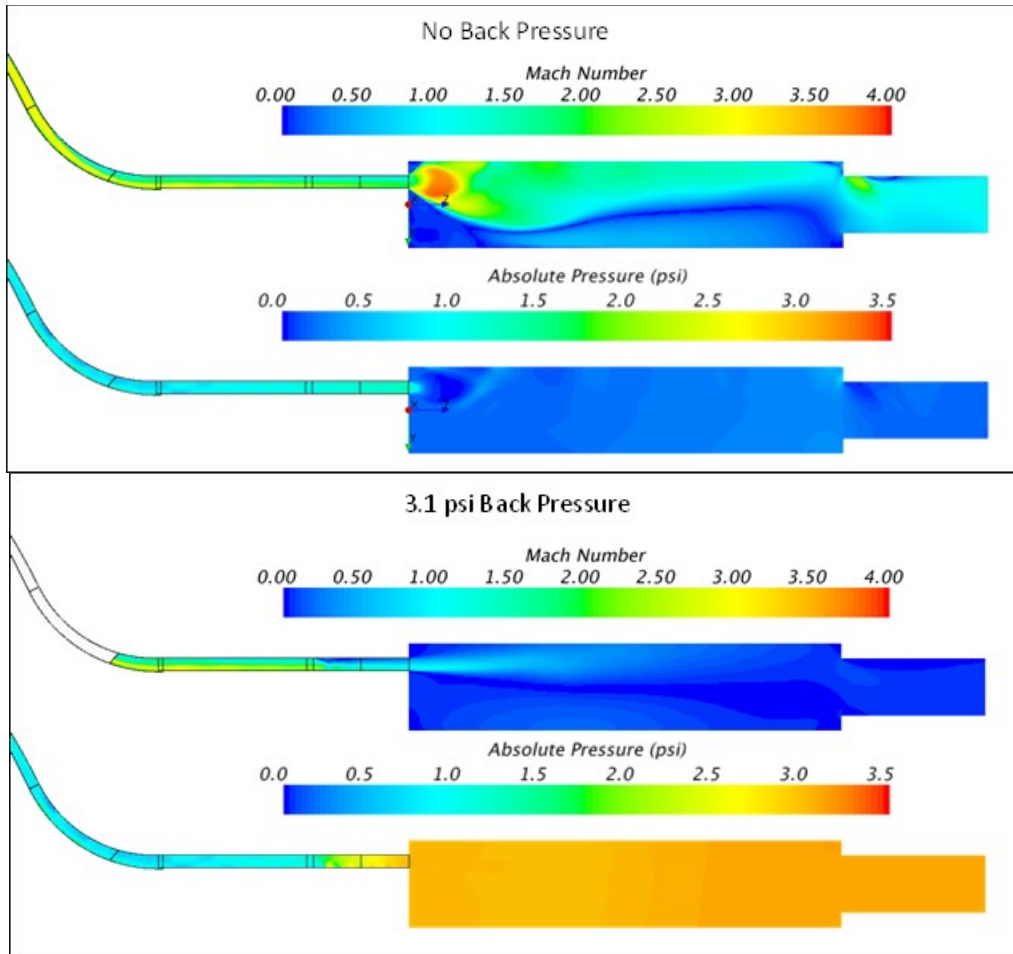
Figure 24 CFD results of ICES vacuum path

The as tested geometry included a knife-edge splitter plate between the diffuser and capture duct. There was an increase in diffuser duct area immediately downstream of the splitter plate. The diffuser itself was straight duct with a short expansion section at the end. These geometric features were all different than any analyzed prior to the release of the final design to manufacturing. Three dimensional analysis of the flow path downstream of the turning duct was performed to ensure that back pressure capabilities had not been reduced when compared to the previous designs analyzed. The CFD solutions (Figure 25) showed no adverse effect on diffuser performance of the blunt splitter plate or the expansion waves introduced by the area relief immediately downstream of the splitter.
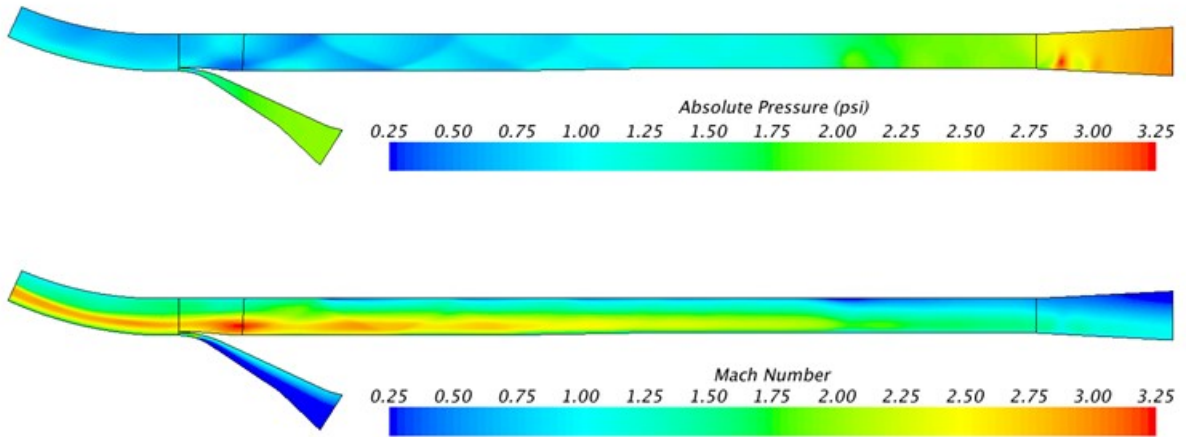
Figure 25 Pressure and Mach number results of diffuser and splitter plate/capture duct

3.1.3 Bench-scale Testing

In further support of the capture duct and diffuser demonstration, a CAD layout of the new hardware assembled to the existing ICES nozzle and curved duct was developed to ensure efficient integration into the Orbital ATK test laboratory. As seen in Figure 26, the test article was installed between existing Test Legs #1 and #2 with a new vacuum connection made to the current Leg #1 exhaust pipe. Additional details of the updated test article installation and backpressure control system are presented in Figure 27 and Figure 28.
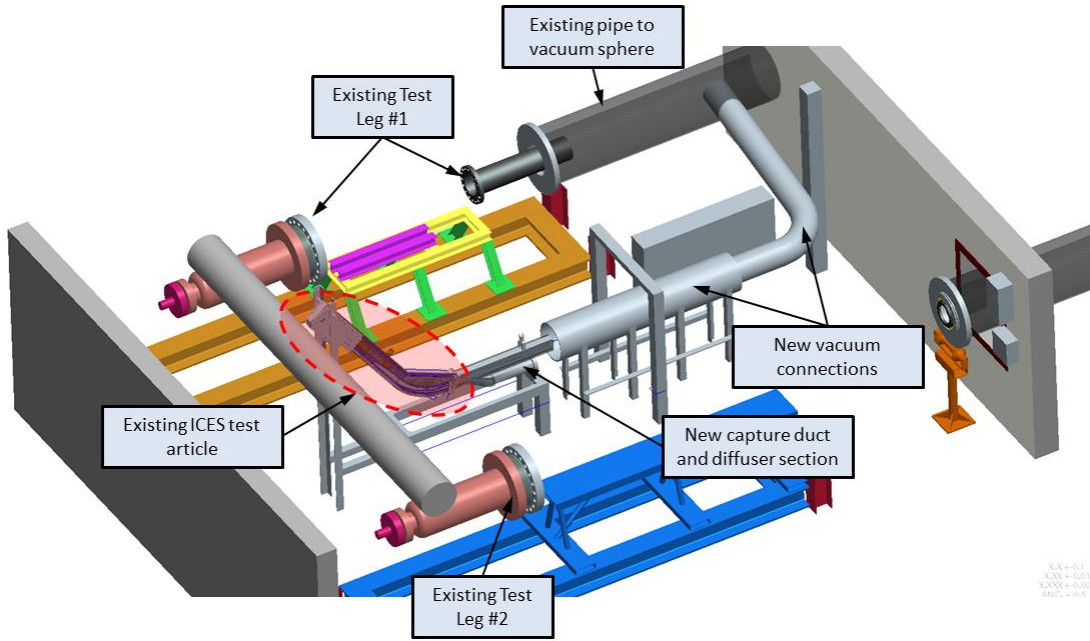
Figure 26 CAD rendering of ICES test article integrated between Orbital ATK Test Leg #1 and #2
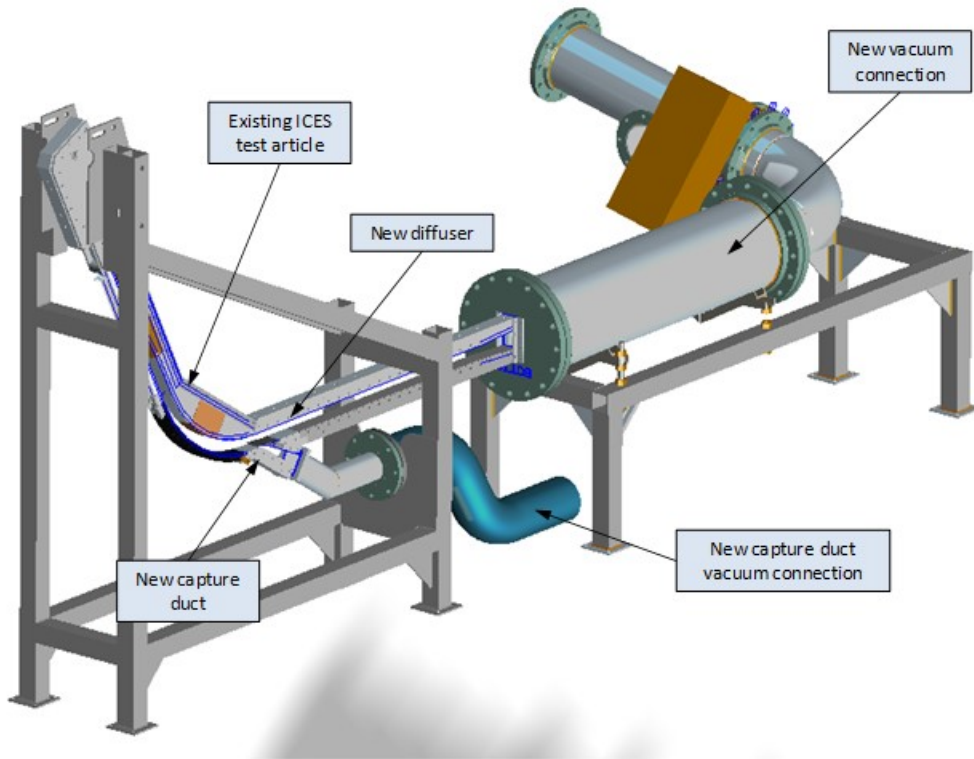
Figure 27: Isometric view of ICES Installation with capture duct and diffuser
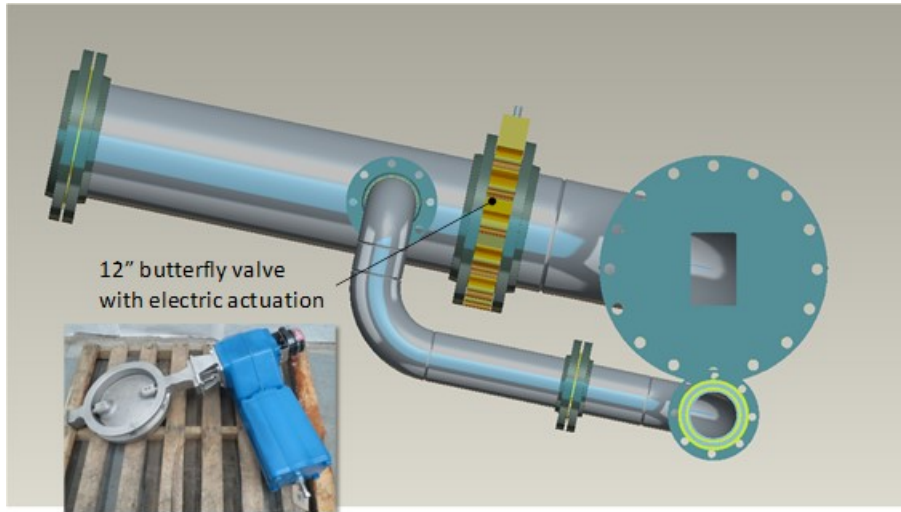
Figure 28: Exhaust system with backpressure control

A zoomed-in view of the capture duct geometry is shown in Figure 29 and the associated hardware (pre-assembly) is shown in Figure 30.
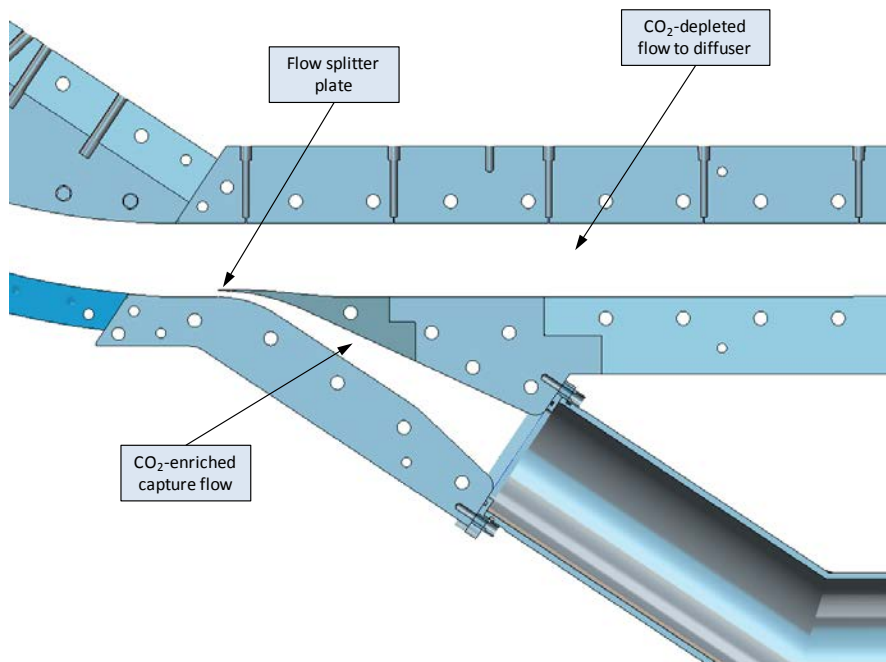
Figure 29: Zoom in on capture region

Figure 30. Assembly of the diffuser/capture duct

Additional photos of the test article assembly are shown in Figure 31 and Figure 32.

Figure 31. ICES test article during assembly

Figure 32. ICES test article support frame and exhaust piping.

Finally, Figure 33 shows the locations of two gas sampling probes connected to an on-line gas chromatograph (GC). Measurements using the "Primary Flow" probe are most valuable as the flow in that region is subsonic and therefore expected to be single-phase due to diffusion through shock waves emanating from the diffuser into the large pipe. The measurement in the capture duct is subject to a complex 2-phase flow with large particles and is therefore not considered reliable since the probe design is not iso-kinetic (i.e. large particles may not enter the tube).

Capture flow GC probe station

Primary flow GC probe station
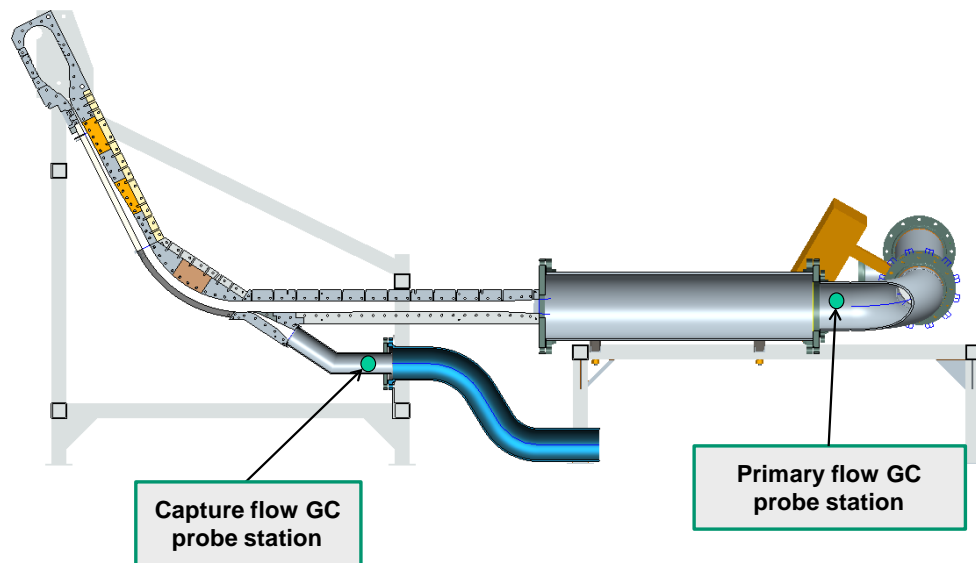
Figure 33: Gas Sampling Probe Locations for Gas Chromatography (GC) Measurements

Optical diagnostics and liquid CO$_2$ injection testing

The objective of this work was to ensure that capture duct testing was supported by robust optical diagnostics to obtain measureable and repeatable solid CO_2 particle sizes. For these tests, liquid CO_2 at high pressure (~800psia) is throttled to low pressure in what is referred to as a shroud tube based on prior work at the Air Force Institute of Technology (AFIT) and Orbital ATK.
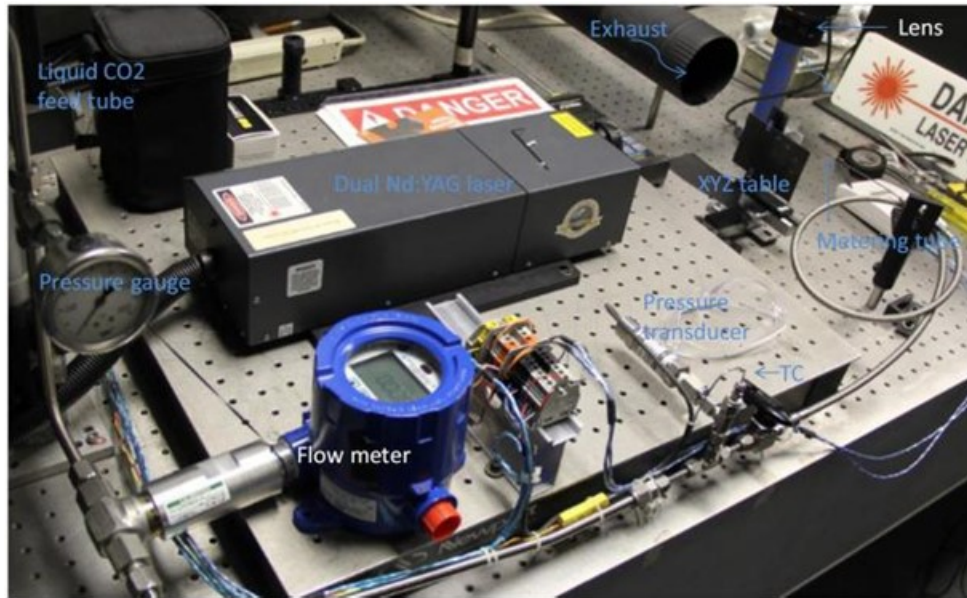
Figure 34: CO_2 Particle Size Test Bench

The experimental arrangement as assembled in the Orbital ATK laboratory is shown in Figure 34, containing the hardware layout of the liquid CO_2 injection system and the key components of the Planar Laser Light Scattering (PLLS) instrument, i.e. the laser illumination source and the image capture system. The liquid CO_2 bottle and the CCD camera mounted collinear with the optical axis of the lens are not shown in this picture.

The liquid CO_2 injector system consisted of a metering orifice nozzle (or metering tube) concentric with a shroud tube exhausting to atmosphere mounted on a high precision xyz translation table. The flow of liquid CO_2 was turned on or off using a manual orifice valve mounted on the supply line right before the nozzle assembly. The experiment was further instrumented with a SIXNET data acquisition system (DAS) consisting of 8 differential analog input channels. The measured properties were the liquid CO_2 temperature, the pressure, the flow rate, and the ambient temperature. One analog input voltage channel was used to record the time evolution of the CCD camera synchronization pulse (TTL logic) during a test. This feature helped correlate the flow properties inferred from each image with the measured liquid CO_2 properties. Two high speed Ethernet lines were used to transmit data from the DAS and from the CCD camera to a computer.

The PLLS instrument relied on a laser sheet (nominal thickness of about 1 mm) to visualize the CO_2 particles, as shown in Figure 35. The source of the light was a dual-pulse Nd:YAG laser (532 nm wavelength, laser energy up to 120 mJ/pulse, 5-7 ns pulse

length). Sheet forming optics at the outlet of the beam allowed for control of sheet thickness and orientation. The light scattered from the CO_2 particles was captured by a receiving lens and a high resolution CCD camera (MANTA G-504B, 2452 pixels x 2056 pixels area, 3.45 μm x 3.45 μm pixel size). The laser sheet orientation for both lasers was set to horizontal. The CCD camera was mounted perpendicular to the laser sheet to record at the 90 deg scattering angle. A pulse generator (DG535) was used to control the laser energy of each pulse, the time delay between pulses and to synchronize the camera with the laser's q-switch pulse. Each camera frame was therefore associated to the single pulse output of the laser.
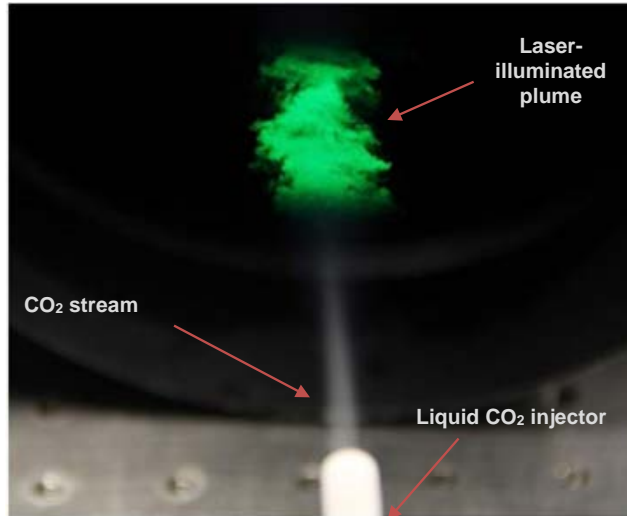
Figure 35: CO_2 particle stream illuminated by laser sheet.

The spatial resolution and the field distortions of the optical system were determined with a transparent grid (Thorlabs, Grid Array R13S3) illuminated by white light.
Figure 36 shows the image of the rectangular grid with the step size of 50 μm. The inset picture is a zoom-in section showing only two grid lines. It was used to determine the spatial resolution of the measurement corresponding to one pixel. The camera lens was a high-quality telecentric system with a focal length of 105 mm mounted with a spacer ring to the camera to increase magnification. The corresponding area in the flow imaged by the camera was about 3 mm x 4 mm. For the current configuration the spatial resolution of the instrument was 1.54 microns per pixel.
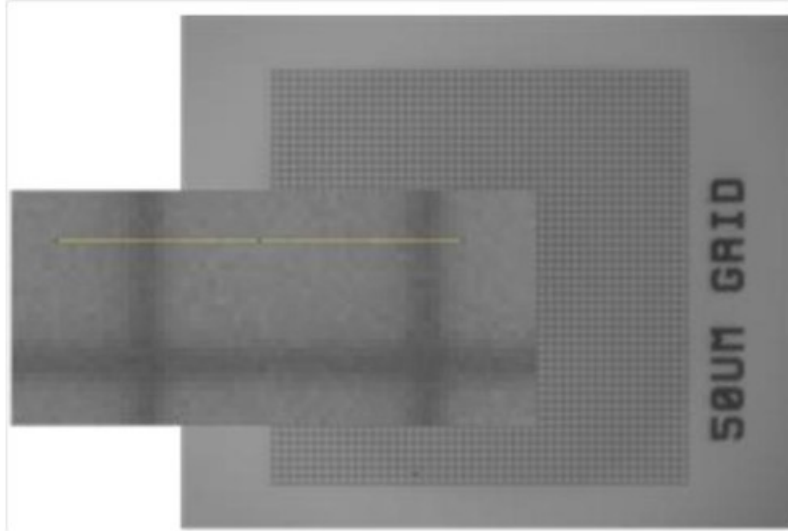
Figure 36: Image of a 50 µm x 50 µm grid illuminated with room light. The image size corresponds to about 3mm x 4 mm of flowfield. The inset picture shows only two grid lines.

The particle size was estimated by direct imaging of the light scattered from the flow field (as seen in Figure 37) and image analysis. For these recordings the laser was operated in single cavity mode so that only one laser pulse was recorded within the image. Analysis of the image proceeded by first determining an instrument function from a region containing an image of a small particle (considered approximately as a point light source). This image was a convolution of the optical instrument point spread function, the entrance pupil function and the diffraction pattern generated by the particle at the laser wavelength. Then, assuming that the larger structures are conglomerates of such small particles, the instrument function was de-convolved from the recorded image. The resulting image was the representation of the particle viewed from a two-dimensional perspective.

3.77 mm x 3.16 mm

Figure 37: CO$_2$ particles image digitally recorded by CCD camera. 0.023" orifice, 6" long shroud tube.

The image was then converted to a binary image by applying a local thresholding function and an edge-detection routine is applied to locate the projected shape and its associated perimeter. An area estimate was produced which was then used to compute an equivalent diameter for the particle assuming it was a spheroid. The equivalent diameter data from several images was then sorted into bins between the minimum and the maximum values of data to produce a distribution function. The particle average diameter and other characteristic properties were obtained directly from fitting this function.

Figure 38 shows the results of particle size measurements for a test using a 0.023" diameter feed tube and 6 inch long shroud. In the plot D$_{mean}$ stands for Sauter Mean Diameter (SMD) - the most probable particle diameter found in the population, D$_{median}$ is a threshold value that separate the higher half part of data from the lower. The SMD is used for particle size characterization in this project. Figure 21 is a result of processing of 10 images, one of which is presented in Figure 20.

We are targeting particles in the 20μm SMD range for our initial ICES migration tests and have developed a solid understanding of the parameters we can vary to control the size range. For the initial test, LCO$_2$ injection setup with 0.023" nozzle and 6"-long shroud tube was baselined. It generates 22 μm SMD particles.
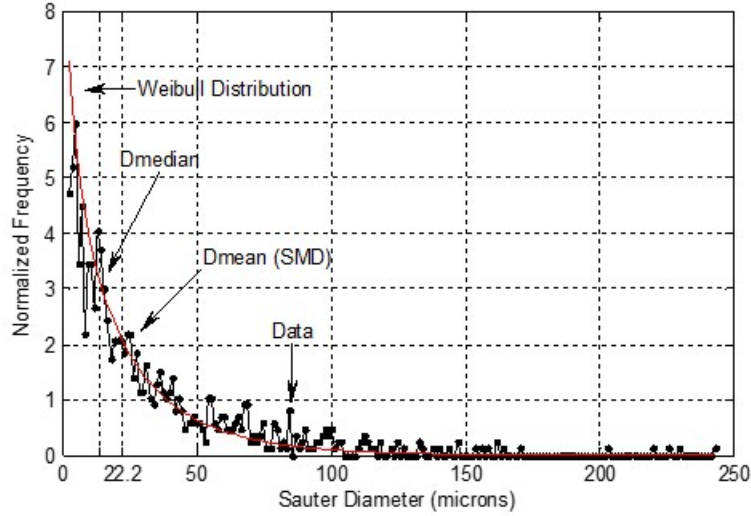
Figure 38: Histogram showing the CO_2 particle size distribution and the Weibull probability density function fit to data. Measurements taken at an axial distance of 5.0 inches downstream of a 0.023" diameter nozzle with a 6" long shroud tube.

CO2 Capture Test Results

CO_2 was injected into the upstream stagnation chamber of the ICES nozzle in an amount approximately equal to 10% (by mass) of the total flow using an array of tubes designed to produce solid particles of ~20μm SMD. Figure 39 shows typical laser sheet image taken in the vicinity of the capture duct.
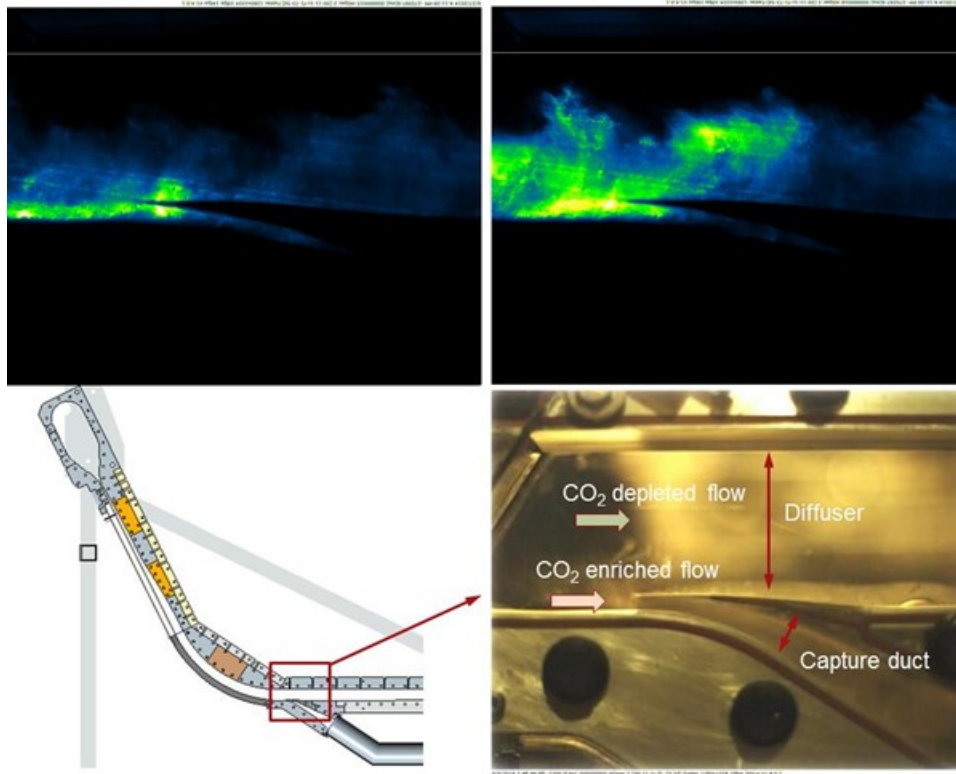
Figure 39: Laser images and photo of the capture duct entrance region.

The bright regions in the image correspond to areas of high solid CO_2 concentration (larger particles), the "wispy" blue areas are the smaller particles and the black region contains little-to-no solid CO_2. The flow pattern is somewhat unsteady in nature and occasional bands of higher concentration are observed above the capture duct.

In general, these images support a high degree of capture. The images in Figure 40 show the CO_2 particle-laden flow upstream of the turning duct. Here we can see that the CO_2 is distributed across the entire flow field, further supporting the observation that the turning duct is functioning as desired.
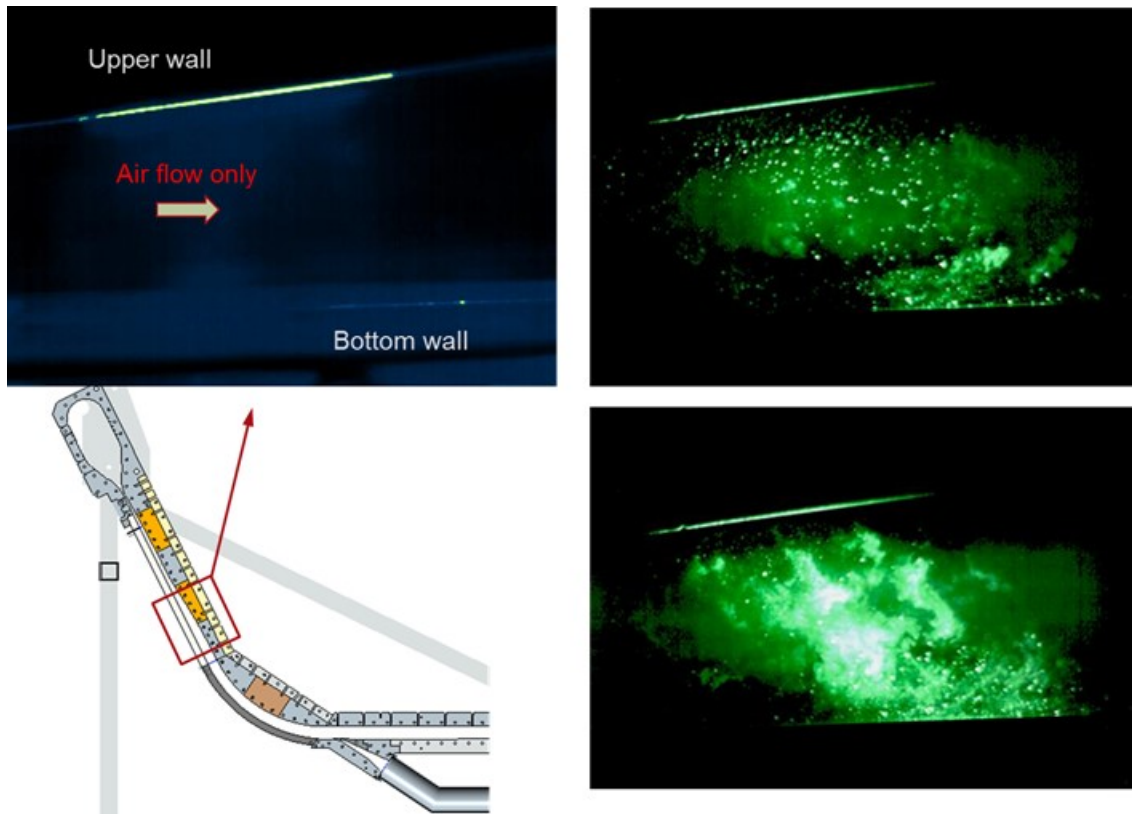
Figure 40: Laser images of the flow upstream of the turning duct (before CO_2 migration).

A summary of all bench-scale tests conducted in the program through October 2, 2014 is presented in Table 4.

Table 4 Summary of the ICES Bench Tests through early Oct 2014

Test Number/Date	Test Setup Configuration	Test Results Description
NETL_104-109, May 22-June 2, 2014	Shakedown runs: tuning air flow, CO_2 flow, instrumentation checkout, laser/camera set up tuning, etc.	
NETL_110, June 5, 2014	Air plenum pressure at 32.6 psi, 6 CO_2 injectors provided 8.4% of CO_2 wt concentration Camera sees straight duct	Large amounts of solid CO_2 particles seen in the pictures Temperature in the plenum had unexplained peak at the moment of GC sampling, therefore estimated 17.6% capture not included in the

Test Number/Date	Test Setup Configuration	Test Results Description
		trend
NETL_111 June 9, 2014	Two sets of air plenum pressure at 30.5 and 76.4 psi 6 injectors provided 9.9% and 4% of CO$_2$ by weight Camera sees capture duct	No individual particles was detected in the pictures Per GC and estimations, 92.6% and 59.3% capture were observed at two pressures
NETL_112 June 9, 2014	Two sets of air plenum pressure at 30.8 and 77.9 psi 6 injectors provided 9.2% and ~4% of CO$_2$ by weight Camera sees capture duct	No individual particles was detected in the pictures Per GC and estimations, 91.1% capture was observed at 30 psi, no separation at 77.9 psi
NETL_113 June 26, 2014	Air only test with backpressure valve. Valve gradually closed till diffuser unstart to collect pressure recovery data	Diffuser unstarted at 3.5 psi backpressure.
NETL_114 June 26, 2014	Same as #113	Same as #113 Data fed into CFD
NETL_115 June 26, 2014	Air plenum pressure at 31.9 psi 6 injectors provided 5.9% of CO$_2$ by weight Camera sees straight duct GC probe switched between diffuser and capture duct locations Concentration was measured 2 times in each location	Large amounts of solid CO$_2$ particles seen in the pictures, no particles during second GC probe in diffuser Very low concentration of 1% was observed in capture duct in the first half Per GC and estimations, 58.9% capture was observed when particles seen in the straight duct, only 22.5 capture when no particles in capture duct (point is not included in the trend)
NETL_116 June 26, 2014	Air plenum pressure at 32.4 psi 6 injectors provided 7.8% of CO$_2$ by weight Camera sees capture duct GC probe switched between diffuser and capture duct locations Concentration was measured 2 times in each location	No individual particles was detected in the pictures Very low concentration of 0.3% was observed in capture duct in the first half Per GC and estimations, 72.9% capture was observed in the first half, only 13.5% capture in the second half (point is not explained but included in the trend)
NETL_117 June 27, 2014	Air plenum pressure at 31.4 psi 2 injectors provided 2.1% of CO$_2$ by weight in plenum Camera sees capture duct GC probe switched between diffuser and capture duct locations Concentration was measured 3 times in each location	No individual particles was detected in the pictures Very low concentration of 0.3% was observed in capture duct in the first measurement Per GC and estimations, 46% capture was observed in the first measurement, only 16.6% capture in the second measurements and 17.5% capture in the third measurement (point are but shown separately included in the trend due to significantly different initial concentration)
NETL_118 June 27, 2014	Air plenum pressure at 32.5 psi 6 injectors provided 7.5% of CO$_2$ by weight in plenum Camera sees capture duct GC probe switched between diffuser and capture duct locations Concentration was measured 2 times in each location	No individual particles was detected in the pictures Per GC and estimations, 12.0% capture was observed in the first half and 11.3% capture in the second half (points are not explained but included in the trend)
NETL_119 July 17, 2014	LCO$_2$ injection only, no air flow. Objective: to obtain video of the particles distribution between diffuser and capture	Video clearly indicated that vast majority of solid particles go to capture duct

Test Number/Date	Test Setup Configuration	Test Results Description
	duct. Vacuum sphere pressure 6 psi, ICES plenum pressure 6.5 psi. Subsonic flow	
NETL_120 Sept 19, 2014	Shakedown test after long no test period	
NETL_121 Sept 19, 2014	Air plenum pressure at ~17.5 psi 6 injectors provided ~8% of CO_2 by weight in plenum No laser. Camera sees capture duct and beginning of the turning duct GC probe in diffuser location only Concentration was measured 2 times	No individual particles was detected in the pictures Per GC and estimations, 57.5% capture was observed in the first measurement and 22.4% capture in the second one Capture duct camera sees "fog" which takes nearly half height of the diffuser duct and all of capture duct. Turning duct camera sees CO_2 migration
NETL_122 Sept 19, 2014	Air plenum pressure at ~30 psi 6 injectors provided ~8% of CO_2 by weight in plenum No laser. Camera sees capture duct and beginning of the turning duct GC probe in diffuser location only Concentration was measured 4 times	Same as #121. CO_2 capture goes down in four consecutive measurement 82.4%-36.9%-19.9%-15.0%
NETL_123 Sept 25, 2014	Air plenum pressure at ~33 psi 6 injectors provided ~9.6% of CO_2 by weight in plenum No laser. Camera sees capture duct and beginning of the turning duct GC probe in diffuser location only One discrete GC measurement	Same as #122. CO_2 capture estimated at 97.1%
NETL_124 Sept 25, 2014	Air plenum pressure at ~30 psi 6 injectors provided ~8.8% of CO_2 by weight in plenum No laser. Camera sees capture duct and beginning of the turning duct GC probe in diffuser location only One discrete GC measurement	Same as #123. CO_2 capture estimated at 85.2%
NETL_125 Sept 25, 2014	Air plenum pressure at ~30 psi 6 injectors provided ~9.5% of CO_2 by weight in plenum No laser. Camera sees capture duct and beginning of the turning duct GC probe in diffuser location only One discrete GC measurement	Same as #124. CO_2 capture estimated at 91%
NETL_126 Sept 25, 2014	Air plenum pressure at ~30 psi 6 injectors provided ~8.5% of CO_2 by weight in plenum Same as #125	Same as #125. CO_2 capture estimated at 82.7%
NETL_127 Sept 25, 2014	Air plenum pressure at ~75 psi 6 injectors provided ~3.6% of CO_2 by weight in plenum Same as #126	Same as #125. CO_2 capture estimated at 70.5%
NETL_128 Sept 25, 2014	Air plenum pressure at ~30 psi 6 injectors provided ~9.9% of CO_2 by weight in plenum Same as #127 Two consecutive GC measurements	Same as #127. CO_2 capture estimated at 83.7% and 30.3%

Test Number/Date	Test Setup Configuration	Test Results Description
NETL_129 Sept 25, 2014	Air plenum pressure at ~30 psi 6 injectors provided ~8.6% of CO_2 by weight in plenum Same as #128 Three consecutive GC measurements	Same as #128. CO_2 capture estimated at 75.7%, 22.8%, and 15.5%
NETL_130 Oct 2, 2014	Air plenum pressure at ~31 psi 6 injectors provided ~8% of CO_2 by weight in plenum No laser. Schlieren imaging is arranged for the capture duct. Camera sees capture duct and beginning of the turning duct GC probe in diffuser location only Concentration was measured 3 times	No individual particles were detected in the pictures. Schlieren image shows stable dual shock on the splitter of the capture duct as expected. No shock change was observed during test (hypothesis of capture duct unstart due to back pressure increase was not confirmed). Per GC and estimations, CO_2 capture estimated at 97.8%, 73.6%, and 39.9%
NETL_131 Oct 2, 2014	Air plenum pressure at ~31 psi 6 injectors provided ~8.4% of CO_2 by weight in plenum Same as #130 Discrete single GC measurement	Same as #130 Per GC and calculations, CO_2 capture estimated at 88.8%
NETL_132 Oct 2, 2014	Air plenum pressure at ~29 psi 6 injectors provided ~8.7% of CO_2 by weight in plenum Same as #131	Same as #131 Per GC and calculations, CO_2 capture estimated at 49.4%
NETL_133 Oct 2, 2014	Air plenum pressure at ~31 psi 6 injectors provided ~8.7% of CO_2 by weight in plenum Same as #131	Same as #131 Per GC and calculations, CO_2 capture estimated at 54.4%
NETL_134 Oct 2, 2014	Air plenum pressure at ~31 psi 6 injectors provided ~8.7% of CO_2 by weight in plenum Same as #131	Same as #131 Per GC and calculations, CO_2 capture estimated at 50.1%

Gas samples taken from the primary flow stream were processed with an online gas chromatograph to assess CO_2 mole fraction in the primary flow exiting the diffuser. The % CO_2 capture was estimated using measured air and liquid CO_2 flow rates and a flow distribution between the diffuser and capture duct derived from CFD (9.3% of the gaseous flow goes into capture duct).

The observed % CO_2 capture (capture efficiency) varied in the wide range from 11.3% to 97.8%. It was originally suggested that capture efficiency depends on supply plenum gas temperature, i.e., temperature of the mixture of the air and injected liquid CO_2. Later tests did not confirm this hypothesis. As seen in Figure 41 which summarizes all test data, a relatively high capture of 60% can be seen at a temperature of 270-275K and very low capture of 15-20% can be seen at as low as 245K.
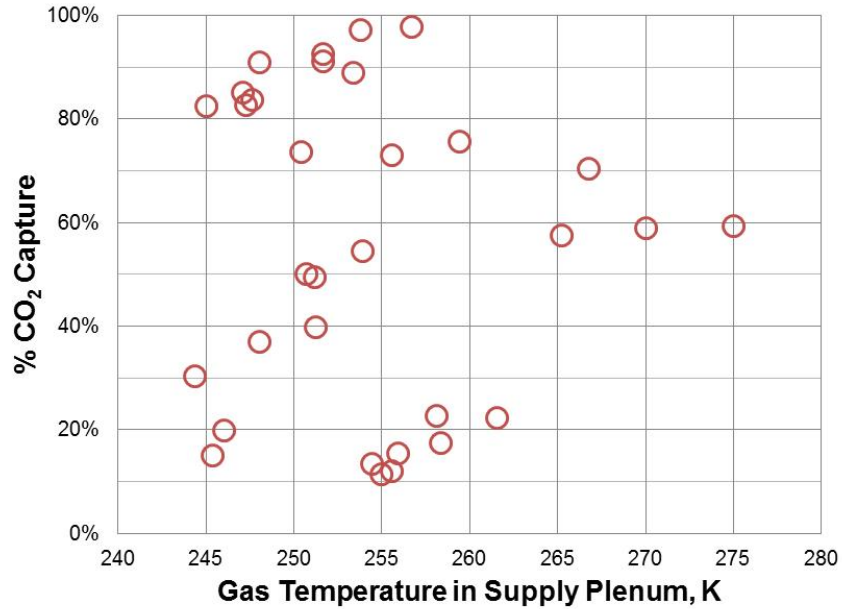
Figure 41 Bench Scale Test Results – percent CO_2 captured as a function of incoming temperature

In this test series it was observed that capture efficiency depends on the duration of the test run. There are several physical parameters which change with the time. One of the important parameters is test article back pressure which depends on vacuum sphere pressure which goes up as the sphere is filled with the flow. It was suggested that increasing back pressure may impact capture duct flow by pushing a shock wave from the capture duct into the diffuser duct culminating by capture duct unstart which was obtained in one of the early tests.

To check this hypothesis, in test series #130-134 schlieren visualization of the capture duct entrance flow was arranged. The expectation was that when back pressure will increase beyond a certain level, the shock wave sitting beneath the lip of the capture duct splitter will move upstream redistributing flow between diffuser and capture duct consequently diverting the CO_2 particles away from the capture duct.

Most of the runs in that test series were intentionally conducted at an elevated back pressure up to 3.2 psi but the expected phenomena did not occur. This can be concluded from both schlieren visualization (see Figure 6) where the shock position did not change and test data presented shown as a plot of capture% vs. sphere pressure (which closely follows capture duct pressure) shown in Figure 7.
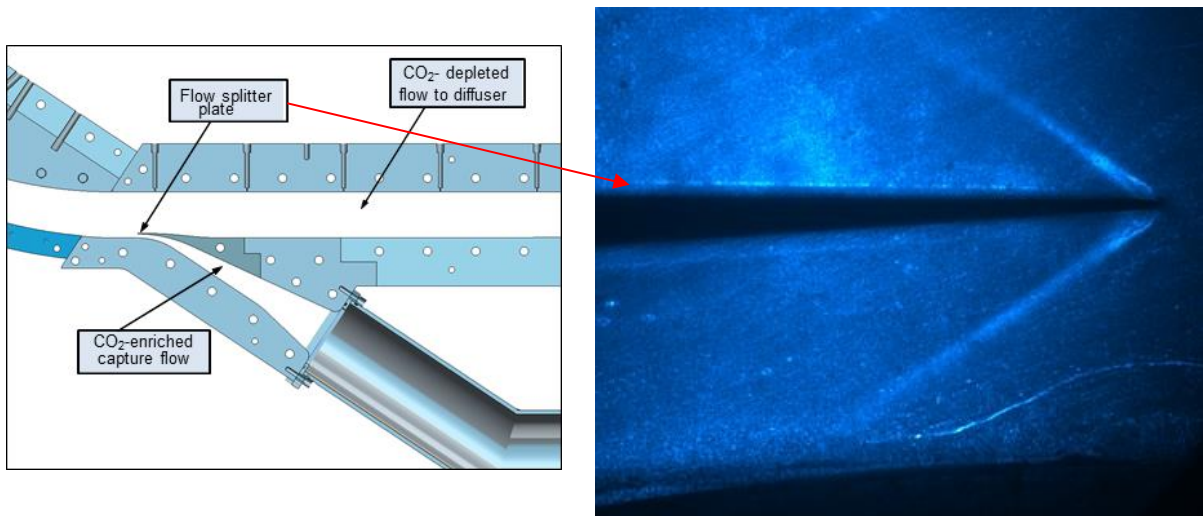
Figure 42 Capture duct configuration and Schlieren image of the splitter plate lip.
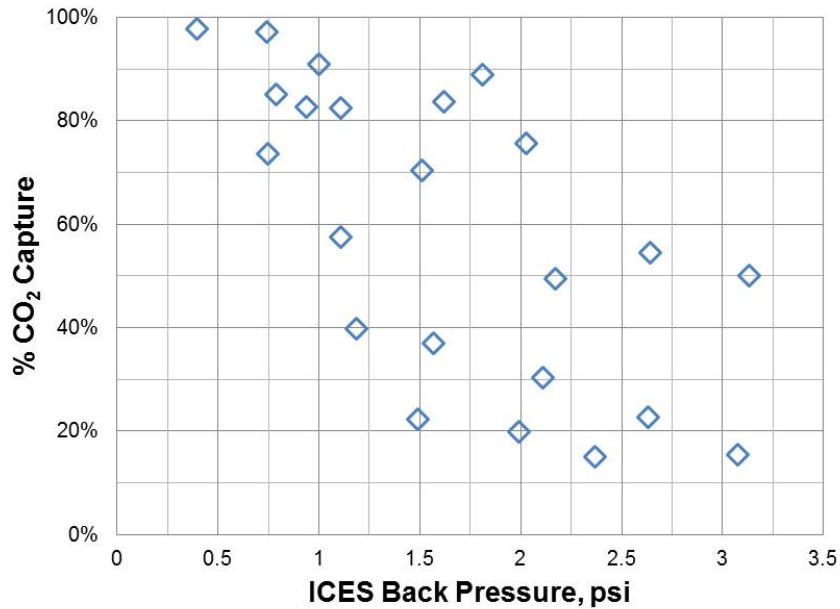
Figure 43 Bench Scale Test Results – percent CO_2 captured as a function of the back pressure.

Figure 43 does show some trend relating capture/back pressure to capture% – this, however, cannot be attributed only to the pressure change since pressure variation in time also influences other parameters such as the thermal environment in the ICES duct. Figure 44 summarizes results of the all significant tests in terms of capture efficiency versus ICES run time. This time is measured between CO_2 injection ON signal and the moment the diffuser flow sample is sent to the GC.
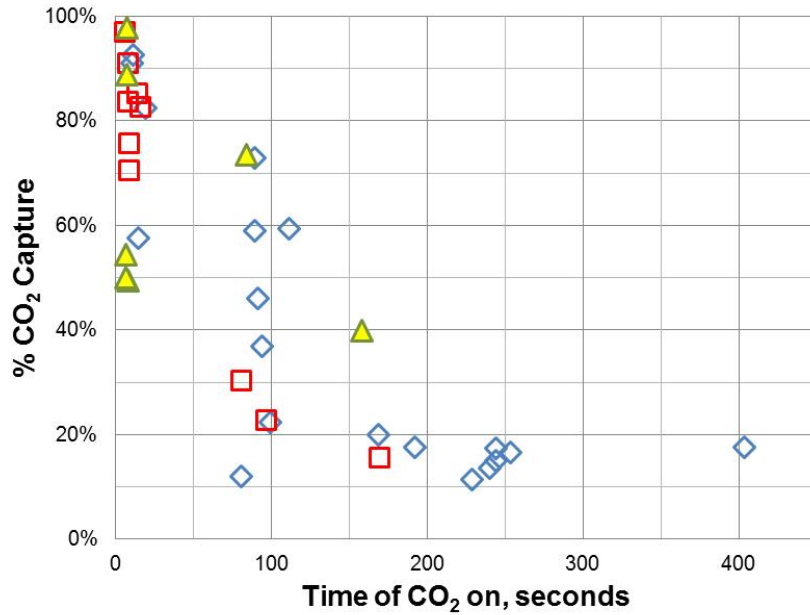
Figure 44 Bench Scale Test Results – percent CO_2 captured as a function of test run time.
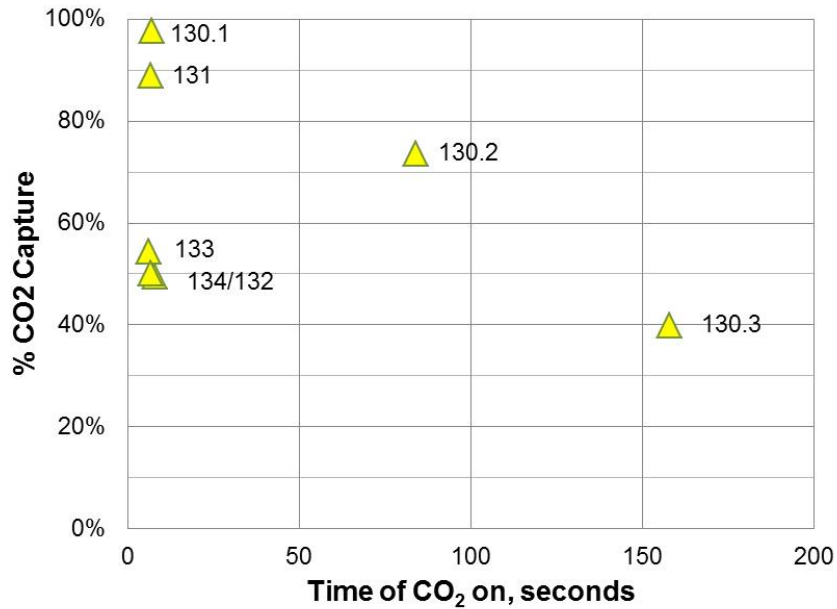
Figure 45 Bench Scale Test Results – percent CO_2 captured as a function of test run time.

The final test series (#130-134) was designed to check the time-dependence hypothesis. It consisted of five runs, one of which included three GC measurements shown in Figure 45 as 130.1, 130.2, and 130.3. In these runs, back pressure was low and very unlikely to be a factor affecting concentration change. In these tests, CO_2 concentration measured in the diffuser increased with time which reflected a decline of the CO_2 capture efficiency.

41

Table 4. Bench Scale Test Summary.

Parameter	Value
Number of CO_2 capture measurement	36
Highest observed capture efficiency	97.8%
Lowest observed capture efficiency	11.3%
Average observed capture efficiency	51.9%
Above 50% capture cases	19 of 36
Above 80% capture cases	10 of 36
Above 90% capture cases	4 of 36

1) Change in temperature of incoming flow and/or hardware. No consistent/repeatable correlation were found to support this explanation;

2) Accumulation of solid CO_2 particles in the piping post diffuser with further sublimation. No physical basis was found for this, not correlated to test time;

3) Impact of the growing backpressure in the capture duct in CO_2 flow distribution. Schlieren visualization specifically introduced to check this hypothesis in the Tests #130-134 revealed that shock position did not change with back pressure.

4) Cumulative measurement system error due to progressive air absorption in vacuum pump upstream of the GC. Current results were found consistent with this issue.

A final test series (#135 and 136 not shown in Table 4) conducted Dec 1, 2014 was intended for root cause investigation of CO_2 capture decrease with time. Significant instrumentation/test rig upgrades where implemented including:

- Modification of the laser visualization system to cross sectional view;
- Introduction of two heat guns pointed at visualization area in order to prevent window fogging;
- Cutting access doors in the diffuser duct downstream of capture duct and cleaning visualization area from inside;
- Introduction of liquid CO_2 flow meter in addition to bottle weight measurement before and after each test;
- Introduction of two real time optical non-dispersive infrared (NDIR) CO_2 sensors calibrated together with gas chromatograph.
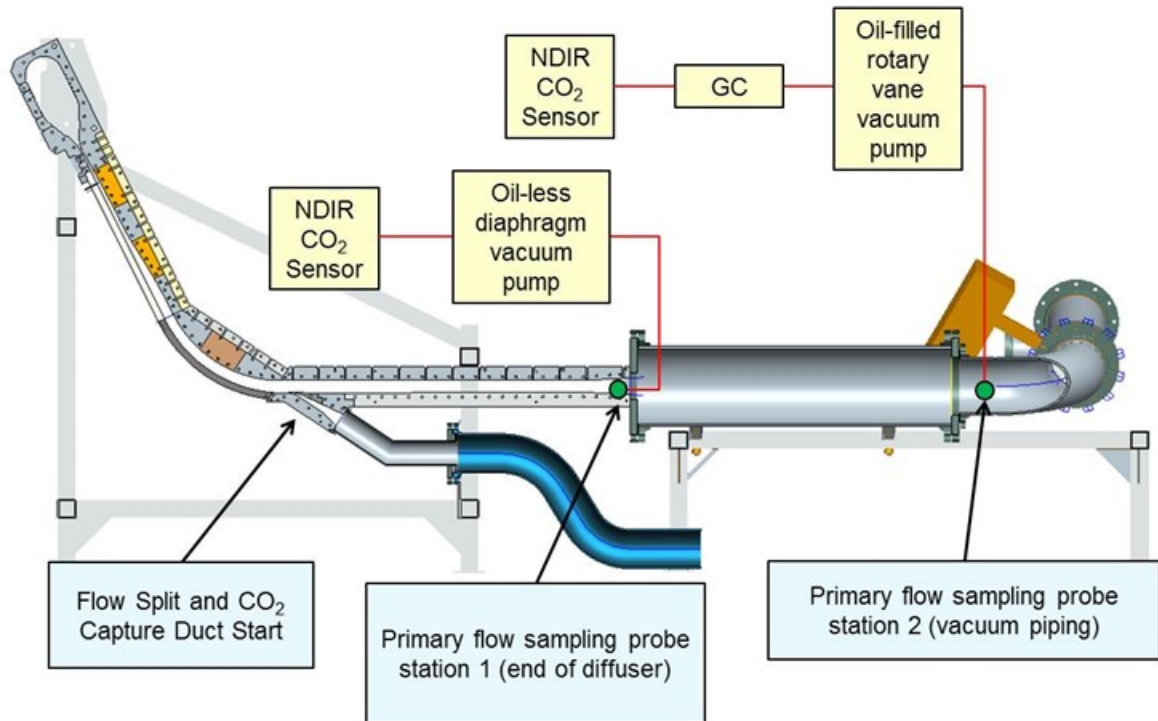
Figure 46 Gas sampling arrangement in the last test series.

Figure 46 shows gas sampling arrangement in Tests #135 and 136 where it is seen that both NDIR sensor and GC (Sample probe station 2) are fed by the oil-filled rotary vane vacuum pump whereas Sample probe 2 uses an oil-less vacuum pump. It was found that vacuum pump oil in Station 2 absorbs a small quantity of air thereby increasing CO_2 content. Flow rate of the sample is so small (air mass counts for 0.00055% of the oil mass) that microscopic amounts of air removal can impact measurement significantly.

In order to confirm this explanation a short experiment was conducted utilizing the GC to measure ambient room air CO_2 concentrations with and without the use of the Varian SD-451 rotary vane vacuum pump. The Varian <u>oil seal</u> rotary vane vacuum pump, which utilizes approximately one liter of mineral oil, was utilized consistently for extracting all of the low pressure sample gas, a mixture of air and CO_2, from the ICES diffuser and delivering the sample to the gas chromatographer (GC) at ambient atmospheric pressure. It is believed that as a result of the fundamental mode of operation of an oil seal vacuum pump, mainly the contact between the sample gas and the pump oil, it is possible for small amounts of air to be absorbed by the pump oil during sample extraction yielding erroneous results for the concentration of CO_2 measured by the gas chromatographer.

The experiment with ambient CO_2 concentration measurements <u>without</u> the Varian SD-451 pump yielded no significant changes as a function of time in the CO_2 measurement values taken with the GC several times over a period of approximately 200 seconds, at intervals of 40 seconds. The experiment was repeated with the Varian SD-451 placed upstream of the GC (in an identical set-up as that being used for sampling during ICES

tests) and the results are shown in Table 5. The data shows and increase in ambient CO$_2$ concentration level as a function of time elapsed from the time the vacuum pump was turned on; an increase of approximately 7.5% and 29% CO$_2$ level was measured at 10 and 65 seconds from the time of pump operation initiation (t=0 seconds), respectively. This trend of increasing CO$_2$ levels is similar to the previous ICES tests and thus confirmed suspicions regarding this issue.   The next phase of tests would be designed to mitigate this problem.

Table 5 Ambient CO$_2$ measurements with and without Varian SD-451 vacuum pump.

EVENT	Room Air	Room air
applies only to room air samples	CO2 %mole	% diff. increase
		from previous sample
Pump OFF	0.04775	
Pump ON sample taken after 10 seconds	0.05134	7.52%
PUMP ON sample 65 seconds after previous sample	0.06605	28.65%

In order to begin the process of resolving this pump contamination issue, two new oil-less vacuum pumps (as shown in Figure 47) were acquired and installed into the Orbital ATK test system.

Free Air Displacement cfm (l/min.) @60Hz	1.2(35)
Free Air Displacement m3/hr (l/min.) @50Hz	1.75(29)
Ultimate Pressure	2(2.7)
Maximum Vacuum	29.85
Motor Horsepower (watts)	1/5(150)
Adjustable Vac. / Gas Ballast	Yes
Tubing Needed	1/4(7)
Intake Thread NPT	M14(1/8)
Overall Dimensions LxWxH in. (cm)	13.8x6.8x8.8 (35.2x7.2x22.3)
Adjustable Vacuum	Knob

Figure 47 Welch Dry Fast Ultra 2042 vacuum pump
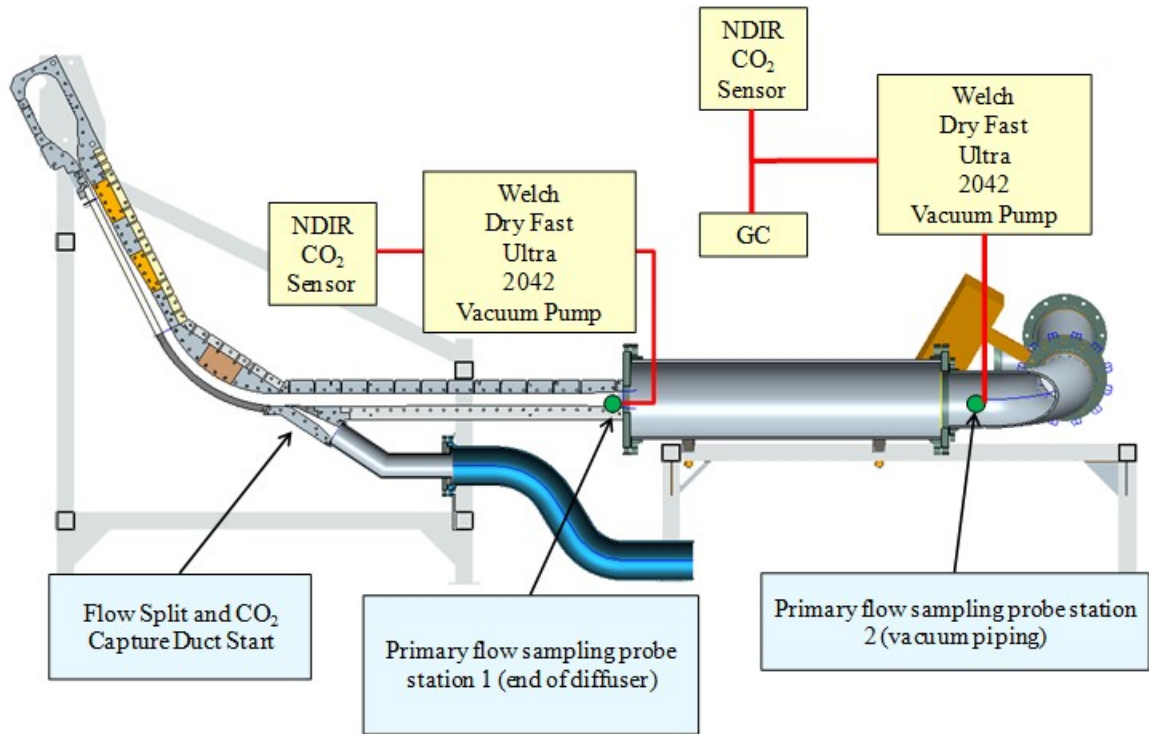
Figure 48 Orbital ATK test arrangement with new vacuum pumps

As shown in Figure 48, the Orbital ATK test setup was modified to include two gas measurement locations, one at the end of the diffuser section (Station 1), and one near the entrance of the 12" pipeline leading to the facility vacuum sphere (Station 2). A sample probe was installed at both of these locations and connected to the new vacuum pumps and a commercial NDIR CO_2 sensor. The downstream measurement was also connected in line with a gas chromatograph (GC). The NDIR sensors provide continuous data while the GC enables selected point measurements due to the ~30 sec time required to obtain a result.

Preliminary shakedown tests were carried out at conditions very close to the last test series ending with Test #134:
- Chamber Pressure: 30 psia
- Back Pressure: < 3 psia
- CO_2 Injectors: 6
- CO_2 Injection

Gas sampling approach was reworked to mitigate several sources of error including time lag, pump oil contamination. Also, in-situ sensors calibration was conducted. New test series was conducted with different amounts of LCO_2 injection in the plenum. Review of results indicate >50% capture of solid CO_2 in several tests. Figure 49 provides summary of these results which verify our goal of capturing >50% of the solid CO_2.

Test Number	% Solid CO_2 Capture
GS03a	62%
GS03b	81%
GS07	72%
GS08	76%

Figure 49 Summary of final results.

Design of CO_2 Seeding System

Since the OSU effort resulted in the conclusion that seeding the flow would be necessary to obtain particles able to migrate effectively, a design effort was undertake to modify the ICES test article to enable seed injection. Since testing with powder (vs. CO_2 or liquid seed) has the advantage of controlled particle size, hardware and associated test article modifications were designed for this purpose. Calculations were carried out based on using 3 micron talc injected at a mass flow of up to 1X the CO_2 mass flow rate (i.e. to simulate the equivalent CO_2 recirculation). In order to provide uniform particle distribution, an injection system with two ¼" OD tubes was developed as shown in Figure 50. Not shown in this figure for convenience are a series of metal screens that are installed in the ICES plenum to reduce the scale of the flow turbulence caused by the large feed holes as shown in Figure 51. These screens serve to support the new tubes which appear cantilevered in Figure 50.
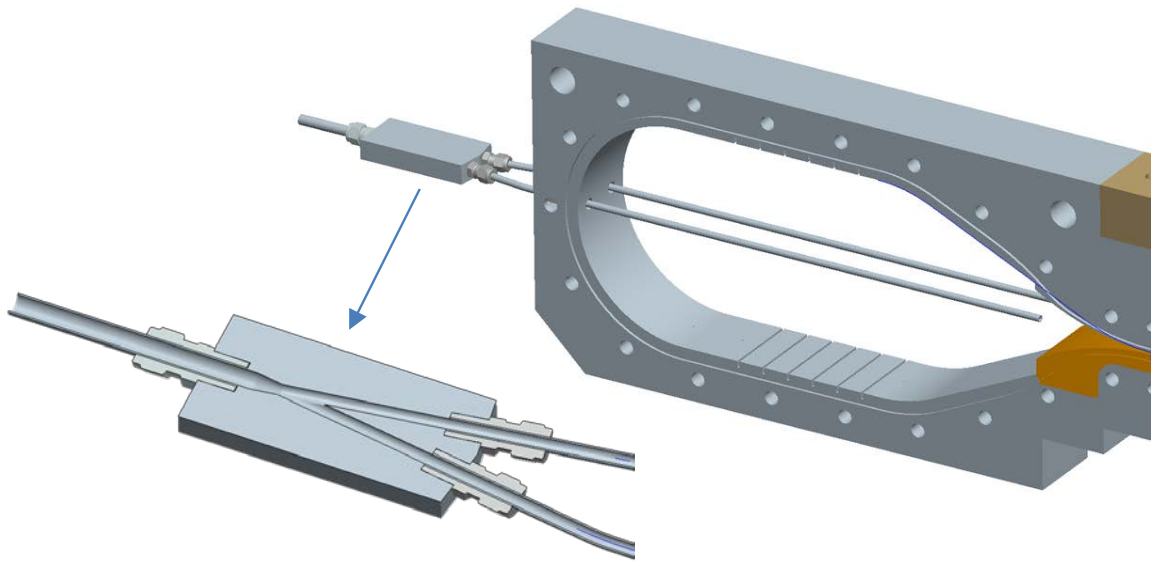
Figure 50 Powder seeder tubing in ICES plenum
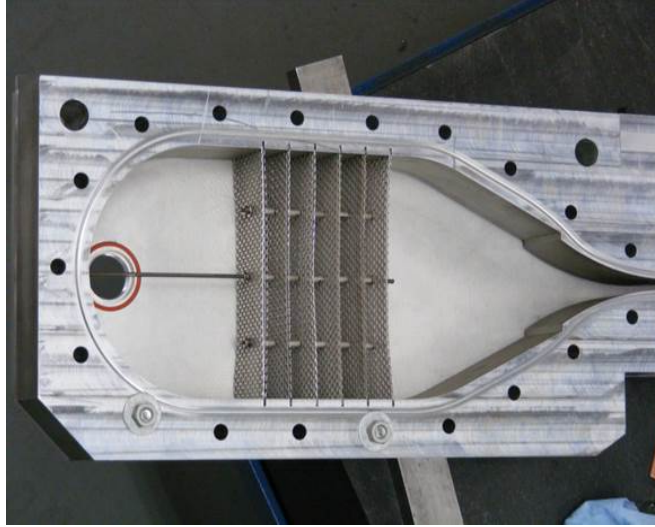
Figure 51 Current ICES plenum showing turbulence-reducing screens

The powder delivery system shown schematically in Figure 52 consists of a powder screw feeder and a gas eductor (or ejector) pump. Air is injected at relatively high pressure into the motive port of the eductor. An internal nozzle accelerates the flow to supersonic speeds, resulting in low suction pressure on the port connected to the powder feed which "doses" the powder at a controlled flow rate. The air and powder mix and flow through the discharge port which connects to the flow splitter shown in Figure 50. As seen in Figure 53, both of these items are commercial products that, with some minor customization/modification were intended to be adapted to the current purpose.

Construction and testing of this system was deferred after updated system thermodynamic analyses (reported in the next section) resulted in a redirection to partial subsonic condensation of CO$_2$ as the "in-situ" seeding mechanism.
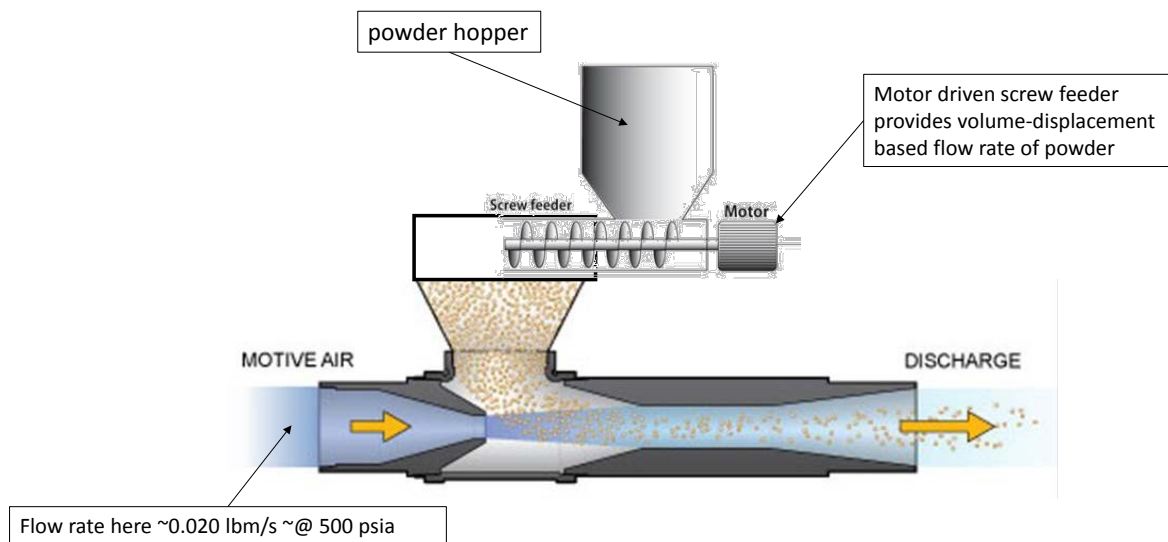
Figure 52 Powder seeder system schematic
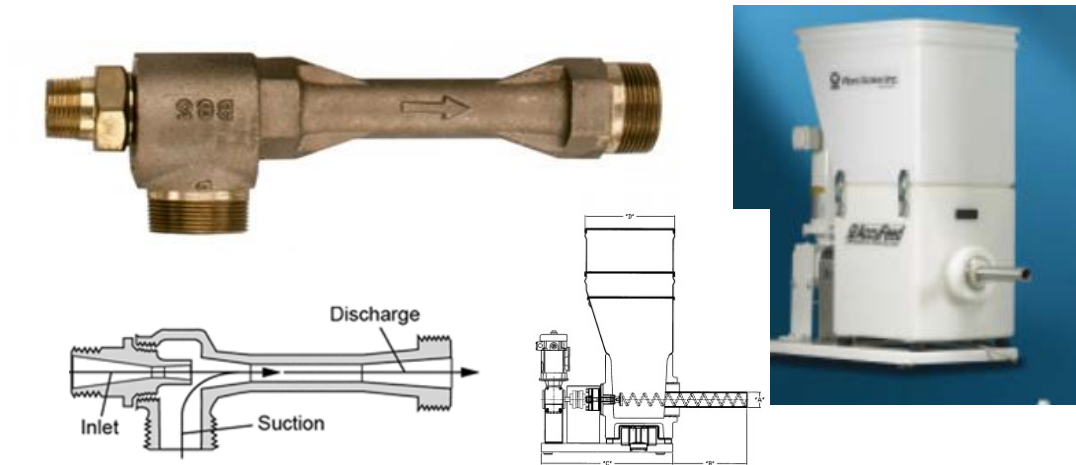
Figure 53 Commercial components for powder seeder

3.1.4 Thermodynamic Modeling

At this stage of the project, attention was focused on thermodynamic modeling in collaboration with project partner EPRI.   Below is excerpt from an interim EPRI technical report which provides a good summary of the initial effort:

> The Electric Power Research Institute (EPRI) has created a suite of tools for modeling the thermodynamic behavior of flue gas accelerated to supersonic speeds through a converging diverging nozzle, removal of the precipitated solids, and subsequently slowed down in a diffuser section. These modeling tools were used to provide an initial calculation of the thermodynamic impact of the solidification and separation of solid CO$_2$ in the ICES process. This model does not incorporate fluid flow calculations, solids separation calculations, kinetics, particle growth or particle size impacts but instead focuses on the equilibrium state of the flue gas with CO$_2$ as it undergoes acceleration, phase transition, solids removal, and deceleration with and without recirculated solid CO$_2$ particles. The results presented show the optimal theoretical results, and actual operation will have additional losses not accounted for in this model.
>
> The model for CO$_2$ capture requires an understanding of CO$_2$ behavior at the temperature and pressures of interest for this system. While many equations of state for CO$_2$ have been developed, these tend to be focused on gaseous and liquid CO$_2$, with little study given to solid CO$_2$ properties. For the operation of the ICES process, solidification of CO$_2$ is required, so understanding the phase behavior, heats of sublimation, saturation temperatures, densities, and other properties are necessary to understand the performance in this process. The equation of state that we implemented is an extended Peng-Robinson equation of state that is applicable for solid / gaseous CO$_2$ properties below the triple point temperature of -216.6 K [Martynov Sergey, Solomon Brown, and Haroun Mahgerefteh. *An Extended Peng-Robinson Equation of State for Carbon Dioxide Solid-Vapor Equilibrium.* Greenhouse Gases: Science and Technology 3.2(2013):136-47.].
>
> The implementation of the equation of state included calculating the full thermodynamic state of pure CO$_2$ (pressure, temperature, density, enthalpy, entropy, phase composition) from any two of the listed properties. These calculations were used in conjunction with NIST developed Refprop software [NIST Standard Reference Database 23: NIST Reference Fluid Thermodynamic and Transport Properties Database (REFPROP): Version 9.1] for fluid property calculations to calculate the thermo-properties of the gas mixture above the triple point of CO$_2$ and the non-CO$_2$ components below the triple point of CO$_2$. For mixed gas properties below the triple point, pure CO$_2$ properties were first calculated at the temperature and partial pressure of interest, and non-CO$_2$ gas properties were calculated through REFPROP. These results for the gaseous CO$_2$ properties and non-CO$_2$ mixed gas properties were combined using linear combining rules to calculate the gas-phase properties.

Simulation of the steady state Inertial CO$_2$ Extraction System (ICES) was undertaken using a solver developed in Matlab. This simulation assumes steady flow and uses velocity as the prime variable that changes along the length of the reactor. Instead of focusing on area, flow dynamics, separation, friction, turbulence, particle growth and particle migration towards the capture duct, this model assumes frictionless flow, equilibrium thermodynamics, and a perfectly designed reactor module. The main equations used to calculate the flow through the accelerating and decelerating portions of the flow are the conservation of mass equation, momentum equation, and conservation of energy equation. The gas and solid CO$_2$ particles are taken to be a single stream at the same velocity and in thermodynamic equilibrium with the density of two phase mixture. Solids separation is modeled by removing a specified portion of the precipitated CO$_2$ as well as a portion of the gaseous stream. For the results shown in this report, we assume ideal separation with 100% of the solid product removed with no slipstream gas removed in the capture duct.

In the simulations run for this study, the maximum velocity attained was calculated as the point at which the target percentage of the inlet gaseous CO$_2$ was captured. For the runs presented below, this threshold was 90% of the inlet CO$_2$, not counting the CO$_2$ used for the recycle. The inlet plenum was assumed to have 0 velocity, as was the diffuser outlet. The CO$_2$ recycle calculations were based on the premise that a certain quantity of solid CO$_2$ (measured in moles of solid CO$_2$ per moles of flue gas) was injected into the gas stream. While all of the gas-phase kinetics were assumed to be instantaneous, we assume that the solid-phase kinetics are slow with no CO$_2$ sublimation into the gas phase. The temperature of the solid particles was taken to be the saturation temperature at the partial pressure of CO$_2$ present in the gas stream to maintain the phase equilibrium between the gaseous and solid components.

We performed several verification tests for the developed models, including running simulations of pure N$_2$, a non-condensing species, and comparing the results to isentropic supersonic flow calculations (Figure 1). We similarly compared the effect of nitrogen + heat addition using the heat addition profile from the condensing CO$_2$ case compared to the Rayleigh flow calculations using the same heat addition, velocity, pressure, and temperature profiles and found excellent agreement. The results from the heat addition, however showed a significant decrease in the stagnation pressure of the overall system.

The results from the simulation using the flue gas containing CO$_2$ and allowing for CO$_2$ precipitation but without CO$_2$ recycle are shown in Figure 2. This shows the effect of the inlet temperature and pressure into the reactor on the discharge pressure from the system after capture of 90% of the CO$_2$ from an initial mixture of 14% CO$_2$, 86% N$_2$ simulated flue gas. In order to achieve atmospheric discharge, the initial conditions have to be approximately 4 bar inlet at 200 K, 6 bar inlet at 250 K. Atmospheric discharge is also possible with 10 bar inlet and temperatures above 300K.
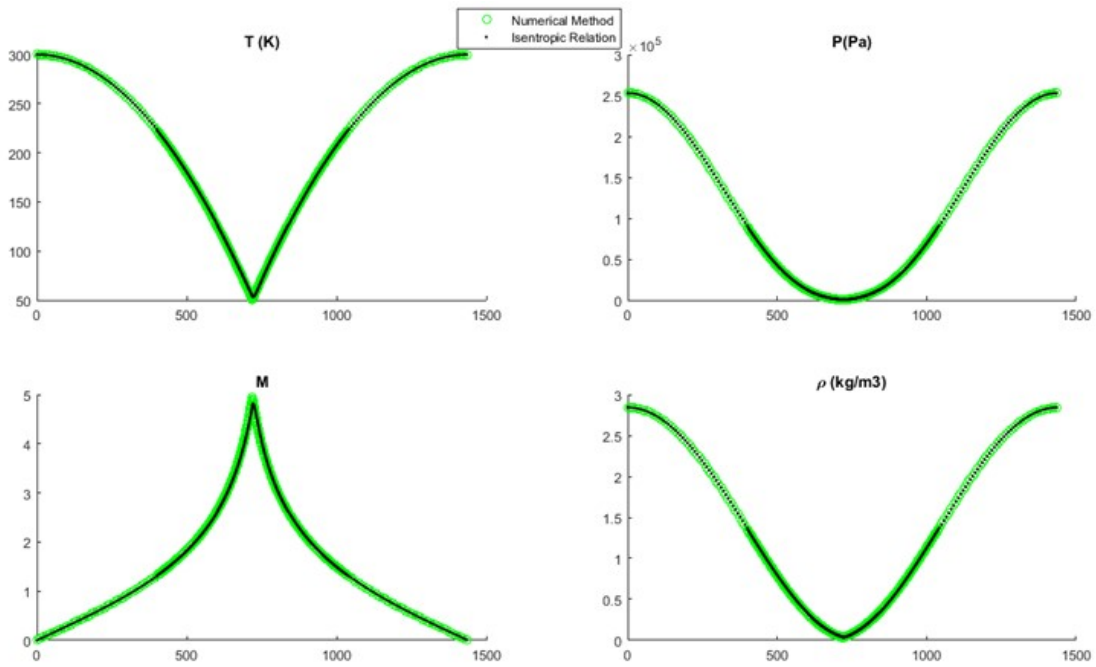
Figure 54: Numerical vs isentropic model verification for N$_2$
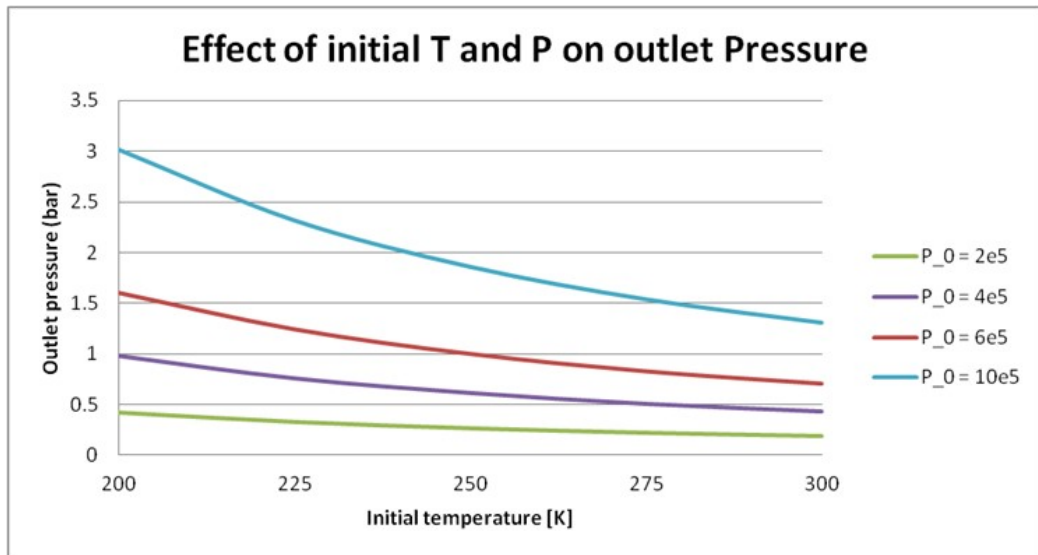
Figure 55 Effect of initial temperature and pressure on diffuser outlet pressure. Outlet pressure > 1 bar required for atmospheric discharge.

The effect of CO$_2$ recycle is to reduce the pressure recovery. For the same conditions and assumptions as above, figure 3 shows the effect of a 10% recycle rate. Atmospheric discharge now requires 6 bar, 210 K or 10 bar, 270 K inlet conditions.
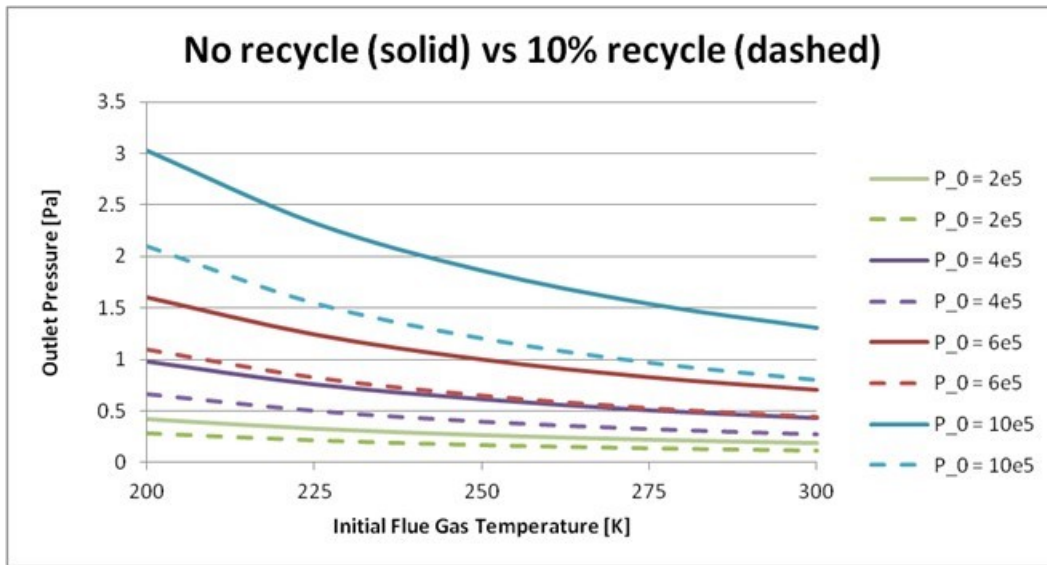
Figure 56 Effect of CO_2 recycle rate and initial temperature and pressure on diffuser outlet pressure. Outlet pressure > 1 bar required for atmospheric discharge.

After initial discussions with EPRI regarding the analysis above, the ACEnT Labs quasi-1D (Q1D) analysis tool was updated to incorporate the new EPRI state model for solid CO_2 below the triple point. The tool was then quickly checked against the EPRI results with very good correlation, despite using a different solution scheme. Using the ACEnT code, plots of the CO_2-depleted stream exhaust pressure vs. incoming temperature for several system feed pressures are presented in Figure 57 and Figure 58 for cases with and without external seeding of the flow with solid CO_2.
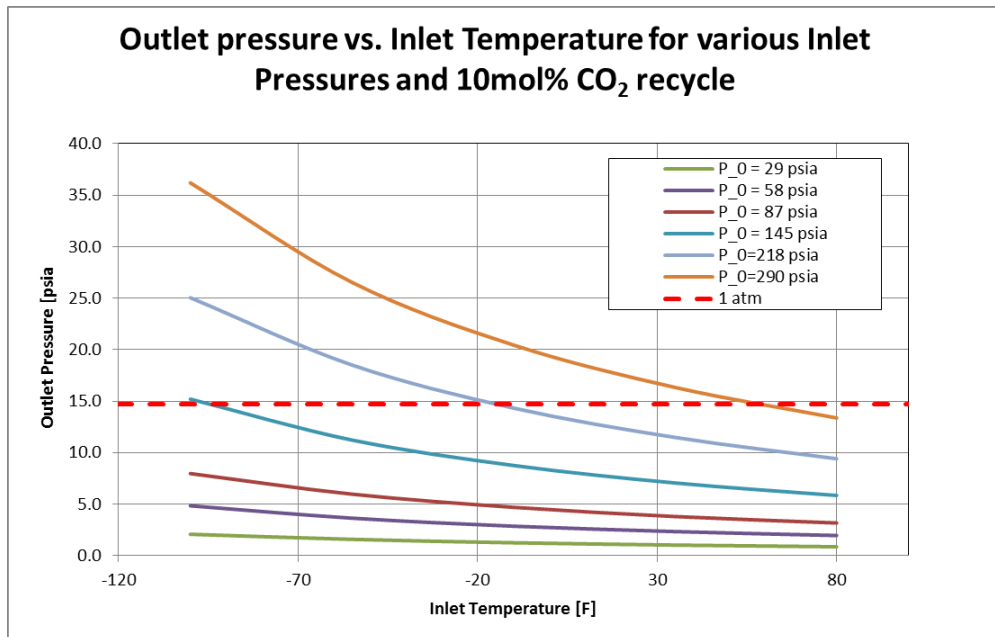
Figure 57 ICES Pressure recovery assuming 10mol% CO_2 seeding
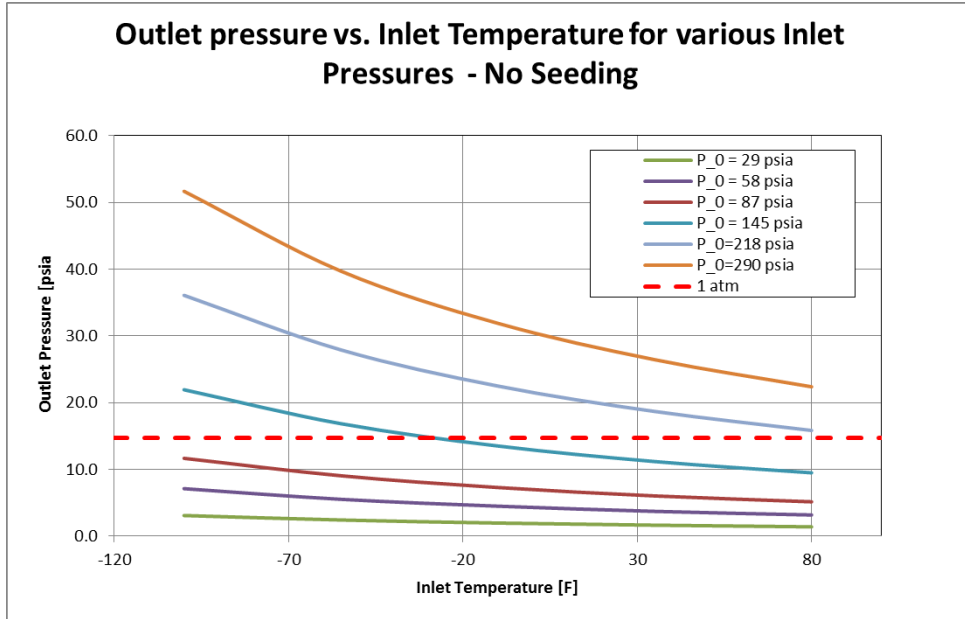
Figure 58 ICES Pressure recovery assuming no seeding

Translating the above into pre-compression requirements results in the compression ratio plot shown in Figure 59. The net result was that we were now predicting the need for compression ratios in the range of 10-15 instead of approximately 2.5 as previously thought. This prompted a re-look at the system integration to identify means to reduce overall pressure drop.
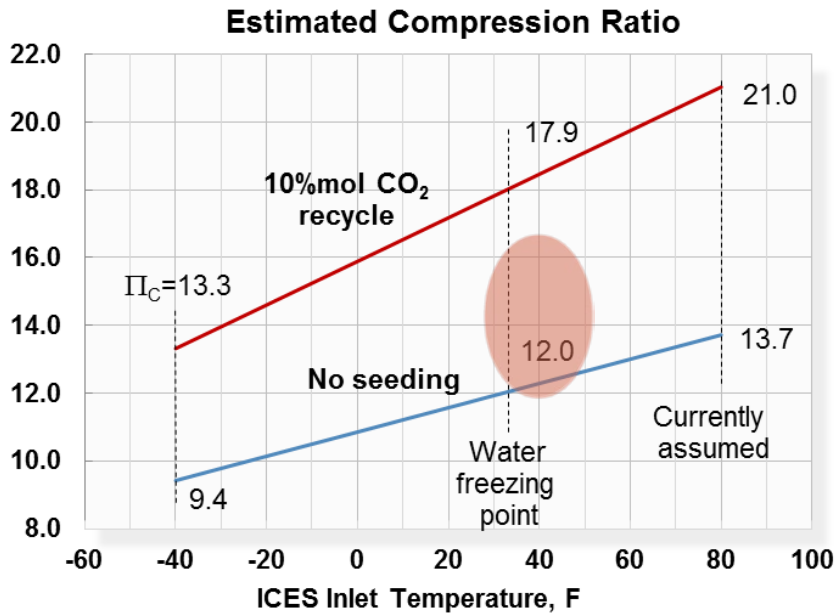
Figure 59 ICES Derived upstream compression ratio requirements

The most attractive and promising method to reduce compression requirements was deemed to be lowering the temperature of the incoming flue gas by heat exchange with

the captured solid CO_2.

In the process of developing a new integrated thermodynamic model for the complete system, another challenge was uncovered. Since the CO_2 leaving the ICES nozzle is flowing at supersonic speed, a significant portion of its total enthalpy is in the form of kinetic energy due to high velocity ($V^2/2$). As this captured stream is decelerated toward the subsonic cyclone (used to separate the slip stream from the solids), the kinetic energy is converted to heat and a portion of the CO_2 will evaporate.

One conceptual means to address this would be to include an impulse turbine that would theoretically convert a portion of the kinetic energy to external shaft work as shown in Figure 60, however the speeds and mixed phase nature of the flow make this solution not currently practical.
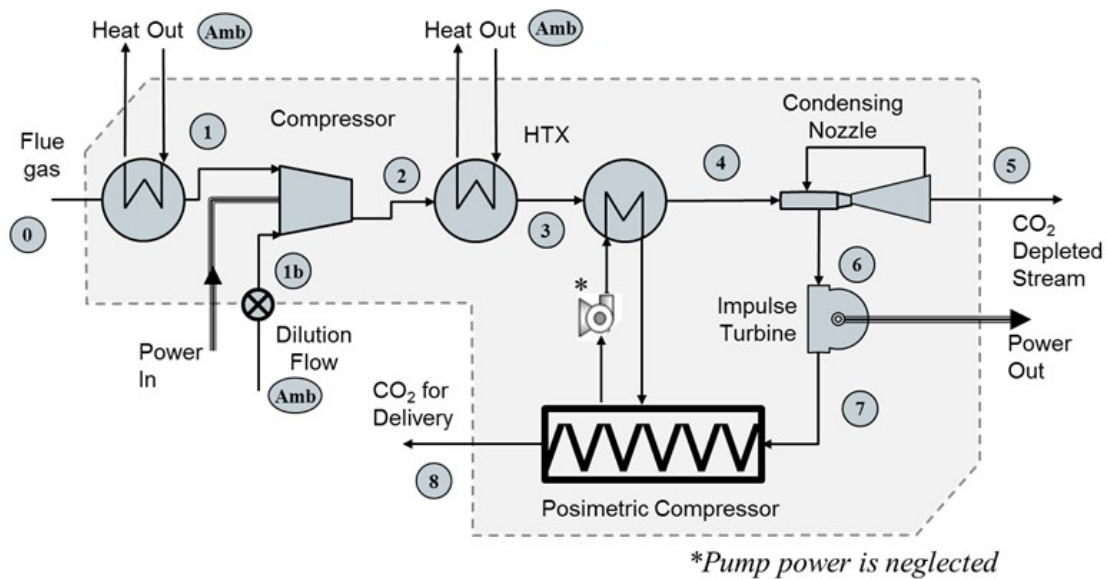
Figure 60   ICES System with Precooling Loop and Impulse Turbine

Another version was then developed (in collaboration with EPRI) wherein the evaporated CO_2 stream is recirculated and recompressed as shown in Figure 61, which also includes a brief description of each component.
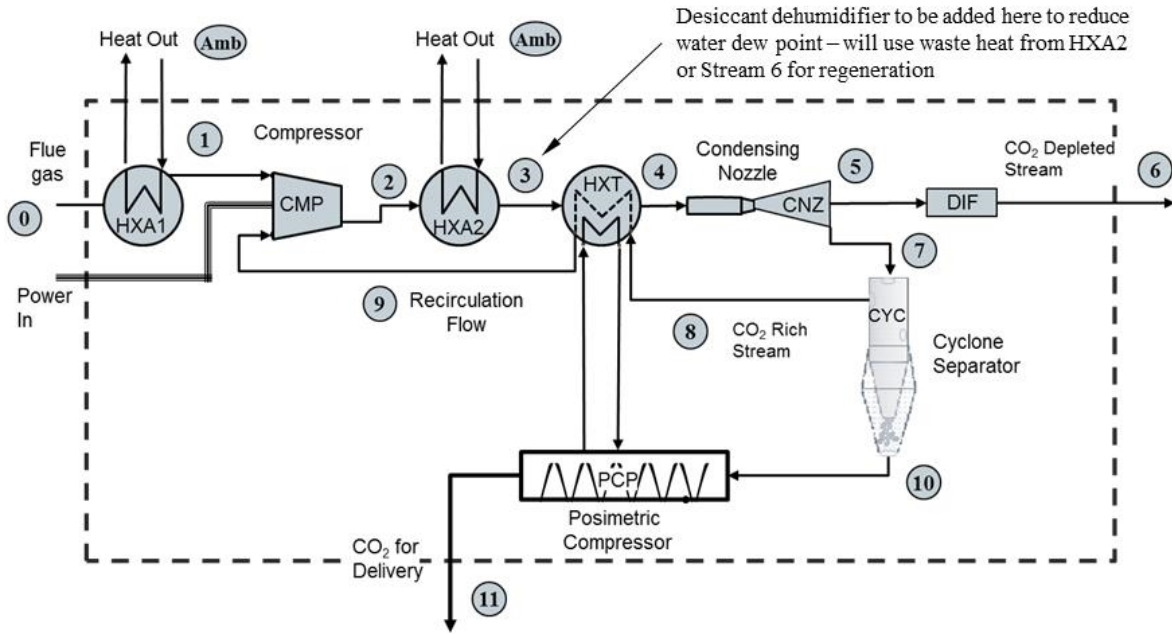
NAME	COMPONENT	DESCRIPTION
HXA1	Ambient Heat Exchanger 1	Cool flue gas to ambient temperature
CMP	Main Compressor	Compress flue gas for processing
HXA2	Ambient Heat Exchanger 1	Cool compressed gas to ambient temperature
HXT	Sub-Cooling Heat Exchanger	Cool to sub-ambient temperatures using heat sink from captured streams
CNZ	Condensing Nozzle	Condensing nozzle for CO_2 separation
CYC	Cyclone Separator	Captured flow separation into two streams: Dry ice and CO_2-rich gas
DIF	Supersonic Diffuser	Diffuse flow for exhaust to ambient
PCP	Posimetric Compressor	Constant volume phase change-based compressor

Figure 61 Updated Operating Schematic with Evaporated CO_2 recirculation

Finally, after additional optimization, the team arrived at the system schematic shown in Figure 62 which highlights the key changes from the original ICES system.
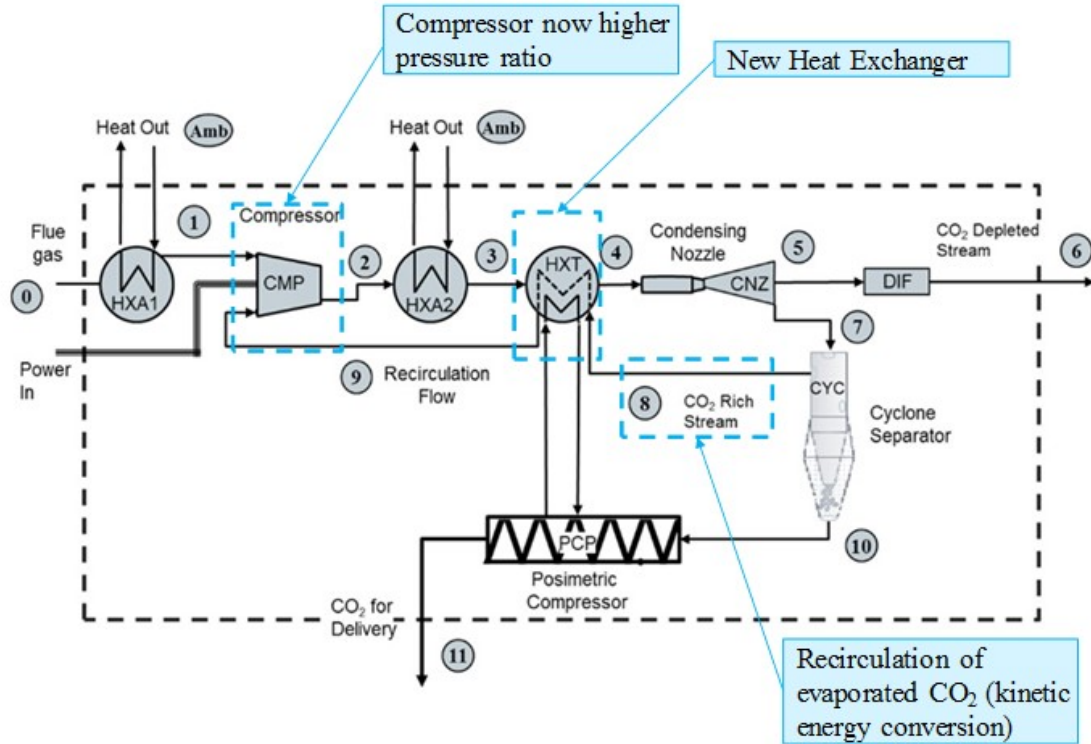
Figure 62 Final ICES System Schematic

A stream table for the final system is presented in Table 6.

Table 6 Final ICES Stream Table

	Compressor			Condensation Onset			CO2 Capture Plane				Cyclone		Recirc Gas	
PR	Recirc Gas	P exit	ΔT sat	CO2 pPress	M start	Velocity	CO2 Cond.	g / glnf	Tsat		ICE	EVAP	% Cap	% CO2
	kg/kg_0	MPa	C	MPa		m/s	rel to plane	rel to flue gas	C					
9.96	12%	1.009	6	0.19	0.51	664	90.4%	90.0%	137.6		74%	26%	5.0%	64%

Station Number		0	1	2	3	4	5	6	7	8	9	10	11
Mass Flow	kg/kg_0	1.000	1.000	1.120	1.120	1.120	0.792	0.792	0.328	0.126	0.126	0.202	0.202
Gas Specie													
Nitrogen	mols	0.8053	0.7729	0.7729	0.7729	0.7729	0.9342	0.9342	0.9342	0.4510	0.4510	0.00	0.00
Argon	mols	0.0096	0.009	0.0092	0.0092	0.0092	0.0111	0.0111	0.0111	0.0054	0.0054	0.00	0.00
Oxygen	mols	0.0280	0.027	0.0269	0.0269	0.0269	0.0325	0.0325	0.0325	0.0157	0.0157	0.00	0.00
CO2	mols	0.1571	0.191	0.1910	0.1910	0.1910	0.0222	0.0222	0.0222	0.5279	0.5279	0.00	0.00
water	mols	0.000	0.000	0.000	0.000	0.000	0.000	0.0000	0.0000	0.0000	0.0000	0.00	0.00
Solid CO2	mols	0.000	0.000	0.000	0.000	0.000	0.000	0.000	0.243	0.000	0.000	1.00	1.00
State													
TT	C	57	20	306	20	-65	81	81		-76	15	-76	20
PT	Mpa	0.101	0.101	1.009	1.009	1.009	0.131	0.101	0.128	0.125	0.112	0.125	15.10
RHOT	kg/m3	1.14	1.30	6.54	13.08	18.88	1.27	0.98		2.819	1.870		
HT	kJ/kg	742	693	984	690	606	818	818		512	592.3	-205.8	235.7
ST	kJ/kg-K	4.08	3.91	3.99	3.29	2.95	4.28	4.35		2.99	3.33		1.05
TT	°	135	68	582	68	-84	179	178		-106	59	-106	68
PT	psia	14.7	14.7	146.4	146.4	146.4	19.0	14.7	18.6	18.1	17.7	18.1	2190.1
RHOT	BTU/lb	0.071	0.081	0.408	0.817	1.179	0.079	0.061		0.176	0.117		
HT	lb/ft3	319	298	423	297	260	352	352		220	255	-89	101

Another key benefit of pre-cooling the flue gas is the ability to condense a small portion of the CO$_2$ (and trace water) to produce in-situ seeding without the need to recirculate solid CO$_2$. This is a very valuable side benefit to the pre-cooled approach since the updated thermodynamic models showed that injecting and accelerating additional mass to high speed was yet another penalty that increased compression requirements (see

comparison of Figure 57 and Figure 58)

3.1.5 Subsonic ICES Testing

Subsonic/transonic condensation is known to promote large (micron scale) particles due to particle collisions caused by non-monodisperse particles and longer residence time.

In order to confirm large particle formation resulting from subsonic/transonic condensation, a subsonic ICES test article intended to permit visualization of subsonic condensation was conceptualized in the region immediately upstream of the nozzle throat as shown in Figure 63. It consists of a transparent 1.25 in ID quartz tube with a plastic, 3-D printed solid centerbody that forms an annular flow path whose smallest cross-section is defined by the throat. The flow proceeds from left to right then up and through a T-section of duct as shown in the upper right hand corner of the figure.
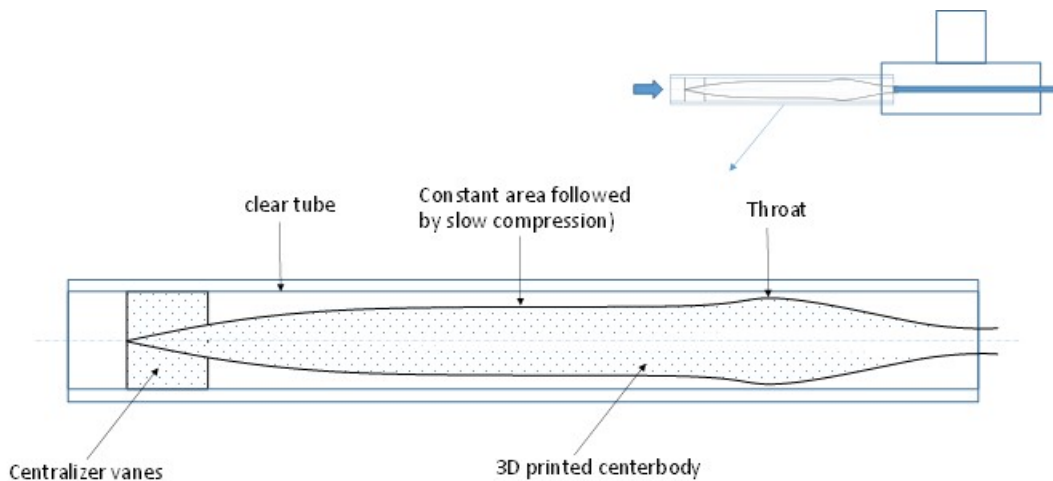
Figure 63 Conceptual Subsonic ICES Test Article

After the conceptual subsonic ICES design was completed, CFD analysis was performed to determine critical test article geometries. The objective of the analysis was to assess two different configurations in which the center bodies had 0.919 in and 0.988 in outer diameter sections. The different cross sectional areas were designed to produce Mach 0.5 and 0.7 "incubators" for condensation and agglomeration. Figure 64 through Figure 68 show results from the test article CFD analysis which supported the prediction of temperatures cold enough for condensation given the expected boundary layer growth. Based on these results, the test article design with the 0.988 sq.in. constant area section was selected for fabrication due to colder temperatures resulting in better/more condensation.
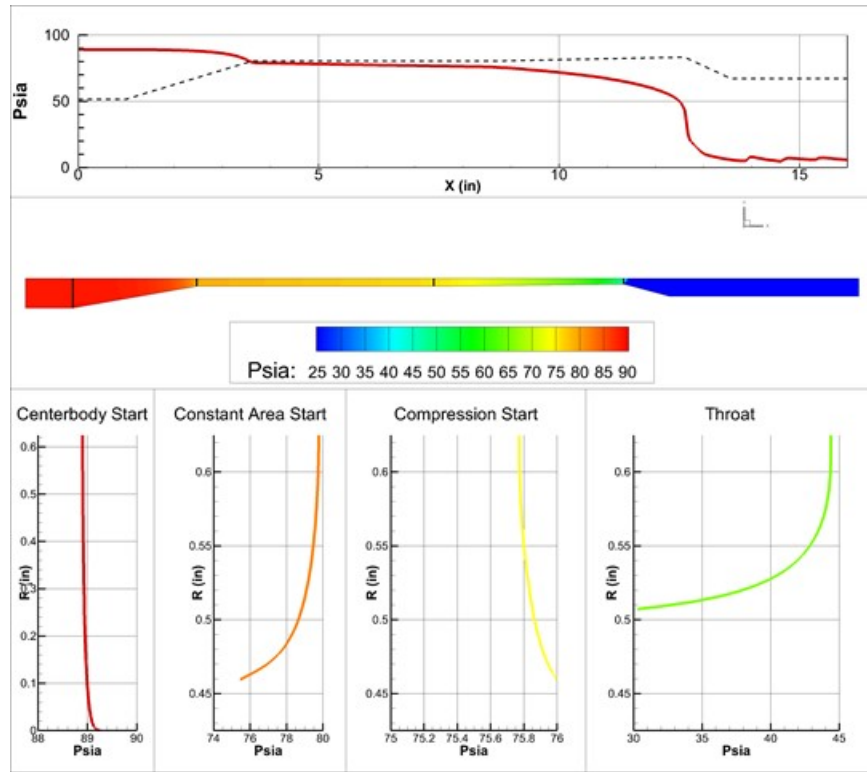
Figure 64 CFD Results for 0.919 OD Centerbody - Pressure
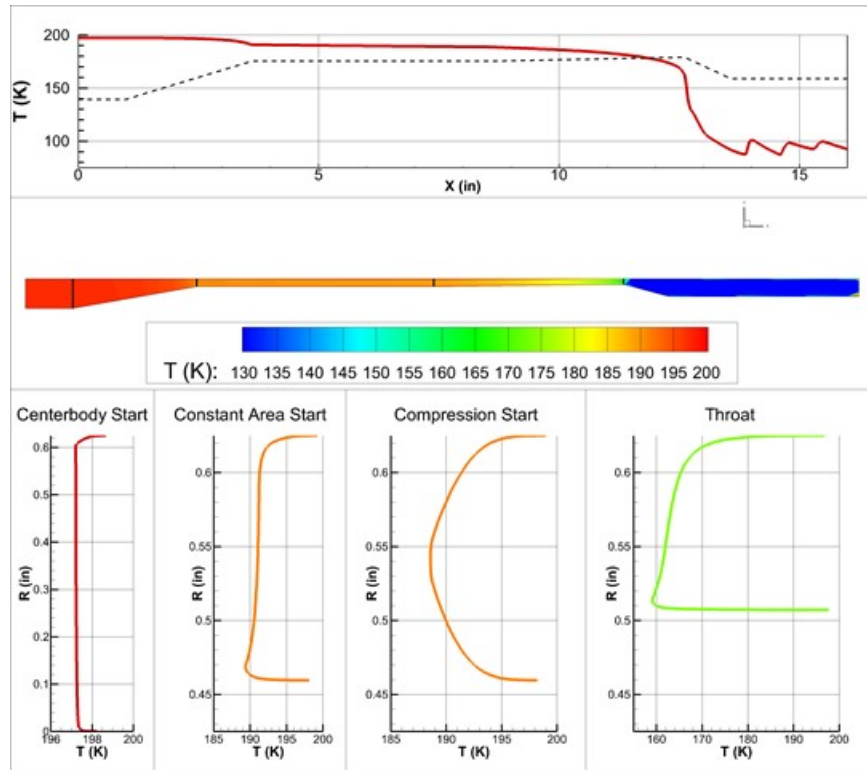
Figure 65 CFD Results for 0.919 OD Centerbody - Temperature
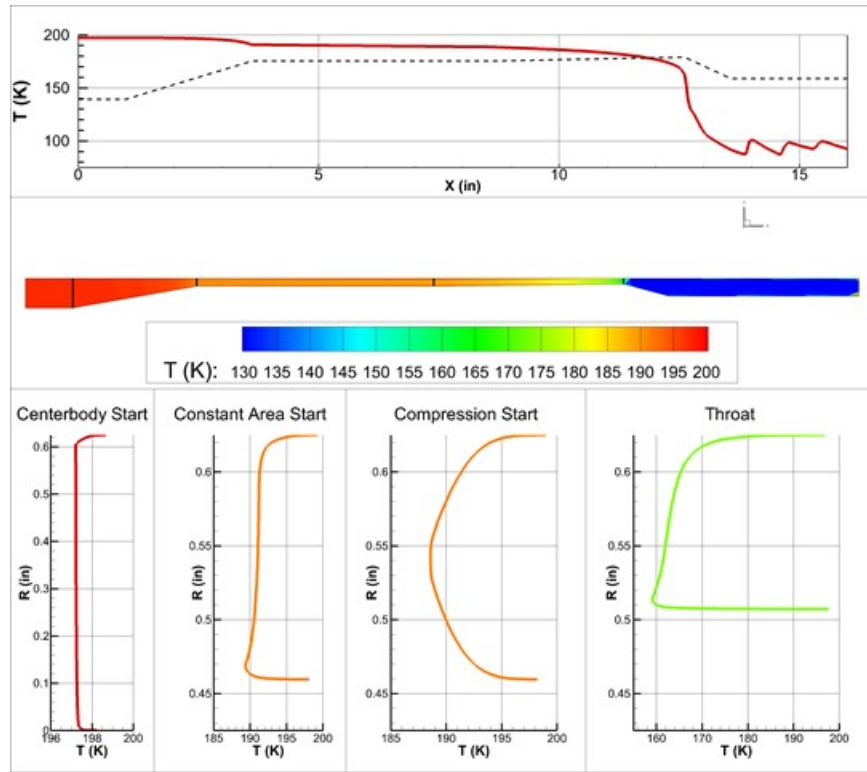
Figure 66 CFD Results for 0.919 OD Centerbody – Mach Number
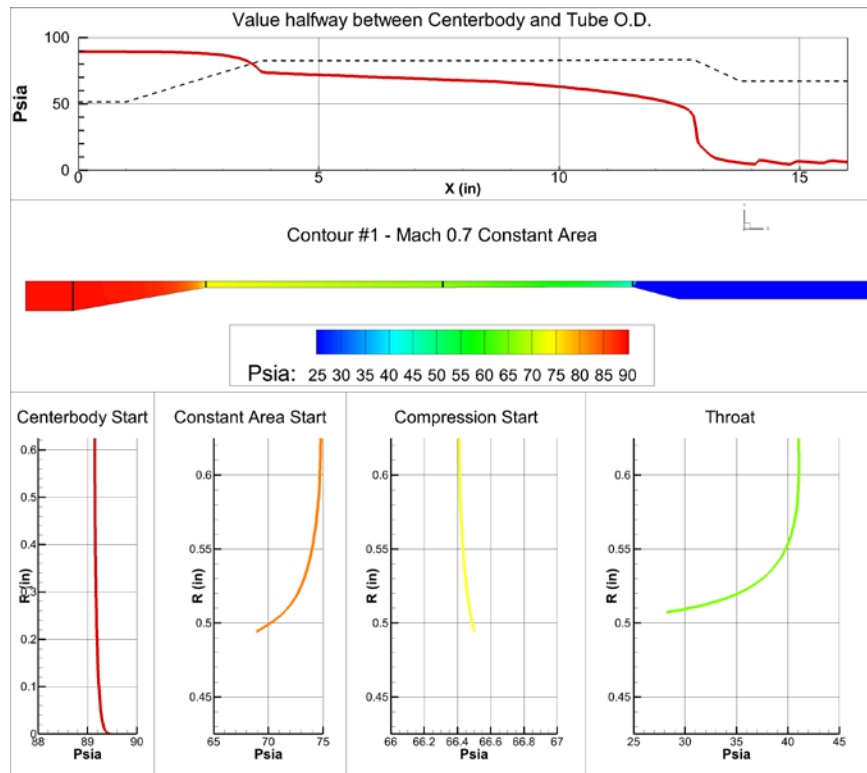
Figure 5.3.7: CFD Results for 0.988 OD Centerbody - Pressure
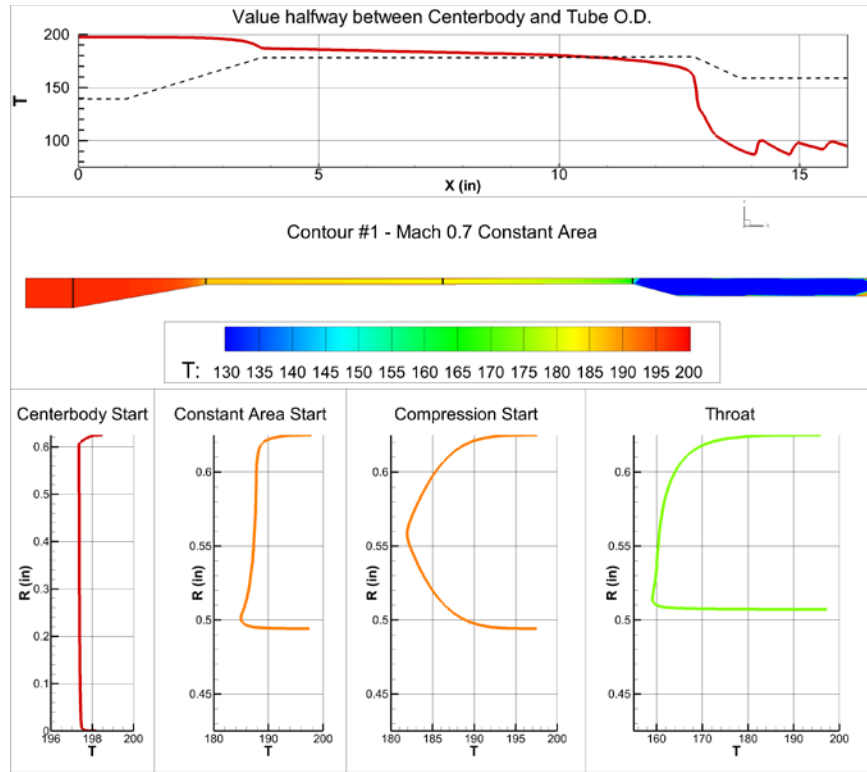
Figure 67 : CFD Results for 0.988 OD Centerbody - Temperature
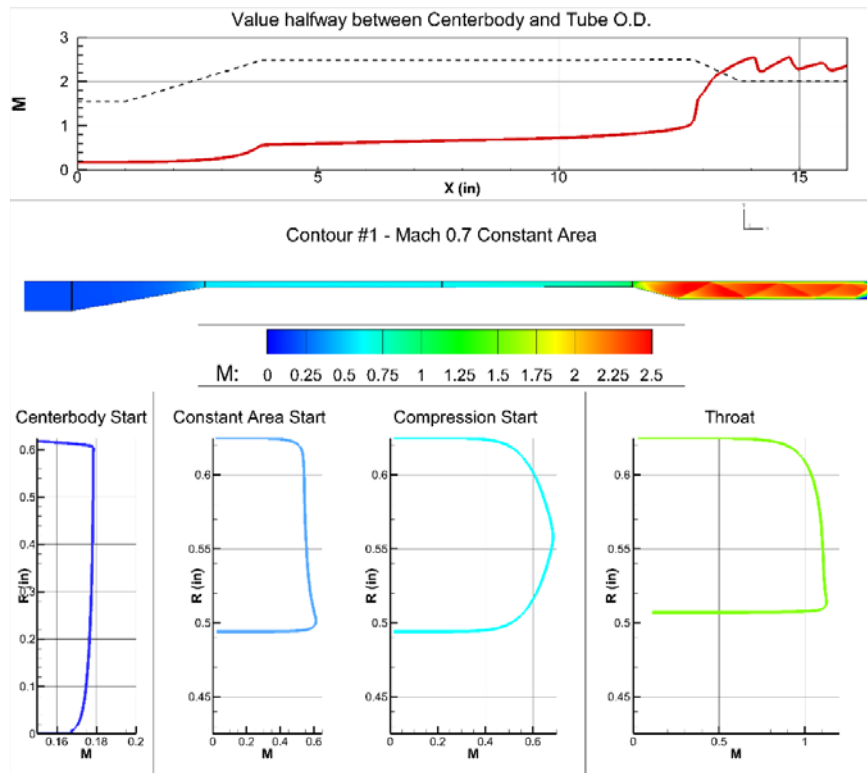
Figure 68 CFD Results for 0.988 OD Centerbody – Mach Number

With CFD analysis complete, detail design of the test article commenced. Rendering of the solid 3D model are shown in Figure 69 through Figure 71. Flow in these images is from right to left and then down the exhaust duct.
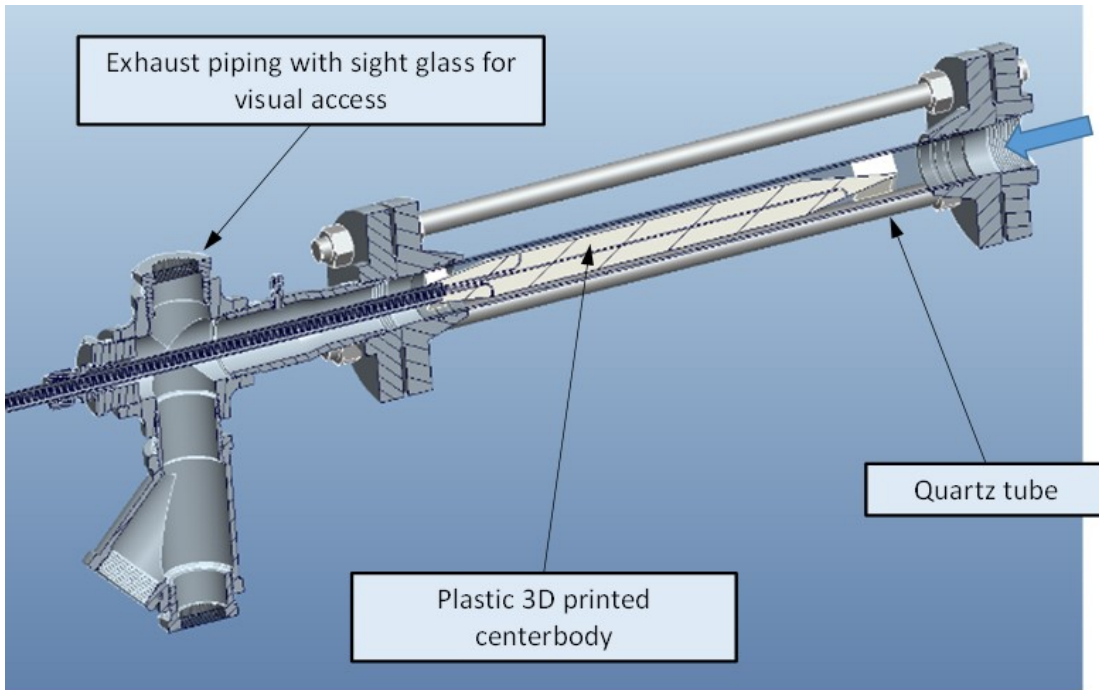
Figure 69: Subsonic ICES Test Article Assembly Key Components
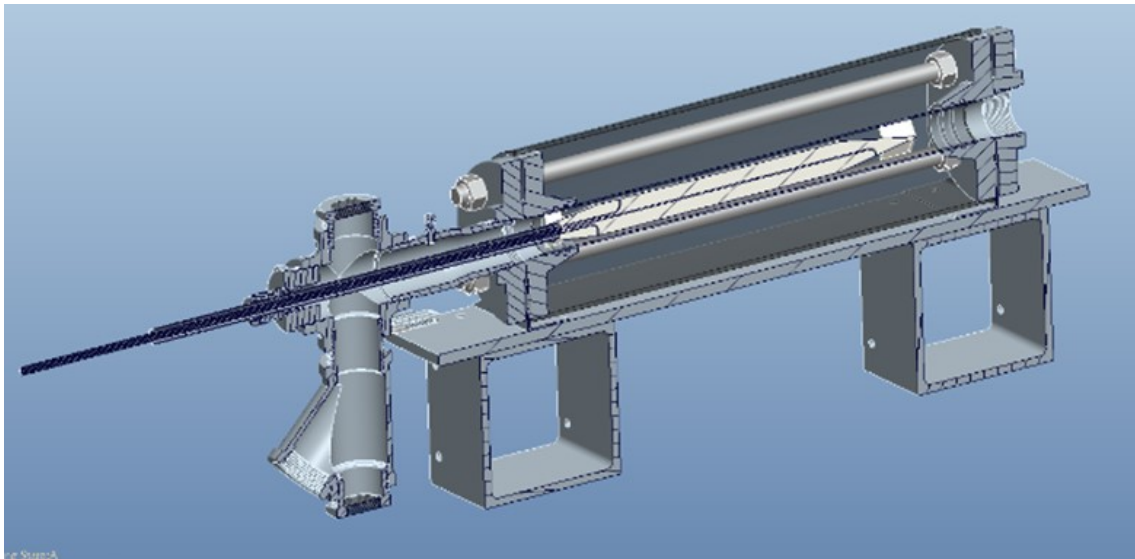
Figure 70: Subsonic ICES Test Article Assembly Cross Section
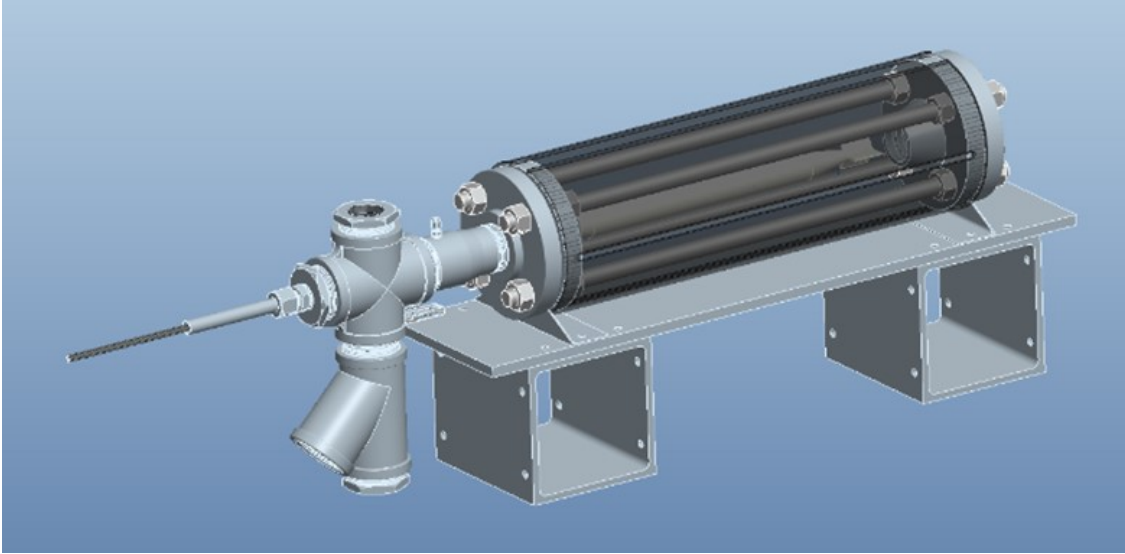
Figure 71: Subsonic ICES Test Article Assembly

Figure 72 is a picture of the completed 3D printed centerbody painted flat black to reduce laser sheet reflection and glare. The centerbody is attached to a metal sting whose axial position can be moved relative to the fixed quartz glass tube. The centerbody was fabricated with integral pressure taps.

Figure 72: Subsonic ICES 3D Printed Centerbody

The integrated test set up is shown in Figure 73. Prior to CO$_2$ addition and subsonic acceleration of the triple mixture, air flow was precooled in the direct HEX/mixer by injection of the liquid nitrogen (LN$_2$). LN$_2$ was stored in the dewar shown in Figure 74. The large dewar on the right of the photo served as a run tank while the smaller one on the left is used to maintain the desired constant pressure in the large dewar.

Using main air and CO$_2$ controls in conjunction with fine tuning valves for LN$_2$, bypass air and CO$_2$, the upstream mixing chamber was brought to approximately 100 psia, 20% CO$_2$ mass flow with no LN$_2$ cooling flow. LN$_2$ flow rate was then gradually increased while using the CO$_2$ and bypass valves to maintain a constant pressure and desired CO$_2$ level.
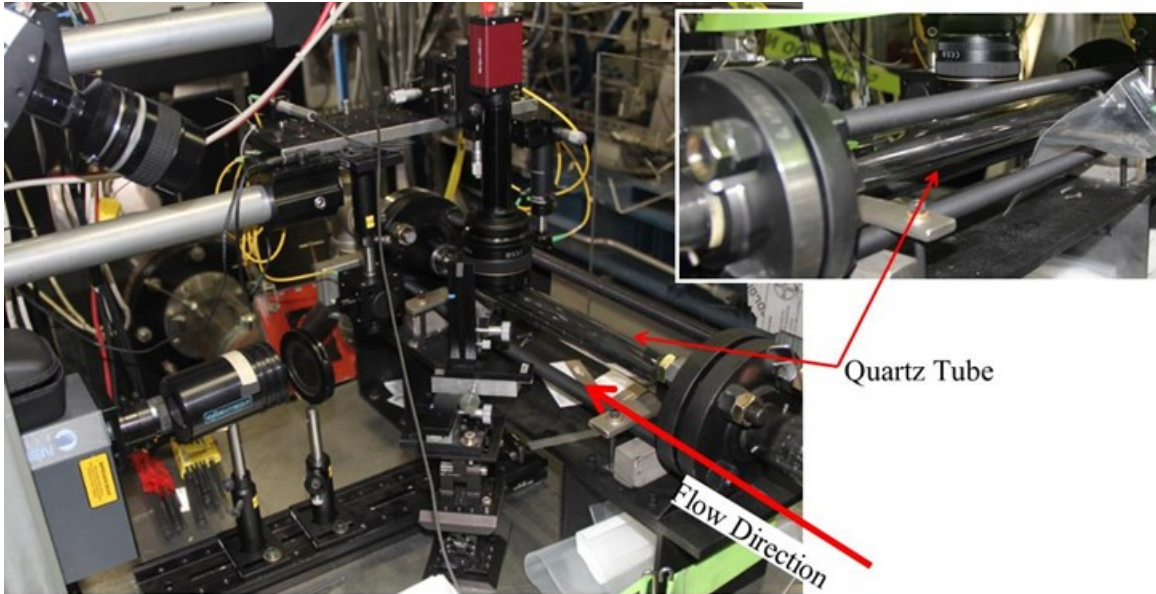
Figure 73: Initial Subsonic ICES Test Configuration

Figure 74: LN2 storage/supply dewars.

Updated Particle Size System

A Particle Sizing and Monitoring System (PSMS) was been developed in the laboratory for the real-time monitoring of CO$_2$ particle formation and particle size distribution prediction. The experimental arrangement of the system is shown in Figure 75. The technique uses a laser sheet (nominal thickness of about 1 mm) to visualize the CO$_2$ particles through surface scattering (opaque particles). The source of the light sheet is a

pulsed Nd:YAG laser (532 nm wavelength, laser energy up to 120 mJ/pulse, 5-7 ns pulse length). Sheet forming optics allow for control of the sheet thickness and orientation. The light scattered from particles is received by the complex lens L1 and recorded with a high resolution CCD camera (MANTA G-504B, 2452 pixels x 2056 pixels area, 3.45 μm x 3.45 μm pixel size). The CCD camera is mounted in a perpendicular direction to the laser sheet to record the laser light scattered at 90o angle. A pulse generator is used to control the laser energy and to synchronize the camera with the laser Q-switch pulse (not shown). The real-time particle monitoring system consists of a low energy CW laser source (< 5 mW), and an alignment mirror M1. After passing through the test area the signal is received by the collimator C2 coupled to a photodetector using an optical fiber.
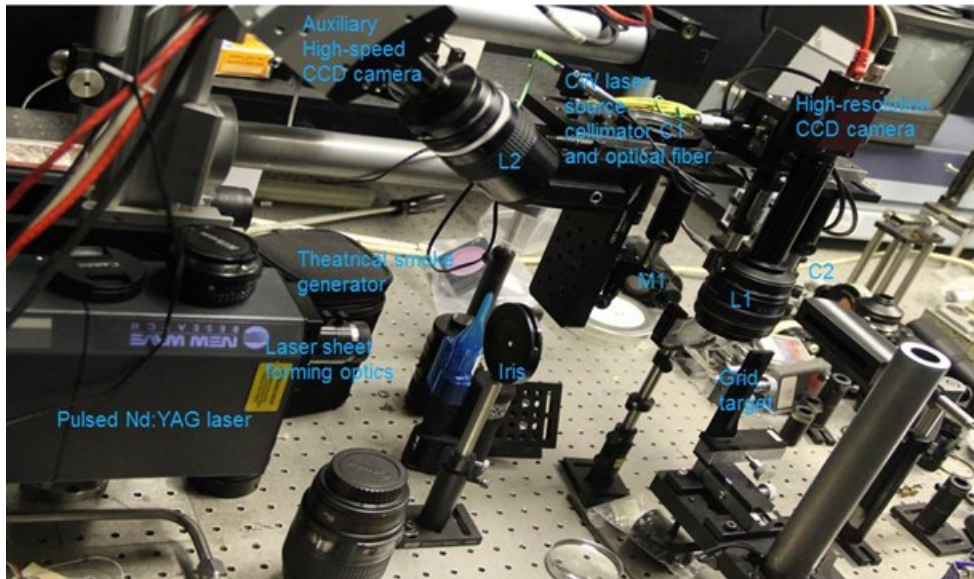
Figure 75 Particle Sizing and Real-Time Monitoring System (PS-RTM).

Tests were performed in the laboratory to characterize the optical system performance and to verify the image post-processing and analysis software tools. The spatial resolution and the field distortions of the optical system were determined with a transparent grid illuminated by white light. The flow field containing particles was simulated using a theatrical smoke generator. Images containing light scattered from submicron particles were recorded with the system and the image processing algorithms and analysis tools were verified on experimental data collected previously.

Figure 76 shows the real time oscillogram recorded during the smoke test. The beginning of the trace in Figure 76 (a) shows the condition when no particles are present in the flow field (very low signal noise). The particles are detected by a short variation in the signal intensity shown in the second part of the trace. Figure 76 (b) shows the signal when the particles are detected (at a shorter time scale).

(a)

(b)
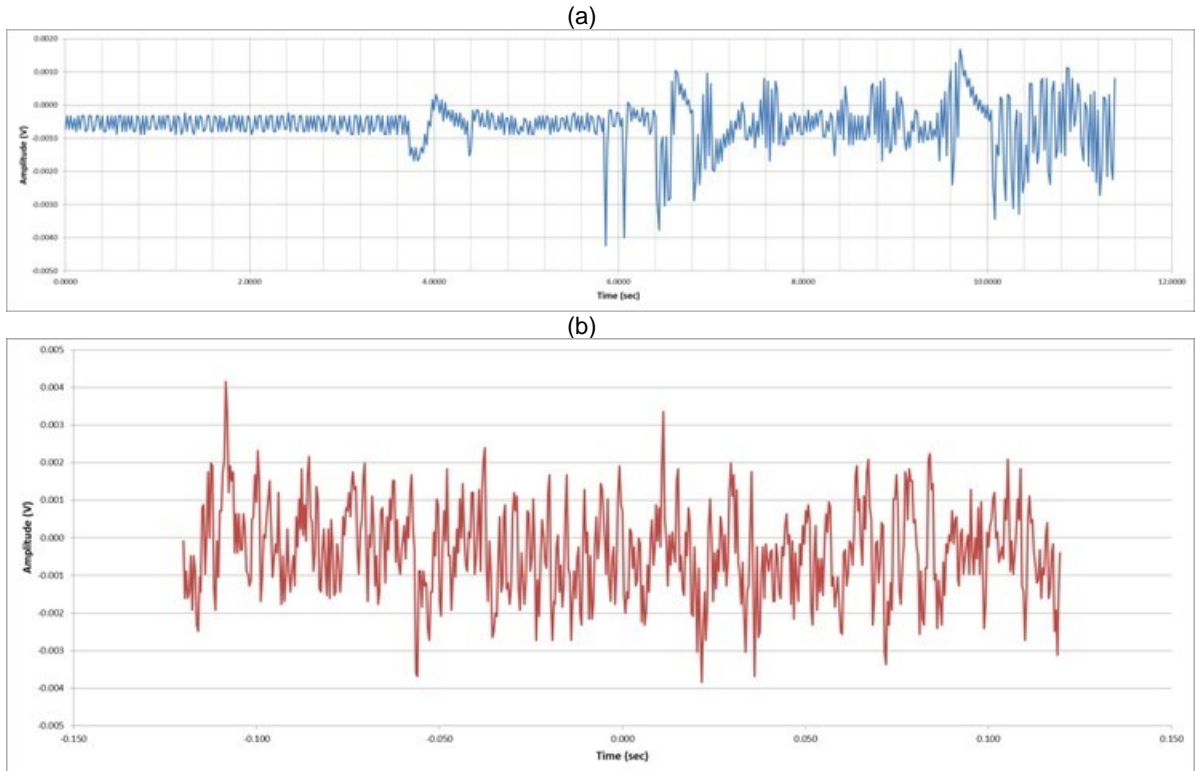
Figure 76: Real time oscillogram showing the detection of particle in a flow field generated by theatrical smoke. The beginning of the trace in Fig. 3 (a) shows no particles. Figure (b) shows particles detected signal at a shorter time scale.

Spatial resolution and field distortions of the optical system are determined with a transparent grid (Thorlabs, Grid Array R13S3) illuminated by white (room) light. Figure 77 shows the image of a rectangular grid with the step size of 50 μm. The picture is a zoomed-in section showing only three grid lines. It is used to determine the spatial resolution of the measurement corresponding to one pixel. The camera lens is a high-quality telecentric system with a focal length of 50 mm mounted with a spacer ring to the camera to increase magnification. The corresponding area in the flow imaged by the camera is about 3.5 mm x 4 mm. For the current configuration the spatial resolution of the instrument was 1.56 microns per pixel.
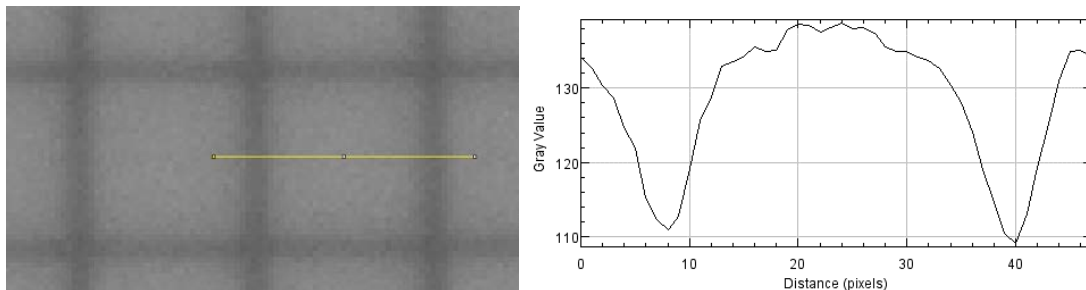
Figure 77 (a), Zoom-in image of a 50 μm grid illuminated with room light, and (b), intensity plot across two gridlines (region shown in (a) with in yellow) used to imply the field of view and the spatial resolution of the camera.

The particle size is estimated by direct imaging of the light scattered from the flow field and image analysis post-test. Figure 78(a) shows a typical image of the flow field containing CO_2 solid particles recorded in previous experiments. Figure 78(b) shows an image containing submicron particles recorded with the actual setup in the laboratory. The particle field is generated using theatrical smoke.

(a)   (b)
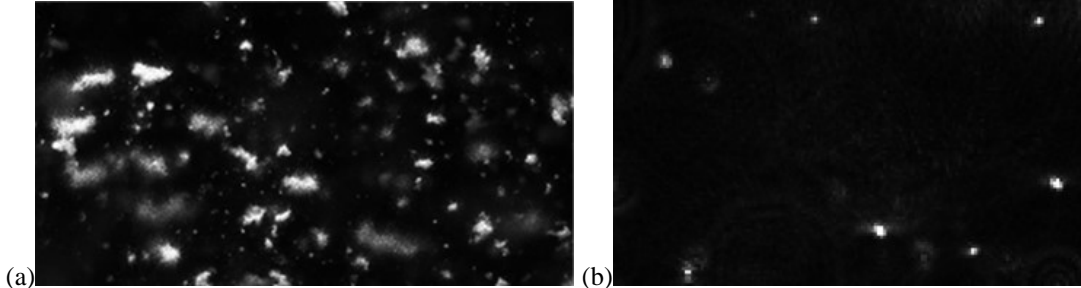
Figure 78 (a), Typical image of a flow field containing CO_2 solid particles recorded in previous experiments. (b), Image of scattered light from submicron particles recorded with the actual setup in the laboratory. The particle field is generated using theatrical smoke.

The analysis of the image containing light scattered from particles (diffraction patterns) consists of four steps: first, the instrument function is determined from a region containing an image of a small particle that generates the smallest diffraction pattern from the set (considered approximately a point source). This image is a convolution of the optical instrument point spread function the pupil function and the diffraction pattern generated by the particle at the laser wavelength; then, assuming that large particles are conglomerate of such small particles, the instrument function is de-convolved from the recorded pattern. The resulting image is a good representation of the particle viewed from a two-dimensional perspective.

For particle sizing, the image is converted to a binary image by applying a local threshold function and an edge-detection routine is applied to locate the projected shape and its associated perimeter. An area estimate is then used to compute an equivalent diameter for the particle assuming it is a spheroid. The equivalent diameter data from several images is then sorted into bins between the minimum and the maximum values of data to produce a distribution function. The particle average diameter and other characteristic properties are obtained directly from fitting this function. A re-computation of the particle apparent diameter distribution generated from two measurements obtained during previous experiments (blue and brown color coding) is shown in Figure 79. A software module is used to fit a Weibull probability density function to the data and determine the statistical properties, the Sauter mean diameter (SMD) and the median value of the particle size.
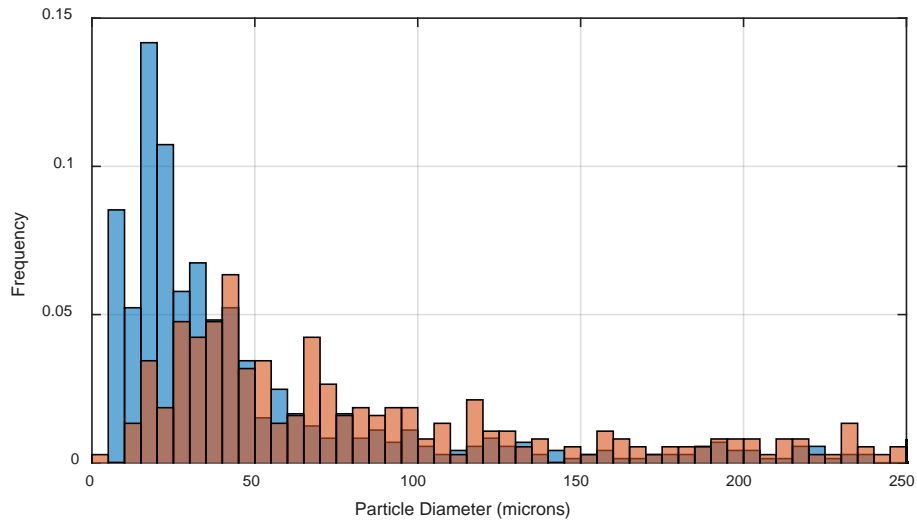
Figure 79: Re-computation of the particle apparent diameter distribution generated from two measurements obtained during previous experiments (blue and brown color coding).

When this approach was applied to the subsonic ICES test rid, as temperatures dropped, a fine fog was observed inside the duct. This temperature was still well above the saturation temperature of CO_2 indicating that what condensation of H_2O in the compressed air supply was being observed. As the temperature was dropped further and passed below the CO_2 saturation temperature large chunks of material were observed at the upstream end of rig. However at this point the outer surface of the quartz tube was too fogged-over in the area where the flow path approached the throat and no laser based particle quantification (size and number density) was possible.

A series of modifications were made to the rig to reduce condensation on the exterior of the quartz tube. These were partially successful, however with the less obstructed view it became clear that the surface of the center body and the inner surface of the quartz tube were accumulating frozen material. Eventually this accumulation resulted in a large amount of material clogging the throat and caused severe light scattering of the laser light source. Again, no laser based particle quantification was possible.

A new free-test test article was quickly designed, fabricated and installed in order to obtain particle size data in the near-field of the sonic jet as shown in Figure 80. The same facility system was used as shown in Figure 81 which also shows the optics aligned with the open jet.
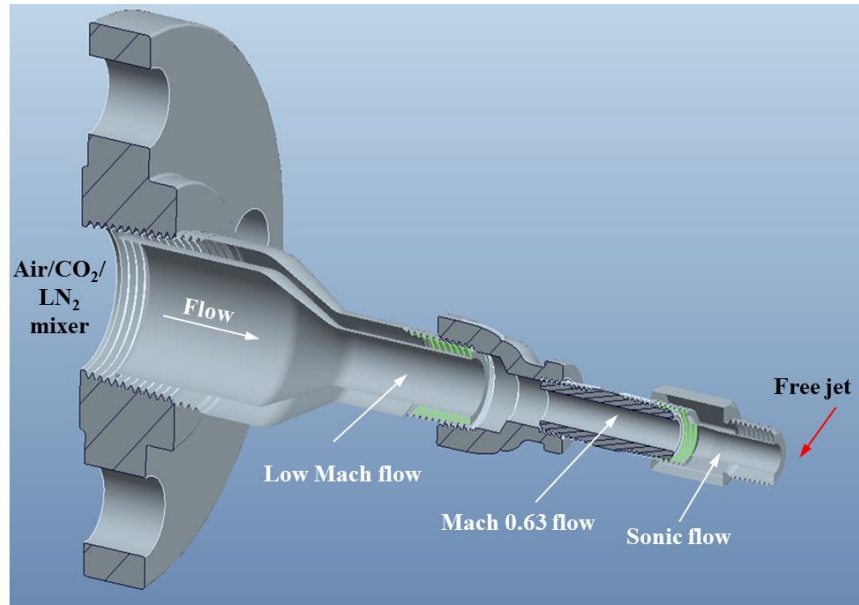
Figure 80: New configuration of the test article (subsonic ICES).
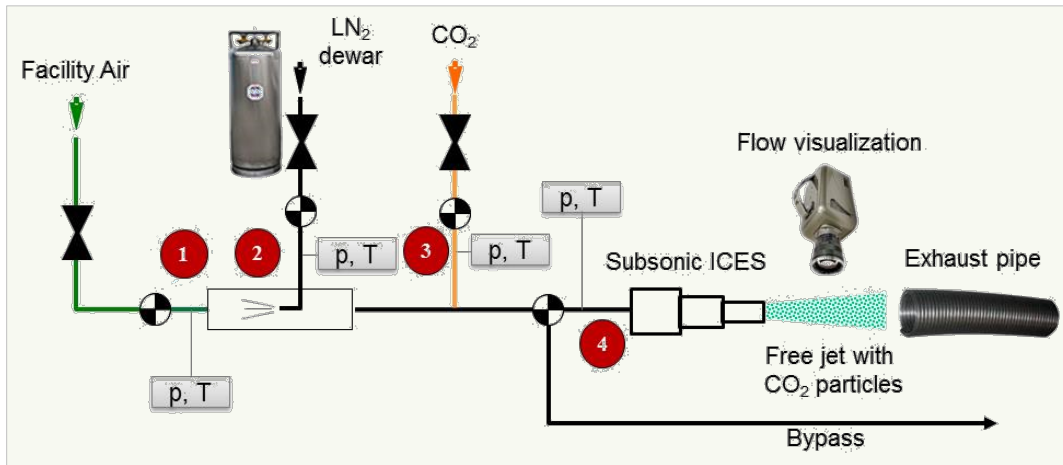
Figure 4.
Figure 81: Major components of the test rig and flow splits.

Table 7 shows temperature of the flow when CO_2 starts to desublimate at corresponding mixture pressure and fractions of the air, LN_2, and CO_2 required to reach these temperatures. The P-T diagram in Figure 82 illustrates the process occurring in the subsonic test article. This information provided some initial guidance for the subsonic ICES demonstration.

Table 7: CO2 sublimation line conditions and amounts of flow components required to reach these conditions

Pressure, psi	80	90	100	120	150
Temperature, K (sublimation line)	191.6	193.0	194.3	196.6	199.3
Temperature, F	-115.1	-112.6	-110.3	-106.2	-101.2
Mass fraction air	0.552	0.555	0.558	0.563	0.569
Mass fraction LN2	0.248	0.245	0.242	0.237	0.231
Mass fraction CO2	0.200	0.200	0.200	0.200	0.200
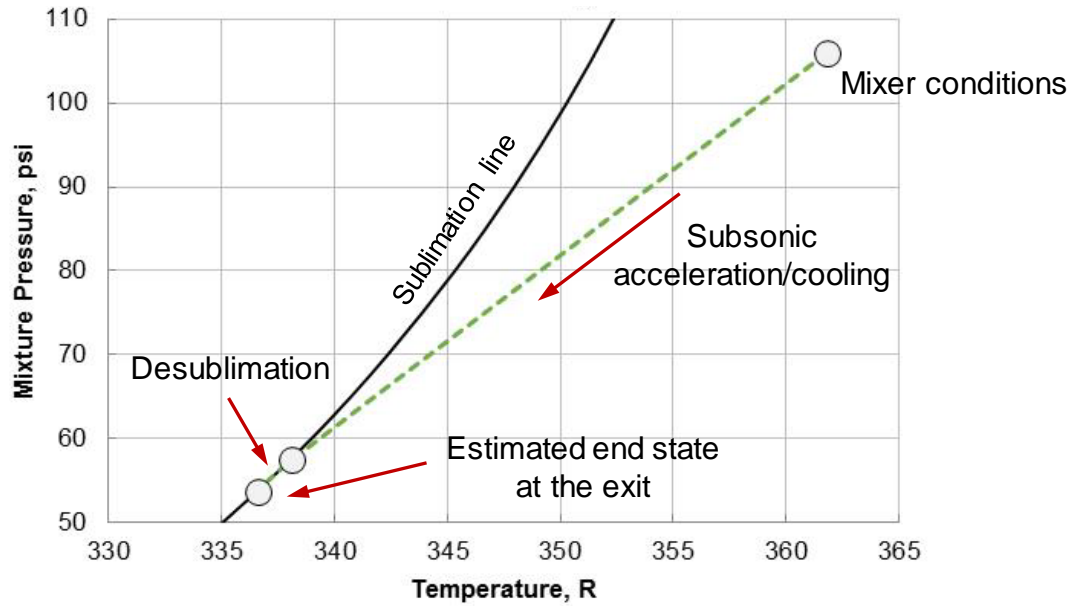
Figure 82 CO2 sublimation and condensation lines in P-T diagram.

Figure 83 shows major components in the vicinity of the updated test article and Figure 84 shows exhaust system views.
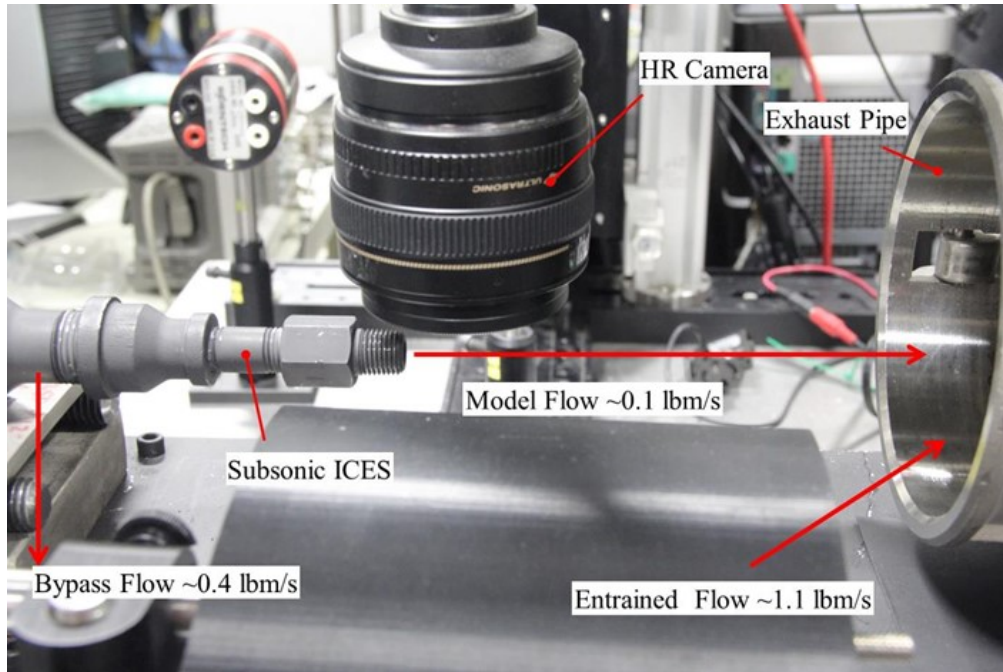
Figure 83 Major Components of the Updated Subsonic ICES Rig with Flow Splits
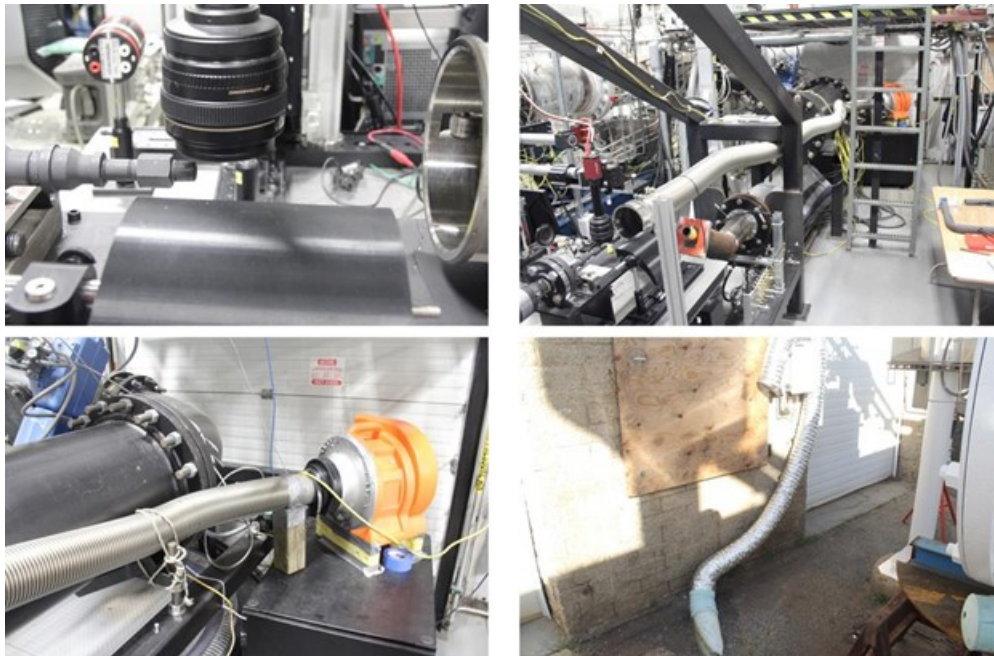
Figure 84 Updated Subsonic ICES Exhaust System

Optical Results

A near field digital camera was setup such that only a very small portion of the plume near the nozzle exit could be observed. The camera field of depth was made as small as possible. The intent being that only particles directly illuminated by the laser beam would be in focus.

For tests ICES16 and ICES17 the field of view began approximately 1 x/d after the nozzle exit and could be traversed more than half the plume. For tests ICES16 and ICES17 the sync trigger which caused the camera to take a sequence of 20 pictures was recorded by the data set.

Figure 85 shows one of the near-field images. These images were used to detect and characterize particles, i.e., provide information on particles number and size.
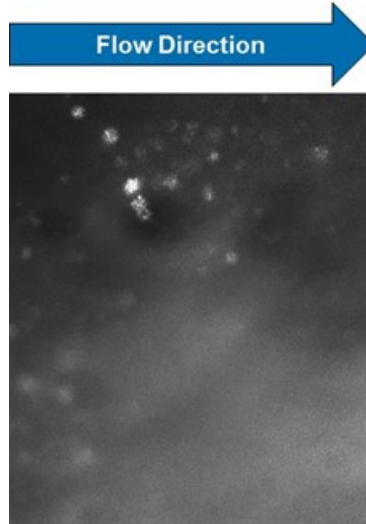
Figure 85 Near-field HRC image for particles count and size evaluation.

A far field digital camera was setup such that the majority of the plume could be observed. Data from this camera was not synced to flow rates, temperatures, pressures or other quantitative data from the test rig. This camera provided qualitative data on the flow field and clearly indicated generation of the substantial amounts of particles as seen in Figure 86. The near field camera partially blocks the reflected laser light. This results in a small visual asymmetry in the observation plane at the bottom of the image.
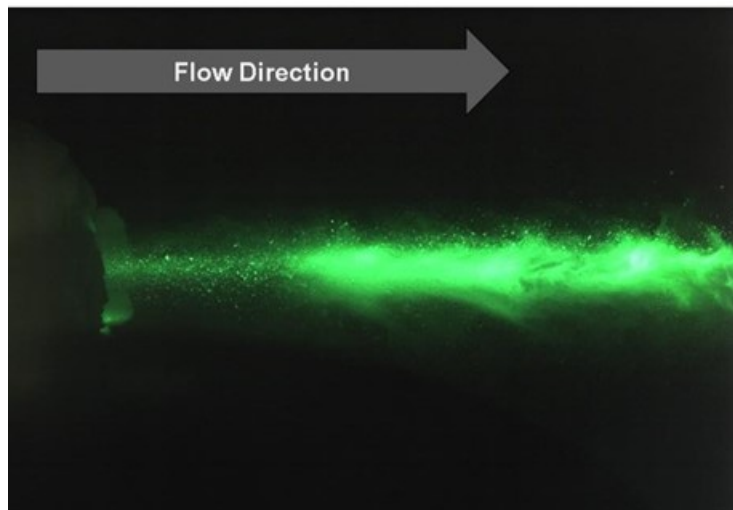
Figure 86 Far field HSC image.

For near field camera calibration, a calibrated target was placed in the camera field of

view (Figure 87). The left side of the target grid was 100 microns while the right side was 500 microns. A full size camera image was used for the measurement (2452 pixels x 2056 pixels).

A grey value trace was created along the yellow line in Figure 87 to determine the number of pixels between the 500 micron grid lines resulting in the plot shown in Figure 88. For the ICES17 camera configuration, the calibration constant was 1.56 (500/320) micron/pixels.
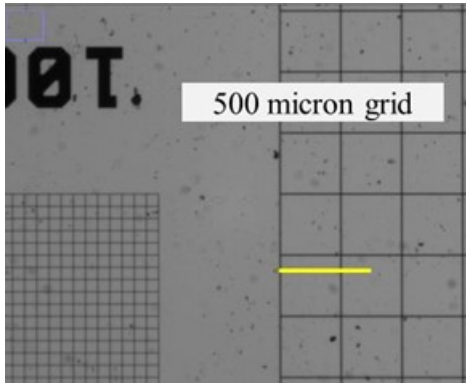
Figure 87 Calibrated target.
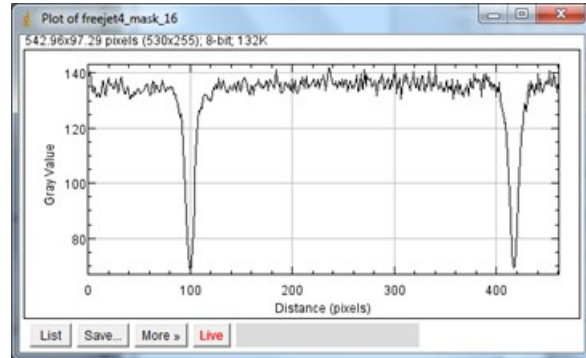
Figure 88 Gray scale value along yellow trace line.

Particle Sizing Algorithm

As before, the particle size is estimated by direct micro-imaging of laser light scattered from the flow field and image analysis. The image processing steps include:

- Image correction, i.e., correcting the recorded image by removing the background light noise;
- Image filtering, de-convolution of the instrument function from the corrected image to obtain the filtered image;
- Particle detection. A detection algorithm applied to the filtered image detects independent particles and estimate their approximate area.

The estimated particle area was used to compute an equivalent particle diameter *assuming* the particle is a spheroid. If enough particles are detected in a dataset the equivalent diameter of particles is sorted into bins between the minimum and the maximum values of data to produce a distribution function. The particle average diameter and other characteristic properties are obtained directly from fitting this function. This process is illustrated in Figure 89 using image post processing for ICES17/image 371.

Raw Image
(3.8 mm x 3.2 mm)

Corrected Image
(3.2 mm x 3.2 mm)

Filtered Image
(3.2 mm x 3.2 mm)
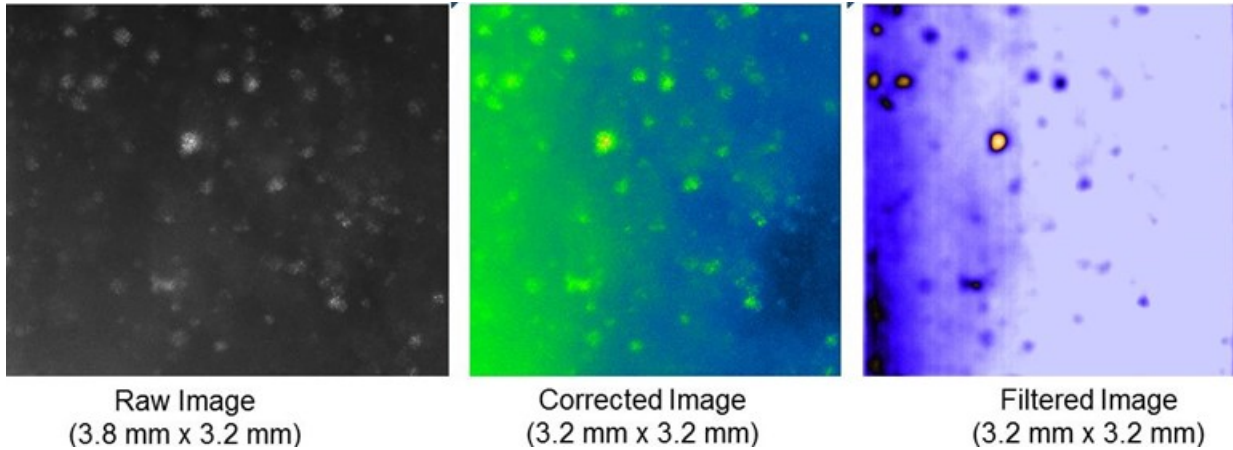
Figure 89 Example of image post-processing (ICES17/Image 371).

Final Subsonic ICES Test Program Summary

- Sequence 1: **ICES14** (10/11/2016)
  - No functional LN$_2$ control
    - Insufficient turndown in LN$_2$ control valve
  - Significant clogging
    - 150 psi pressure relief valve tripped several times
    - The critical flow venturi used for air flow measurement unchoked, resulting in loss of air flow measurement
  - No camera sync signal was recorded
  - Near field camera at about x/d 2.36 x/d on the jet centerline.

- Sequence 2: **ICES15** (10/13/2016)
  - 0.05" Orifice added in LN$_2$ line to improve turndown
    - This resulted in insufficient maximum LN$_2$ flow
  - The 0.2" critical flow venturi used to measure air flow, was replaced with a 0.3" venturi to decrease back pressure sensitivity
  - No camera sync signal was recorded
  - Near field camera at x/d ~1.0 ;
  - Far field camera at 30 deg.

- Sequence 3: **ICES16** (10/13/2016)
  - Orifice in LN$_2$ increased to 0.10" to increase max LN$_2$ flow
    - Marginally sufficient maximum LN$_2$ flow
  - Camera sync signal recorded
  - Near field camera imaging at about X/D 1.0 x/d

- - Limited data available due to camera malfunction during test
  - Likely caused by proximity to field flow and sensitivity to jet noise
- Sequence 4: **ICES17** (10/14/2016)
  - o Orifice in LN_2 line increased to from 0.1" to 0.125" to increase maximum LN_2 flow
    - Sufficient max LN_2 flow
  - o Camera sync signal recorded
  - o Near field camera
    - x-direction – ~1 x/d
    - y-direction – centerline (up to 1 y/d)

Data Set Selection

ICES Test 17 had the most robust camera operation and the most stable flow conditions. The times the near field camera was in operation and recording data were compared to measured pressures, temperatures and flow rates. Image sequences were identified where: a) stable flow was observed and; b) data indicated a robust set of flow measurements. Thus the measurement of %CO_2 had high confidence and was close to the target value of 20%. Images from this test were post processed to determine mean particle size

A detection algorithm was applied on a piecewise basis to the filtered image. Clearly the out-of-plane particles seen by the human eye are removed by the algorithm. Particular to this flow-field, in regions with significant scatter due to large numbers of small particles, large particles are not detected. Particle count is low and likely to be conservative and biased towards larger particles. Since the particles are assumed to be sphere, the apparent diameter was computed from the projected area of the particle imaged by the camera.

Detected particles obtained from the filtered image (white circles in Figure 90) super-imposed on the corrected image to emphasize particle detection. The color scale is the same as for the filtered image which was used to detect the particles.
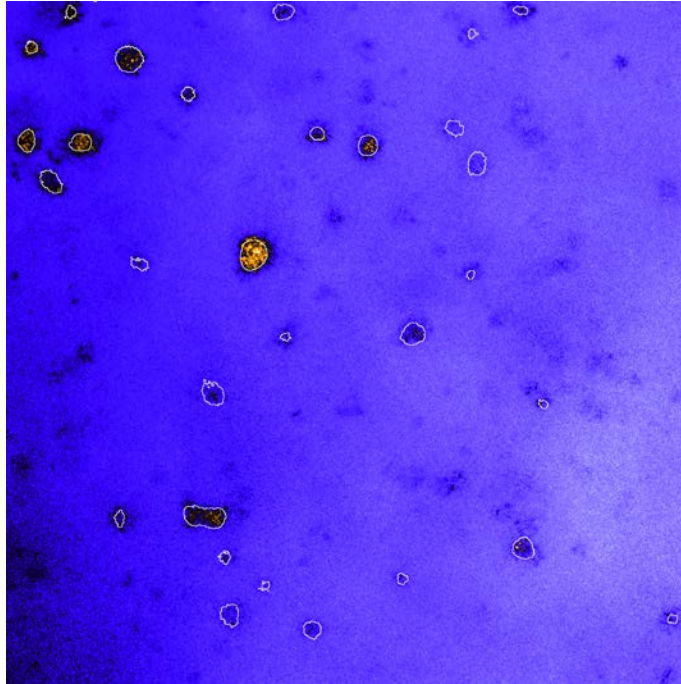
Figure 90 Example of image post-processing (ICES17/Image 371).

In all three experimental cases subjected to detailed analysis CO_2 desublimation in the test article is estimated at 3.0-3.5% of the total CO_2 contained in the surrogate flue gas. The data on the following pages summarizes typical groups of images from test ICES17 and major associated data.

Image 188

Image 192

Test	ICES17
Image Range	181-200
$d_{ave}(\mu m)$	39.2
$\sigma d(\mu m)$	42.1
% CO2	19%
Mixing Tube Pressure (psia)	104
Mixing Tube Temperature (R)	368°
Saturation Temp @ Mixing Tube (R)	348°
Mixing Tube Delta T Sat (R)	20° above
Temperature at Mach 1 (R)*	307°
Pressure at Mach 1 (psia)*	55.3°
Aprox. Saturation Temp @ Mach 1 (R)	337.3°
Estimated amount of desublimated CO2	3.0%

Image 351

Image 358

Test	ICES17
Image Range	341 - 360
$d_{ave}(\mu m)$	38.4
$\sigma d(\mu m)$	7.4
% CO2	19%
Mixing Tube Pressure (psia)	106
Mixing Tube Temperature (R)	362°
Saturation Temp @ Mixing Tube (R)	348°
Mixing Tube Delta T Sat (R)	14° above
Temperature at Mach 1 (R)*	302°
Pressure at Mach 1 (psia)*	57.4°
Aprox. Saturation Temp @ Mach 1 (R)	338.1°
Estimated amount of desublimated CO2	3.5%

Test	ICES17
Image Range	361 - 380
$d_{ave}(\mu m)$	**39.2**
$\sigma d(\mu m)$	6.7
% CO2	19%
Mixing Tube Pressure (psia)	102
Mixing Tube Temperature (R)	363°
Saturation Temp @ Mixing Tube (R)	346°
Mixing Tube Delta T Sat (R)	17° above
Temperature at Mach 1 (R)*	303°
Pressure at Mach 1 (psia)*	53.7°
Mach 1 Delta to Tsat at Mach 1 (R)	336.7°
Estimated amount of desublimated CO2	3.3%

The volume and mass of condensate were estimated using Image 371 shown in Figure 91 where dimenensions of all 33 visible particles are also summarized. A statistical analysis to assess the %CO2 from these images is very difficult, but estimations made indicate evidence of a very **significant amount** of the CO_2 in the form of large migratable particles.
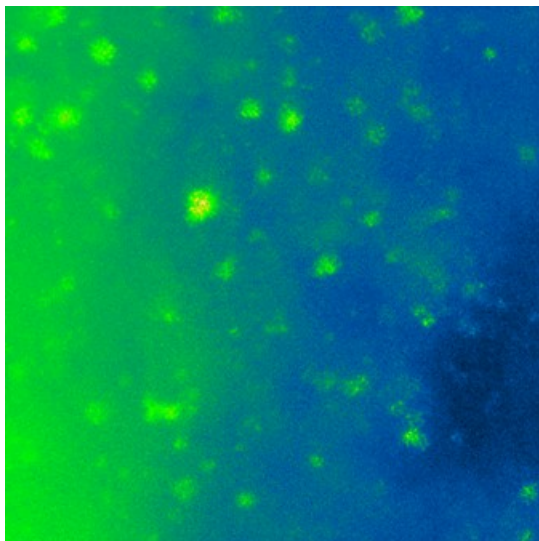
	$d_{371}(\mu m)$	Volume,μ		$d_{371}(\mu m)$	Volume,μ
1	32.3	17667.8	18	30.3	14617.5
2	39.6	32506.0	19	28.2	11766.2
3	39.1	31356.5	20	28.3	11835.0
4	47.8	57139.8	21	37.9	28451.8
5	36.2	24933.7	22	35.7	23882.7
6	33.5	19669.8	23	41.6	37643.4
7	38.2	29285.4	24	52.0	73538.1
8	30.7	15212.0	25	36.8	25999.6
9	32.0	17120.2	26	36.8	25999.6
10	38.8	30597.9	27	19.6	3919.6
11	27.7	11086.2	28	32.3	17589.2
12	37.0	26538.2	29	23.2	6526.6
13	41.8	38150.5	30	31.0	15625.4
14	26.1	9319.1	31	27.1	10452.8
15	43.1	41972.5	32	32.5	18022.9
16	40.9	35737.2	33	29.5	13380.6
17	27.9	11356.6			

Figure 91 Particle count and size data for Image 371

Conclusions from Subsonic ICES Testing
- Large particles were detected throughout the tests;
- Mean particle sizes for the sequences were on the order of 30-40 microns. These are large enough for inertial separation;
- Volume estimates show that a "significant amount" of CO_2 has condensed into large migratable particles;
- Excessive amount of particles compared to equilibrium estimates can be explained by local formation of subcooled particles in the CO_2 mixing zone.

3.1.6 Updated Techno-economic Analysis

After the test program was completed, the team focused on updating the previous Techno-ecomonic analysis (TEA) carried out by WorleyParsons in 2013.   This effort was led by EPRI and performed again by WorleyParsons.   A detailed report is included here as Appendix B, but brief summary is included here.

Based on the updated schematic (Figure 62) and stream table (Table 6), an updated plant system block diagram was created as shown in Figure 92.
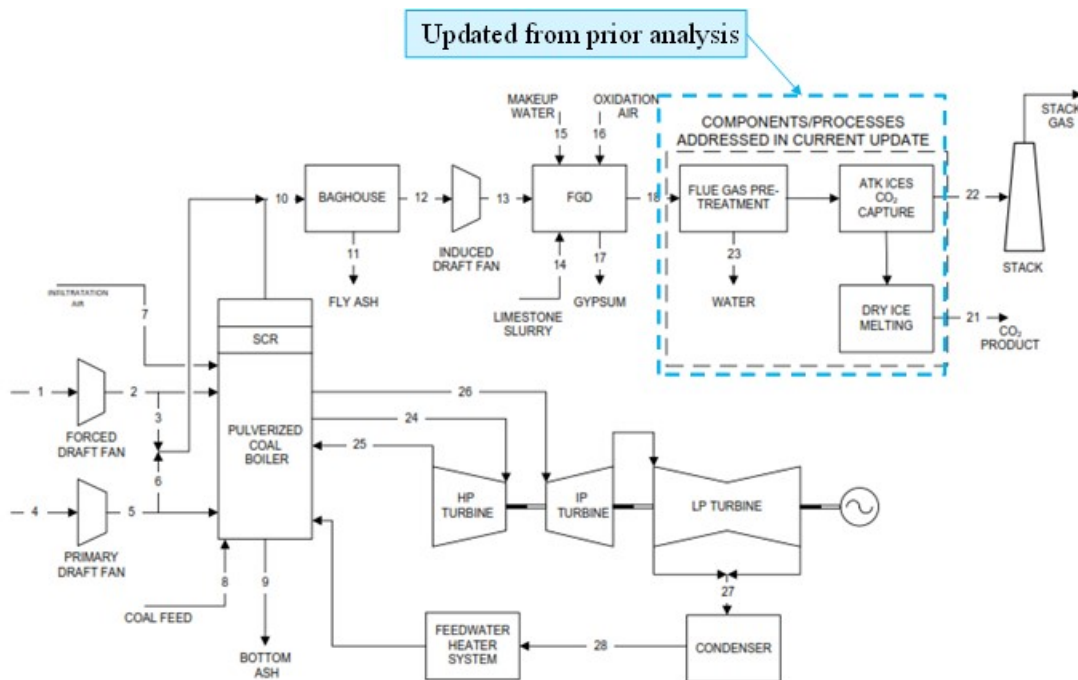
Figure 92 Updated Plant Block Diagram

Details of the flue-gas pre-treatment system including compressors and heat exchangers is shown in Figure 93.
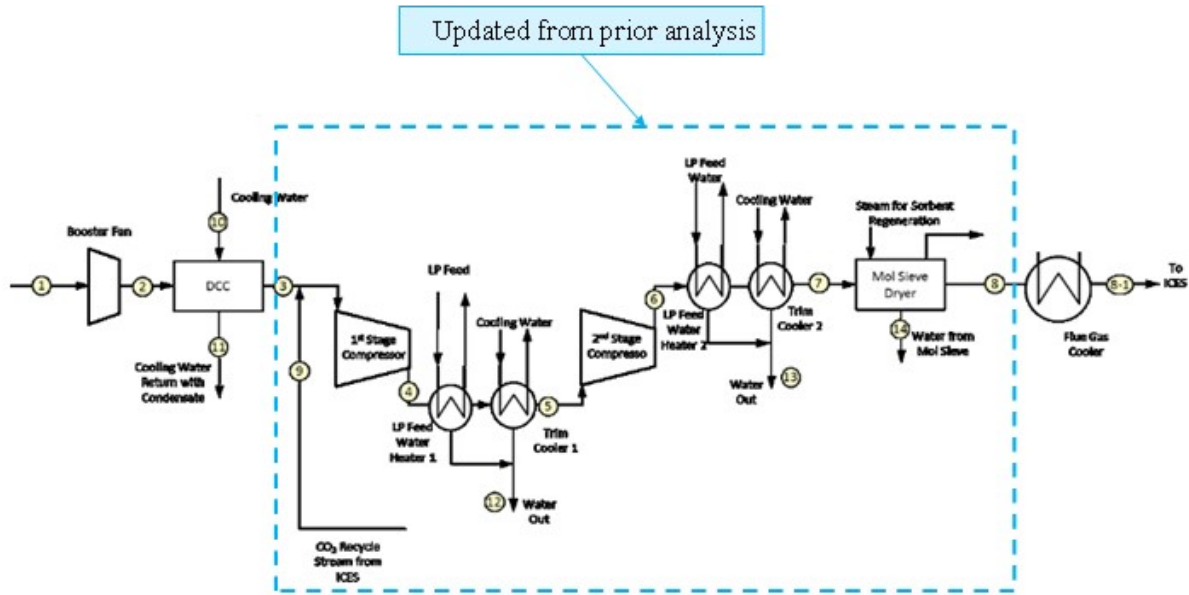
Figure 93 Details of Flue Gas Pre-treatment System

The essential result of the updated TEA is that the updated ICES system economics are on par with the Case 12 from the DOE Bituminous Baseline Report which includes an amine-based capture system.   Graphical and tabular comparative data is presented in Figure 94 and Table 8 respectively.
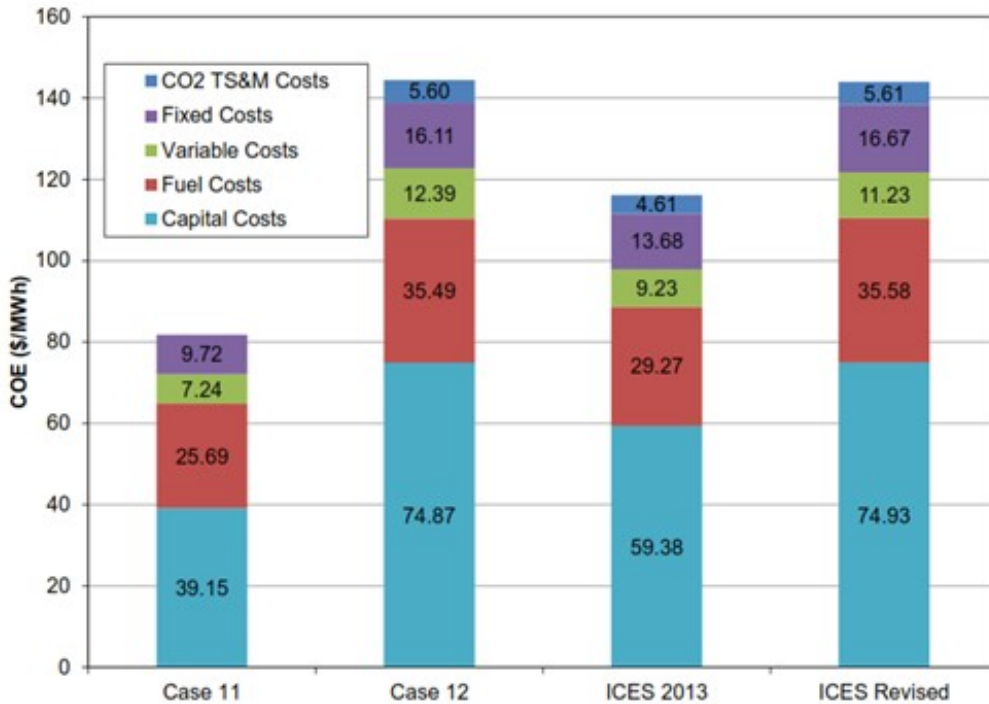
Figure 94 Summary of Economic Comparison of ICES to Case 11 and Case 12 of Bituminous Baseline Report

Table 8 Tabulated Comparison of Operating Parameters and Economics

	Case 11	Case 12	ICES 2013	ICES Revised
PLANT DESCRIPTION				
Steam Cycle	Supercritical	Supercritical	Supercritical	Supercritical
CO_2 Capture	No	Yes	Yes	Yes
OPERATING PARAMETERS				
Net Plant Output, MWe	550.0	550.0	550.0	451.80
Net Plant Heat Rate, Btu/kWh HHV (kJ/kWh)	8,686 (9,165)	12,002 (12,663)	9,896 (10,441)	12,030 (12,693)
Net Plant Efficiency, HHV	39.3%	28.4%	34.5%	28.4%
CO_2 Captured, lb/MWh (kg/MWh)	-	2,200 (998)	1,813 (822)	2,204 (998)
CO_2 Emitted, lb/MWh net (kg/MWh net)	1768 (802)	244 (111)	201 (91)	245 (111)
CAPITAL AND OPERATING COSTS				
Total Overnight Cost (2012$/kW)	2,513	4,496	3,565	4,499
Variable Operating and Maintenance ($/MWh)	7.24	12.39	9.23	11.24
Fixed Operating and Maintenance ($/yr)	39,826,084	65,958,457	56,039,860	56,079,253
ECONOMIC METRICS				
COE ($/MWh, 2012$)	81.81	144.45	116.17	144.02
Cost of CO_2 Captured ($/tonne CO_2)	NA	62.79	41.79	62.79
Cost of CO_2 Avoided ($/tonne CO_2)	NA	90.67	48.36	90.67

As summarized in the updated TEA report, ICES still has a number of key advantages over adsorption and membrane-based systems due to the lack of a consumable media and no hazardous chemicals in the process. Additionally, ICES is expected to have comparatively favorable economics for applications requiring less capture (~50%) and/or applications with lower CO_2 concentration (~8mol%) since compression costs scale with these parameters.

4. Summary and Recommendations for Future Research

Several key accomplishments were achieved in the development of the ICES system in this program including the demonstration of large CO_2 particle formation through partial subsonic condensation. This was enabled by introducing a flue gas pre-cooling scheme that was developed to address increases to flue gas compression requirements that evolved from a better understanding of system thermodynamic modeling.

With new analysis tools developed in this program, we recommend that future work will continue optimization of ICES process and related cycles for range of CO_2 concentrations and/or CO_2 capture levels to identify performance sensitivities and to find most favorable operating conditions. Include possible operation in conjunction with other technologies (e.g., stage 2 of membrane system).

Appendix A. OSU Final Report

(separate file appended)

Supersonic Post-combustion Inertial CO2 Extraction System
Final Report

Submitted to:
ATK

Submitted by:

B. Wyslouzil
The Ohio State University
Columbus OH 43210

December 31, 2014

TABLE OF CONTENTS

1. LIST OF FIGURES

growth corresponds to the first "kink" in the *p-T* curve, close to the extrapolated vapor-liquid curve. At the conditions corresponding to heterogeneous nucleation, the vapor is highly supersaturated with respect to the solid. The effect of particle size is observed indirectly; heterogeneous CO_2 condensation is delayed at lower water vapor concentrations, because the seed particle size decreases as roughly $(y_{H2O})_0^{1/3}$.

2. LIST OF TABLES

3. EXECUTIVE SUMMARY

A team of researchers at the Ohio State University was engaged by ATK to provide data that would help ATK and ACENT researchers understand the key parameters that control particle formation and growth when flue gas expands across a supersonic nozzle. An extensive set of experiments was completed to explore the basic physcis, and complementary modeling studies of particle growth in one-dimensional supersonic flow were conducted for particles in the nanometer and micron size ranges.

Initial experiments established that in the presence of water, condensation of CO_2 occurs via heterogeneous nucleation onto homogeneously nucleated water droplets. Positive consequences are that condensation starts at much warmer temperatures than required if homogeneous CO_2 nucleation controlled the phase transition, and the large surface area lets condensation occur on very short time scales. The challenge remains that the number of particles created by the nucleation of water, typically on the order of 10^{12} cm^{-3}, controls the ultimate size of the CO_2-rich particles. Thus, the composite particles are expected to have diameters on the order of 25 nm making inertial separation difficult. Brownian coagulation is not expected to reduce the number density enough to make a significant difference to the final particle size, and the schemes that were attempted to enhance coagulation by introducing turbulence appeared to add additional energy to the flow and thereby reduce the degree of condensation. Depending on how ICES is integrated into a power plant, particles in the flue gas could potentially act as more appropriate condensation seeds and make ICES a particulate control as well as a CO_2 capture device. This could have positive economic benefit by enhancing process intensification.

Studies that investigated the injection of CO_2 particles were largely computational with limited light scattering experiments conducted to validate the basic modeling approach. The models showed that it was important to add the particles close to the throat in order to avoid evaporation, that small particles with their larger surface area increased the rate of condensation, and that changing the scale of the device could be helpful. Although our modeling studies covered a wide range of parameter space, additional work in this area is clearly required, in particularly moving to more sophisticated models of the injection process and the two-phase flow.

4. Background, Tasks, and Deliverables: Supersonic Post-combustion Inertial CO_2 Extraction System

4.1 Background:

ATK and ACENT researchers are developing an Inertial Carbon Extraction System (ICES) with an initial application designed to remove CO_2 from the flue gas stream of a coal fired power plant (~14.5mol% CO_2, 1.5mol% H_2O, balance N_2). ICES relies on the supersonic condensation of the CO_2 component of the flue gas and inertial separation of the solid particles. Condensation of CO_2 into particles with diameters above approximately 3 microns is critical to the success of this technique. A lack of detailed understanding of the parameters that govern particle size evolution has hindered technical success to date.

The OSU team was engaged to provide data that would help ATK and ACENT researchers understand the key parameters that control particle formation and growth in supersonic flow. This report summarizes the work completed at OSU.

4.2 Primary Objectives for the OSU team:

Perform experiments to provide data on how proposed design modifications are likely to influence CO_2 particle size. Results should be traceable to 3-5 micron particle size in the eventual ATK test article

Provide ICES team with data required to model condensation phenomena and make informed design decisions during trade studies.

4.3 Tasks to be performed by OSU research team:

4.3.1 Analytical tasks

1.1. Generate database of existing data on CO2 condensation data germane to ATK ICES effort. – **Early Q1**
1.2. Generate database of existing OSU test data germane to supersonic condensation as inputs to proposed models. – **Early Q1**
1.3. Support efforts of the ICES CFD analysis team to simulate supersonic condensation. – **Ongoing**
1.4. Review existing 1-D modeling tools – **Early Q1**
1.5. Using data from 1.4, suggest a baseline nozzle contour which encompasses known behaviors which should maximize particle growth within practical constraints. – **Mid Q1**

4.3.2   Baseline experimental tasks

2.1 Perform a baseline CO_2 condensation test using an appropriate contour at OSU using OSU's in-house diagnostics – **End of Q1**
2.2 Rerun test at appropriate lab with high frequency light source to determine particle diameters and number densities – **Early Q2**
2.3 Cross correlate infra-red laser scatter to higher frequency light source data. **– Early Q2**

4.3.3   Perturbation / Growth Impact Experiments

3.1. Test using alternate nozzle contours **- Q2 through Q3, Baseline – Four (4) Tests**
3.2. Turbulence-enhanced growth **- Q2 through Q3, Baseline – Four (4) Tests**
3.3. Humidity-enhanced growth **- Q2 through Q3, Baseline – Four (4) Tests**
3.4. Particle seeding effects **- Q2 through Q**
   - Recoverable third component injection **- Q2 through Q3**, **Baseline – Four (4) Tests**
   - CO_2 recirculation **- Q2 through Q3 Baseline – Four (4) Tests**

4.4 Deliverables

Deliverables include monthly reports in Power Point format with attached Excel spreadsheets and Final Technical Report in MS Word format at the end of the effort.

Specific deliverables include:

4.4.1   Analytical tasks
   1.1 Excel spreadsheet and technical memorandum with literature based data and data sources
   1.2 Excel spreadsheet and technical memorandum with experimental data
   1.3 Attend Bi-weekly telecom with CFD working group, review data comparisons as they become available
   1.4 Report on existing models and suggested areas of improvement
   1.5 Excel spreadsheet with contour definition and technical memorandum on expected performance

4.4.2   Baseline experimental tasks
   2.1 Technical memo outlining results, geometric definition of contour used and data in an agreed upon format
   2.2 Technical memo outlining results and data in an agreed upon format
   2.3 Technical memo outlining results and data in an agreed upon format

4.4.3   Perturbation / Growth experiments
   3.1 Short technical memo outlining results and data in an agreed upon format at the completion of each test
   3.2 Short technical memo outlining results and data in an agreed upon format at the completion of each test
   3.3 Short technical memo outlining results and data in an agreed upon format at the completion of each test
   3.4 Short technical memo outlining results and data in an agreed upon format at the completion of each test

4.5 Project Close out
   A final Technical Report summarizing the project results cross referenced to the delivered technical memos shall be prepared

5. Analytical Tasks

5.1 Existing data transferred to ATK (Deliverable 1.2)

In response to ATK's request for data that could be used to validate three-dimensional models describing condensation in supersonic flows, OSU provided an extensive set of unary and binary condensation data for D_2O - nonane mixtures in N_2 carrier gas. These data were measured by Harshad Pathak as part of his PhD dissertation and are published.[1, 2] **Figure 1** illustrates the nozzle profile used in the experiments, where the defined contour was provided to ATK.

Figures 2 and **3** illustrate typical examples of the data that were delivered. Spreadsheets included all of the directly measured variables including the incoming flow rates of
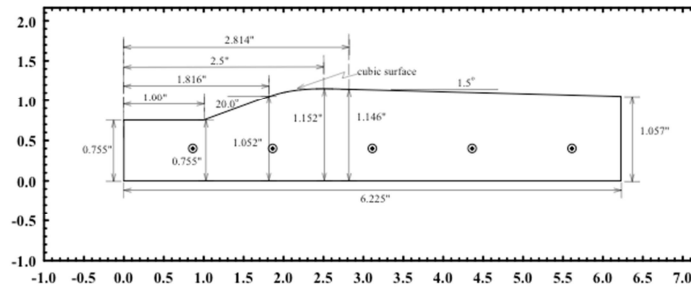
Figure 1. The profile of the nozzle used in the D2O-nonane condensation experiments.
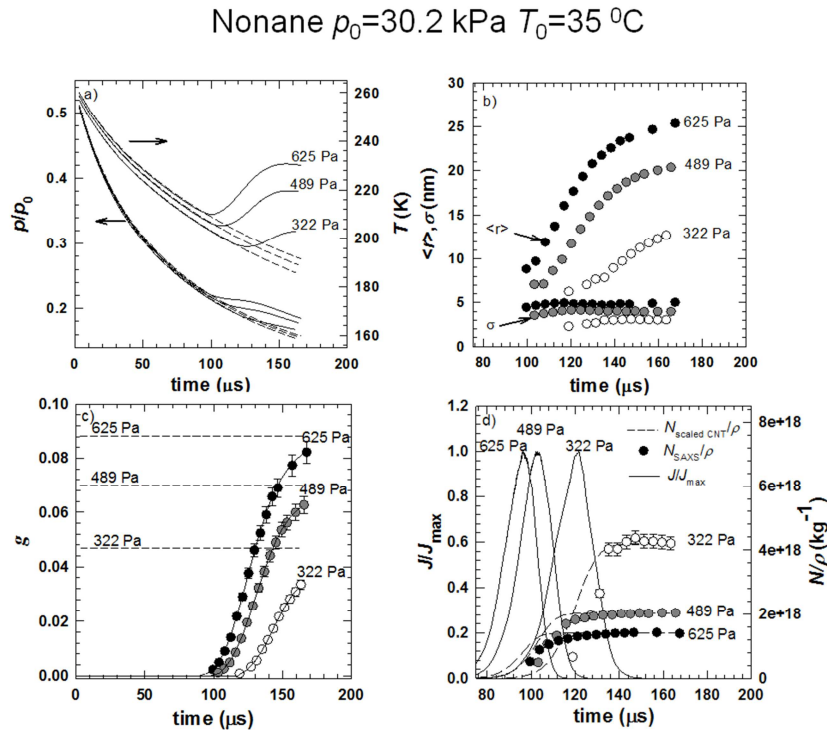
Figure 2. Position resolved measurements of nonane condensation in a supersonic nozzle.

D$_2$O p_{v0}=538 Pa and nonane p_{v0}=487 Pa
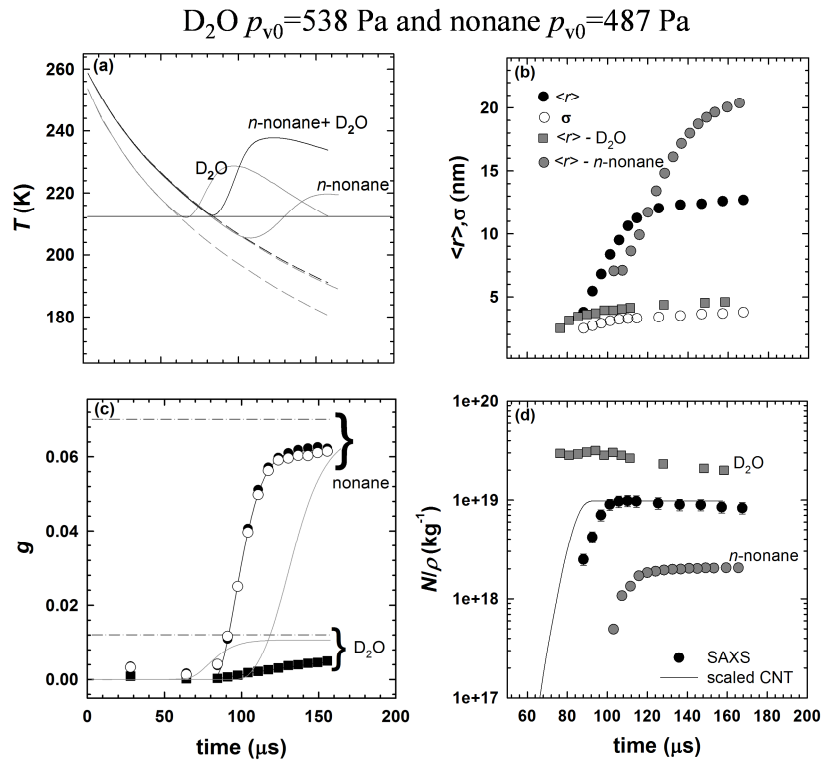
Figure 3. Position resolved measurements of nonane-D$_2$O co-condensation in a supersonic nozzle.

condensable and carrier gas, stagnation temperature and pressure, and position resolved static pressure profiles, particle size distribution parameters derived from small angle X-ray scattering (SAXS) measurements, and the mass fraction of condensable in the vapor and liquid states measured by Fourier Transform Infra-red (FTIR) spectroscopy. The values for the other flow variables – temperature, density, velocity, area ratio, time – derived from an integrated data analysis approach, assuming a one-dimensional flow, were also included.

5.2 CO$_2$ condensation in supersonic nozzles literature review (Deliverable 1.1)

Homogeneous nucleation and condensation of CO$_2$ in supersonic flow was studied in detail by Duff,[3] and to a more limited extent by Erbland et al.[4] and Ramos et al.[5] Although these studies are interesting, our analysis suggests that the presence of residual water vapor in the gas mixture means that homogeneous nucleation of CO$_2$ is highly unlikely in the ICES process. This is best understood by examining both the process cartoon and the phase diagrams of CO$_2$ and water, illustrated in **Figure 4**. Since the vapor pressures of these two species differ by about 3 orders of magnitude, water vapor will condense at temperatures where the stable state of CO$_2$ is the vapor. At lower temperatures CO$_2$ then condense via heterogeneous nucleation on these seeds. Consequently, as illustrated in **Figure 4** heterogeneous
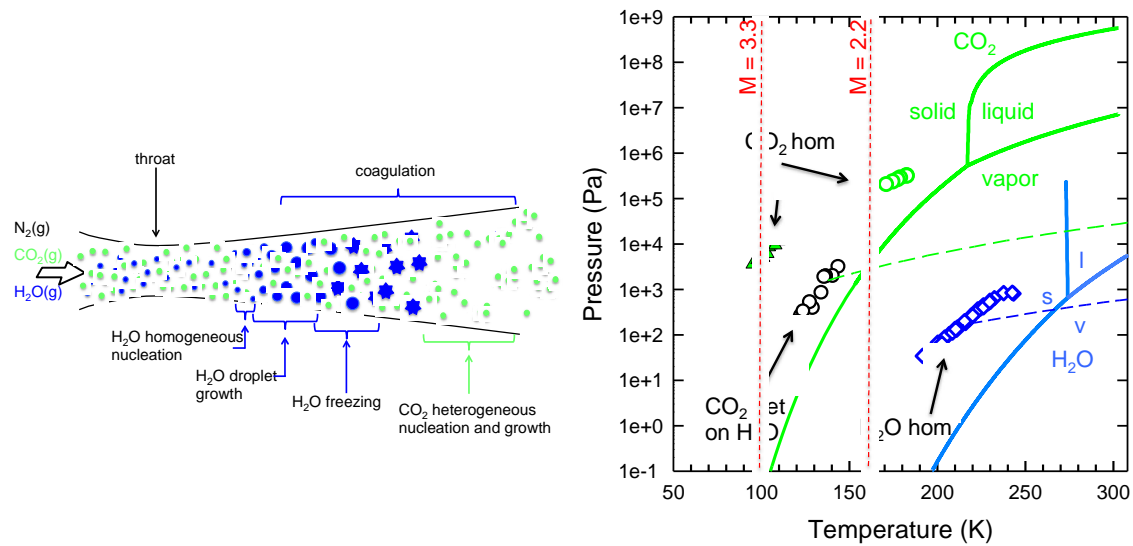
Figure 4: Heterogeneous nucleation in a supersonic nozzle. **(left)** As water vapor and CO_2 flow through a supersonic nozzle, water condenses and freezes at temperatures well above the sublimation temperature for CO_2. Further cooling of the flow initiates heterogeneous nucleation of CO_2 onto the frozen water droplets. **(right)** On a combined phase diagram for CO_2 (green) and H_2O (blue), the solid lines indicate the equilibrium phase boundaries for the solid, liquid and vapor regions. The conditions corresponding to the homogeneous nucleation of water[6] and CO_2 in supersonic flows are indicated by the blue and green symbols. The circles are from Duff[3] and the triangles are our estimates based on the theory corresponding states.[7] The black symbols are our very recent measurements for the onset of heterogeneous nucleation of CO_2 on water particles. The dashed lines trace the *p-T* history of CO_2 (green) and H_2O (blue) as a mixture (14.5% CO_2, 0.75% H_2O, balance N_2) containing these species expands across the nozzle from $T_0 = 308$ K and $p_0 = 2$ atm. The red vertical lines correspond to the indicated Mach numbers. Water condenses when the blue dashed line intersects the blue diamonds. CO_2 condenses heterogeneously when the green dashed line intersects the black circles. To our knowledge these are the first deliberate and well characterized heterogeneous nucleation experiments conducted in a supersonic nozzle.

CO_2 condensation is initiated at much higher temperature or lower pressure/Mach number than expected for homogeneous condensation, greatly affecting separator design.

5.3 A condensation model in 1-D supersonic flow (Deliverable 1.4)

5.3.1 Flow equations

One-dimensional adiabatic steady flow of a gas mixture in a supersonic nozzle is governed by the following four equations.

$$\rho u du = -dp \qquad \text{(momentum equation)}, \qquad (1)$$

$$\rho u A = \rho^* u^* A^* \qquad \text{(continuity equation)}, \qquad (2)$$

$$h + u^2/2 = h_0 \qquad \text{(energy equation)}, \qquad (3)$$

$$p = \rho(R/\mu_{av})T = \rho n^m RT \qquad \text{(equation of state)}, \qquad (4)$$

where ρ, u, and p are the mass density, velocity, and static pressure of the flowing gas, respectively, A is the effective flow area, and the asterisk denotes the values of the variable at the nozzle throat. The specific enthalpy of the gas mixture, including the condensate, is denoted by h and h_0 is the value of h under the stagnation conditions, i. e., when $u = 0$. μ_{av} denotes the average molecular weight of the gas mixture, including any particles (clusters + droplets). R is the universal gas constant and $n^m = 1/\mu_{av}$ denotes the total moles of gas molecules (monomers) and particles per unit mass of the mixture.

In the condensing flow h can be expressed as

$$h = h_0 + \int_{T_0}^{T} c_{p-gas}^0 dT - q, \qquad (5)$$

where q is the heat release per unit mass of the system either by a phase change (particle formation/growth) or by small cluster formation. The isobaric specific heat capacity of the gas mixture in the fictitious state where neither condensation nor clustering occurs, c_{p-gas}^0, is given by

$$c_{p-gas}^0 = \omega_{inert} c_{p-inert} + \sum_i \omega_i c_{p-i(v)}^0 . \qquad (6)$$

Here $c_{p-inert}$ is the isobaric specific heat capacity of the carrier gas (nitrogen in our case), and $c_{p-i(v)}^0$ is that of condensable species i (CO_2 and H_2O) in the ideal gas state (i.e. at infinitely low density). The mass fraction of the condensable species i, ω_i, is constant across the nozzle as is ω_{inert}, the mass fraction of the carrier gas. (g_{inf} used in the expression g/g_{inf} is the same as $\omega_\square$). The molar density per unit mass, n^m, is expressed by

$$n^m = \frac{\omega_{inert}}{\mu_{inert}} + \sum_i \left(\frac{\omega_{vi}}{\mu_{vi}} \right) + \frac{\omega_{cls}}{\langle \mu_{cls} \rangle} + \frac{\omega_c}{\langle \mu_c \rangle} . \qquad (7)$$

Here, the molecular weight and mass fraction are μ and ω, respectively, and the subscripts, *inert*, *vi*, *cls*, and *c* denote the inert carrier gas, the condensable vapor of species *i*, the small clusters, and the condensate (droplets) respectively. The angle brackets $\langle \ \rangle$ indicate the number-averaged value. Generally, and in this study, the term $\omega_c/\langle\mu_c\rangle$ can be neglected because the average molecular weight of the droplets $\langle\mu_c\rangle$ is large. We also neglected the effect of the clustering. That is, in Eq. (7) we set

$$\frac{\omega_{cls}}{\langle\mu_{cls}\rangle} = \frac{\omega_c}{\langle\mu_c\rangle} = 0 . \tag{8}$$

The mass fraction of condensate of species *i*, g_i, is related to *q* by

$$q = \sum_i g_i \, \Delta h_{vap-i} \big/ \mu_{vi} \quad , \tag{9}$$

where Δh_{vap-i} is the molar heat of vaporization of species *i* in the bulk phase at the same temperature as in the gas phase. For CO_2 solid or H_2O solid (ice), molar heat of sublimation, Δh_{sub} was used. The mass fraction ω_{vi} (Eq. 7) is related to g_i by $\omega_{vi} = \omega_i - g_i$.

5.3.2 The OSU condensation model

A model of particle formation and evolution in the ICES device or the OSU supersonic nozzles solves Eqns. (1) – (4), where the value of g_i includes contributions from nucleation as well as particle growth. A fully predictive model would include accurate expressions for the homogeneous nucleation of water, the growth and subsequent freezing of the water droplets, heterogeneous nucleation of CO_2 onto the water-ice particles and further condensational growth, as well as particle coagulation.

The basic physics of the problem can still, however, be explored without this level of detail. In the simplified OSU model we introduce an exiting aerosol, either nanometer sized water particles or micron size CO_2 particles of a prescribed size, into the supersonic flow. We then estimate CO_2 condensation or evaporation using the appropriate growth model, and track the state of the flow (*p, T, ρ, u*) as well as the particle size and the distribution of CO_2 between the phases. The shape of the expansion is also an input parameter and lets us explore alternative nozzle profiles.

5.3.3 Droplet Growth models

Droplet growth is a dynamic process. The net growth rate is governed by the difference between the rate at which vapor molecules are incorporated into the droplet and the rate with which monomers evaporate from the droplet. Since the condensing vapor releases heat, the temperature of a growing droplet is higher than that of the surrounding gas and the monomer evaporation rate increases above that for a droplet in thermal equilibrium with its surroundings.

The equations used to describe the coupled mass and heat transfer problem depend on the Knudsen number, $Kn = l_{mf}/2\langle r \rangle$, where l_{mf} is the mean free path of a vapor molecule and $\langle r \rangle$ is the average radius of the droplet. In the free molecular regime, $\langle r \rangle$ is significantly smaller than l_{mf} and Kn is much larger than 1. In the continuum regime $\langle r \rangle$ is significantly larger than l_{mf} and Kn is much smaller than 1. Since experiments were conducted in both regimes, we will present the droplet growth laws applicable to each regime.

5.3.3.1 Free molecular regime

In the free molecular regime droplet growth is described by the Hertz-Knudsen (HK) droplet growth model,

$$\frac{dr}{dt} = \frac{v_l}{\sqrt{2\pi m_v k_B}} \left(q_c \frac{p_v}{\sqrt{T}} - q_e \frac{p_{eq}(\langle r \rangle, T_d)}{\sqrt{T_d}} \right), \tag{1}$$

an expression that is based on the kinetic theory of gases.[8] In Equation (1), t is time, m_v is the mass of a monomer, k_B is the Boltzmann constant, T is the temperature of the vapor phase, v_l is the molecular volume of the condensate, q_c and q_e are condensation and evaporation coefficients, respectively, p_v is the partial pressure of the vapor, and $p_{eq}(\langle r \rangle, T_d)$ is the equilibrium vapor pressure above the drop of radius $\langle r \rangle$ at temperature T_d. The Kelvin-Helmholtz equation relates $p_{eq}(\langle r \rangle, T_d)$ to the physical properties of the condensate by,

$$p_{eq}(\langle r \rangle, T_d) = p_{eq}(T_d) \exp\left(\frac{2\zeta v_l}{k_B T_d \langle r \rangle} \right) = p_{eq}(T_d) \exp(Ke) \tag{2}$$

where $p_{eq}(T_d)$ is the equilibrium vapor pressure over a flat surface at temperature T_d, and ζ is the surface tension of the liquid. Finally, $Ke = 2\zeta v_l/(k_B T_d \langle r \rangle)$ is the Kelvin number.

When modeling in the free-molecular regime, we simplified this equation by assuming
  1. $T_d = T$ (isothermal droplet growth)
  2. the Kelvin effect is negligible i.e pressure above the small drop is the same as the pressure above a flat surface.
  3. and $q_e = q_c$.

Although the finer details of the process are not described accurately by this approach, the basic physics is still captured adequately. Incorporating these assumptions, the change in the droplet radius due to the condensation of CO_2, can be written as

$$\frac{dr}{dt} = \text{Impingement Rate} \times \left(1 - 1/S_{CO2}\right) \times v_{CO2} \times q_c \tag{10}$$

where S_{CO2} denotes the supersaturation ratio of CO_2 relative to the vapor pressure of solid CO_2 or (supercooled) liquid CO_2. The molar volume of CO_2, $v_{CO2} = \mu_{CO2}/\rho_{CO2}$, where ρ_{CO2} is the density of CO_2 and μ_{CO2} is the molar weight of CO_2. q_c is the condensation coefficient of CO_2.

The impingement rate is given by

$$\text{Impingement Rate} = \frac{p_{CO2}}{RT} \sqrt{\frac{RT}{2\pi\mu_{CO2}}} \tag{11}$$

where p_{CO2} is the partial pressure of CO_2, and T is the temperature.

The initial value of r at the onset point of CO_2 condensatation, r_0 is given by

$$\rho_{H2O} N_{drop} \frac{4\pi}{3} r_0^3 = g_{H2O} = \omega_{H2O}, \tag{12}$$

where we assume all of the H_2O in the flow has condensed and frozen before the flow reaches the onset point of CO_2 condensation. That is $g_{H2O} = \omega_{H2O}$ and ρ_{H2O} is the density of ice. N_{drop} denotes the number of the ice particles per unit mass, which was estimated to be about 4×10^{19} kg^{-1} based on our extensive studies of H_2O condensation.[6] N_{drop} was assumed to be constant downstream of the onset point, that is, the effect of the coagulation was neglected.

Finally, the mass fraction of condensate of CO_2, g_{CO2} is determined by

$$g_{CO2} = \frac{4\pi}{3}\left(r^3 - r_0^3\right)\rho_{CO2} N_{drop} \tag{13}$$

5.3.3.2 Continuum regime

When the particle size is significantly larger than mean free path of the condensing molecules, particle growth is in the continuum regime. Under these conditions, the non-isothermal growth model is given by Eqs. (15) - (17).

$$J_m = \mu_{vi}\left(\frac{D(T_m)}{rRT_m}\right)\left(p_{vi} - p_i(T_d)\right), \tag{15}$$

$$J_h = \left(\frac{k(T_m)}{r}\right)\left(T_d - T_g\right), \tag{16}$$

$$T_m = (2T_d + T_g)/3, \tag{17}$$

where, mass flux (kg m^{-2}s^{-1}), J_m, and heat flux (J m^{-2}s^{-1}), J_h, are expressed by the diffusion coefficient D and thermal conductivity k at the intermediate temperature T_m, respectively. The equilibrium vapor pressure of condensate (CO$_2$) is denoted by $p_i(T_d)$, the effect of curvature on which was neglected here. The partial pressure of condensate in vapor phase is p_{vi}. The droplet temperature T_d was determined by solving the Eq. (18)

$$J_h = J_m \left\{ \Delta h_{vap-i}(T_d) \middle/ \mu_{vi} - (T_d - T_g) c^0_{p-i(v)} \right\}. \tag{18}$$

The change in the droplet radius due to the condensation of CO$_2$, dr/dt is calculated as

$$\frac{dr}{dt} = v_{CO2} J_m \tag{19}$$

$$g_{CO2S} = \frac{4\pi}{3} r^3 \rho_{CO2} N_{drop}, \tag{20}$$

where, N_{drop} denotes the number of the droplets per unit mass, which was estimated from the g_{CO2S} and the diameter of the droplet. N_{drop} was assumed to be constant downstream of the onset point, that is, the effect of the coagulation was neglected. The molar volume of CO$_2$ is v_{CO2}.

5.3.4 Droplet Coagulation

We did not consider the role of coagulation in any of the modeling. For particle number densities on the order of 10^{13} cm^{-3}, particle coagulation will reduce the number density by about an order of magnitude on the order of 100 microseconds. Since the coagulation rate depends on N^2 reducing the concentration by another order of magnitude with take correspondingly longer.

5.3.5 Light Scattering

The equations used to estimate the energy reaching the detector during the light scattering experiments are summarized in the appropriate sections of the report.

6. Experimental and Modeling Tasks (Deliverables 2 and 3)

Experiments were conducted to
1. Demonstrate that the 2 step condensation process predicted by analysis of the phase diagram is correct (**Baseline Experiment, Deliverable 2**).
2. Quantify the degree of CO_2 recovery as a function of H_2O and CO_2 concentration and nozzle expansion rate (**Baseline Experiment, Deliverable 2**).
3. Characterize the size of the particles produced (**Baseline Experiment, Deliverable 2**).
4. Investigate the effect of inducing turbulence in the flow on particle size. (**Flow Perturbation Experiment, Deliverable 3**).
5. Investigate the feasibility of injecting micron size CO_2 droplets (particles) into the flow to collect CO_2 (**Seed Particle Injection Experiment, Deliverable 3**).

Models of particle growth were completed to complement and better understand the experiments.

6.1 Experimental setup

The basic experimental setup used in this work is illustrated in **Figure 5**. Modifications made to incorporate light scattering or CO_2 liquid injection are detailed in the results sections. As illustrated in **Figure 5**, the carrier gas, N_2, is supplied from the gas side of two liquid N_2 tanks. This flow is heated to room temperature, the pressure is regulated, and the flow rates are controlled using MKS mass flow controllers. One of the streams is split further into two streams, heated to ~ 50 C and enters the vaporizer where liquid water is dispersed as a fine spray and then evaporated. CO_2 is supplied by two high pressure cylinders. The CO_2 flows are heated, combined and the mass flow rates is controlled by a third MKS mass flow controller. The temperature of the combined carrier
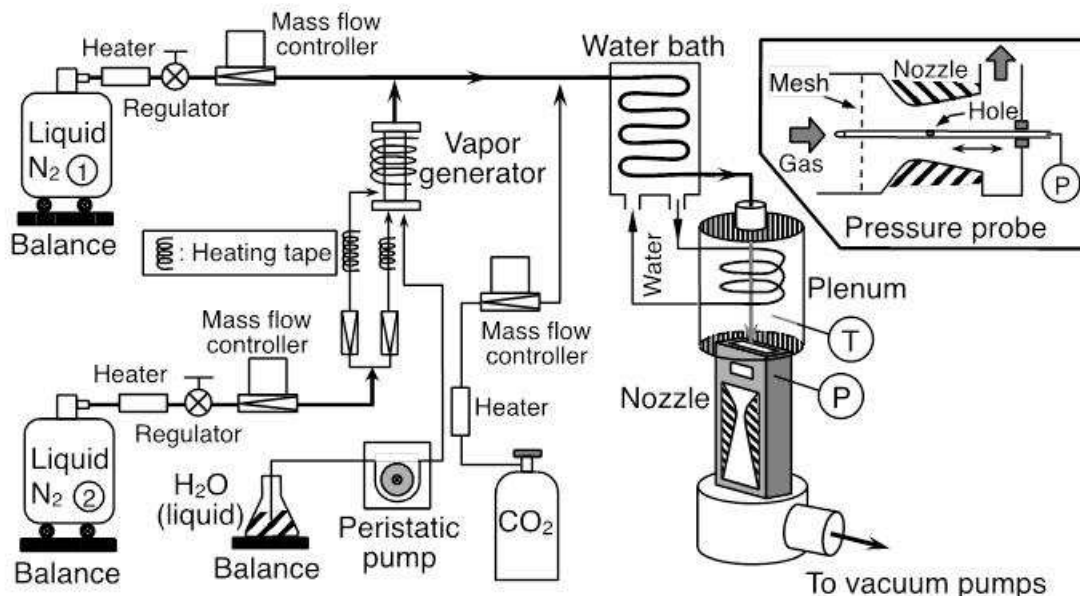
Figure 5: A schematic diagram of the experimental setup.

gas – condensable mixture is controlled by the water bath. As the gas mixture flows through the plenum the Mach number is ~0 and the stagnation temperature and pressures are measured. The flow then enters the nozzle, expands and cools inducing particle formation and growth. The pressure drop required for supersonic flow is provided by two rotary vane vacuum pumps.

6.2 Pressure trace measurements (PTM)

In these experiments we measure the static pressure p along the nozzle axis for both the pure carrier gas and the condensing vapor mixtures using a movable static pressure probe (Fig. 5 inset). In the absence of condensation, we can directly determine the effective area ratio $(A/A^*)_{dry}$ of the nozzle, where A^* is the area of the throat. Because phase transitions are accompanied by latent heat release, we observe condensation as a deviation of the pressure (or ρ or T) from the isentropic profile. We derive initial estimates for the other properties of the condensing flow (u, T, ρ, condensate mass fraction g), by integrating the diabatic flow equations (Equations 1 – 4) using p and $(A/A^*)_{dry}$ as the known quantities. We can improve these estimates by incorporating light scattering results, and iteratively solve the flow equations using p and g as the known quantities. Either way, the pressure trace measurements rapidly establish the limits to which the vapor (liquid) can be supersaturated before the vapor-to-liquid (liquid-to-solid) phase transitions of water occur and the subsequent heterogeneous nucleation of CO_2 onto the seed particles takes place.

6.3 Baseline Experiments

After demonstrating that we could run under the desired inlet conditions ($p_0 = 2$ atm), we adjusted the nozzle shape until we could reach temperatures low enough to induce CO_2 heterogeneous condensation. The nozzle shapes are characterized in Table 1 with respect to their effective expansion rates for N_2 starting at $p_0 = 2$ atm.

   Figure 6 illustrates a typical pressure trace made using nozzle T1R1. As illustrated in this figure, the heat release is first observed at temperatures and partial pressures where water vapor is highly supersaturated but CO_2 vapor is still subsaturated with respect to the condensed phases. As the first fragments of the new liquid phase grow, the heat released into the surrounding gas mixture due to the phase transition increases the temperature and the pressure slightly above that of the isentropic expansion of the same gas mixture in the absence of condensation. This heat release then quenches nucleation after ~10 μs, leaving a relatively monodisperse liquid H_2O aerosol. Shortly after their formation, the rapidly growing droplets are hotter than the carrier gas, but as growth slows, the droplets quickly cool to closely match the temperature of the carrier gas. Once most of the H_2O vapor has condensed, the pressure and temperature start to decrease

Table 1: Characteristics of the nozzles used.

Nozzle	d(A/A*)/dx (cm^{-1})	A* (cm^2)	Mexit
T1	0.17	0.290	2.6
T2	0.28	0.168	3.0
T3	0.38	0.126	3.3
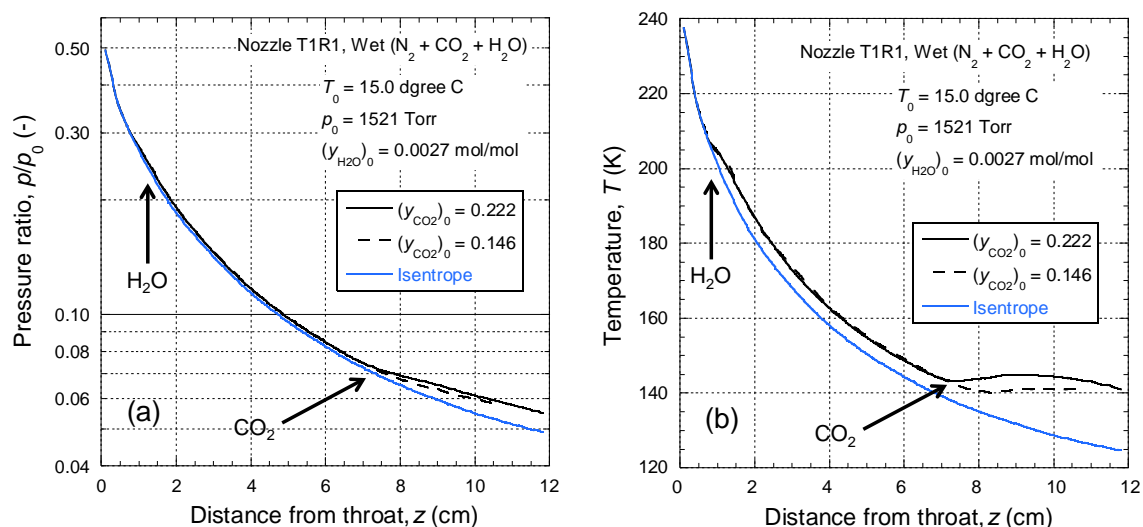
Figure 6. Heterogeneous nucleation of CO_2 on H_2O. The static pressure ratios **(a)** and temperatures **(b)** in the presence (black lines) and absence (blue line) of H_2O. The expansion is isentropic and CO_2 does not condense when H_2O is absent. The inlet concentration of water is fixed at a mole fraction of 0.0027, and the onset of water condensation is indicated by the leftmost arrow in the pressure/temperature plots. The onset of CO_2 condensation (right arrow) moves to higher pressure and temperature as the mole fraction of CO_2 $(y_{CO2})_0$ increases, but always occurs at temperatures significantly colder than those required for the condensation of water.

again, roughly parallel to the isentropic expansion, and the water droplets freeze. At still lower temperatures, the supersaturation of CO_2 increases to the point where heterogeneous nucleation begins. The large heat release seen in **Figure 6** as CO_2 condenses relative to that observed for H_2O, reflects the much higher concentration of CO_2 in the incoming stream.

Despite their apparent simplicity, PTMs provide significant insights into heterogeneous nucleation. As illustrated in **Figure 7**, as the vapor mixture expands and cools (from right to left) along an isentrope, the heat release due heterogeneous CO_2 condensation produces a "kink" in the curve. In all cases, heterogeneous nucleation is delayed far beyond the saturated solid-vapor line. Instead, heterogeneous nucleation consistently starts near the extrapolated vapor-liquid equilibrium line. In the context of the water ice-nucleation literature,[9] this means that solid water is a poor CO_2 ice nucleator. The effect of particle size is also quite clear. Comparing two cases with the same nominal CO_2 mole fraction, heterogeneous nucleation is significantly delayed for the lower water vapor experiment (dashed green curve) where the ice seed particles are smaller.

Finally, **Figure 7** also suggests that even if heterogeneous nucleation is initiated by the formation of liquid-like critical clusters, continued heat release at temperatures above the
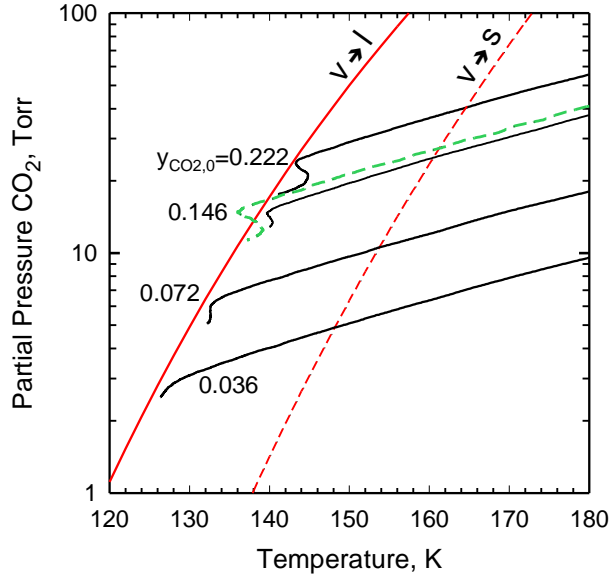
Figure 7. Five expansions histories in *p-T* space, including those illustrated in Fig. 6, together with the solid-liquid[10] (dashed red line) and extrapolated vapor-liquid[11] (solid red line) equilibrium curves of CO_2. The black lines correspond to heterogeneous condensation experiments at an initial H_2O mole fraction $(y_{H2O})_0 = 0.0027$ and the indicated values of $(y_{CO2})_0$. The dashed green line corresponds to fixing $(y_{CO2})_0 = 0.146$ and decreasing H_2O to $(y_{H2O})_0 = 0.0009$. The onset of heterogeneous CO_2 nucleation and growth corresponds to the first "kink" in the *p-T* curve, close to the extrapolated vapor-liquid curve. At the conditions corresponding to heterogeneous nucleation, the vapor is highly supersaturated with respect to the solid. The effect of particle size is observed indirectly; heterogeneous CO_2 condensation is delayed at lower water vapor concentrations, because the seed particle size decreases as roughly $(y_{H2O})_0^{1/3}$.

extrapolated vapor-liquid equilibrium curve means that the growing particles are solid. If the droplets were liquid, they would evaporate.

Although experiments in Nozzle T1R1 clearly confirmed that CO_2 condensation in the ICES device would be driven by heterogeneous rather than homogeneous nucleation, the fraction of CO_2 entering the nozzle that had condensed by the exit was rather low – at most ~9%. Thus, nozzles T2 and T3 were designed to decrease the temperature and increase the CO_2 removal efficiency. **Figure 8** summarizes the results of the pressure measurements conducted with nozzle T3. Although the fraction of CO_2 condensed increases over that observed in Nozzle T1R1, when the mole fraction of CO_2 =14.5%, the amount of solid CO_2 condensed (20%) is still far below the target value of 90% CO_2.

A well recognized problem associated with working with small nozzles is that condensation can change the shape of the effective expansion by compressing the boundary layer.[12] Thus, the pressure measured down stream of condensation is lower than it would be if the boundary layer were stable, as are the estimates for *T* and *g*, and condensation appears to slow rather abruptly. To investigate whether this could be an issue in the current experiments we modeled heterogeneous condensation of CO_2 in the
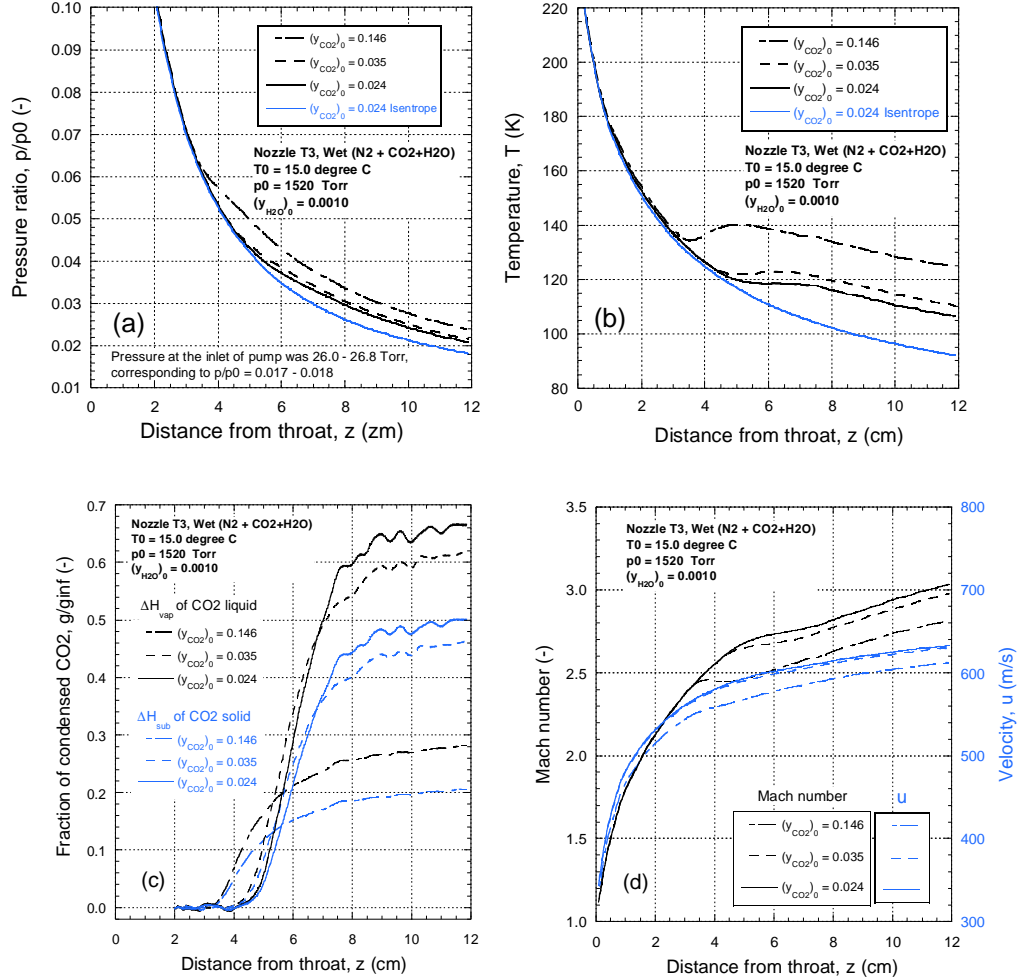
Figure 8: Heterogeneous nucleation experiments of CO_2 on H_2O in Nozzle T3. **(a)** The static pressure ratios, **(b)** temperatures, **(c)** fraction of CO_2 condensed, and **(d)** Mach number and velocity. Although the fraction of CO2 condensed calculation shows the results for condensation of the liquid and solid, the results in Figure 7 suggest that the particles consist of solid CO_2.

nozzle using the modeled described earlier. The simplifying assumptions include:
  (i) the flow is one dimensional
  (ii) droplet growth is isothermal, governed by Eq (10), but q_c is not necessarily 1
  (iii) the number of ice particles per unit mass, $N_{drop} = 4 \times 10^{19}$ kg^{-1} (based on previous experimental results)
  (iv) CO_2 condensation starts when the saturation relative to the liquid, $S_{CO2} = 1$ (based on current experiments)
  (v) CO_2 is assumed to condense either as a liquid or as a solid
  (vi) the mass fraction of CO_2 condensate is given by Eq. (13) and the seed particle size is set by the mass fraction of water and N_{drop}.

Figure 9 illustrates the results of modeling CO_2 condensation on ice particles in Nozzle T3. The conditions correspond to the experiments summarized in **Figure 8** for the highest concentration of CO_2. In these models we assumed that the condensate consisted of either

17
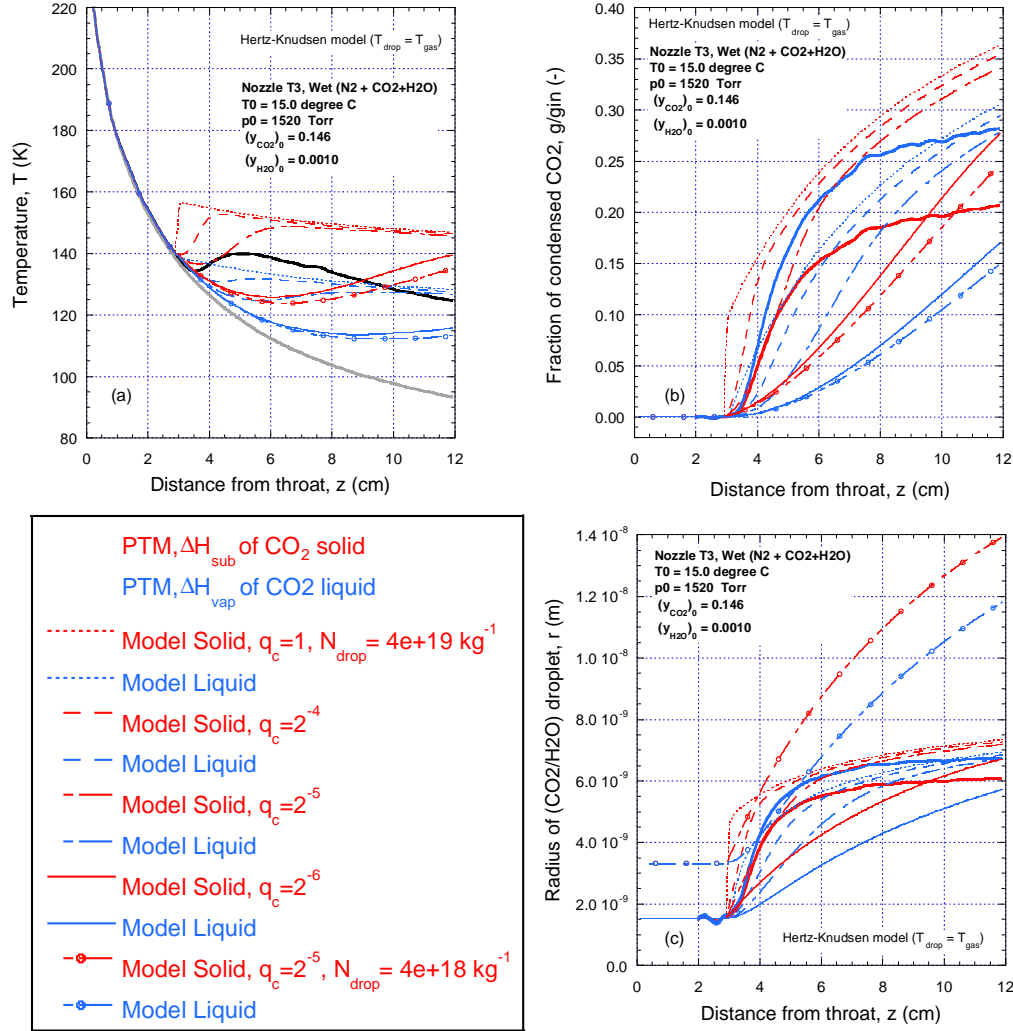
Figure 9: Heterogeneous nucleation of CO_2 on H_2O. **(a)** The static pressure ratios **(b)** temperatures **(c)** fraction of CO_2 condensed, **(d)** Mach number and velocity.

liquid or solid, and we adjusted the condensation coefficient q_c to find the value that best matched the experimental results. During rapid condensation, using $q_c<1$ is an easy way to mimic the effect of non-isothermal growth. We also considered the case of $N_{drop} = 4\times10^{18}$ kg^{-1} in order to test the sensitivity of the model to the assumed particle concentration.

As illustrated in all parts of **Figure 9**, the model does not match the data when we assume that the condensate is liquid. Even when $q_c = 1$, the temperature does not increase rapidly enough, and condensate mass fraction is generally lower than the experimental values. This result confirms our earlier analysis, based on **Figure 7**, that the condensate is solid. In contrast, assuming the condensate is solid the model matches the data quite nicely over the initial stages of condensation when $q_e=2^{-5}$. For z >~5 cm, however, the model predicts that condensation should continue and reach significantly higher values than those derived from the PTM. The mismatch between the observed and modeled condensate mass fraction suggests that boundary layer compression plays a role in these

experiments. Finally, decreasing N by an order of magnitude increases the predicted size of the droplets at the nozzle exit but decreases the condensate mass fraction (for $q_c=2^{-5}$).

Based on the modeling results, we therefore turned to light scattering as an alternate way to estimate the mass fraction of condensate, and to confirm our estimates for N and $<r>$. Although small angle X-ray scattering (SAXS) would be a better technique than visible light scattering, we did not have time to do SAXS experiments as part of this program.

6.4 Light Scattering Experiments

Figure 10 illustrates the final light scattering setup developed to investigate the growth of aerosol formed by heterogeneous condensation of CO_2 on water ice. With slight variations, this setup was calibrated by comparing light scattering from pure water droplets and pure nonane droplets to previous X-ray scattering measurements as described below.
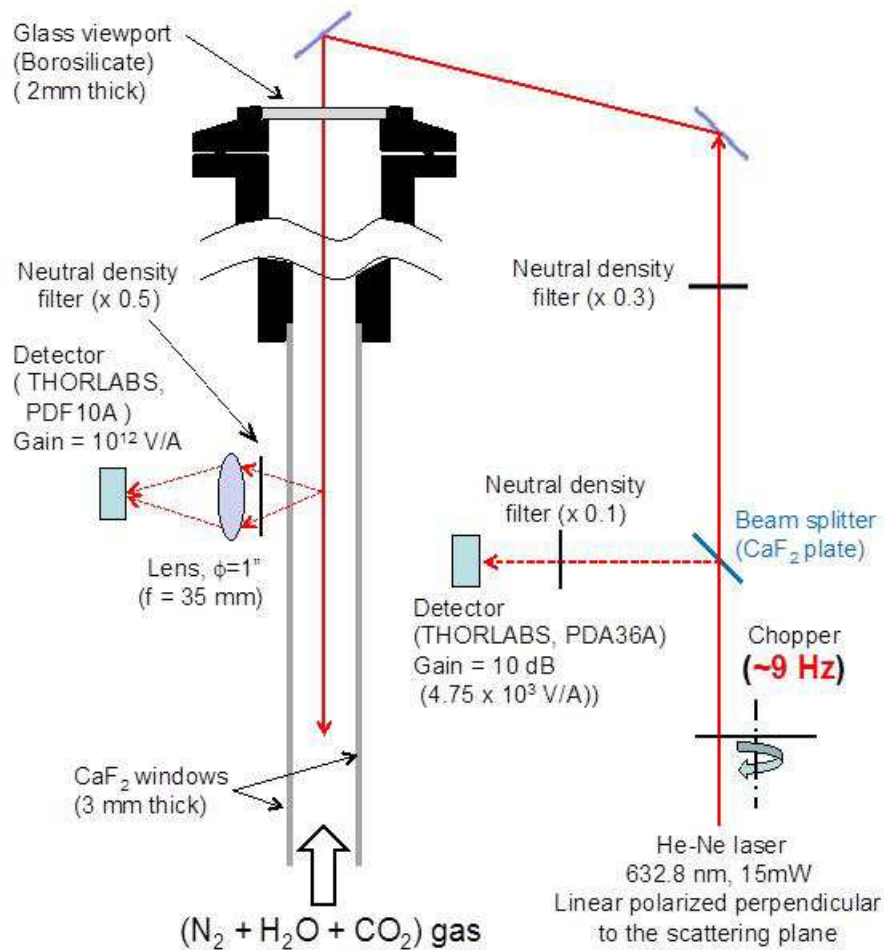
Figure 10: In the light scattering setup, the beam travels along the nozzle axis entering from the downstream end of the nozzle. Scattered light is detected at 90 degrees.

6.4.1 Light Scattering Theory: Rayleigh scattering

For the particles formed by heterogeneous condensation of CO_2 on homogeneously nucleation ice particles, the radius of the particles, r is much smaller than the wavelength of the laser light, λ, and scattering is in the Rayleigh regime. For the Rayleigh scattering, the relationship of the intensities of the incident light I_i and the scattered light from a single particle, $(I_s)_{one}$, is expressed by Eq. (21) or Eq. (22) depending on the polarization of the light.

When the incident light polarized perpendicular to the scattering plane,

$$\left(I_s\right)_{one} = \frac{16\pi^4 n^4 r^6}{\lambda^4 l^2} \left(\frac{m^2 - 1}{m^2 + 2}\right)^2 I_i \ , \tag{21}$$

and when the incident light polarized parallel to the scattering plane

$$\left(I_s\right)_{one} = \frac{16\pi^4 n^4 r^6}{\lambda^4 l^2} \left(\frac{m^2 - 1}{m^2 + 2}\right)^2 \left(\cos^2 \theta\right) I_i \ . \tag{22}$$

Here n is the refractive index of medium, and $m \equiv n_1/n$, where n_1 is the refractive index of particle. The scattering angle and distance from the particle to the lens are denoted by θ and l, respectively.

In dilute systems, that is, when the number density of particles is low as in the case of condensation in supersonic nozzle, the intensity of light scattered from the particles is the summation of the single particle scattering intensities $(I_s)_{one}$, and the total energy of the scattering light, which reach a detector, $(E_s)_{detect}$ is calculated by

$$\left(E_s\right)_{detect} = I_i N_{drop} \iint \left(I_s\right)_{one} l^2 d\Omega dv_s \ , \tag{23}$$

where $(I_s)_{one}$ is integrated with respect to the scattering volume v_s and solid angle Ω as shown in **Figure 11**. The number density of particles is denoted by N_{drop}, and l is the distance between the particles and the lens. Combining Eqs. (22) and (23) gives
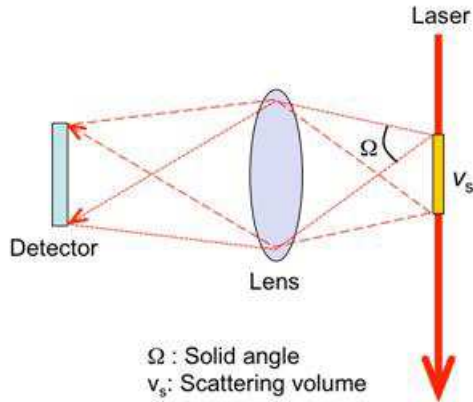
Figure 11: Geometric constraints determine the amount of light reaching the detector.

$$\left(E_s\right)_{\det ect} = I_i N_{drop} \frac{16\pi^4 n^4 r^6}{\lambda^4}\left(\frac{m^2-1}{m^2+2}\right)^2 \iint (\text{Function of } \theta)d\Omega dv_s , \qquad (24)$$

where the integral depends on the geometry of the detector, lens, and laser beam, and is independent of the properties of the particles.

6.4.2 Calibrating the light scattering setup

The parameters in Eq. (24) that depend on the condensable species are r, m, and N_{drop}. The refractive index of medium (carrier gas in our case) can be assumed to be unity. If the setup of the light scattering measurement does not change, λ and the integral quantity do not change, and $(E_s)_{detect}$ can be expressed using a constant correction factor f_c, as

$$\left(E_s\right)_{\det ec} = f_c I_i N_{drop} V_{drop}^2 \left(\frac{n_1^2-1}{n_1^2+2}\right)^2 , \qquad (25)$$

where V_{drop} denotes the volume of a particle and comes from r^6.

We can also rewrite Eq. 25 in terms of the energy of incident laser E_i

$$\left(E_s\right)_{\det ec} = f_c' E_i N_{drop} V_{drop}^2 \left(\frac{n_1^2-1}{n_1^2+2}\right)^2 , \qquad (26)$$

and determine the correction factor f_c' in Eq. (26), by comparing the measured energy of the scattered light to that expected based on the SAXS measurements. Any loss of energy due to reflections throughout the system is incorporated into the correction factor. We did this for a H_2O condensation experiment[1] in nozzle C3 at $T_0 = 308$ K, $p_0 = 227$ Torr, $(y_{H2O})_0 = 0.019$. The values of the parameters in Eq. (26) at $z = 4.9$ cm determined from SAXS or measured in the light scattering experiment were:

$(E_s)_{detect} = 7.1 \text{ x } 10^{-13}$ W
$E_i = 1.7 \text{ x } 10^{-3}$ W
$N_{drop}V^2_{drop} = 3.1 \text{ x } 10^{-30}$ m^3 (from SAXS)
refractive index of water: $n_1 = 1.33$

These values yielded the value of $f_c' = 3.3 \text{ x } 10^{21}$ m^{-3}.

We then tested the robustness of our approach by measuring the light scattering from nonane droplets formed in the same nozzle and for which we also have position resolved SAXS data.[1] As illustrated in **Figure 12**, the agreement between the measured values of $(E_s)_{detect}$ (output voltages of detector (PDF10A)) and those predicted using $f_c' = 3.3 \text{ x } 10^{21}$ m^{-3}, the index of refraction for nonane $n_1 = 1.405$, and the values of $N_{drop}V^2_{drop}$ determined from SAXS is quite good. The differences between the two at the lowest values of z are most likely due to the rapid increase in scattering from the nozzle walls near the throat. Thus, near the throat the difference signal is the result of subtracting two relatively large numbers and is therefore more uncertain.
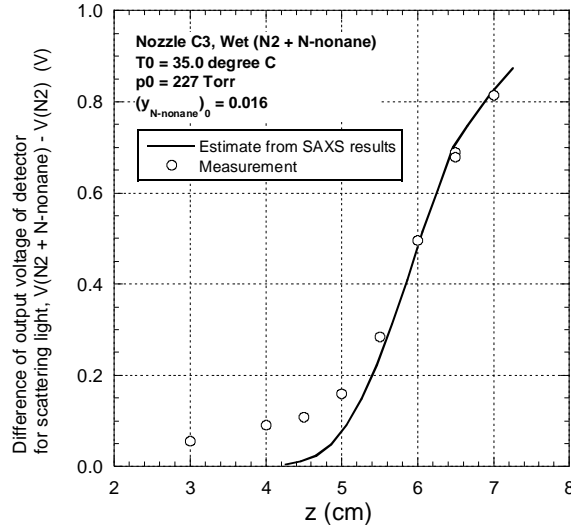
Figure 12: The difference in voltage between the experiments in which nonane is condensing and the dry trace. The symbols are the experimental values the black line is estimated based on the calibration factor established for water and the SAXS measurements.

6.4.3 Light scattering measurements (LSM): heterogeneous CO_2 condensation

Two heterogeneous CO_2 condensation light scattering experiments were conducted using the "standard conditions" i.e. $p_0 = 1520$ Torr (2 atm), $T_0 = 15$ C, $y_{H2O} = 0.001$, and $y_{CO2} = 0.143$ or $y_{CO2} = 0.035$. The differences in the output voltage of the detector for scattering light between the condensing flow and dry flow are shown in **Fig. 13**. As indicated by the black filled circles in **Figure 13(left)**, the intensity of scattering light from the H_2O droplets is negligibly small. The open circles suggest that condensation of CO_2 starts
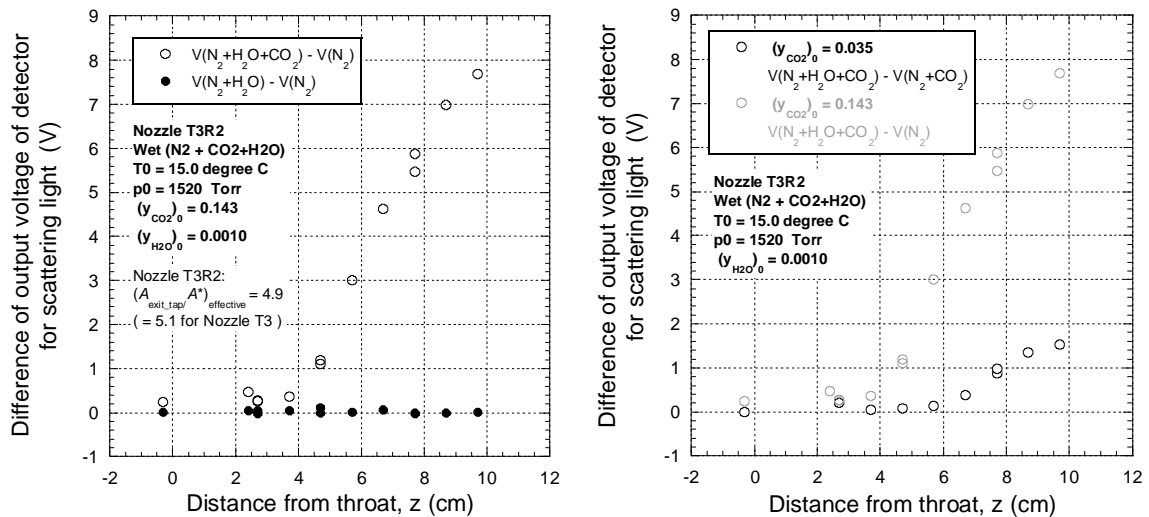
Figure 13: (left) The difference in voltage between the experiments in which H_2O alone (filled circles) or CO_2 + H2O (open circles) are condensing and the dry trace. **(right)** The difference in voltage between the experiments in which CO_2 + H_2O (open circles) are condensing and the dry trace – either N2 or N2+CO2 - for the experiments with $y_{CO2} = 0.035$ (dark) and those for $y_{CO2} = 0.143$ (light).

around z = 3 - 4 cm when y_{CO2} = 0.143 and near z = 6 cm y_{CO2} = 0.035, in agreement with our earlier pressure measurements.

To interpret the scattering signals more quantitatively we used the correction factor f_c established in the calibration measurements and the value of n_1 was assumed to be that of CO_2 solid, i.e. n_1 = 1.42 at λ = 632.8 nm because, as confirmed in **Figure 13**, the contribution of condensed H_2O on the intensity of scattering light is negligible. The value of $N_{drop}V^2_{drop}$ was determined as a function of the distance from the throat from the light scattering measurement using Eq. (26).

The quantity $N_{drop}V_{drop}$ can also be estimated from the mass fraction of condensed CO_2, g_{CO2}, derived from pressure trace measurement (PTM) as,

$$g_{CO2} = \left(N_{drop}V_{drop} / \rho - g_{H2O} / \rho_{H2O} \right) \rho_{CO2}. \tag{27}$$

In Eq. 27, ρ denotes the density of the gas mixture, derived from PTM, and ρ_{H2O} (= 930 kg/m^3) and ρ_{CO2} (= 1170 kg/m^3) are the densities of H_2O solid and CO_2 solid, respectively. The mass fraction of condensed H_2O, g_{H2O} should be the same as the mass fraction of all H_2O molecules, g_{inf}, because all H_2O molecules are expected to condense prior to the onset of CO_2 condensation.

Thus, N_{drop} and V_{drop} can be determined independently by combining the results of LSM and PTM as follows. The number density per unit volume, N_{drop} is related to the number density per unit mass, n_{drop} as

$$N_{drop} = \rho n_{drop}. \tag{28}$$

If we assume n_{drop} is constant in the nozzle, i.e. coagulation of droplets is neglected, then for a given value of value n_{drop}, g_{CO2} can be derived from the result of LSM, $N_{drop}V^2_{drop}$ using Eq. (27). We determined the value of n_{drop} so that the value of g_{CO2} from LSM agrees with that of g_{CO2} derived from PTM assuming that solid CO_2 grows on the droplet. We only considered the value of g_{CO2} slightly downstream of the onset point of CO_2 condensation because the values of g_{CO2} from PTM are known to be underestimated further downstream.

For $(y_{CO2})_0$ = 0.035 we estimated that the number density of the droplets per unit mass was n_{drop} = 9 x 10^{18} kg^{-1}. This value is about a factor of two larger than the estimate n_{drop} = 5 x 10^{18} kg^{-1} found for $(y_{CO2})_0$ = 0.143 - 0.146. The reason for this difference is not entirely clear. Flow disturbances due to the onset of condensation may affect the coagulation of the droplets, and/or the increase in temperature downstream of the onset point may accelerate Ostwald ripening – the evaporation of the smallest droplets and growth of the larger drops – more significantly at higher CO_2 concentrations. Both values of n_{drop} lie between the values we used in our initial modeling effort.

The chart shows the following legend and annotations:

$(y_{CO2})_0 = 0.035$
○ Light scattering (Nozzle T3R2)
-------- Model for solid droplet (Nozzle T3)
Number density, $n_{drop} = 9e{+}18$ kg^{-1}
Condensation coefficient, $q_c = 0.22$
$(y_{CO2})_0 = 0.143 - 0.146$
○ Light scattering (Nozzle T3R2)
Model for solid droplet (Nozzle T3)
$n_{drop} = 5e{+}18$ kg^{-1}
$q_c = 0.055$

Nozzle T3, T3R2
Wet (N2 + CO2+H2O)
T0 = 15.0 degree C
p0 = 1520 Torr
$(y_{H2O})_0 = 0.0010$

$(A_{exit\_tap}/A^*)_{effective} =$
5.1 in Nozzle T3
4.9 in Nozzle T3R2

Y-axis: Fraction of condensed CO$_2$, g/ginf (-)
X-axis: Distance from throat, z (cm)

Figure 14: The fraction of CO_2 condensed that was derived from pressure trace measurement (PTM, solid black line), light scattering measurement (LSM, open circles), and model calculations (dashed line).

Figure 14 summarizes the fraction of condensed CO_2, g/g_{inf} as estimated from the light scattering measurements (LSM), the PTM, and from model calculations. For both levels of $(y_{CO2})_0$ the value of g/g_{inf} from LSM, $(g/g_{inf})_{LSM}$ starts to deviate from $(g/g_{inf})_{PTM}$ near z = 6 cm. At the exit of nozzle, $(g/g_{inf})_{LSM}$ is about 70 % higher than $(g/g_{inf})_{PTM}$ at $(y_{CO2})_0$ = 0.143 - 0.146, and about 80 % higher at $(y_{CO2})_0$ = 0.035. At the lower CO_2 concentration these experiments suggest that *close to 80% of the CO_2 has condensed by the nozzle exit*!

The model calculations agree with the measured values of $(g/g_{inf})_{LSM}$ quite well for condensation coefficients q_c = 0.055 for $(y_{CO2})_0$ = 0.143 - 0.146, and q_c = 0.22 for $(y_{CO2})_0$ = 0.035. The difference in q_c is thought to be due to the effect of non- isothermal condensation. The droplet temperatures should be higher for higher $(y_{CO2})_0$ because the droplets are growing more quickly. Thus, the evaporation rate of molecules from the droplet should be higher at higher $(y_{CO2})_0$ leading to an apparent condensation coefficient q_c that is less than 1 and that decreases as $(y_{CO2})_0$ increases.

Figure 15 illustrates the change in the estimated radius of the H_2O/CO_2 particles as condensation proceeds. Particles are estimated to reach about 14 nm in radius at the exit of the nozzle for $(y_{CO2})_0$ = 0.143 - 0.146, or about 10 nm for $(y_{CO2})_0$ = 0.035. Thus, these particles are extremely difficult to remove via inertial separation.

24
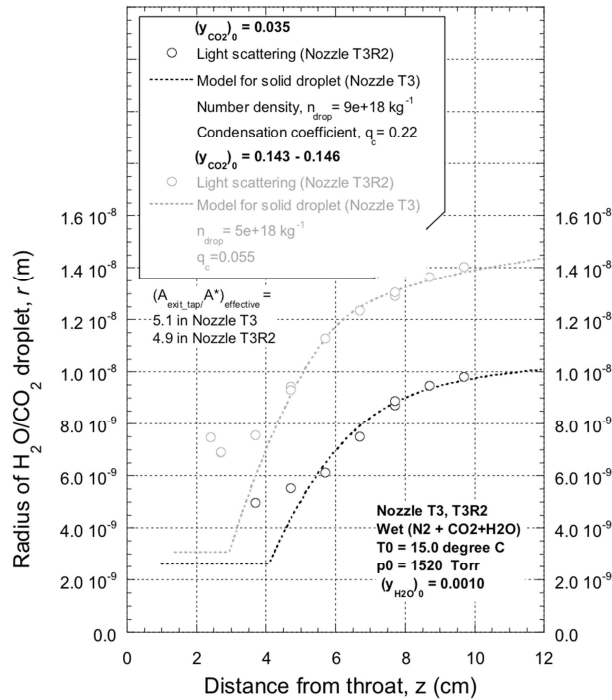
Figure 15: The size of the CO_2 particles derived LSM (circles) and model calculations (dashed lines).

6.5 Flow Perturbation Experiments

A limited set of experiments was conducted to investigate the possibility that perturbing the flow could enhance droplet coagulation and therefore increase the particle size. The light scattering setup illustrated in **Figure 10** was used to investigate this possibility with the one modification that a metal rod was inserted into the nozzle in order to disturb the supersonic flow. The rod and the arrangement of the rod in the flow is illustrated in **Figures 16.** In these experiments we changed the position (distance from throat) and angle (θ) of the metal rod and observed the intensity of scattered light at $z = 9$ cm, i.e. ~6 cm downstream of the onset of CO_2 condensation.
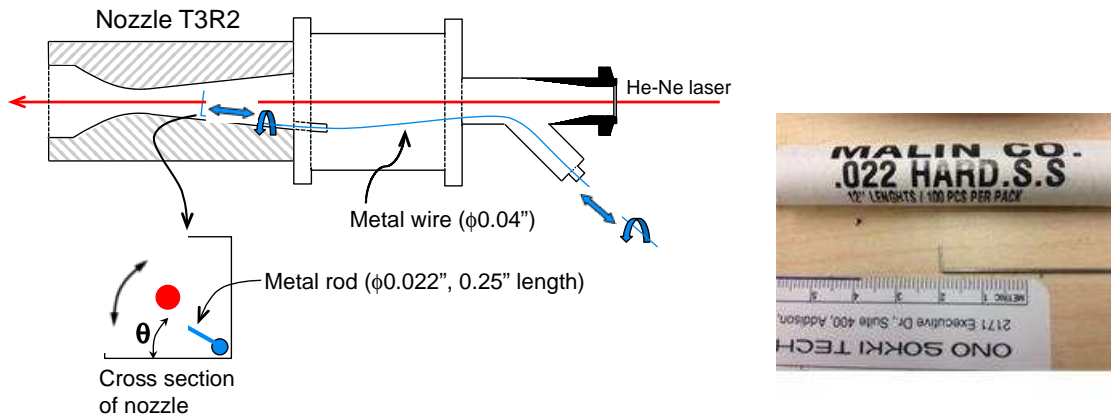
Figure 16: The experimental setup for the flow perturbation experiments.
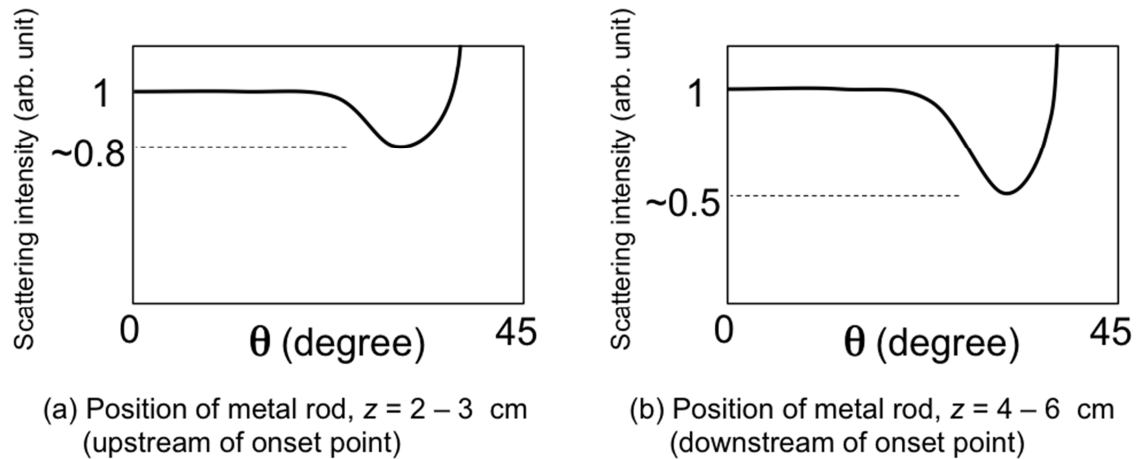
Figure 17: Qualitative light scattering intensity measured as a function of the angle of the flow perturbing rod.

The intensity of scattering light was very sensitive to the direction (θ) of the rod when the rod is near the laser light path, and it was not possible to determine the direction (θ) accurately. Hence, we could only qualitatively investigate the effect of the rod on the intensity of scattering light.

As shown in **Figs. 17(a) and 17(b)**, when θ is small, that is, when the rod is far from the region of the flow illuminated by the laser beam, the rod does not affect the intensity of scattering light. However, as the rod approaches the illuminated region, the light scattering intensity decreases, and then increases steeply as the rod crosses the region of the flow illuminated by the laser beam. The decrease in the intensity is more significant when the rod is downstream of the onset point of CO_2 condensation than it is when the rod is upstream of the onset point. At the same time that the intensity of scattered light decreases due to the presence of the rod, we also observed a decrease in the exit pressure. This suggests that the heat release due to condensation is lowered by the presence of the rod and, thus, the decrease in light scattering intensity may be due to a decrease in particle size/condensed CO_2.

The rod can raise the gas temperature both by decreasing the flow area (A/A^*) and by introducing warm air from the boundary layer around the rod into the flow. Any increase in the gas temperature caused by the rod will naturally slow droplet growth. A possible explanation for observation that the effect of the rod is smaller when the rod is upstream of the onset point is that only H_2O droplets exist in this region. Furthermore, the gas temperature is still far below the equilibrium value for H_2O at the experimental partial pressures, and thus evaporation of H_2O from the droplets should be insignificant even when the gas temperature increases. Furthermore, according to our model calculations, the effect of the number of H_2O droplets on the amount of CO_2 condensate at the exit of nozzle is insignificant. The concept that heat is added to the flow by the presence of additional surfaces in the flow was further explored by ATK modeling efforts and the results support the ideas discussed here.

In summary, we found that perturbing the flow – using rods or even more streamlined shapes – in the nozzle is not effective at increasing the size of the droplets. Rather, the additional surface area increases the temperature of the flow and slows the condensation of CO_2 with no evidence that it accelerates the coagulation of the droplets.

6.6 CO_2 Injection: Experiments and Modeling – OSU nozzle

CO_2 injection experiments at OSU used the experimental setup shown in **Figure 18**. The liquid CO_2 is injected into the subsonic region of the nozzle through an orifice in order to minimize evaporation of the CO_2 particles. The orifice is not on the centerline of the flow to avoid the reflection of laser light on the surface of orifice. The setup has the added benefit that we can easily change the location of CO_2 injection.

During an experiment the flow rate of N_2 gas is controlled by mass flow controllers, but the flow rate of CO_2 through the orifice is not easily controlled or directly measured. Instead, the flow rate was first measured before or after the light scattering experiments using a mass flow meter and a metal tank as shown in **Figure 18 (right).** The flow rate was measured at room temperature (~ 25 degree C) even though the inlet N_2 temperature in the light scattering experiment is 15 degree C. The flow rate of CO_2 liquid through the orifice is, however, expected to depend on the temperature as will be discussed below. In the end the flow rate and the mass fraction of CO_2 in the mixed flow were determined by comparing the experimental LSM and either the static pressure at the nozzle exit or the flow rate of N_2 to the predictions of model calculations. Since the micron size CO_2 particles produced in the injection experiments scatter light more intensely than the nanoscale particles investigated earlier, the light scattering setup was modified slightly from that in **Figure 10** by changing the neutral density filter to decrease the intensity of light reaching the detector. **Figure 19** shows two views of the final CO_2 droplet injection setup, and confirms that the particles persist far downstream of the injection point.
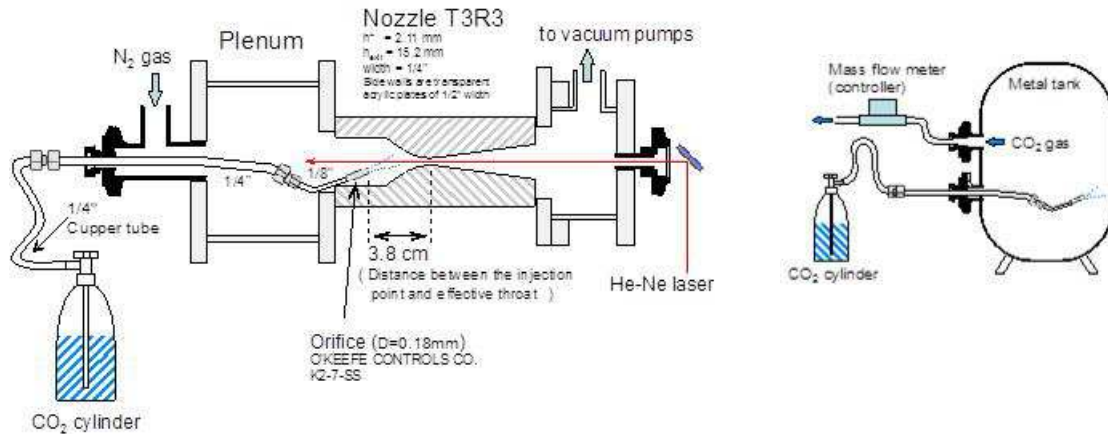
Figure 18: (left) OSU experimental setup for CO_2 injection into the nozzle. **(right)** The CO_2 flow calibration setup.
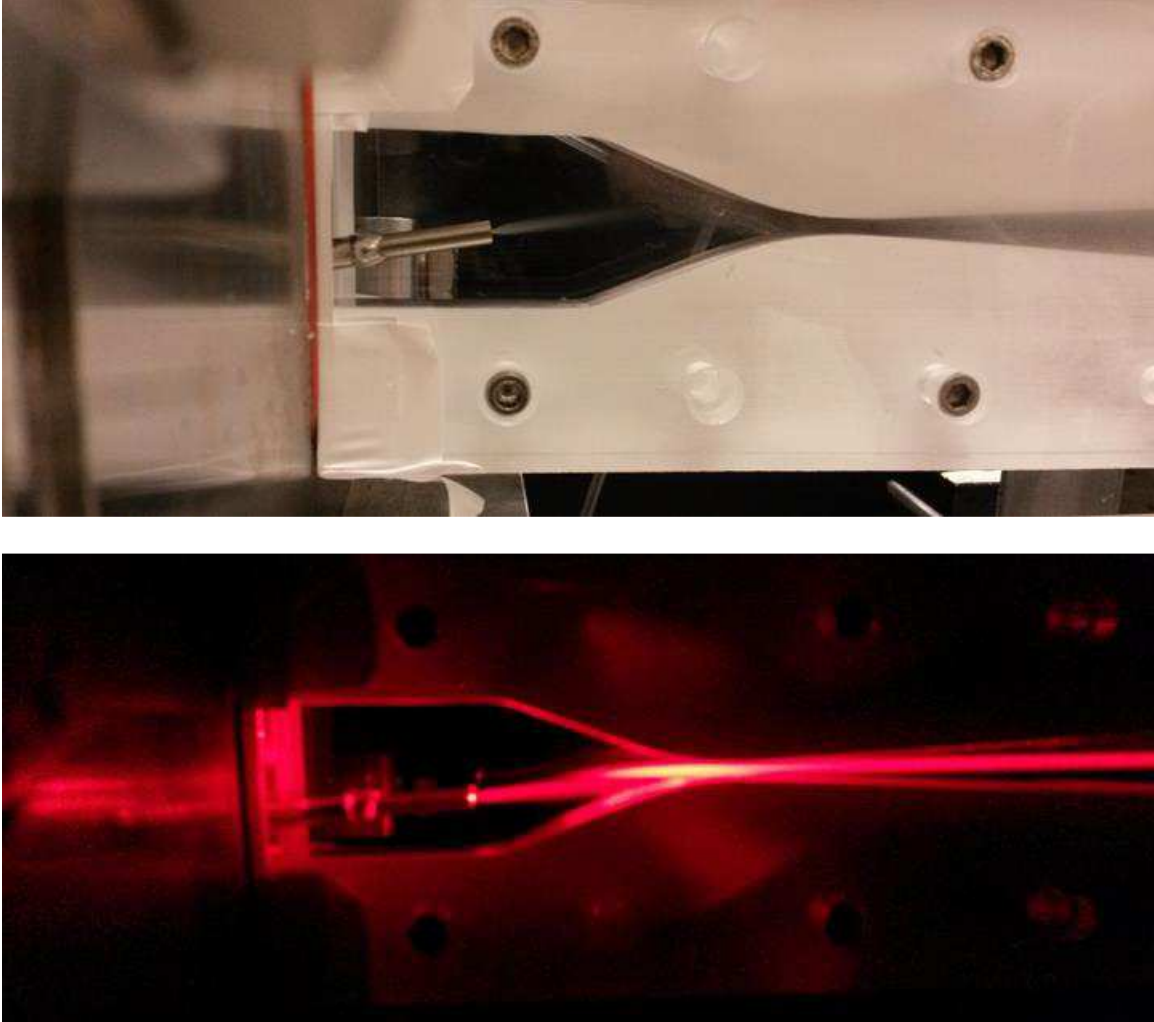
Figure 19. (top) The CO_2 injector nozzle integrated into Nozzle T3. **(bottom)** Light scattering confirms the presence of particles far downstream of the injection point.

The two light scattering measurements made as liquid CO_2 was injected into the nozzle were conducted under the same nominal operating conditions. The results are summarized in **Figure 20**. As demonstrated by the points at $z = 7.7$ cm, reproducibility was good for a particular experiment, but agreement between the two experiments was not good. Both flow and pressure measurements suggest that the CO_2 injection orifice had clogged during the first experiment, thereby reducing the flow of CO_2 entering the nozzle significantly (see experimental report from 9/24/2014 for more detail). In order to determine the weight fraction of CO_2, w_{CO2}, and the radius of droplet, r, we therefore modeled droplet growth in the nozzle and compared the predicted values of $(E_s)_{detect}$ and the exit pressure (or N2 flow rate) to those measured in the experiments.
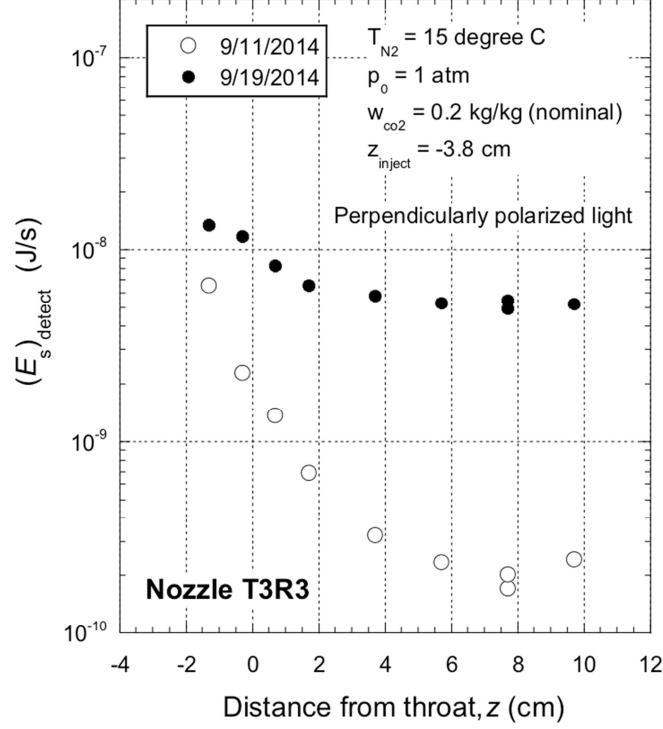
Figure 20. The energy reaching the detector during light scattering measurements made when liquid CO_2 is injected into the nozzle forming micron size particles.

To predict the values of $(E_s)_{detect}$ presented in **Figure 20**, we first recognize that for the wavelength of light used in these experiments, light scattering from micron sized particles is governed by Mie theory rather than Rayleigh theory. **Figure 21** illustrates the intensity of the scattered light (of wave length λ) from a single particle (radius r, refractive index n_1), $(I_s)_{one}$, calculated using Mie theory, where I_i is the intensity of incident light and l denotes the distance from the scattering point to the lens.

We define a function $f_s(r, \theta)$ according to the y-axis in **Figure 21** as

$$f_s(r,\theta) \equiv \left\{ (I_s)_{one} / I_i \right\} \times \left(4\pi^2 l^2 / \lambda^2 \right) \tag{29}$$

In a dilute system such as ours, the intensity of light scattered from the particles is a summation of $(I_s)_{one}$, and the total energy of the scattering light that reaches the detector, $(E_s)_{detect}$ is calculated by

$$\begin{aligned}
(E_s)_{detect} &= N_{drop} \iint (I_s)_{one} \, l^2 \, d\Omega dv_s \\
&= N_{drop} I_i \lambda^2 / 4\pi^2 \iint f_s(r,\theta) d\Omega dv_s
\end{aligned} \tag{30}$$

where N_{drop} denotes the number density of droplets per unit volume, and $(I_s)_{one}$ is integrated with respect to the scattering volume v_s and solid angle Ω.
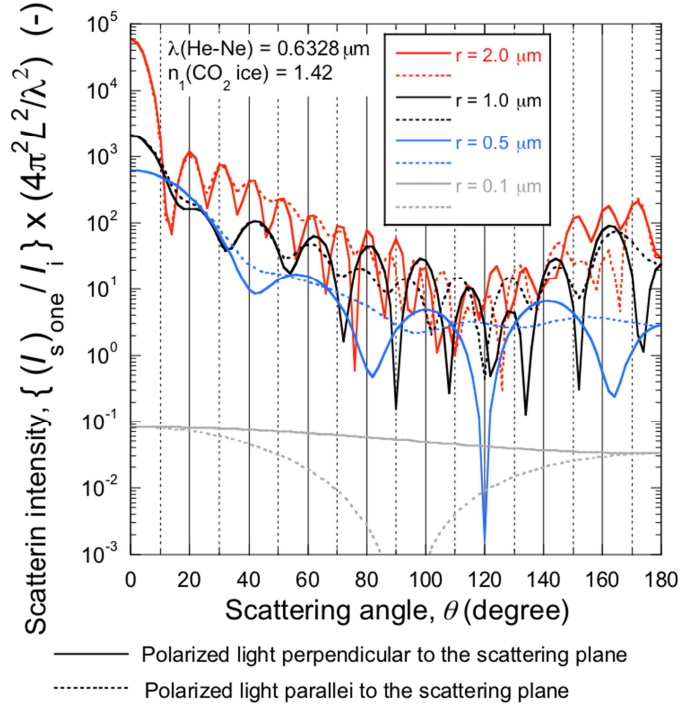
Figure 21: Scattering intensity from micron sized particles is calculated using Mie theory for the noted wavelength and index of refraction.

In this study, we approximated Eq.(30) as follows. In the configuration of our light scattering measurement, the scattering angle for the most of the light reaching the detector lies between 80 and 100 degree. Hence, we used an average value of $f_s(r,\theta)$ for $80 \le \theta/\text{degree} \le 100$, denoted by $f_s(r, \square\square\square\square\square)$, and obtained.

$$
\begin{aligned}
(E_s)_{\det ect} &\approx N_{drop} I_i f_s(r,80\text{-}100)\lambda^2/4\pi^2 \iint d\Omega dv_s \\
&\approx N_{drop} I_i f_s(r,80\text{-}100)\lambda^2/4\pi^2 \Delta\Omega\Delta v_s
\end{aligned}
\tag{31}
$$

Furthermore, in our experiments the scattered light is dominated by light polarized perpendicular (or parallel) to the scattering plane, and hence, only the $f_s(r, \square\square\square\square\square)$ for perpendicularly (or parallel) polarized light need be considered.

We previously defined a correction factor f_c' for Rayleigh scattering of perpendicularly polarized light as

$$
f_c' \equiv \frac{9\pi^2 I_i}{E_i \lambda^4} \iint (\text{Function of } \theta) d\Omega dv_s \approx \frac{9\pi^2 I_i}{E_i \lambda^4} \Delta\Omega\Delta v_s,
\tag{32}
$$

where (Function of θ) = 1 was used, because, in the Rayleigh scattering, (Function of θ) = 1 for the perpendicularly polarized light. Combining Eqs. (31) and (32), leads to the following relationship for the energy of the light hitting the detector during the experiments with micron size particles,

$$(E_s)_{\det ect} = \frac{\lambda^6}{36\pi^4} N_{drop} E_i f_c' f_s(r, 80\text{-}100),\qquad(33)$$

where $f_c' = 3.4 \times 10^{21}$ m^{-3} and $E_i = 5.0$ mW .

Finally, f_s(r, 80-100) was averaged over $0.6r < r < 1.4r$ assuming a normal size distribution, with a standard deviation of $0.2r$. This averaging was necessary to obtain a smooth line for $(E_s)_{detect}$ because $f_s(r, \theta)$ has sharp fringes as shown in **Figure 21**, and because it is unlikely that the particles we are producing during the injection process are monodisperse. We note that the size distribution was not considered in the model calculation for the growth of CO_2 droplet. Nevertheless, we can estimate $(E_s)_{detect}$ by substituting the values of N_{drop} and r derived from the model calculation into Eq.(33).

Model calculations of the evolution of injected CO_2 particles were conducted and **Figure 22** illustrates the comparisons between the LSMs conducted on 9/19/2014 and 9/11/2014. The model calculations using different assumptions for the initial radius of the droplet, r_0 and the weight fraction w_{CO2} for each r_0 was chosen either so that the pressure at z = 10 cm, $p(z=10cm)$, agreed with the measured value multiplied by a small correction factor, or that the flow rate of N_2 matched the measured value. Further details are available in experimental report of 9/24/2014.
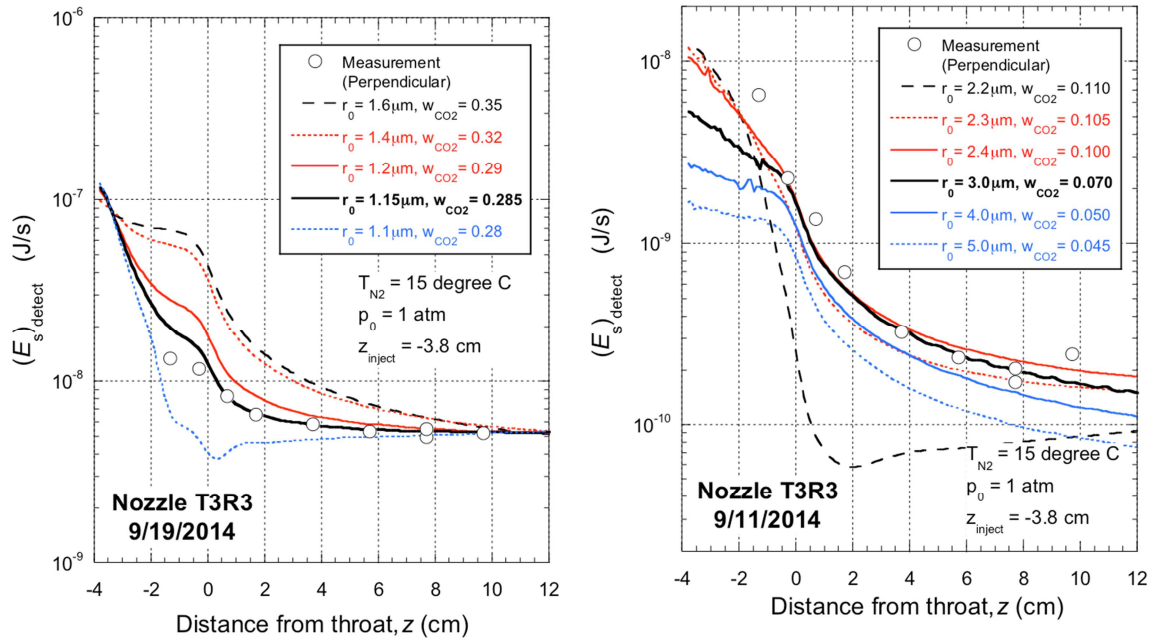
Figure 22: The energy predicted to reach the detector is a function of the average particle size and the mass fraction of CO_2. **(left)** For the experiment conducted on 9/19, the calculations suggest that the average particle size is $r_0 = 1.15$ μm. **(right)** For the experiment conducted on 9/11, the calculations suggest that the average particle size is $r_0 = 3$ μm.

As shown in the **Figure 22 (left),** the $(E_s)_{detect}$ values calculated when $r_0 = 1.15$ μm and $w_{CO2} = 0.285$ reproduce the measured results quite well. The weight fraction $w_{CO2} = 0.285$ corresponds to a CO_2 flow rate of 35.1 SLM. This flow rate is slightly higher than that measured at room temperature (25.4 SLM) and is consistent with the lower temperature of the CO_2 feed tube during the experiment. Further details are available in experimental report from 9/24/2014. In **Figure 22 (right)** for the experiments conducted on 9/11, the $(E_s)_{detect}$ values calculated for $r_0 = 3.0$ μm and $w_{CO2} = 0.070$ reproduce the measured result. In both cases, the estimated diameters are in the range of the values, 0.5 to 11 μm reported in Ref. 13. The weight fraction of 0.070 corresponds to CO_2 flow rate of 6.9 SLM, a value that is much smaller than that the 35.1 SLM observed for the measurements on 9/19, and suggests that the orifice tube was clogged.

The larger droplet size, $r_0 = 3.0$ μm, observed during the 9/11 experiment can be explained as follows. When the tube is clogged the pressure drop will increase and, therefore, result in more significant evaporation of CO_2 liquid and a decrease in the temperature within the tube. Since the small CO_2 droplets are thought to form in the flashing spray by the boiling of CO_2 in the primary droplets,[14] a decrease in the temperature of CO_2 liquid should slow down boiling in the droplet and thus increase the final size of the droplets.

An additional experiment with the CO_2 injection system in which we added water vapor to the flow did not work because ice deposits on the nozzle surface around the throat and the nozzle flow became unstable.

6.7 CO$_2$ Injection: Modeling – ATK nozzle

In addition to modeling the experiments conducted in the OSU nozzle, significant effort was expended modeling CO_2 injection scenarios in the ATK nozzle profile and modifications to the profile. In the case of CO_2 injection modeling we must first determine the inlet conditions since these are a function of the amount of CO_2 liquid injected into the nozzle and the distribution of this liquid between vapor and solid particles. To estimate the inlet conditions we consider the following steps.

(a) Expand the pressurized CO_2 liquid adiabatically into the inlet at a pressure of p_0.

$$g_{CO2}CO_2 \text{ liquid}(T_{CO2L}, p_{CO2L}) \rightarrow g_{CO2S}CO_2 \text{ solid}(T_{CO2}, p_0) + g_{CO2G}CO_2 \text{ vapor}(T_{CO2}, p_0) \quad (34)$$

$$p_{CO2S}(T_{CO2}) = p_0 \quad (35)$$

$$\left(g_{CO2S} + g_{CO2G}\right)\left\{\Delta h_{\text{vap}-i}(T_{CO2L})\big/\mu_{vi} + \int_{TCO2L}^{TCO2} c_{p-i(v)}^0 dT\right\} - g_{CO2S}\,\Delta h_{\text{sub}-i}(T_{CO2})\big/\mu_{vi} = 0 \quad (35)$$

where, the temperature after the expansion, T_{CO2}, is determined by Eq. (35), that is the equilibrium pressure of CO_2 solid, $p_{CO2S}(T_{CO2})$ is equal to the inlet pressure p_0. The mass ratio between the solid and vapor, g_{CO2S}/g_{CO2G}, is derived from Eq. (35), where $\Delta h_{\text{vap}-i}$ ($\Delta h_{\text{sub}-i}$) is the molar heat of vaporization (sublimation) of species i in the bulk liquid (solid) phase, and μ_{vi} is molecular weight of species i. The isobaric specific heat capacity of the species i in the ideal gas state is denoted by $c_{p-i(v)}^0$. The work, which is done by the

expanding CO_2 gas was assumed to change to the heat and is distributed in the gas in the inlet of nozzle. Hence the term of this work does not appear in this analysis.

This calculation generally leads to about a 50-50 split of the CO_2 between the vapor and condensed phases and initial particle temperatures on the order of 180 – 205 K.

(b) CO_2 vapor is mixed with N_2 vapor.

$$g_{CO2G} CO_2 \text{ vapor} \left(T_{CO2}, p_0\right) + g_{N2} N_2 \text{ vapor} \left(T_{N2}, p_0\right) \rightarrow CO_2/N_2 \text{ mixture}(T_{g0}, p_0), \quad (36)$$

$$g_{CO2G} \int_{TCO2}^{TG0} c_{p\text{-}CO2(v)}^0 dT + g_{N2} \int_{TN2}^{TG0} c_{p\text{-}N2(v)}^0 dT = 0. \quad (37)$$

The inlet gas temperature, T_{G0}, was determined by solving Eq. (37). The temperature of CO_2 solid was assumed to remain at T_{CO2} during the mixing process between the CO_2 and N_2.

The parameters that are chosen for a simulation include:

(i)   Mass fraction of CO_2, g_{CO2} $(= g_{CO2S} + g_{CO2G} = 1 - g_{N2})$
(ii) Temperature of liquid CO_2, T_{CO2L}
(iii) Pressure of liquid CO_2, p_{CO2L}
(iv) Inlet pressure, p_0
(v) Temperature of N_2 gas, T_{N2}

The inlet conditions that are derived from Eqns. (34) – (37) include:

(vi) Inlet mass fractions of CO_2 solid and vapor, g_{CO2S} and g_{CO2G}
(vii) Inlet temperature of CO_2 solid, T_{CO2S}
(viii) Inlet gas temperature, T_{G0}

(c) Size of CO_2 solid droplet

The size distribution of CO_2 solid particles produced in the flashing spray of CO_2 liquid through an orifice (0.25 mm diameter) has been reported in Ref. 13. In these experiments, the liquid pressure is the equilibrium pressure at 25 degree C = ~57 bar, and the output pressure is 1 atm. The liquid temperature was varied from 25 to -30 degree C. At low temperatures, CO_2 vapor boiling occurred outside of the orifice. At high temperatures, boiling occurred inside the flow tube, and the flow pattern changed drastically. Nevertheless, the average diameter of the CO_2 solid particle was in the narrow range of 3.5 - 4.0 µm.

In most of our modeling the particle size was treated as a free parameter and the number density of particles was adjusted to agree with the mass fraction of solid CO_2 at the inlet to the nozzle.

6.7.1 Preliminary Studies

Our initial modeling efforts focused on conditions comparable to the CO_2 injection experiments conducted at ATK and assumed all of the CO_2 in the flow came from liquid injected into the nozzle. The mass fraction of CO_2 was $w_{CO2} = 0.2$ (or 0.1). At the point of injection ~half of the CO_2 is in the gas phase, and half is in the condensed phase, i.e $g_{CO2s}/ w_{CO2} = $ ~0.5. The key findings are as follows.

(1) Injecting particles as close as possible to the throat is critical since CO_2 particles shrink at the higher temperatures upstream of the throat and, furthermore, the residence time is long (for a given distance) because of the velocities are low. Small (2 μm radius) droplets evaporate when they are injected ~12 cm upstream of the throat but survive when injected ~3 cm upstream of the throat (see report 8/27/14). In the latter case, the mass fraction of solid CO_2 approaches 0.6 at the nozzle exit and the droplets are still growing. The effect of injection location was explored further for $r = 2$ μm droplets (see report 9/17/2014), and the mass fraction of CO_2 condensate at the nozzle exit g_{CO2s}/ w_{CO2} reached ~0.64 when the droplets were injected 1 cm upstream of the throat.

(2) Large particles (20 μm radius) pass through the nozzle essentially unchanged. Even if they are injected ~12 cm upstream of the throat their sizes only decrease by ~1%. The stability of the large particles directly reflects the 1000-fold change in surface area available for evaporation/growth when the droplet radius is increased from 2 to 20 microns while maintaining the mass fraction constant. On the other hand, there was still a net evaporation of CO_2 rather than any net condensational growth, i.e. at the nozzle exit $g_{CO2s}/ w_{CO2} < $ ~0.5. (see report 9/10/14). This effect was explored further (see report 9/17/14) where droplets ranging in size from 2 to 10 μm were injected ~12 cm upstream of the throat. Droplets 3 μm in size survived and were growing rapidly, but did not regain the mass they had lost by the nozzle exit. Droplets 10 μm in size lost much less mass but did not regain any of the lost mass either.

6.7.2 Modifying ATK nozzle shape

The ATK nozzle shape was modified in several ways to explore the issues of residence time and further expansion on the maximum recovery of CO_2. The ability of the injected CO_2 particles to collect CO_2 injected with the gas stream was also explored.

The two initial nozzle shapes explored are illustrated in **Figure 23** and are denoted as the "Long Flat" and "Long Fast" ATK nozzles. Based on the preliminary studies, the injection point was fixed at 1 cm upstream of the throat.

Initial modeling efforts using these nozzles (see modeling report 09/24/14 for detailed results) found that condensation was enhanced by decreasing the particle size further to $r = 1.25$ μm, the smallest size that can be realistically removed by inertial separation, by decreasing the temperature of the incoming CO_2 to 225 K from 300 K, and by expanding the flow more significantly. **Figure 24** illustrates the key performance parameters – the
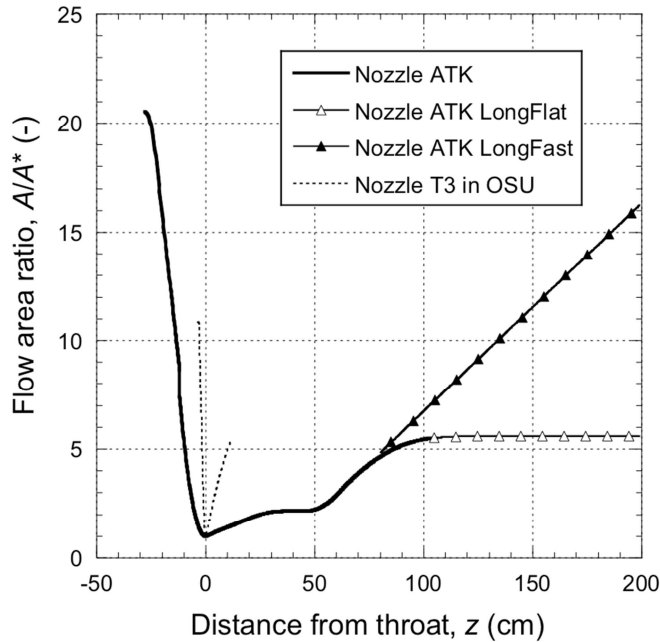
Figure 23. The nominal flow area ratios of the ATK nozzle and the two modified versions.

mass fraction ratio g_{CO2S}/w_{CO2} and particle size – as a function of the distance from the throat when all of the CO_2 entering the nozzle is injected as liquid. Although both nozzle shapes enhance condensation, g_{CO2S}/w_{CO2} is still less than 1 at the nozzle exit even for the Long Fast nozzle. The pressure at the exit of the Long Fast nozzle is also extremely low, ~ 12 Torr (~0.23 psia) and so using this nozzle may not be realistic.
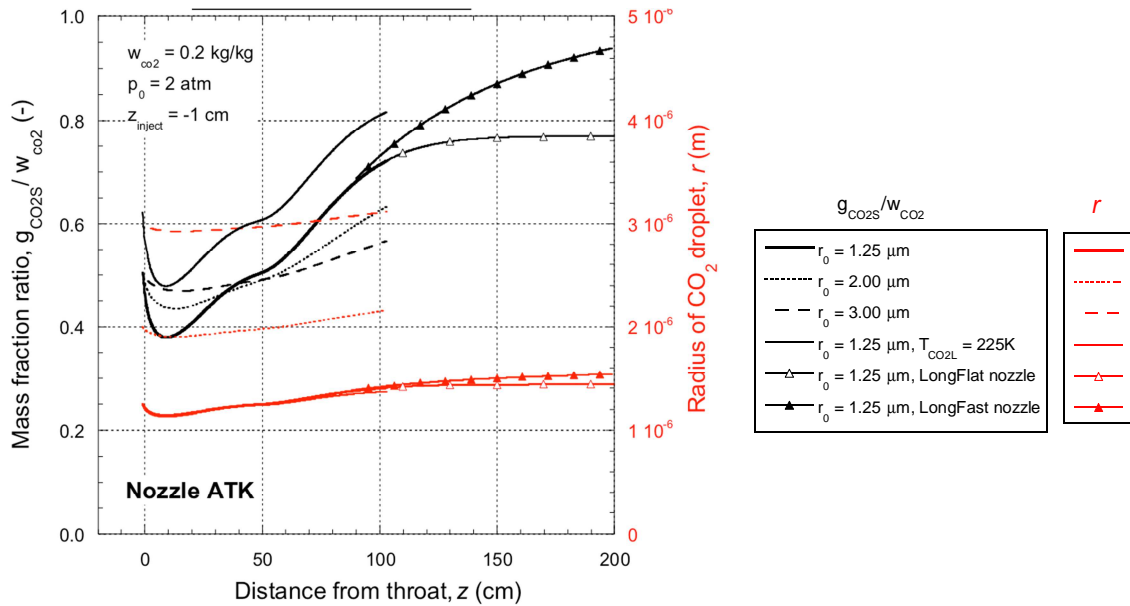
Figure 24. The mass fraction ratio and particle size predicted for the ATK nozzle as a function of the initial particle size and CO_2 liquid temperature. The default liquid temperature is 300 K. The results for two alternate nozzle shapes are also shown.

35

Table 2: Injection conditions for model calculations of the growth of CO_2 solid particles in Long Flat ATK nozzles.

	Case 1	Case 2	Case 3
Mass fraction of CO_2 liquid, w_{CO2L}	0.1, 0.2	0.1, 0.2	0.1, 0.2
Initial mass fraction of CO_2 gas, w_{CO2g0}	0	0	0.2
Inlet pressure, p_0 (atm)	2.0	2.0	2.0
Initial radius of CO_2 solid particle, r_0 (mm)	1.25	1.25	1.25
Temperature of liquid CO_2, T_{CO2L} (K)	300	225	300
Temperature of N_2 gas, T_{N2} (K)	288	288	288
Pressure of liquid CO_2, p_{CO2L} (atm)	66	66	66
Injection point, z_{inject} (cm) [a]	-1	-1	-1
Inlet mass fraction ratio of CO_2 solid and vapor, g_{CO2S}/w_{CO2}	0.51	0.62	0.17, 0.25
Inlet temperature of CO_2 solid, T_{CO2S} (K)	203.6	203.6	203.6
Inlet gas temperature, T_{G0} (K)	284.6, 280.8	285.4, 282.4	284.5, 280.5
Inlet partial pressure of CO_2, $(p_{CO2})_0$ (Torr)	51, 111	40, 86	281, 366
Number density of CO_2 droplet, N'_{drop} (10^{12} kg^{-1})	5.3, 10.6	6.5, 13.0	5.3, 10.6

The behavior of the Long Flat nozzle was investigated further for the cases outlined in **Table 2** (see report 09/30/2014 for more detailed results) and the key results are illustrated in **Figure 25.** Cases 1 and 2 are for pure CO_2 liquid injection whereas Case 3 corresponds to the ICES operating mode in which injected CO_2 particles collect CO_2 vapor. As illustrated in **Figure 25** in both Cases 1 and 2, g_{CO2S}/w_{CO2} is initially higher when $w_{CO2L} = 0.2$ than when $w_{CO2L} = 0.1$ due to the higher partial pressure of CO_2 in the gas phase. However, for $w_{CO2L} = 0.2$ the value of g_{CO2S}/w_{CO2} reaches a ceiling, as the droplets reach equilibrium with the CO_2 in the gas phase at the gas/particle temperature. When z > ~130 cm, the values of g_{CO2S}/w_{CO2} for $w_{CO2L} = 0.1$ surpass the values for $w_{CO2L} = 0.2$ because less heat has been released to the flow and, thus, gas/particle temperatures and equilibrium pressures are lower.

When CO_2 is also added to the incoming gas stream, the mass fraction ratio g_{CO2S}/w_{CO2} is significantly lower. This is largely because the total mass fraction of CO_2 entering the nozzle in Case 3 ($w_{CO2} = 0.3$ or 0.4) is significantly higher than in Case 1 or 2 ($w_{CO2} = 0.1$ or 0.2). One problem of the high levels of CO_2 in the gas phase is that the gas and droplet temperatures are significantly higher than in the more dilute cases – there is less bath gas to absorb the energy of the condensing material and cool the growing droplets. We do note that for Case 3 when $w_{CO2L} = 0.1$, the initial fraction of CO_2 entering the system as a liquid (prior to flashing) is 0.33 (=0.1/0.3), and the final value of $g_{CO2S}/w_{CO2} \sim 0.38$. Thus
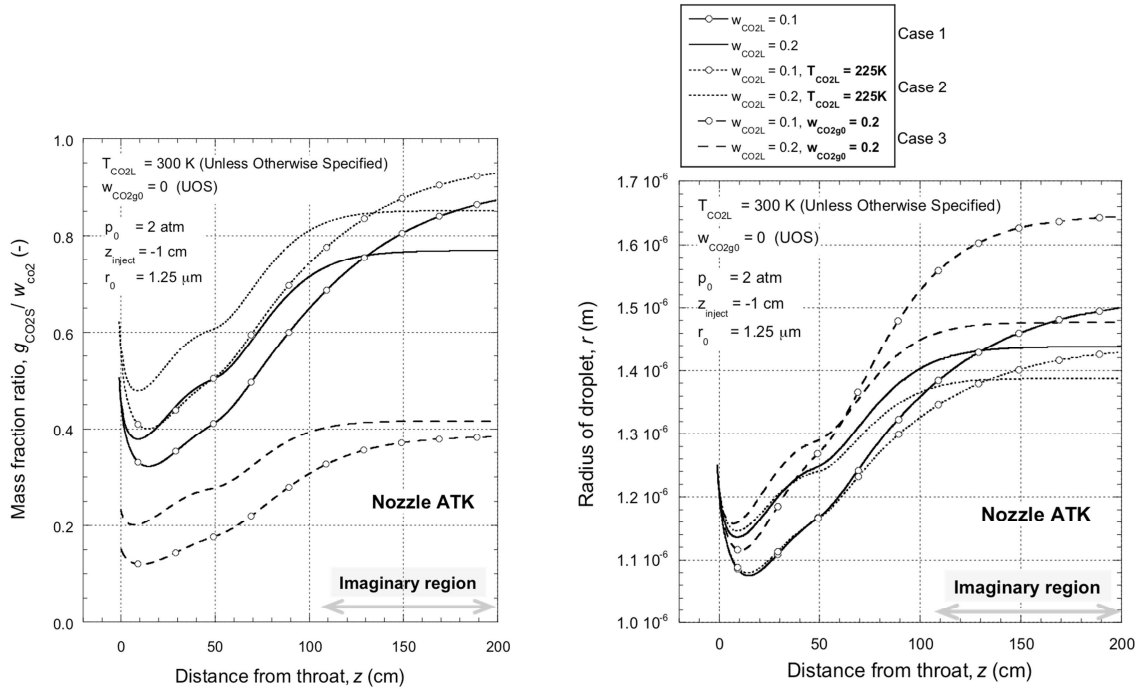
Figure 25. The mass fraction ratio **(left)** and particle size **(right)** predicted for the ATK Long Flat nozzle as a function of the initial CO_2 liquid mass fraction w_{CO2L}, liquid temperature, and CO_2 gas mass fraction w_{CO2g0}.

all of the initial liquid entering the nozzle has condensed and about 7.5% of the incoming gas has been recovered.

A similar set of calculations was conducted for $r_0 = 2$ μm, but the values of g_{CO2S}/w_{CO2} at the nozzle exit were always lower than when $r_0 = 1.25$ μm.

The question of nozzle scale (see report from 11/19/14) is also of interest since for the same $(A/A^*)_{exit}$ there is more time available for condensation when the size of the nozzle is increased. **Figure 26** illustrates the base ATK nozzle and the two scaled nozzles that we considered. In all cases the area ratio was not scaled for z<0 to minimize droplet evaporation in the subsonic region. **Table 3** summarizes the injection conditions for the model calculations.

For Case 1 and 2 – liquid injection only – the major effects of scaling were as follows:
  (1) In general, increasing the nozzle scale increased condensation.
  (2) The 1 μm droplets, however, evaporated completely near the nozzle throat in the $z \times 20$ nozzle.
  (3) For 1 μm droplets the maximum value of g_{CO2S}/w_{CO2} was 0.9 (0.78) for $w_{CO2L} = 0.1$ (0.2) in the $z \times 10$ nozzle.
  (4) For 2 μm droplets the values of g_{CO2S}/w_{CO2} were very close to those for 1 μm droplets in the $z \times 10$ nozzle.
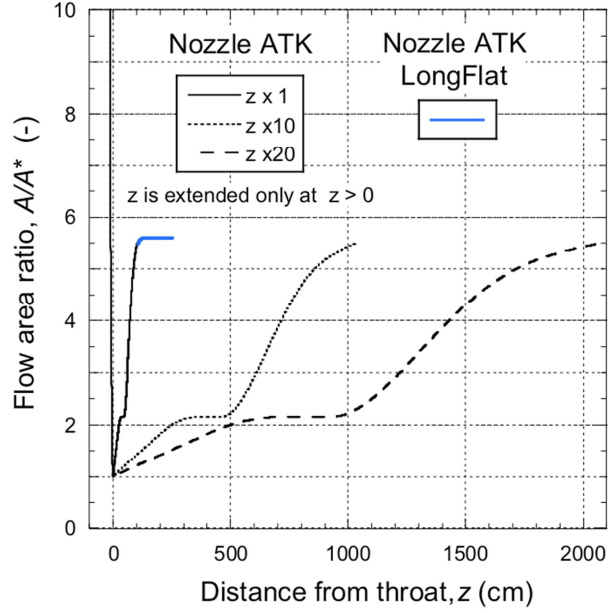
Figure 26. The nominal flow areas of the scaled ATK nozzles.

Table 3: Injection conditions for model calculations of the growth of CO_2 solid particles in scaled ATK nozzles.

	Case 1	Case 2	Case 3	Case 5
Mass fraction of CO_2 liquid, w_{CO2L}	0.1	0.2	0.1	0.1
Initial mass fraction of CO_2 gas, w_{CO2g0}	0	0	0.2	0.2
Inlet pressure, p_0 (atm)	2.0	2.0	2.0	2.0
Initial radius of CO_2 solid particle, r_0 (μm)	1 - 5	1 - 5	1 - 2	1
Temperature of liquid CO_2, T_{CO2L} (K)	300	300	300	**(73)**[a]
Temperature of N_2 gas, T_{N2} (K)	288	288	288	288
Pressure of liquid CO_2, p_{CO2L} (atm)	66	66	66	66
Injection point, z_{inject} (cm) [a]	-1	-1	-1	-1
Inlet mass fraction ratio of CO_2 solid, g_{CO2S}/w_{CO2}	0.51	0.51	0.17	0.33
Inlet temperature of CO_2 solid, T_{CO2S} (K)	203.6	203.6	203.6	203.6
Inlet gas temperature, T_{G0} (K)	284.6	280.8	284.5	287.9
Inlet partial pressure of CO_2, $(p_{CO2})_0$ (Torr)	51	111	281	235
Number density of CO_2 droplet, N'_{drop} (10^{12} kg^{-1})	10.3 - 0.08	20.6 - 0.17	10.3 - 1.3	20.2

[a]Temperature of liquid CO2 was set at an unrealistic value of 73 K so that the inlet mass fraction ratio of CO2 solid is gCO2S/wCO2L = 0.99.

(5) For 5 μm droplets condensation is still significantly below that for 2 μm droplets when $w_{CO2L} = 0.1$, but reasonably close when $w_{CO2L} = 0.2$ in the $z \times 20$ nozzle.

(6) The reduced maximum values of g_{CO2S}/w_{CO2} for $w_{CO2L} = 0.2$ relative to $w_{CO2L} = 0.1$ are a consequence of the higher gas and droplet temperatures due to increased heat release at the higher w_{CO2L}.

For Case 3, **Figure 27** illustrates the mass fraction of CO_2 solid (black lines), rather than the mass fraction ratio, as a function of position. Two particle sizes – 1 and 2 μm – are considered and the corresponding traces for Case 1 (orange lines) with $r = 2$ μm is also included. As in most of the other calculations, the value of g_{CO2S} has almost reached its maximum at the exit ($z \approx 1000$ cm) of the $z \times 10$ nozzle and going to larger nozzles does not improve performance significantly. The maximum value, $g_{CO2S} \sim 0.12$, is higher than that reached the case 1 (orange lines) but only by about 0.03, and furthermore, g_{CO2S} only exceeds the value of $w_{CO2L} = 0.1$, by 0.02. Therefore, the CO_2 droplets capture only about 10 % of the incoming CO2 gas.

Droplet growth slows significantly near the nozzle exit because supersaturation ratios approach 1 and droplets are growing under near equilibrium conditions (temperature and supersaturation figures are available in report of 11/19/14). More CO_2 can only condense if the flow is expanded more severely. Thus, we examined an additional set of long flat nozzles where the expansion ratio (A/A^*) scaled by factors of 2, 4, 8 and 32 times higher than the standard ATK design. In addition we increased the inlet pressure by a factor of 5 to examine the effect increased CO_2 concentration on condensation. **Figure 28** summarizes the results.
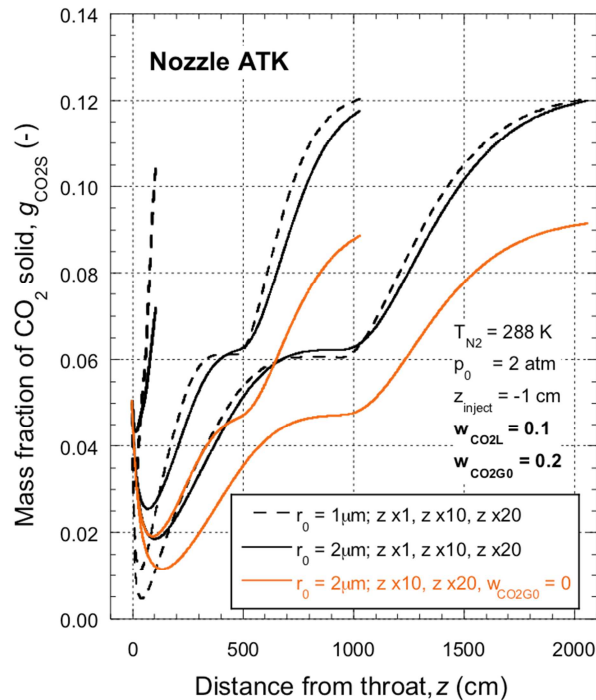
Figure 27. The mass fraction of CO2 solid as a function of position in the scaled ATK nozzles. Conditions correspond to Case 3 (black lines) and Case 1 (orange lines).
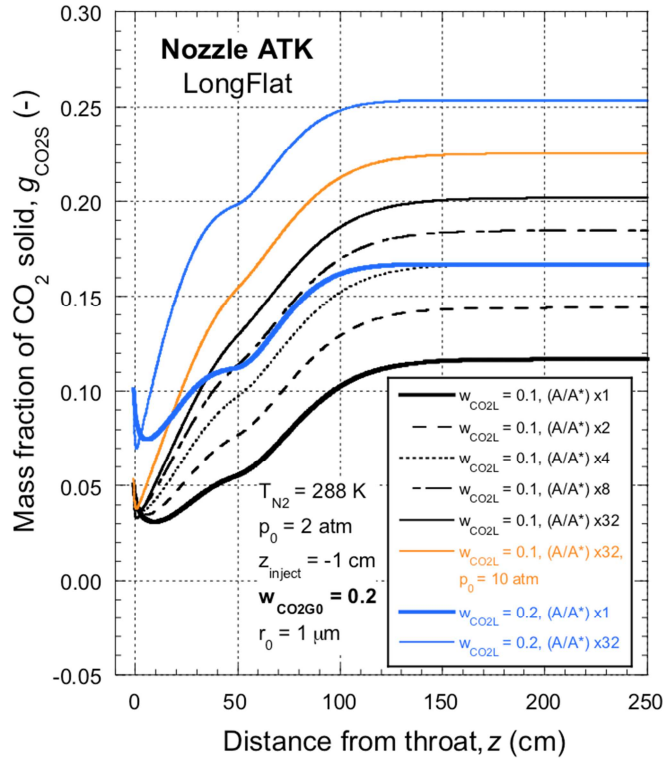
Figure 28. The mass fraction of CO_2 solid, g_{CO2S} as a function of position in the more rapidly expanding Long Flat ATK nozzles. Conditions are indicated in the legend. The mass fraction of CO_2 in the incoming gas stream was fixed at 0.2.

The heavy solid black line in **Figure 28** corresponds to Case 3 in the standard ATK geometry with an extended flat section, and here ~10% of the CO_2 present in the gas $((0.12-0.1)/0.2)$ is condensed. The heavy solid blue line is a comparable calculation but with $w_{CO2L} = 0.2$. In this case, ~84% of the CO_2 entering as liquid is condensed $(0.168/0.2)$ or, equivalently, ~ 42% of the total CO_2 entering $(0.168/0.4)$ is condensed.

The remaining black lines in **Figure 28** correspond to Case 3 and nozzles that have area ratios that expand at 2×, 4×, 8×, and 32× that of the standard ATK nozzle. The maximum value reached by g_{CO2S} is about 0.2 even for the extremely fast 32× nozzle. This corresponds to 50 % of the CO_2 entering in the gas stream $((0.2 - 0.1)/0.2)$ being captured by the CO_2 droplets in the nozzle. The lighter solid blue line is a calculation similar to the heavy blue line but in a nozzle with a 32× expansion. Doubling the flow of liquid, increases g_{CO2S}, but now for the fastest nozzle only 25% of the CO_2 entering in the gas stream $((0.25 - 0.2)/0.2)$ is captured. Finally we considered one additional case, that of $p_0 = 10$ atm and the 32× nozzle. Again, the value of g_{CO2S} increases relative to the p0 = 2 atm case, but not proportionally to the increase in incoming CO2.

Increases in the total amount of CO_2 entering the nozzle - either as a liquid or in the vapor phase consistently increase the temperature making it difficult to remove additional

material from the vapor phase. Furthermore the extremely low pressures inherent in the much faster nozzles may not be realistic for industrial operation.

To determine how much CO_2 we would expect to condense from the gas stream if all of the CO_2 injected into the nozzle was a solid at 203.6 K, we conducted an additional modeling study. The parameters used for this calculation correspond to Case 5 in Table 3. The results are illustrated in **Figure 29.** There is a clear increase in the mass fraction of solid. For the 1×, 4× and 32× nozzles ~30%, 55% and 73% of the incoming CO_2 gas is condensed at the nozzle exit, respectively.

To summarize the modeling studies, this work showed that it was important to add the particles close to the throat in order to avoid evaporation, that small particles with their larger surface area increased the rate of condensation, and that changing the scale of the device can be helpful. Although our modeling studies covered a wide range of parameter space, additional work in this area is clearly required, in particularly moving to more sophisticated models of the injection process, the droplet size distribution, and any effects these large particles have on the two-phase flow.
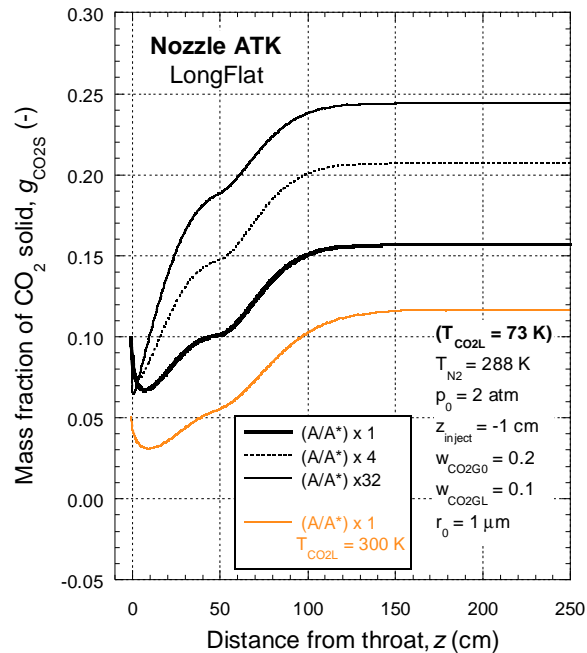
Figure 29. The mass fraction of CO_2 solid, g_{CO2S} as a function of position in the more rapidly expanding Long Flat ATK nozzles. Conditions are indicated in the legend. The orange line corresponds to Case 3.

Conclusions

Separation of condensable species via condensation in a supersonic flow apparatus is an attractive approach from the standpoint of process simplification and intensification. The challenges inherent in developing a full scale device with the goal of separating 90% of the CO_2 from flue gas are, however, not negligible. The extensive set of experimental and modeling studies conducted at OSU provided insight into this process and led to the following conclusions. Items 1-5 below pertain to the tests with trace water and vapor phase CO_2 only.

1. CO_2 condensation from flue gas undergoing supersonic flow will be driven by heterogeneous nucleation and condensation. In the absence of injected liquid or solid media, the most likely scenario is CO_2 condensation onto homogeneously nucleated water droplets. The role that native solid particulate matter in the flue gas (e.g. fly ash) could play in this scenario was not considered in these studies because there was no information regarding this parameter and it may not be a variable that is easily controlled in the full scale process.

2. Heterogeneous nucleation appears to start near the extrapolated CO_2 vapor-liquid equilibrium line, and the supersaturation required to initiate heterogeneous nucleation increases as the water/ice particle size decreases.

3. The high number density of water droplets ($\sim 10^{12}/cm^{-3}$) results in CO_2 particles with diameters less than ~ 30 nm making inertial separation extremely challenging.

4. For the water/CO_2 cases, the maximum CO_2 recovery observed in lab scale experiments was about 80% for an inlet CO_2 concentration of 3.5 mol%. The maximum recovery was $\sim 30\%$ for an inlet concentration of 14.5 mol% that is typical of flue gas. All experiments started from a stagnation pressure of 2 atm.

5. A 1-D model considering Browning coagulation showed that this effect is unlikely to increase particle size on the timescale available in the supersonic flow. Furthermore, since particles are solid, they are likely to form fractal-like objects thereby changing their drag and their ability to be separated.

6. Limited flow perturbation experiments (turbulent wake) suggested that the heat introduced into the flow by the relatively warm surfaces was detrimental to CO_2 recovery and did not increase particle size significantly. Modeling by ATK confirmed this observation.

7. Light scattering experiments validated a model developed to explore throttled CO_2 liquid injection as a means to provide micron size particles with which to remove CO_2 from the gas phase.

8. Models of the experiments showed that small CO_2 particles initially shrink at the high temperatures upstream of the throat. Thus, injection close to the throat is critical.

9. For a fixed CO_2 injection rate, particles should be as small as possible to ensure a large surface area for CO_2 condensation, but not so small that they evaporate completely.

10. In experiments, the addition of water vapor to the flow led to ice formation on the nozzle surfaces near the throat and unstable operating conditions. This may be a consequence of the geometry of the experiments and the small size of the test nozzle, but could also be an issue at full scale.

11. Modeling of the ATK nozzle, and variants thereof (longer, faster, and scaled up nozzles), confirmed that CO_2 droplet injection close to the throat was critical, that for a fixed CO_2 injection rate recovery is maximized when particles are as small as possible given that they should be recovered by inertial separation and not evaporate fully, and that increasing the scale of the device was helpful. When CO_2 was present both in the incoming flow and injected in the flow as a liquid to produce particles, some net CO_2 recovery was observed.

Suggestions/considerations for future work.

1. The role of particles present in the flue gas should be considered. These particles are inert and, unlike CO_2 liquid droplets, will not evaporate in the flow. Their ability to suppress H_2O homogeneous nucleation should also be considered.

2. The models used to describe droplet growth were somewhat simplified – especially in the free molecular regime – and should be examined more carefully.

3. If CO_2 injection is pursued further, a more sophisticated approach to determining the stagnation conditions is required.

4. Minimizing heat release to the flow is critical since heat release drives the temperature of the flow and the particles toward the equilibrium line cutting off condensation and limiting recovery.

Appendix A: Thermodynamic properties of CO_2 and N_2

$C_{p\text{-}N2(v)} = 29.124$ J/mol K   at $p_{N2} = 1$ atm and $T = 298.15$ K. (Ref. 15)
Same value is reported for ideal gas state (Ref. 16)

$C^0_{p\_CO2(v)} = 25.92 + 2.930 \times 10^{-2}\, T + 2.38 \times 10^{-5}\, T^2$ (J/mol K)
fitted to the data for $T = 100 - 400$ K in Ref. 16

$C^0_{p\_H2O(v)} = R(4.00 + 2.69 \times 10^{-4}\, T - 2.10 \times 10^{-6}\, T^2 + 5.66 \times 10^{-9}\, T^3)$
fitted to the data for T = 160 - 340 K in Ref. 17
This equation can be extrapolated safely down to 0 K.

$\Delta h_{sub\text{-}H2O} = 46.7825 + 0.0358925T - 7.414 \times 10^{-5}\, T^2 + 0.5415\exp\{-(T/123.75)^2\}$ (kJ/mol)
for $T > 30$ K (Ref. 18)

$\Delta h_{sub\text{-}CO2} = 2.303 \times 10^{-3}$ R x $1301.679 T^2/(T - 3.494)^2$ (solid) (kJ/mol)
obtained by applying Clausius-Clapeyron equation to the following vapor pressure of
solid CO_2.

$Log(p_{CO2}/bar) = 6.81228 - 1301.679/(T - 3.494)$ for $154 <= T/K <= 196$ (NIST web)
fitted to the data in Ref. 10
This equation can be extrapolated down to 65 K. (Ref. 19)

$\Delta h_{vap\text{-}CO2} = 2.303 \times 10^{-3}$ R$(1.353202 \times 10^3 - 8.142537T/2.303 + 6.259156 \times 10^{-3}\, T^2)$ (liquid)
(kJ/mol)
obtained by applying Clausius-Clapeyron equation to the following vapor pressure of
liquid CO_2.

$Log(p_{CO2}/atm) = -1.353202 \times 10^3/T - 8.142537 Log(T) + 6.259156 \times 10^{-3}\, T + 24.61930$
for $217 <= T/K <= 276$ (Ref. 11)

$\rho_{H2O} = 930$ kg/m^3 for ice (Ih) at $T < 200$ K (Ref. 20)
$\rho_{CO2} = 1170$ kg/m^3 for liquid at $T = 220$ K and $p = 2$MPa (Ref. 21)

$\mu_{CO2} = 44.01$ g/mol
$\mu_{H2O} = 18.02$ g/mol
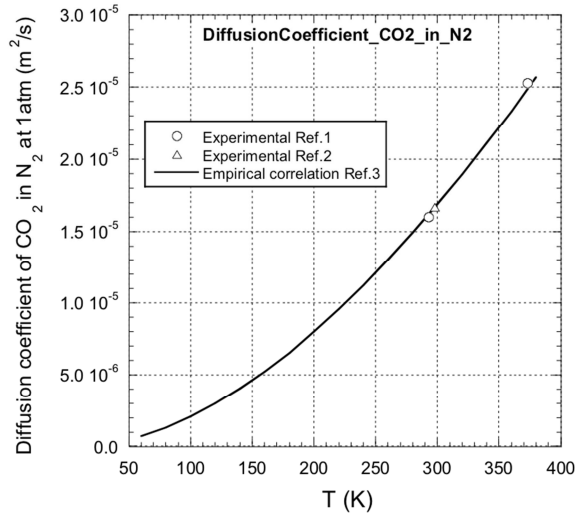
Figure A-1: The diffusion coeffient of CO_2 in N_2 (Ref 20, 22). The diffusion coefficient is inversely proportional to the pressure when pressure is less than a few atmosphere.
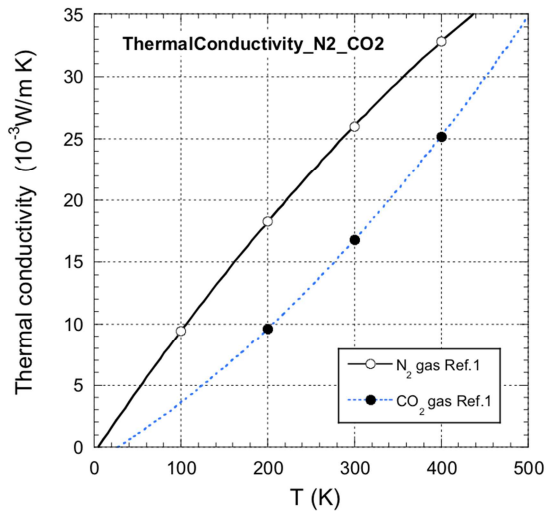
Figure A-2. The thermal conductivities of CO_2 and N_2 (Ref. 22). The dependence of thermal conductivity on pressure is negligible at pressures below 10 atm.

References

1. Pathak, H.; Mullick, K.; Tanimura, S.; Wyslouzil, B. E., Nonisothermal Droplet Growth in the Free Molecular Regime. *Aerosol Science and Technology* 2013, 47, 1310-1324.

2. Pathak, H.; Woelk, J.; Strey, R.; Wyslouzil, B. In *Co-condensation of Nonane and D2O in a Supersonic Nozzle*, 19th International Conference on Nucleation and Atmospheric Aerosols (ICNAA), Colorado State Univ, Ctr Arts, Fort Collins, CO, 2013 Jun 23-28; Colorado State Univ, Ctr Arts, Fort Collins, CO, 2013; pp 51-54.

3. Duff, K. Condensation of CO2 in Supersonic Nozzles. Massachusetts Institute of Technology, 1964.

4. Erbland, P. J.; Rizzetta, D. P.; Miles, R. W. In *Numerical and experimental investigation of CO2 condensate behavior in hypersonic flow*, AIAA Aerodynamic Measurement Technology and Ground Testing Conference, Denver, CO, Denver, CO, 2000; pp AIAA-200 - 2379.

5. Ramos, A.; Fernandez, J. M.; Tejeda, G.; Montero, S., Quantitative study of cluster growth in free-jet expansions of CO2 by Rayleigh and Raman scattering. *Physical Review A* 2005, 72.

6. Kim, Y. J.; Wyslouzil, B. E.; Wilemski, G.; Wolk, J.; Strey, R., Isothermal nucleation rates in supersonic nozzles and the properties of small water clusters. *Journal of Physical Chemistry A* 2004, 108, 4365-4377.

7. Bhabhe, A.; Wyslouzil, B., Nitrogen nucleation in a cryogenic supersonic nozzle. *Journal of Chemical Physics* 2011, 135, 244311-1 - 244311-11.

8. Hill, P. G., CONDENSATION OF WATER VAPOUR DURING SUPERSONIC EXPANSION IN NOZZLES. *Journal of Fluid Mechanics* 1966, 25, 593-&.

9. Hoose, C.; Moehler, O., Heterogeneous ice nucleation on atmospheric aerosols: a review of results from laboratory experiments. *Atmospheric Chemistry and Physics* 2012, 12, 9817-9854.

10. Giauque, W. F.; Egan, C. J., Carbon dioxide. The heat capacity and vapor pressure of the solid. The heat of sublimation. Thermodynamic and spectroscopic values of the entropy. *Journal of Chemical Physics* 1937, 5, 45-54.

11. Michels, A.; Wassenaar, T.; Zwietering, T.; Smits, P., THE VAPOUR PRESSURE OF LIQUID CARBON DIOXIDE. *Physica* 1950, 16, 501-504.

12. Tanimura, S.; Zvinevich, Y.; Wyslouzil, B. E.; Zahniser, M.; Shorter, J.; Nelson, D.; McManus, B., Temperature and gas-phase composition measurements in supersonic flows using tunable diode laser absorption spectroscopy: The effect of condensation on the boundary-layer thickness. *Journal of Chemical Physics* 2005, 122, 194304-1 - 194304-11.

13. Lin, T.-C.; Shen, Y.-J.; Wang, M.-R., Effects of superheat on characteristics of flashing spray and snow particles produced by expanding liquid carbon dioxide. *Journal of Aerosol Science* 2013, 61, 27-35.

14. Hulsbosch-Dam, C. E. C.; Spruijt, M. P. N.; Necci, A.; Cozzani, V., Assessment of particle size distribution in CO2 accidental releases. *Journal of Loss Prevention in the Process Industries* 2012, 25, 254-262.

15. *Lange's Handbook of Chemistry, 14th Edition*. McGraw-Hill: New York, 1992.

16.   Jr., C. M. W., *NIST - JANAF Thermochemical Tables, 4th Edition*. J. Phys. Chem. Ref. Data, Monograph 9: 1998.

17.   Friedman, A. S.; Haar, L., HIGH-SPEED MACHINE COMPUTATION OF IDEAL GAS THERMODYNAMIC FUNCTIONS .1. ISOTOPIC WATER MOLECULES. *Journal of Chemical Physics* 1954, 22, 2051-2058.

18.   Murphy, D. M.; Koop, T., Review of the vapour pressures of ice and supercooled water for atmospheric applications. *Quarterly Journal of the Royal Meteorological Society* 2005, 131, 1539-1565.

19.   Azreg-Ainou, M., Low-temperature data for carbon dioxide. *Monatshefte Fur Chemie* 2005, 136, 2017-2027.

20.   *Handbook of Chemistry and Physics*. CRC Press: 2002.

21.   NIST Chemistry WebBook. http://webbook.nist.gov/chemistry/.

22.   Poling, B. E.; Prausnitz, J. M.; O'Connell, J. P., *Properties of Gases and Liquids, 5th Edition*. McGraw-Hill: New York, 2001.

Appendix B. Techno-Economic Analysis Update

(separate file appended)

EPRI Technical Report

Updated Techno-Economic Analysis for Inertial CO_2 Extraction System

Final Report, February 2017

Prepared in support of US Department of Energy National Energy Technology Laboratory award DE-FE0013122

Orbital ATK

77 Raynor Ave, Ronkonkoma, NY 11779

Project Manager
Bon Calayag

ACENT Laboratories

Project Manager
Anthony Castrogiovanni

EPRI Project Manager
A. Berger

DISCLAIMER OF WARRANTIES AND LIMITATION OF LIABILITIES

ORDERING INFORMATION

CITATIONS

This report was prepared by

Advisian WorleyParsons
2675 Morgantown Road, Reading, PA 19607
Contact: Vlad Vaysman, 610-855-2588, Vladimir.vaysman@advisian.com

Principal Investigators
V. Vaysman
J. Simpson
Y. Lu

The report is a corporate document that should be cited in the literature in the following manner:

Updated Techno-Economic Analysis for Inertial CO$_2$ Extraction System, EPRI, Palo Alto, CA, Orbital ATK, Ronkonkoma, NY and ACENT Laboratories, 2017.

ABSTRACT

This report presents results from the performance and cost analysis of the Inertial CO_2 Extraction System (ICES) developed by Orbital ATK and ACENT Laboratories in support of the DOE National Energy Technology award DE-FE0013122.

The ICES process is a carbon capture process for post-combustion capture. This process uses the cooling effect of supersonic expansion to lower the temperature of flue gas and cause CO_2 to form solids that can be removed from the gas stream inertially. An initial techno-economic analysis of this process was undertaken in 2013. However, subsequent simulations have shown that the embodiment of the process analyzed in 2013 would not perform as reported. As a result of this analysis, a new process configuration with updated operating conditions was identified.

The configuration, operating conditions, performance, and cost analysis of the updated ICES system are presented in this report as an update of the 2013 TEA. While these results do not show a significant energetic or cost improvement over the DOE Bituminous Baseline Case 12 Econamine carbon capture technology, they do represent the performance of a unique form of capture that does not share many of the drawbacks or requirements of existing solvent-based CO_2 removal technologies.

CONTENTS

LIST OF FIGURES

LIST OF TABLES

1 BACKGROUND AND EVALUATION BASIS

Introduction and Background

Orbital ATK and ACENT laboratories have developed an Inertial CO_2 Extraction System (ICES) for separating and capturing the CO_2 emitted in the flue gas of fossil-fired power plants. The ICES process involves the acceleration of flue gas to supersonic speeds in order to cool the flue gas to such a degree that the carbon dioxide forms solid particles that can be inertially separated from the remaining flue gas. This technology is being developed under the award DE-FE0013122 from the Department of Energy (DOE) National Energy Technology Laboratory (NETL). EPRI and Advisian WorleyParsons (WP) are both project partners in this effort.

WP completed an initial techno-economic analysis (TEA) of this process in March of 2013 that was based on the initial embodiment of the ICES process. This included determining the size, type, and quantity of all major equipment necessary for this process as well as estimating the capital and operating costs for the carbon capture process. However, the ICES process modeled in that initial TEA has evolved substantially due to improved process modeling and system optimization. In order to determine whether the evolved ICES process can be economically viable, an update of the initial TEA has been performed and its results are presented here.

Objectives and Evaluation Basis

The objective of this TEA update is to perform analysis of the modified ICES process using the initial TEA completed in March, 2013 as a baseline. Only the major changes to the ICES process, including the required inlet flue gas condition to the ICES reaction duct have been incorporated. Other components of the power plant, such as boiler, steam turbine, balance of plant systems for both the ICES process and the power plant itself used in this study are the same as in the WP initial TEA, and are based on the pulverized coal plants in the National Energy Technology Laboratory's (NETL) report titled "Cost and Performance Baseline for Fossil Energy Plants – Volume 1: Bituminous Coal and Natural Gas to Electricity".

The final results of this TEA update, including overall plant efficiency, \$/tonne CO_2 captured, and \$/tonne CO_2 avoided are consistent with the NETL Bituminous Baseline Studies (rev 2, November 2010) Case 12 reported on a \$/MW net basis using a June, 2011 cost basis.

The tasks performed for this TEA update include:

1. Modification of equipment train from the FGD outlet to the ICES nozzles inlet (flue gas dehydration, cooling, and compression)

2. A conceptual level update of the overall cycle (power plant and CO_2 capture) efficiency

3. An update of the CAPEX associated with the above changes

4. An update of OPEX associated with the above changes

5. An update of the levelized cost of electricity and cost per ton of CO_2 captured or avoided

ICES Process Description

ICES was designed as a means of harnessing the cooling power of accelerating supersonic flow to solidify and capture CO_2 from post-combustion flue gas. At sufficiently low temperatures determined by the gas-solid phase behavior of CO_2, 90% or any predetermined quantity of the initial CO_2 can be solidified. The solid CO_2 can then be separated from the remaining gas stream through turning the gas flow, which causes the solid particles to be inertially pushed against the outer wall in the turning duct. A knife-edge separator can then be used to capture the solid flow along with a small slip-gas stream. The solid particles can be further separated from the slip-gas stream in a cyclone. Meanwhile, the remaining CO_2-lean gas in the main duct can be decelerated in a diffusor to increase the pressure to allow atmospheric discharge.

The solid CO_2 particles are pressurized by a process using solids pumping, heating to melt the CO_2 to become a liquid and further liquid pumping and heating to make the CO_2 a supercritical fluid. As the solid CO_2 heating, melting, and liquid CO_2 heating take place at significantly sub-ambient temperatures, there is the possibility for thermal integration of this process to cool the incoming flue gas to facilitate the cryogenic capture. This capture process makes use of some process equipment that is common with other capture processes, such as the initial flue gas treatment and compression and solid CO_2 pressurization, but overall the capture process and capture mechanism is fundamentally different from all other capture processes as it does not rely on chemistry or any sort of separation medium.

ICES Process Update

The original embodiment of the ICES process studied in the March 2013 TEA was based on the gas inlet conditions of 2.5 bar pressure and ambient temperature entering the supersonic expansion and capture duct. However, simulations and modeling showed that these conditions were not sufficient to allow pressure recovery of the remaining CO_2-lean flue gas in the diffusor in order to allow discharge to atmospheric pressure. Specifically, the heat released during the phase change of the CO_2 from gas to solid and the transfer of momentum from the gas to the solid phase reduced the total pressure of the system to significantly sub-ambient once the solid CO_2 particles were removed. Further analysis showed that a significant portion of the CO_2 that was captured as a solid was reconverted to a gas upon being decelerated from supersonic speeds and reabsorbing the kinetic energy of the supersonic particle flow. This meant that capturing 90% of the incoming CO_2 would not be possible without a redesign of the system.

To allow discharge to atmospheric pressure, a new process configuration was determined by ACENT Labs and EPRI that would allow for 90% capture of the incoming CO_2 in the flue gas stream. This configuration differed from the original embodiment in four main ways:

1. The inlet pressure of the flue gas to the supersonic duct was increased to 11.86 bar

2. The inlet temperature of the flue gas to the supersonic duct was reduced to -62°C. This was accomplished through thermal integration of the CO_2 pressurization system.

3. The flue gas was dehydrated so that solid H_2O would not plug sub 0°C heat exchanger surfaces.

4. The CO_2 that volatilized in the cyclone along with the additional gas that was captured in the capture duct was recycled back to the inlet of the flue gas conditioning step.

The current evaluation is based on the updates of the ICES process provided by EPRI as presented on Figure 1-1, and in Table 1-1.
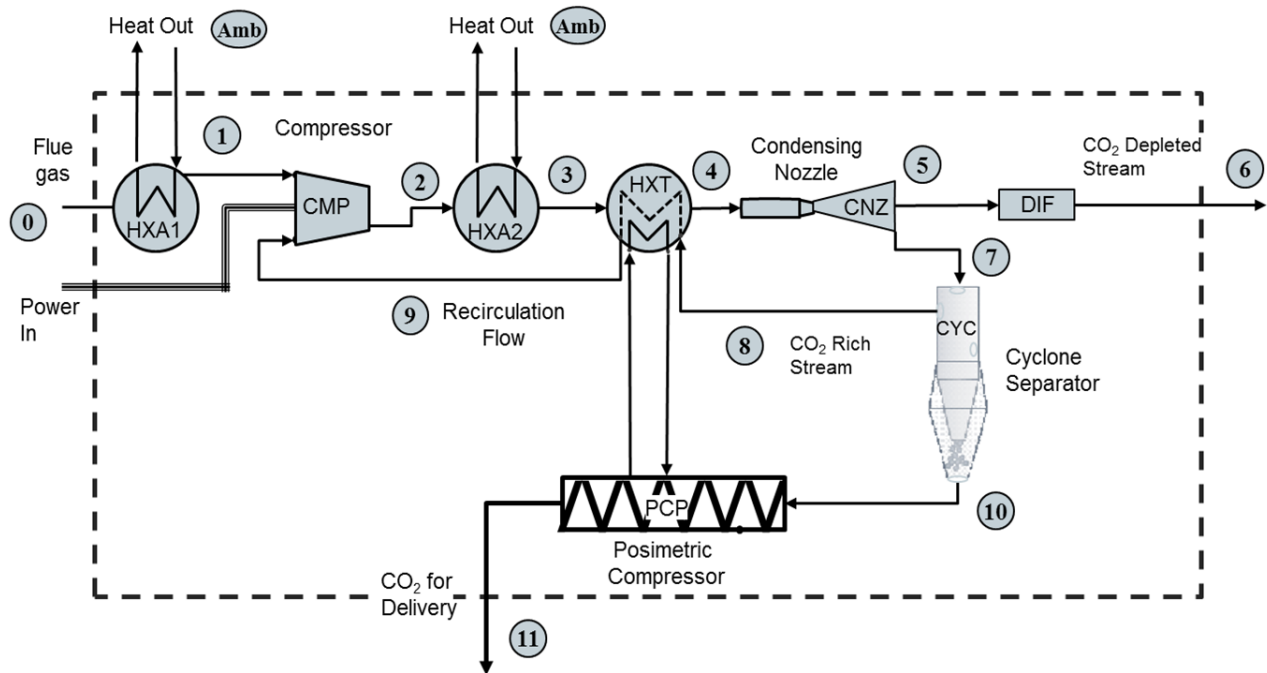
Figure 1-1
Block Flow Diagram of the Updated ICES Process

Table 1-1
Stream Table of the Updated ICES Process

		Compressor	Compressor	Compressor	Condensation Onset	Condensation Onset	Condensation Onset	CO2 Capture Plane	CO2 Capture Plane	CO2 Capture Plane	CO2 Capture Plane	Cyclone	Cyclone	Recirc Gas	Recirc Gas	CMP
		PR	Recirc Gas	PT exit	ΔT sat	CO2 pPress	M start	CO2 Cond.	M cap	Velocity	Tsat					INLET
			kg/kg_0	MPa	C	MPa		rel to plane		m/s	C	ICE	EVAP	% Slip Gas	% CO2	
		11.7	12.7%	0.1029	6	0.231	0.51	92.3%	2.88	678	136.0	73%	27%	5.0%	66%	
	Station Number	0	1	2	3	4	5	6	7	8	9	10	11	1A
Mass Flow	kg/kg_0	1.000	1.000	1.127	1.127	1.127	0.793	0.793	0.334	0.127	0.127	0.207	0.207	1.127
	# moles	32.518	32.518	35.955	35.955	35.955	27.742	27.742	8.151	3.438	3.438	4.713	4.713	35.956
Gas Specie														
Nitrogen	mols	0.8053	0.8053	0.7693	0.7693	0.7693	0.9379	0.9379	0.9379	0.4289	0.4289	0.00	0.00	0.7693
Argon	mols	0.0096	0.0096	0.0092	0.0092	0.0092	0.0112	0.0112	0.0112	0.0051	0.0051	0.00	0.00	0.0092
Oxygen	mols	0.0280	0.0280	0.0267	0.0267	0.0267	0.0326	0.0326	0.0326	0.0149	0.0149	0.00	0.00	0.0267
CO2	mols	0.1571	0.1571	0.1948	0.1948	0.1948	0.0183	0.0183	0.0183	0.5511	0.5511	0.00	0.00	0.1948
water	mols	0.000	0.0000	0.000	0.000	0.000	0.000	0.0000	0.0000	0.0000	0.0000	0.00	0.00	0.0000
Solid CO2	mols	0.000	0.000	0.000	0.000	0.000	0.000	0.000	0.252	0.000	0.000	1.00	1.00	
Average MW of gas phase		30.7523	30.7523	31.3447	31.3447	31.3447	28.5689	28.5689	41.0320	36.9491	36.9491	44.01	44.01	31.3447
State														
TT	C	57	20	331	20	-62	89	89		-77	10	-77	10	7
PT	Mpa	0.101	0.101	1.186	1.186	1.186	0.133	0.103	0.130	0.115	0.113	0.115	15.10	0.1013
RHOT	kg/m3	1.14	1.30	7.37	15.42	22.07	1.26	0.98		2.643	1.776			1.364
HT	kJ/kg	742	692	1010	688	606	827	827		506	582.3	-206.8	213.9	680
ST	kJ/kg-K	4.08	3.90	3.98	3.24	2.91	4.30	4.37		2.97	3.30		0.97	3.86
TT	°F	135	68	628	68	-80	192	192		-107	50	-107	50	45
PT	psia	14.7	14.7	171.9	171.9	171.9	19.3	14.9	18.9	16.7	16.3	16.7	2190.1	14.7
RHOT	BTU/lb	0.071	0.081	0.460	0.963	1.378	0.079	0.061		0.165	0.111			
HT	lb/ft3	319	298	434	296	261	356	356		218	250	-89	92	292

2 TECHNICAL ANALYSIS

Flue Gas Pretreatment System

Modified Flue Gas Pretreatment system configuration is presented on Figure 2-1.

Prior to introducing the flue gas stream to the ICES CO_2 capture equipment, the flue gas from the FGD will be boosted through a booster fan and cooled from 57°C (136°F) to 17°C (63°F) in a direct contact cooler (DCC) and thus the flue gas volume into the compressor is reduced to minimize the flue gas compression power. The flue gas is compressed to 12 barA (174 psia) in a two stage axial compressor. The compressor inter-stage cooling will be achieved by LP boiler feedwater and cooling water. The LP boiler feedwater heater 1 will make use of high quality waste heat from the flue gas after the 1st stage compressor. The plant cooling water will provide the trim cooling to further decrease the flue gas temperature before entering the 2nd stage compressor. The flue gas exiting the 2nd stage compressor passes through the similar cooling arrangement, except that after being initially pre-cooled by the plant cooling water, the flue gas is cooled to approximately 3°C (37°F) in the trim cooler 2 using cold heat transfer fluid from ICES. Such cooling arrangement minimizes volume and moisture content of the flue gas entering the molecular sieve dryer, and it is beneficial for reducing steam demand for adsorbent regeneration in the molecular sieve dryer. The molecular sieve dryer reduces the flue gas moisture content to less than 5 ppm so that there is no ice formation in the final flue gas cooler. Temperature of the dehydrated flue gas exiting the molecular sieve dryer and prior to entering the ICES system is further reduced to minus 62°C (minus 80°F) by using the cold heat transfer fluid from the ICES system.
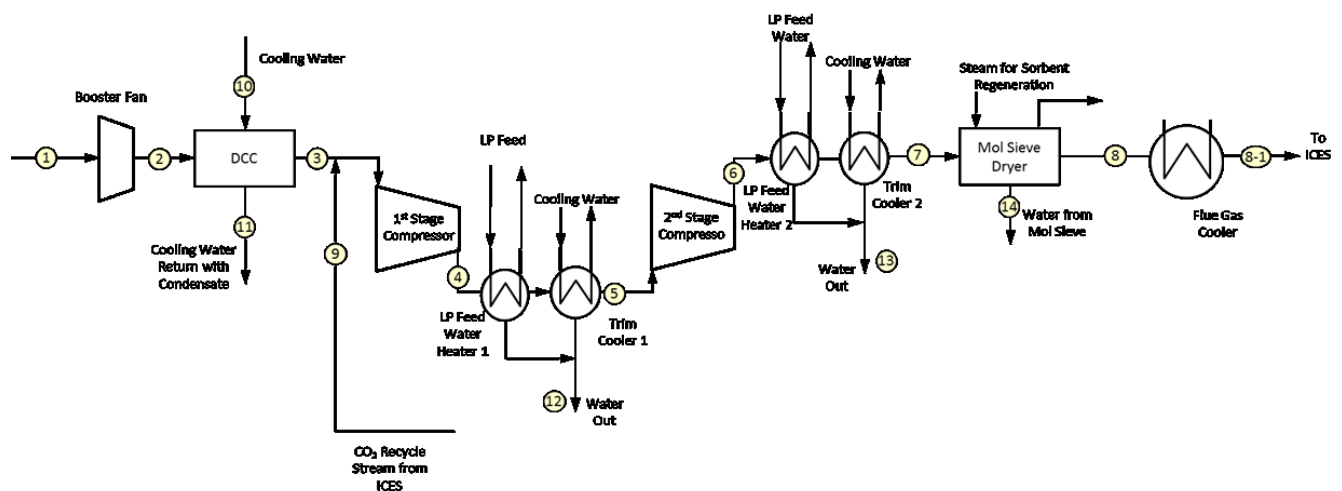
Figure 2-1
Block Flow Diagram of the Modified Flue Gas Pretreatment System

Heat and Material Balance details of the modified flue gas pretreatment system are shown in Table 2-1.

Table 2-1
Stream Table of the Modified Flue Gas Pretreatment System

Stream Description	Flue Gas From Plant FGD	Flue Gas After Booster Fan	Flue Gas After DCC	Flue Gas After Compressor Stage 1	Flue Gas Entering Compressor Stage 2	Flue Gas After Compressor Stage 2	Flue Gas Entering Mol Sieve Dryer	Flue Gas After Mol Sieve Dryer
Stream ID	1	2	3	4	5	6	7	8
Mole Frac								
ARGON	0.008	0.008	0.009	0.009	0.009	0.009	0.009	0.009
CO_2	0.135	0.135	0.156	0.194	0.195	0.195	0.197	0.197
H_2O	0.154	0.154	0.020	0.018	0.009	0.009	0.001	0.000
N_2	0.679	0.679	0.787	0.753	0.760	0.760	0.766	0.767
O_2	0.024	0.024	0.028	0.026	0.027	0.027	0.027	0.027
Mass Flow kg/hr								
ARGON	27,285	27,285	27,281	28,817	28,817	28,817	28,817	28,817
CO_2	500,988	500,988	499,188	684,253	684,240	684,240	684,158	684,158
H_2O	233,485	233,485	25,750	25,751	13,509	13,509	1,022	1
N_2	1,604,620	1,604,620	1,604,530	1,694,860	1,694,860	1,694,860	1,694,860	1,694,840
O_2	64,218	64,218	64,210	67,825	67,825	67,825	67,825	67,825
Total Flow kmol/hr	84,314	84,314	72,739	80,320	79,640	79,640	78,945	78,887
Total Flow kg/hr	2,430,600	2,430,600	2,220,960	2,501,510	2,489,250	2,489,250	2,476,680	2,475,640
Total Flow cum/hr	2,311,050	2,206,750	1,752,720	817,940	565,130	240,830	148,929	149,679
Temperature C	57	64	17	156	25	163	3	3
Pressure bar	1.0	1.1	1.0	3.5	3.5	12.0	12.0	11.9
Density kg/cum	1.05	1.10	1.27	3.06	4.40	10.34	16.63	16.54
Average MW	28.83	28.83	30.53	31.14	31.26	31.26	31.37	31.38

Table 2-1
Stream Table of the Modified Flue Gas Pretreatment System (Continued)

Stream Description	Flue Gas Into ICES	CO$_2$ Recycled Stream from ICES	Cooling Water to DCC	Cooling Water from DCC	Water Condensed from Compressor Interstage Cooler	Water Condensed from Compressor After Cooler	Water Removed from Mol Sieve Dryer
Stream ID	8-1	9	10	11	12	13	14
Mole Frac							
ARGON	0.009	0.005	0.000	0.000	0.000	0.000	0.000
CO$_2$	0.197	0.555	0.000	0.000	0.000	0.003	0.000
H$_2$O	0.000	0.000	1.000	1.000	1.000	0.997	0.989
N$_2$	0.767	0.425	0.000	0.000	0.000	0.000	0.011
O$_2$	0.027	0.015	0.000	0.000	0.000	0.000	0.000
Mass Flow kg/hr							
ARGON	28,817	1,536	0	4	0	0	0
CO$_2$	684,158	185,065	0	1,786	12	82	0
H$_2$O	1	0	5,803,360	6,011,080	12,241	12,487	1,021
N$_2$	1,694,840	90,335	0	97	1	3	17
O$_2$	67,825	3,615	0	8	0	0	0
Total Flow kmol/hr	78,887	7,581	322,135	333,711	680	695	57
Total Flow kg/hr	2,475,640	280,551	5,803,360	6,013,000	12,254	12,573	1,039
Total Flow cum/hr	111,778	157,418	5,808	6,021	12	13	2
Temperature C	-62	10	15	35	25	3	3
Pressure bar	11.9	1.1	1.0	1.0	3.5	12.0	11.9
Density kg/cum	22.15	1.78	999.22	998.65	996.22	998.96	476.91
Average MW	31.38	37.01	18.02	18.02	18.03	18.09	18.12

Power Plant with Updated ICES System

The plant configuration with the updated ICES CO_2 capture system incorporated into a supercritical pulverized coal plant is the same as is the initial TEA except for:

- Modified Flue gas pretreatment

- Modified ICES CO_2 capture

A block flow diagram of the pulverized coal power plant equipped with the modified ICES and flue gas pretreatment systems is presented on Figure 2-2. The process stream data is shown in Table 2-2
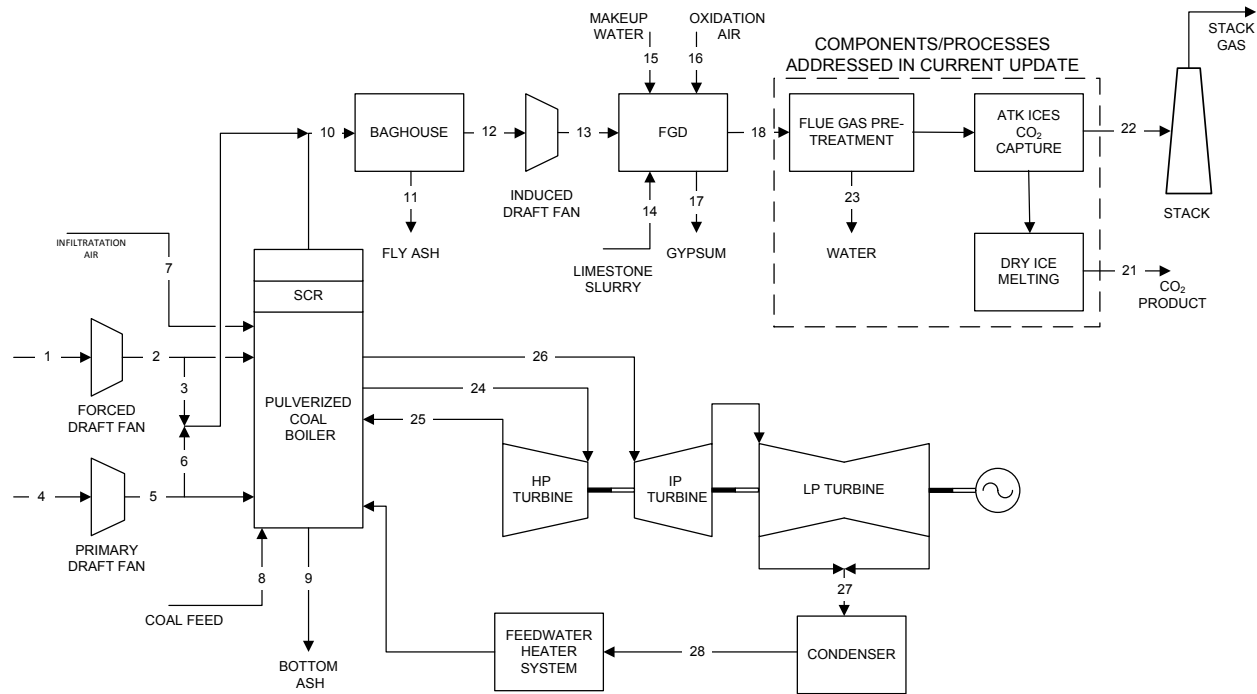
Figure 2-2
Block Flow Diagram of the Power Plant Equipped with modified ICES system

Table 2-2
Stream Table of the Power Plant Equipped with modified ICES system

	1	2	3	4	5	6	7	8	9	10	11	12	13	14
V-L Mole Fraction														
Ar	0.0092	0.0092	0.0092	0.0092	0.0092	0.0092	0.0092	0.0000	0.0000	0.0087	0.0000	0.0087	0.0087	0.0000
CO_2	0.0003	0.0003	0.0003	0.0003	0.0003	0.0003	0.0003	0.0000	0.0000	0.1450	0.0000	0.1450	0.1450	0.0000
H_2	0.0000	0.0000	0.0000	0.0000	0.0000	0.0000	0.0000	0.0000	0.0000	0.0000	0.0000	0.0000	0.0000	0.0000
H_2O	0.0099	0.0099	0.0099	0.0099	0.0099	0.0099	0.0099	0.0000	0.0000	0.0870	0.0000	0.0870	0.0870	1.0000
N_2	0.7732	0.7732	0.7732	0.7732	0.7732	0.7732	0.7732	0.0000	0.0000	0.7324	0.0000	0.7324	0.7324	0.0000
O_2	0.2074	0.2074	0.2074	0.2074	0.2074	0.2074	0.2074	0.0000	0.0000	0.0247	0.0000	0.0247	0.0247	0.0000
SO_2	0.0000	0.0000	0.0000	0.0000	0.0000	0.0000	0.0000	0.0000	0.0000	0.0021	0.0000	0.0021	0.0021	0.0000
Total	1.0000	1.0000	1.0000	1.0000	1.0000	1.0000	1.0000	0.0000	0.0000	1.0000	0.0000	1.0000	1.0000	1.0000
V-L Flowrate (kg mol /hr)	66,876	66,876	1,990	20,544	20,544	2,818	1,546	0	0	94,107	0	94,107	94,107	3,385
V-L Flowrate (kg/hr)	1,588,354	1,588,354	47,044	487,926	487,926	67,152	36,705	0	0	2,799,052	0	2,799,052	2,799,052	60,975
Solids Flowrate (kg/hr)	0	0	0	0	0	0	0	211,193	4,096	16,383	16,383	0	0	25,966
Temperature (°C)	15	19	19	15	25	25	15	15	15	169	15	169	181	15
Pressure (MPa, abs)	0.1	0.11	0.11	0.1	0.11	0.11	0.1	0.1	0.1	0.1	0.1	0.1	0.11	0.1
Enthalpy (kJ/kg)A	30.23	34.36	34.36	30.23	40.78	40.78	30.23	---	---	327.37	---	308.94	321.02	---
Density (kg/m^3)	1.2	1.2	1.2	1.2	1.3	1.3	1.2	---	---	0.8	---	0.8	0.8	---
V-L Molecular Weight	28.857	28.857	28.857	28.857	28.857	28.857	28.857	---	---	29.743	---	29.743	29.743	---
V-L Flowrate (lb mol /hr)	121,348	121,348	3,594	37,276	37,276	5,130	2,804	0	0	170,755	0	170,755	170,755	5,938
V-L Flowrate (lb/hr)	3,501,716	3,501,716	103,714	1,075,690	1,075,690	148,044	80,920	0	0	5,078,777	0	5,078,777	5,078,777	106,983
Solids Flowrate (lb/hr)	0	0	0	0	0	0	0	465,600	9,029	36,119	36,119	0	0	46,211
Temperature (°F)	59	66	66	59	78	78	59	59	59	59	59	59	59	59
Pressure (psia)	14.7	15.3	15.3	14.7	16.1	16.1	14.7	14.7	14.7	14.7	14.7	14.7	14.7	14.7
Enthalpy (Btu/lb)A	13	14.8	14.8	13	17.5	17.5	13	---	---	140.7	---	132.8	138	---
Density (lb/ft^3)	0.076	0.078	0.078	0.076	0.081	0.081	0.076	---	---	0.05	---	0.049	0.052	---

Table 2-2
Stream Table of the Power Plant Equipped with modified ICES system (Continued)

	15	16	17	18	21	22	23	24	25	26	27	28
V-L Mole Fraction												
Ar	0.0000	0.0128	0.0000	0.0081	0.0000	0.0112	0.0000	0.0000	0.0000	0.0000	0.0000	0.0000
CO_2	0.0000	0.0005	0.0004	0.1350	1.0000	0.0144	0.0110	0.0000	0.0000	0.0000	0.0000	0.0000
H_2	0.0000	0.0000	0.0000	0.0000	0.0000	0.0000	0.0000	0.0000	0.0000	0.0000	0.0000	0.0000
H_2O	1.0000	0.0062	0.9996	0.1537	0.0000	0.0000	0.9890	1.0000	1.0000	1.0000	1.0000	1.0000
N_2	0.0000	0.7506	0.0000	0.6793	0.0000	0.9414	0.0000	0.0000	0.0000	0.0000	0.0000	0.0000
O_2	0.0000	0.2300	0.0000	0.0238	0.0000	0.0330	0.0000	0.0000	0.0000	0.0000	0.0000	0.0000
SO_2	0.0000	0.0000	0.0000	0	0.0000	0.0000	0.0000	0.0000	0.0000	0.0000	0.0000	0.0000
Total	1.0000	1.0000	1.0000	1.0000	1.0000	1.0000	1.0000	1.0000	1.0000	1.0000	1.0000	1.0000
V-L Flowrate (kg mol /hr)	13,485	975	250	84,314	10,464	60,843	721	103,260	87,211	87,211	45,984	79,441
V-L Flowrate (kg/hr)	242,941	28,289	4,498	2,430,600	460,507	1,734,580	13,196	1,860,231	1,571,110	1,571,110	828,397	1,431,132
Solids Flowrate (kg/hr)	0	0	40,138	0	0	0	0	0	0	0	0	0
Temperature (°C)	15	167	57	57	35	89	32	593	354	593	38	39
Pressure (MPa, abs)	0.10	0.31	0.10	0.1	15.27	0.1	1.00	24.23	4.90	4.52	0.01	1.72
Enthalpy (kJ/kg)A	-46.8	177.65	---	298	-9143	65.0	-15667	3481	3082	3655	2346	163
Density (kg/m³)	1003.1	2.5	---	1.1	720.945	0.98	545.777	69.18434	18.67769	11.56543	0.064074	993.2975
V-L Molecular Weight	18.015	29.029	---	28.83	44	28.57	18.30154	18.015	18.015	18.015	18.015	18.015
V-L Flowrate (lb mol /hr)	24,055	1,820	440	185,828	23,063	134,097	1,590	227,649	192,268	192,268	101,377	175,137
V-L Flowrate (lb/hr)	433,364	52,827	7,941	5,358,501	1,015,234	3,824,055	29,091	4,101,100	3,463,700	3,463,700	1,826,300	3,155,100
Solids Flowrate (lb/hr)	0	0	71,920	0	0	0	0	0	0	0	0	0
Temperature (°F)	59	333	136	135	95	192	90	1100	669	1100	101	101
Pressure (psia)	14.7	45	14.9	14.5	2215	14.5	145	3515	711	656	0.982	250
Enthalpy (Btu/lb)A	-20.1	76.4	---	130	-3989	28	-6736	1497	1325	1572	1008	70
Density (lb/ft³)	62.62	0.154	---	0.067	43.9	0.060	34.07	4.32	1.166	0.722	0.004	62.01

Performance Results

The performance summary of the power plant equipped with the modified flue gas preconditioning and ICES systems is presented in Table 2-3.

Table 2-3
Performance Summary of the Power Plant with Modified Flue Gas Pretreatment and ICES Systems

POWER SUMMARY, kWe	
Steam Turbine Gross Power at Generator Terminals	**692,851**
Coal Handling and Conveying	470
Pulverizers	3,170
Sorbent Handling & Reagent Preparation	1,030
Ash Handling	610
Primary Air Fans	1,480
Forced Draft Fans	1,890
Induced Draft Fans	8,530
SCR	60
Baghouse	80
Wet FGD	3,390
Miscellaneous Balance	2,000
Steam Turbine Auxiliaries	400
Condensate Pumps	851
Circulating Water Pumps	6,750
Ground Water Pumps	640
Cooling Tower Fans	3,500
CO_2 Capture - Booster Fan	5,143
CO_2 Capture - Flue Gas Compressor	195,984
CO_2 pressurization	1,850
DCC Cooling Water Pump	533
Heat Transfer Fluid Pump	391
Transformer Losses	2,395
Total Auxiliaries	**241,347**
Net Power	**451,800**
Net Plant Heat Rate, Btu/kWh HHV	12,030
Net Plant Efficiency, HHV	28.4%

Major Equipment List

Major equipment list provided in Table 2-4 includes equipment components utilized for the modified Flue Gas Pretreatment system. All other plant equipment is identical to the initial WP TEA.

Table 2-4
Major Equipment List of Modified Flue Gas Pretreatment System

Equipment No.	Description	Type	Design Condition	Quantity
1	Booster Fan	Centrifugal	Flow: 5,358,550 lb/hr	1 op
			Inlet Pressure: 14.7 psia	
			Outlet Pressure: 29.4 psia	
			Power: 4,700 kW	
2	Direct Contact	Vertical	65 ft dia, 80 ft T/T,	1 op
	Cooler		Operating: 15 psig / 136°F,	
			Design: +-1 psig / 135°F,	
			Pressure Drop: 2 psia	
			Flow: 5,358,550 lb/hr	
			Carbon Steel lined w/ SS	
3	Wet Cooling Tower	Mechanical Draft	Heat Duty: 500 MMBtu/hr,	1 op
4	Flue Gas Compressor /	Two Stage, Axial	Inlet Gas Flow: 5,515,000 lb/hr	1 op
	Motor Driven		Inlet Pressure: 14.7 psia	
			Outlet Pressure: 174 psia	
			Power: 196,000 kW	
5	Compressor Interstage	Heat Exchanger	Heat Duty: 249 MMBtu/hr,	1 op
	Cooler 1	Shell & Tube	Shell Side:	
	(LP Feed Water Heater 1)		Fluid: Flue Gas	
			Flow: 5,515,000 lb/hr	
			81 psia (with 0.4 psi pressure drop)	
			428°F	
			Cold Side (Finned Tube)	
			Fluid: LP Boiler Feedwater	
			Flow: 3,010,581 lb/hr	
			245 psia	
			300°F	
			304 SS Heat Transfer Surface Area: 174,000 ft^2	

Table 2-4
Major Equipment List of Modified Flue Gas Pretreatment System (Continued)

Equipment No.	Description	Type	Design Condition	Quantity
6	Compressor Interstage	Heat Exchanger	Heat Duty: 39 MMBtu/hr,	1 op
	Trim Cooler 1	Shell & Tube	Shell Side:	
			Fluid: Flue Gas	
			Flow: 5,515,000 lb/hr	
			81 psia (with 0.2 psi pressure drop)	
			428°F	
			Cold Side (Finned Tube)	
			Fluid: cooling water (Finned Tube)	
			Flow: 663,000 lb/hr	
			25 psia	
			240°F	
			304 SS	
			Heat Transfer Surface Area: 55,000 ft^2	
7	Compressor After Cooler	Heat Exchanger	Heat Duty: 384 MMBtu/hr,	1 op
	(LP Feed Water Heater 2)	Shell & Tube	Shell Side:	
			Fluid: Flue Gas	
			Flow: 5,488,000 lb/hr	
			174 psia (with 0.4 psi pressure drop)	
			224°F	
			Cold Side (Finned Tube)	
			Fluid: LP Boiler Feedwater	
			Flow: 2,487,000 lb/hr	
			245 psia	
			200°F	
			304 SS	
			Heat Transfer Surface Area: 395,000 ft^2	
8	Compressor After Cooler	Heat Exchanger	Heat Duty: 28 MMBtu/hr,	1 op
	Trim Cooler 2	Shell & Tube	Shell Side:	
			Fluid: Flue Gas (with .2 psi pressure drop)	
			Flow: 5,488,000 lb/hr	
			174 psia	
			224°F	
			Cold Side (Finned Tube)	
			Fluid: Cooling water	
			Flow: 150,000 lb/hr	
			25 psia	
			100°F	
			304 SS	
			Heat Transfer Surface Area: 8,000 ft^2	

Table 2-4
Major Equipment List of Modified Flue Gas Pretreatment System (Continued)

Equipment No.	Description	Type	Design Condition	Quantity
9	Molecular Sieve Dryer	Two Bed Adsorption	Inlet Flow: 5,461,000 lb/hr	1 op
		System	Inlet Pressure: 174 psia	
			Inlet Temperature: 104°F	
			Outlet Product Gas Water Content: < 5ppm	
			Water Removal Eff: >= 99.95%	
10	Flue Gas Cooler	Heat Exchanger	Heat Duty: 154 MMBtu/hr,	1 op
		Shell & Tube	Shell Side:	
			Fluid: Flue Gas	
			Flow: 5,457,850 lb/hr	
			174 psia (with 0.3 psi pressure drop)	
			104°F	
			Cold Side (Finned Tube)	
			Fluid: Heat Transfer Fluid	
			Flow: 6,838,015 lb/hr	
			100 psia	
			110°F	
			304 SS	
			Heat Transfer Surface Area: 715,000 ft^2	
11	ICES System		As Specified by ATK	1 op
12	Screw Feeder		Material: Dry Ice	4 op
			Flow: 254,000 lb/hr	
			150 psia	
			-107 °F	
13	Dry Ice Melting Vessel		Contains One heat exchanger	2 op
			38 MMBtu	
			Inside Diameter:8 ft	
			Length: 14 ft	
			Stainless Steel	
			Internal heat exchanger Surface Area: 7,000 ft^2	

Table 2-4
Major Equipment List of Modified Flue Gas Pretreatment System (Continued)

Equipment No.	Description	Type	Design Condition	Quantity
14	CO$_2$ Product Heater	Shell & Tube	Heat Duty: 67 MMBtu/hr,	1 op
			Shell Side:	
			Fluid: Heat Transfer Fluid	
			Flow: 424,000 lb/hr	
			100 psia	
			150°F	
			Cold Side (Tube)	
			Fluid: Liquid CO$_2$	
			Flow: 1,015,242 lb/hr	
			2215 psia	
			-39 °F	
			304 SS	
			Heat Transfer Surface Area: 20,000 ft^2	
15	Heat Transfer Fluid pump	Centrifugal	Fluid: Heat Transfer Fluid	2 op
			Flow: 3,100,000 lb/hr (each)	
			Inlet:	
			Pressure: 15 psia	
			Temp: 70 °F	
			Outlet:	
			Pressure: 100 psia	
			Temp: 70°F	
16	Recirculating Flow Heater	Shell & Tube	Heat Duty: 20 MMBtu/hr,	
			Shell Side:	
			Fluid: Flue Gas	
			Flow: 618,500 lb/hr	
			20 psia	
			-106°F	
			Tube Side	
			Fluid: Heat Transfer Fluid	
			Flow: 298,000 lb/hr	
			100 psia	
			50°F	
			304 SS	
			Heat Transfer Surface Area: 64,000 ft^2	

Table 2-4
Major Equipment List of Modified Flue Gas Pretreatment System (Continued)

Equipment No.	Description	Type	Design Condition	Quantity
17	CO$_2$ Pump		Fluid: Liquid CO$_2$	4 op
			Flow: 254,000 lb/hr	
			Inlet:	
			Pressure: 145 psia	
			Temp: -50°F	
			Outlet:	
			Pressure: 2,215 psia	
			Temp: -39°F	

3 COST ESTIMATE AND ECONOMIC ANALYSIS

Cost Estimate

The cost estimating methodology used to determine the capital costs and operating costs is identical to the initial WP TEA, with the costs presented on a 2012 cost basis for a generic greenfield Midwestern US location. The total capital cost summary of the power plant equipped with modified flue gas pretreatment in ICES systems is presented in Table 3-1.

Table 3-1
Total Plant Cost Summary

Client:	EPRI									**Report Date:**	2017-Jan-27	
Project:	Acent ICES Revision											
		TOTAL PLANT COST SUMMARY										
Case:	Acent ICES - 1x451.6 MWnet SubCritical PC w/ CO2 Capture											
Plant Size:	451.6 MW,net			**Estimate Type:** Conceptual				**Cost Base (Jun)**	2012	($x1000)		

Acct No.	Item/Description	Equipment Cost	Material Cost	Labor Direct	Labor Indirect	Sales Tax	Bare Erected Cost $	Eng'g CM H.O.& Fee	Contingencies Process	Contingencies Project	TOTAL PLANT COST $	TOTAL PLANT COST $/kW
1	COAL & SORBENT HANDLING	$21,916	$5,568	$13,040	$0	$0	**$40,524**	$3,556	$0	$6,612	**$50,691**	$92
2	COAL & SORBENT PREP & FEED	$14,818	$825	$3,743	$0	$0	**$19,386**	$1,650	$0	$3,155	**$24,192**	$44
3	FEEDWATER & MISC. BOP SYSTEMS	$58,179	$0	$26,854	$0	$0	**$85,033**	$7,476	$0	$15,077	**$107,587**	$196
4	PC BOILER & ACCESSORIES											
4.1	PC Boiler & Accessories	$208,167	$0	$116,889	$0	$0	**$325,056**	$30,821	$0	$35,588	**$391,465**	$712
4.2	SCR (w/4.1)	$0	$0	$0	$0	$0	**$0**	$0	$0	$0	**$0**	$0
4.3	Open	$0	$0	$0	$0	$0	**$0**	$0	$0	$0	**$0**	$0
4.4-4.9	Boiler BoP (w/ ID Fans)	$0	$0	$0	$0	$0	**$0**	$0	$0	$0	**$0**	$0
	SUBTOTAL 4	**$208,167**	**$0**	**$116,889**	**$0**	**$0**	**$325,056**	**$30,821**	**$0**	**$35,588**	**$391,465**	**$712**
5	FLUE GAS CLEANUP	$108,400	$0	$36,301	$0	$0	**$144,701**	$13,322	$0	$15,802	**$173,826**	$316
5B	CO2 REMOVAL & COMPRESSION	$155,383	$51,016	$92,507	$0	$0	**$298,906**	$23,607	$47,830	$64,714	**$435,056**	$963
6	COMBUSTION TURBINE/ACCESSORIES											
6.1	Combustion Turbine Generator	N/A	$0	N/A	$0	$0	**$0**	$0	$0	$0	**$0**	$0
6.2-6.9	Combustion Turbine Accessories	$0	$0	$0	$0	$0	**$0**	$0	$0	$0	**$0**	$0
	SUBTOTAL 6	**$0**	**$0**	**$0**	**$0**	**$0**	**$0**	**$0**	**$0**	**$0**	**$0**	**$0**
7	HRSG, DUCTING & STACK											
7.1	Heat Recovery Steam Generator	N/A	$0	N/A	$0	$0	**$0**	$0	$0	$0	**$0**	$0
7.2-7.9	HRSG Accessories, Ductwork and Stack	$18,458	$950	$12,409	$0	$0	**$31,816**	$2,830	$0	$4,546	**$39,193**	$71
	SUBTOTAL 7	**$18,458**	**$950**	**$12,409**	**$0**	**$0**	**$31,816**	**$2,830**	**$0**	**$4,546**	**$39,193**	**$71**
8	STEAM TURBINE GENERATOR											
8.1	Steam TG & Accessories	$69,548	$0	$8,496	$0	$0	**$78,044**	$6,805	$0	$8,485	**$93,334**	$170
8.2-8.9	Turbine Plant Auxiliaries and Steam Piping	$35,433	$1,276	$16,587	$0	$0	**$53,297**	$4,284	$0	$8,127	**$65,708**	$119
	SUBTOTAL 8	**$104,981**	**$1,276**	**$25,084**	**$0**	**$0**	**$131,341**	**$11,089**	**$0**	**$16,612**	**$159,041**	**$289**
9	COOLING WATER SYSTEM	$19,510	$9,872	$17,605	$0	$0	**$46,987**	$4,265	$0	$6,928	**$58,181**	$106
10	ASH/SPENT SORBENT HANDLING SYS	$6,019	$175	$7,753	$0	$0	**$13,947**	$1,286	$0	$1,566	**$16,799**	$31
11	ACCESSORY ELECTRIC PLANT	$22,032	$8,921	$23,809	$0	$0	**$54,762**	$4,709	$0	$7,418	**$66,889**	$122
12	INSTRUMENTATION & CONTROL	$12,165	$0	$12,303	$0	$0	**$24,469**	$2,158	$1,223	$3,436	**$31,285**	$57
13	IMPROVEMENTS TO SITE	$3,601	$2,070	$7,748	$0	$0	**$13,419**	$1,326	$0	$2,949	**$17,694**	$32
14	BUILDINGS & STRUCTURES	$0	$27,843	$26,869	$0	$0	**$54,711**	$4,845	$0	$8,933	**$68,490**	$125
	TOTAL COST	**$753,628**	**$108,516**	**$422,914**	**$0**	**$0**	**$1,285,058**	**$112,941**	**$49,053**	**$193,337**	**$1,640,388**	**$3,632**

The development of the Bare Erected Costs for the modified ICES CO_2 capture system including the flue gas pretreatment equipment, the ICES CO_2 capture equipment and the dry ice melting system is provided in Table 3-2.

Table 3-2
Buildup of ATK ICES CO_2 Capture System and Supporting Systems Bare Erected Cost (2012$)

Item No.	Item Description	Equipment Cost (Total)	Material Cost	Labor Cost	Bare Erected Cost $
1	Booster Fan	$1,680,000	$616,000	$1,293,600	$3,589,600
2	Direct Contact Cooler	$6,710,720	$2,460,597	$5,167,255	$14,338,573
3	Wet Cooling Tower	$4,961,054	$2,510,330	$4,476,572	$11,947,956
4a	Flue Gas Compressor - First Stage	$43,568,000	$5,809,067	$12,199,040	$61,576,107
4b	Flue Gas Compressor - Second Stage	$42,672,000	$5,689,600	$11,948,160	$60,309,760
5	Compressor Interstage Cooler 1	$2,757,161	$1,194,770	$2,509,016	$6,460,947
6	Compressor Interstage Trim Cooler 1	$2,235,749	$968,824	$2,034,531	$5,239,104
7	Compressor Aftercooler 1	$4,187,106	$1,814,413	$3,810,267	$9,811,785
8	Compressor Aftercooler Trim Cooler 2	$827,788	$358,708	$753,287	$1,939,782
9	Molecular Sieve Dryer	$2,240,000	$1,083,871	$2,276,129	$5,600,000
10	Flue Gas Cooler	$2,909,550	$1,260,805	$2,647,690	$6,818,045
11	ICES System				
	Distribution Duct	$960,000	$320,000	$672,000	$1,952,000
	Expansion Duct	$7,200,000	$2,400,000	$5,040,444	$14,640,444
	Dry Ice Cyclone	$6,646,596	$4,431,064	$9,305,234	$20,382,894
	Collection Duct	$960,000	$320,000	$672,000	$1,952,000
12	Screw Feeder	$16,098,333	$5,366,111	$11,268,833	$32,733,277
13	Dry Ice Melting Vessel	$1,709,186	$1,091,810	$2,292,802	$5,093,798
14	CO_2 Product Heater	$2,285,274	$990,286	$2,079,600	$5,355,160
15	Heat Transfer Fluid pump	$1,072,531	$1,072,531	$2,252,316	$4,397,378
16	Recirculating Flow Heater	$1,491,077	$646,134	$1,356,880	$3,494,091
17	CO_2 Pump	$2,211,223	$2,211,223	$4,643,568	$9,066,013
18	Ductwork, incl. Foundations and Supports	$0	$8,400,000	$3,808,000	$12,208,000
	Total	**$155,383,348**	**$51,016,143**	**$92,507,224**	**$298,906,715**

Economic Analysis

Plant specific inputs, both technical and cost, for the power plant with the modified ICES CO_2 capture system are listed in Table 3-4. This table compares the results to those for the DOE/NETL Case 11 and Case 12.

Table 3-3
Comparison of Operating Parameters and Costs between the DOE/NETL Baseline Cases and the modified ATK ICES Case

	Case 11	Case 12	ICES 2013 (Note)	ICES Revised
OPERATING PARAMETERS				
Net Plant Output, MWe	550.0	550.0	550.0	451.80
Net Plant Heat Rate, Btu/kWh HHV (kJ/kWh)	8,686 (9,165)	12,002 (12,663)	9,896 (10,441)	12,030 (12,693)
CO_2 Captured, lb/MWh (kg/MWh)	-	2,200 (998)	1,813 (822)	2,204 (998)
CO_2 Emitted, lb/MWh net (kg/MWh net)	1768 (802)	244 (111)	201 (91)	245 (111)
COSTS				
Risk	Low	High	High	High
Total Plant Costs (2012$/kW)	2,033	3,651	2,897	3,660
Total Overnight Cost (2012$/kW)	2,513	4,496	3,565	4,499
Bare Erected Cost	1,665	2,815	2,252	2,844
Home Office Expenses	151	256	205	259
Project Contingency	217	456	352	428
Process contingency	0	124	89	128
Owners Costs	480	844	668	840
Total Overnight Cost (2012$x1,000)	1,382,286	2,472,362	1,960,975	2,032,814
Total As Spent Capital (2012$/kw)	2,850	5,125	4,065	5,129
Annual Fixed Operating Costs ($/yr)	39,826,084	65,958,457	56,039,860	56,079,253
Variable Operating Costs ($/MWh)	7.24	12.39	9.23	11.23
Fuel				
Coal Price ($/ton)	69.00			

Note: Subsequent simulations have shown that the embodiment of the process analyzed in 2013 would not perform as reported.

Table 3-3 illustrates the relative changes in the ICES CO_2 system with the increased pressure to the expansion nozzle. With keeping the power plant size the same on a gross basis, the net output of the power plant decreases from 550MW to 451.6MW and the net plant heat rate of the plant increases from 9,896 to 12,035 Btu/kWh, similar to that of the Case 12. Further, in part due to the higher installed costs and the lower net power generation, the total overnight costs have increased from $3,565/kW to $4,499/kW. Both of these changes will have unfavorable impact on the revised case economics.

The comparisons in LCOE between the DOE Case 11 and 12 and the ICES cases are shown in Table 3-4 and Figure 3-1.

The increases in COE from the non-capture, Case 11, are 77% for both the DOE/NETL Case 12 and the revised ICES case. Note that this assessment does not take into account the resizing of the power generation equipment, primarily the boiler and the steam turbine generator. Resizing all of this equipment to produce net power of 550 MW will result in a small improvement in the economics. However, it is not anticipated that these changes will greatly impact the overall results.

Table 3-4
Comparison of the Economic Analysis Results between the DOE/NETL Cases and the Modified ICES Case

	Case 11	Case 12	ICES 2013	ICES Revised
COE ($/MWh, 2012$)	**81.81**	**144.45**	**116.17**	**144.02**
CO_2 TS&M Costs		5.60	4.61	5.61
Fuel Costs	25.69	35.49	29.27	35.58
Variable Costs	7.24	12.39	9.23	11.23
Fixed Costs	9.72	16.11	13.68	16.67
Capital Costs	39.15	74.87	59.38	74.93
LCOE (2012$/MWh)	103.73	183.17	147.30	182.17
Cost of CO_2 Captured ($/tonne CO_2)		62.79	41.79	62.79
Cost of CO_2 Avoided ($/tonne CO_2)		90.67	48.36	90.67
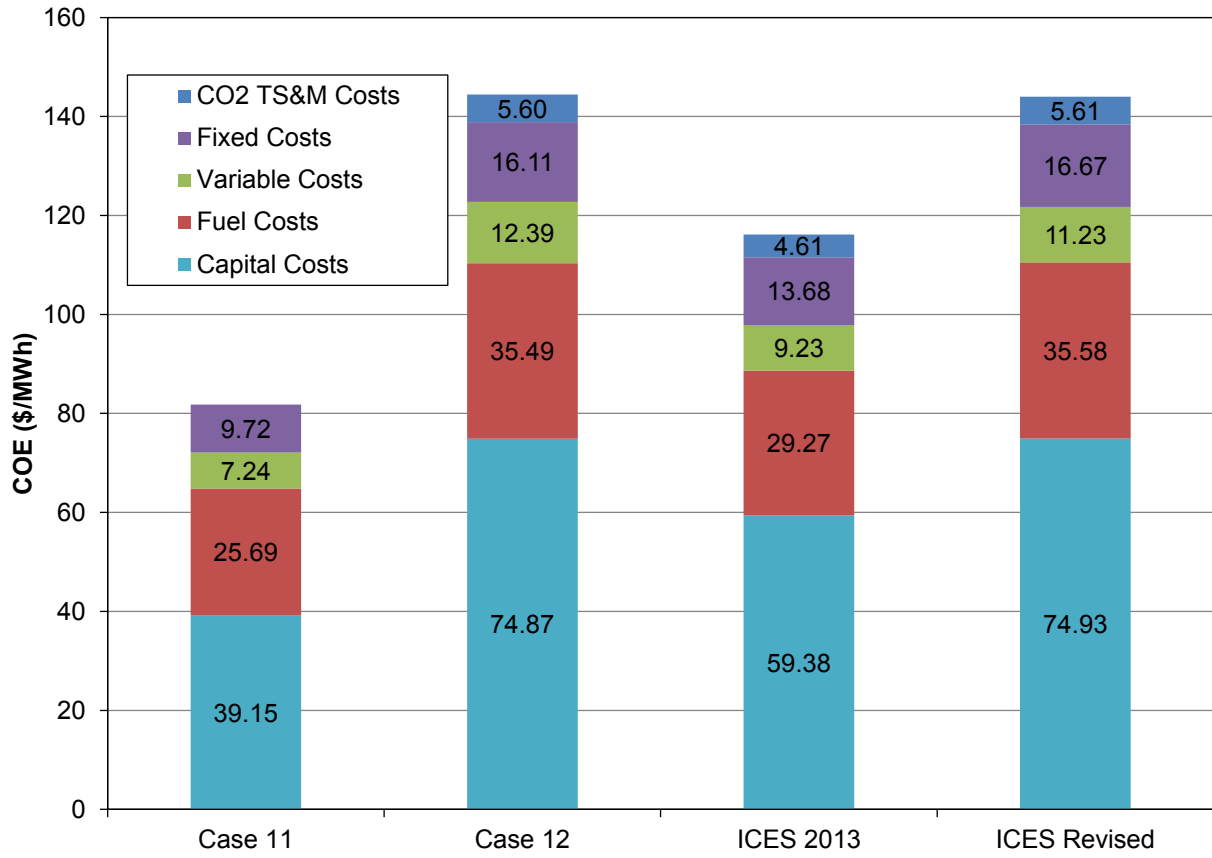
Figure 3-1
Comparison and Breakdown of COE for the DOE/NETL Baseline Cases and the ICES Cases

4 STUDY FINDINGS

Performance and Cost Summary

The current study revises the previously performed TEA, which was based on the original embodiment of the ICES process studied in the March 2013. This revision is based on the latest process design requirements for the flue gas to the ICES expansion nozzle to produce dry ice from the flue gas. The focus of this study was to modify the flue gas pretreatment system to meet the revised flue gas specification and integrate the heat required for melting the dry ice with the flue gas cooling. An additional change included moving the water separation step, required to produce a pipeline quality CO_2 product, to upstream of the expansion step. Other major components of the system were assumed to remain the same. The system was optimized to reduce the auxiliary loads through minimizing the compression energy, integrating the heat of compression with the feedwater heating, and utilizing the cooling potential of the dry ice. A summary of the plant performance, the capital costs, and economic results is provided in Table 4-1.

Table 4-1 Summary of Plant Performance, Capital Costs, and Economic Results.

	Case 11	Case 12	ICES 2013	ICES Revised
PLANT DESCRIPTION				
Steam Cycle	Supercritical	Supercritical	Supercritical	Supercritical
CO_2 Capture	No	Yes	Yes	Yes
OPERATING PARAMETERS				
Net Plant Output, MWe	550.0	550.0	550.0	451.80
Net Plant Heat Rate, Btu/kWh HHV (kJ/kWh)	8,686 (9,165)	12,002 (12,663)	9,896 (10,441)	12,030 (12,693)
Net Plant Efficiency, HHV	39.3%	28.4%	34.5%	28.4%
CO_2 Captured, lb/MWh (kg/MWh)	-	2,200 (998)	1,813 (822)	2,204 (998)
CO_2 Emitted, lb/MWh net (kg/MWh net)	1768 (802)	244 (111)	201 (91)	245 (111)
CAPITAL AND OPERATING COSTS				
Total Overnight Cost (2012$/kW)	2,513	4,496	3,565	4,499
Variable Operating and Maintenance ($/MWh)	7.24	12.39	9.23	11.24
Fixed Operating and Maintenance ($/yr)	39,826,084	65,958,457	56,039,860	56,079,253
ECONOMIC METRICS				
COE ($/MWh, 2012$)	81.81	144.45	116.17	144.02
Cost of CO_2 Captured ($/tonne CO_2)	NA	62.79	41.79	62.79
Cost of CO_2 Avoided ($/tonne CO_2)	NA	90.67	48.36	90.67

Potential Technology Hurdles

The increased pressure and decreased temperature requirements of the flue gas to the ICES expansion nozzle resulted in significant changes in the flue gas pretreatment system. As illustrated in the performance modeling and cost estimating activities, the changes resulted in:

- A significant increase in the plant auxiliary load to compress the incoming flue gas.

- Additional or larger equipment including heat exchangers and compressors.

Meeting the revised ICES flue gas specification of higher pressure and lower temperature poses a technology hurdle for this CO_2 capture approach.

Potential Applications for ICES Technology

While this technology does not show cost or energy savings compared to baseline amine capture technology, it does still have several advantages including:

1. Compact system size

2. No chemical separation agent

3. Significantly lower energy consumption at partial capture rates

4. Improved performance with lower inlet CO_2 concentrations

The compact size and lack of additional chemical agents in contact with the flue gas or product CO_2 could be useful for applications constrained in space or with stringent emissions restrictions for degradation or carryover. However, these are minor benefits that would likely not cause the adoption of this technology in isolation. Applications with lower CO_2 inlet concentration or with less than 90% capture required present potential applications where the ICES process may be better suited than competing technologies.

Unlike other capture technologies that typically use the driving force of the partial pressure of CO_2 in the gas phase to absorb into a chemical agent in a counter-current configuration, the ICES process is a co-current capture system. The role of excess gas in other systems serves only to lower the partial-pressure of the CO_2 and hence driving force of the CO_2 capture process. In ICES, the excess gas is used to absorb the energy released during CO_2 phase change as well as to transfer kinetic energy to the solid CO_2 particles. At lower concentrations of CO_2, the energy released during phase change has less impact on the temperature of the full system and so capture can be accomplished at lower velocities and with less pressure drop, and hence less extreme initial conditions. Similarly, capturing less of the CO_2 from a gas stream does not require such low temperatures and high velocities, meaning that less compression and pre-cooling would be required.

While this analysis was undertaken on the basis of 90% capture from the flue gas of a coal-fired power plant, partial capture or capture from a lower concentration gas stream would show a significantly reduced energy of capture and would exhibit performance that may be substantially more favorable than under these capture conditions.

A APPENDIX
REFINEMENT OF ICES PLANT, CONCEPT OF OPERATION AND PERFORMANCE EVALUATION, PREPARED FOR ATK BY WORLEYPARSONS, MARCH 2013.

Refinement of ICES Plant
Concept of Operation and Performance Evaluation

Prepared for:

Prepared by:

WorleyParsons Group Inc.

March 22, 2013

[Revision 2]

NOTICE

This Report was prepared by WorleyParsons Group Inc. as an account of work contracted by and for the benefit of the ATK.

Reference herein to any specific commercial product, process, or service by trade name, trademark, manufacturer, or otherwise does not necessarily constitute or imply its endorsement, recommendation, or favoring by WorleyParsons.

The information presented in this document represents the collective efforts of ATK and WorleyParsons.

TABLE OF CONTENTS

when experience counts

LIST OF EXHIBITS

Revision Record

Revision	Date	Content
0	2012-12-20	Draft issued to ATK for comments
1	2013-01-09	Final issued to ATK for comments
2	2013-03-22	Final version issued to ATK

List of Abbreviations

AACE	Association for the Advancement of Cost Engineering
ARPA-E	Advanced Research Project Agency– Energy
APC	Air pollution control
Aspen	Aspen Plus®
BEC	Bare erected cost
BFD	Block flow diagram
BFW	Boiler feedwater
Btu	British thermal unit
Btu/hr	British thermal unit per hour
Btu/kWh	British thermal unit per kilowatt-hour
Btu/lb	British thermal unit per pound
CCF	Capital Charge Factor
COE	Cost of electricity
DOE	Department of Energy
EIA	Energy Information Administration
EPA	Environmental Protection Agency
EPC	Engineer/Procure/Construct
EPC	Engineering/Procurement/ Construction Management
ESP	Electrostatic precipitator
FD	Forced draft
FGD	Flue gas desulfurization
FOAK	First-of-a-kind
gal/MWh	Gallon per megawatt hour
HHV	Higher heating value
hp	Horsepower
ICES	Inertial CO_2 Extraction System
ID	Induced draft
ISO	International Organization for Standardization
kJ	Kilojoules
kV	Kilovolt
kW	Kilowatt
kWe	Kilowatt-electric
kWh	Kilowatt-hour
lb	Pound
LCOE	Levelized cost of electricity
MAF	Moisture/Ash-Free
m	meters
mol%	Mole percent
MPa	Megapascals
MVA	Mega volt-amps
MW	Megawatt
MWe	Megawatts electric
MWh	Megawatt-hour
NETL	National Energy Technology Laboratory

NOAK	Nth-of-a-kind
NOx	Oxides of nitrogen
O&M	Operation and maintenance
PA	Primary air
PC	Pulverized coal
PFD	Process flow diagram
PM	Particulate matter
ppm	Parts per million
ppmv	Parts per million volume
psi	Pounds per square inch
psia	Pounds per square inch absolute
psig	Pounds per square inch gage
PSFM	Power systems financial model
SC	Supercritical
SC PC	Supercritical Pulverized Coal
SCR	Selective catalytic reduction
SNCR	Selective non-catalytic reduction
SO_x	Oxides of sulfur
SS	Stainless steel
STG	Steam turbine generator
TASC	Total as-spent cost
TOC	Total overnight cost
Tonne	Metric ton (1000 kg)
TPC	Total plant cost
TPD	Tons per day
TPH	Tons per hour
TPI	Total plant investment
vol%	Volume percent
WB	Wet bulb
wt%	Weight percent
yr	Year
$/MMBtu	Dollars per million British thermal units
$/MMkJ	Dollars per million kilojoule
$/MWh	Dollars per megawatt-hour
°C	Degrees Celsius
°F	Degrees Fahrenheit

ES - Executive Summary

The Inertial CO_2 Extraction System (ICES) technology being developed by ATK is a CO_2 separation process capable of removing CO_2 from coal derived combustion gases and producing solid carbon dioxide. One application of this technology is to capture CO_2 from coal fired steam power plants, in a post-combustion mode to reduce their CO_2 emissions. The captured CO_2 would then be transported by pipeline to a storage site for long term storage.

To assess the feasibility of the ATK ICES technology and to compare this technology to state-of-the-art post-combustion CO_2 capture technologies for power plants, ATK enlisted the help of WorleyParsons to provide guidance and support for incorporating their technology into a supercritical coal fired power plant. Specific support included:

1. Refinement of specific system components to support the integration of the ICES technology into carbon capture at a coal fired power plant, specifically:

    a) Dehydration and compression of the flue case prior to the ICES

    b) Transfer of the dry ice/CO_2 from the ICES to pipeline as supercritical CO_2

    c) Use of dry ice as a cooling source.

2. Integration of the capture system into a supercritical pulverized coal (PC) power plant.

3. Preparation of a preliminary economic assessment.

4. Compare the plant performance and economics to state-of-the-art capture processes as presented in the Department of Energy (DOE)/ National Energy Technology Laboratory (NETL) Bituminous Baseline Report[1].

The supercritical pulverized coal (SC PC) power plant designs with and without CO_2 capture provided in the Bituminous Baseline Report were used as a basis for facilities developed and compared to during this study. The Case 11 configuration from this report is the without capture plant configuration, while Case 12 is the with CO_2 capture configuration. The post-combustion CO_2 capture technology used in Case 12 is the Fluor Econamine FG Plus^{SM}.

Approach

The approach used to develop the assessment of the ATK ICES CO_2 technology included:

*   Selecting technologies and systems that allow for the integration of the ICES technology into a power facility and the production of a CO_2 stream suitable for pipeline transportation.
*   Modeling of the systems and power generation facility to determine the performance of the facility with the ATK ICES CO_2 technology
*   Determining the equipment sizes for the power plant and the ICES CO_2 capture equipment
*   Developing capital and operating and maintenance (O&M) cost estimates based on the performance modeling
*   Performing an economic assessment with the plant performance and cost estimating results. The economic assessment determined:
    o   Cost of electricity (COE)
    o   Levelized cost of electricity
    o   Cost of CO_2 captured
    o   Cost of CO_2 avoided
    o   Increase in COE over non-capture case.

Summary of Findings

Performance and Cost

The current study developed a conceptual supercritical pulverized coal fired unit that incorporated the ATK ICES CO_2 capture technology. As part of this study, systems for pretreating the flue gas prior to the CO_2 capture technology and melting the dry ice after separation were developed. Reducing the auxiliary loads through minimizing the compression energy and utilizing the cooling potential of the dry ice were considered to improve the plant efficiency. A summary of the plant performance, the capital costs, and economic results are provided in Exhibit ES-1.

Exhibit ES-1 Summary of Plant Performance, Capital Costs, and Economic Results.

	Case 11	Case 12	ATK ICES
PLANT DESCRIPTION			
Steam Cycle	Supercritical	Supercritical	Supercritical
CO_2 Capture	No	Yes	Yes
OPERATING PARAMETERS			
Net Plant Output, MWe	550.0	550.0	550.0
Net Plant Heat Rate, Btu/kWh HHV (kJ/kWh)	8,686 (9,165)	12,002 (12,663)	9,896 (10,441)
Net Plant Efficiency, HHV	39.3%	28.4%	34.5%
CO_2 Captured, lb/MWh (kg/MWh)	-	2,200 (998)	1,813 (822)
CO_2 Emitted, lb/MWh net (kg/MWh net)	1768 (802)	244 (111)	201 (91)
CAPITAL AND OPERATING COSTS			
Total Overnight Cost (2012$/kW)	2,513	4,496	3,565
Variable Operating and Maintenance ($/MWh)	7.24	12.39	9.23
Fixed Operating and Maintenance ($/yr)	39,826,084	65,958,457	56,039,860
ECONOMIC METRICS			
COE ($/MWh, 2012$)	81.81	144.45	116.17
Cost of CO_2 Captured ($/tonne CO_2)	NA	62.79	41.79
Cost of CO_2 Avoided ($/tonne CO_2)	NA	90.67	48.36

The implementation of carbon capture to power generation increases capital costs, operating and maintenance costs. Compared to the cost increases incurred with the adding the Fluor Econamine technology to a supercritical power plant, as illustrated by cases 11 and 12 in the Bituminous Baseline report, ATK ICES CO_2 capture technology offers several advantages. The reduction in cost increases are:

- Capital costs: 47%
- Variable Operating and Maintenance Costs: 61%
- Fixed Operating Costs: 38%

Additionally, the improvement in the plant efficiency decreases the additional fuel costs by 63% compared to the Bituminous Baseline Report capture case (Case 12).

The increase in the cost of electricity, as compared to Case 11, for the facility with the ATK ICES CO_2 is 42%. This compares 77% for the CO_2 capture Case 12 in the Bituminous Baseline report. This relatively lower increase of the cost of electricity for the ATK ICES technology is a result of the lower capital and O&M costs and improvements in the overall plant efficiency.

Footprint Compared to MEA Capture Systems

A layout for a 550 MW net generation facility with the ATK ICES CO_2 capture equipment was developed to illustrate the arrangement of the equipment and determine the footprint of the capture system. The footprint for the ATK ICES CO_2 capture equipment was determined to be on the order of 8,000 m^2 which compares to 20,000 to 30,000 m^2 for amine capture systems plants with similar net capacities[2, 3, 4]

Potential Technology Hurdles

During the process development work two potential technical hurdles were identified:

1. The pressurization of the dry ice from atmospheric pressure to ~10 bar to allow the melting to result in liquid CO_2.
2. The future use of the filtration method to remove the solid water ice from the liquid CO_2, or possibly the method of separation of water ice from the CO_2 ice.

These potential hurdles are a result of the unique material characteristics of the flow streams that are encountered in the ATK ICES CO_2 capture technology. While a review of the literature and discussions with equipment vendors provided insight to solutions that would work, the final approach to developing the solution, selection of appropriate equipment and sizing of the equipment, requires testing with the actual materials to be process or at minimum a better understanding of their properties. For the pressurization of the dry ice, the particle size and the resulting behavior in an auger need to be investigated. For the separation of the water ice from the liquid CO_2, characteristics of the water ice particles in the liquid CO_2 are important.

Path Forward

A COE penalty target set forth by the DOE for CO_2 capture implementation including transportation and storage is 35%. Implementation of the ICES technology results in an increase in COE of 42%. While it is a significant improvement over the chemical absorption technology in Case 12 (a 77% COE penalty), it is seven percentage points above the specified target. The COE increase is a result of:

- additional capital costs (24.7% of 42% increase over without capture case):
  - ICES and the flue gas conditioning system (18.7% of 42% increase over without capture case)
  - larger plant size to support the steam and auxiliary loads of the capture system, maintaining the same net output (6.0%),
- operating costs (7.2% of 42.0% increase over without capture case):
- additional fuel cost for decreased efficiency (4.4% of 42.0% increase over without capture case)
- CO_2 transportation and monitoring costs (5.6% of 42.0% increase).

This list illustrates that the majority of the 42% cost increase in COE over the non-capture case is from the additional capital costs. A possibility may exist to improve both capital costs and plant efficiency by investigating the following potential improvements via performing more focused and detailed engineering and cost analysis.

Efficiency

The application of the ICES process is estimated to reduce net plant efficiency by 4.5 percentage points, a 6.4 percentage points improvement over the chemical absorption system in Case 12. Further incremental reduction in efficiency penalty is believed to be possible by optimizing interconnecting ducts configuration to reduce pressure drop and by integrating flue gas cooling surfaces into the FGD structure.

Capital Costs

Capital costs of the ICES based CO_2 capture system are estimated to be approximately half of those for the chemical absorption based system in Case 12. However, there are several areas of the ICES system based design where potential capital costs reduction can be further investigated:

- Integration of flue gas cooling required for the ICES process into the FGD structure
- Associated reduction of the interconnecting ducts
- Modification of the ICES configuration by utilizing staggered opposing arrangement of the ICES flue gas expansion ducts, and reducing quantity of dry ice cyclones in half by combining two expansion ducts per one cyclone
- Refinement of engineering design with input from further testing such as impact of reduced compression requirements prior to expansion.

1   Introduction

1.1   Background

ATK is developing its Inertial CO_2 Extraction System (ICES) technology, capable of separating CO_2 from coal derived combustion gas and producing solid carbon dioxide. One application of this technology is to capture CO_2 from coal fired power plants to reduce their emissions. The captured CO_2 would then be transported by pipeline to a storage site for long term storage. This development is currently funded by the US Department of Energy (DOE) Advanced Research Project Agency– Energy (ARPA-E).

1.2   Project Overview

ATK requested WorleyParsons' support in evaluation of a conceptual CO_2 capture plant based on ATK's ICES. As part of ATK's ARPA-E Phase 2 project, WorleyParsons' support focused on:

1. Refinement of specific system components, specifically:

    d) Dehydration and compression of the flue case prior to the ICES

    e) Transfer of the dry ice/CO_2 from the ICES to pipeline as supercritical CO_2

    f) Use of dry ice as a cooling source.

2. Integration of the capture system into a supercritical pulverized coal (PC) power plant.

3. Preparation of a preliminary economic assessment.

4. Compare the plant performance and economics to state-of-the-art capture processes as presented in the Bituminous Baseline Report.

1.3   Report Objectives

The objective of this report is to provide a summary of the activities performed during this investigation and findings to guide future work on ATK ICES technology. The information provided in this report includes:

*   Basis of evaluation
*   Flue gas pretreatment and dry ice melting technology considered
*   Summary of the evaluation approach
*   Performance of supercritical power plant incorporating ATK ICES CO_2 capture technology
*   Capital and operation and maintenance (O&M) cost estimates
*   Updated performance and capital and O&M costs for supercritical power plants, with and without CO_2 capture, presented in the Bituminous Baseline Report (Cases 11 and 12)[1].
*   Economic analysis
*   Power plant 3D rendering for facility incorporating ATK ICES technology

2   Evaluation Basis

An evaluation basis was developed and presented in the Evaluation Basis Document (EBD) for the ATK ICES evaluation project to specify the evaluation criteria that formed the basis of the subsequent engineering and cost estimating efforts. As such, this document was an important communication tool to ensure the project basis is properly defined and understood by all the parties involved. The following sections provide the evaluation basis used through the project.

2.1   Engineering/Technical Design Specifications

The technical design specifications used in this study are the same as those used in the pulverized coal plants in the National Energy Technology Laboratory's (NETL) report titled "Cost and Performance Baseline for Fossil Energy Plants – Volume 1: Bituminous Coal and Natural Gas to Electricity"[1]. The following sections will highlight specific aspects of importance to the ATK process.

2.1.1   Site Conditions

The power plant used in the study is based on a site in Midwestern United States. A specific location is chosen as the reference site, in order that the performance and cost are developed on a consistent and realistic basis.   These conditions are described completely in the Bituminous Baseline report.   Process modeling work was based on ISO ambient conditions summarized in Exhibit 2-1.

Exhibit 2-1 Site Ambient Conditions Based ISO

Parameter	ISO Value
Elevation, m (ft) (above MSL)	0 (0)
Barometric Pressure, psia	14.696
Dry Bulb Temperature, °C (°F)	15 (59)
Wet Bulb Temperature, °C (°F)	11 (51.5)
Relative Humidity, %	60

Site characteristics are presented in Exhibit 2-2.

Exhibit 2-2 Site Characteristics

Parameter	Value
Cost Basis	Greenfield, Midwestern USA
Topography	Level

The following evaluation considerations are site-specific, and were not quantified for this study. Allowances for normal conditions and construction were included in the cost estimates. Typically the considerations of these factors do not have a significant impact on the cost unless the site specific situation is unusual or extreme.

- Flood plain considerations.
- Existing soil/site conditions.
- Rainfall/snowfall criteria.
- Seismic design.
- Buildings/enclosures.
- Wind loading
- Fire protection.
- Local code height requirements.
- Noise regulations – Impact on site and surrounding

2.1.2 Coal Characteristics

The particulate remaining from the coal ash after bag house and FGD may have a significant impact on the ICES in that it may lead to wear of components in the C/D nozzle and swirl vanes of the ICES system and promote nucleation of the dry ice. The 2010 version of the Bituminous Baseline Report does not provide information regarding the ash composition. Based on other sources [5], the mineral analysis and ash properties for this coal are provided in Exhibit 2-3.

Exhibit 2-3 Typical Illinois #6 Ash Mineral Analysis and Fusion Properties

Typical Ash Mineral Analysis		Weight Percent
Silica	SiO_2	45.0%
Aluminum Oxide	Al_2O_3	18.0%
Titanium Dioxide	TiO_2	1.0%
Iron Oxide	Fe_2O_3	20.0%
Calcium Oxide	CaO	7.0%
Magnesium Oxide	MgO	1.0%
Sodium Oxide	Na_2O	0.6%
Potassium Oxide	K_2O	1.9%
Phosphorus Pentoxide	P_2O_5	0.2%
Sulfur Trioxide	SO_3	3.5%
Undetermined		1.8%
Total		**100.0%**

2.1.3 Product Carbon Dioxide Specification

The CO_2 is to be transported and injected as a supercritical fluid in order to avoid two-phase flow and to reach maximum efficiency [6]. CO_2 is supplied to the pipeline at the plant fence line at a pressure of 15.3 MPa (2,215 psia). The CO_2 product gas composition varies, but is expected to meet the specification described in Exhibit 2-4.

Exhibit 2-4 CO_2 Pipeline Specification

Parameter	Units	Value
Inlet Pressure	MPa (psia)	15.3 (2,215)
Outlet Pressure	MPa (psia)	10.4 (1,515)
Inlet Temperature	°C (°F)	35 (95)
N_2 Concentration	ppmv	< 300
O_2 Concentration	ppmv	< 40
Ar Concentration	ppmv	< 10
H_2O Concentration	ppmv	< 150

2.2 ICS Technology Description

2.2.1 ICES Process Overview

The current evaluation is based on boundaries set by ATK; this boundary is shown in the process flow diagram (PFD) in Exhibit 2-5. The focus of the design basis will concentrate on the pre and post processes. Key pre-processes will include the dehydration and compression of the flue gas post the desulfurization unit. Post process design will concentrate on the movement of the solid CO_2 from the cyclone to pipeline.

Exhibit 2-5 ICES Process Flow Diagram
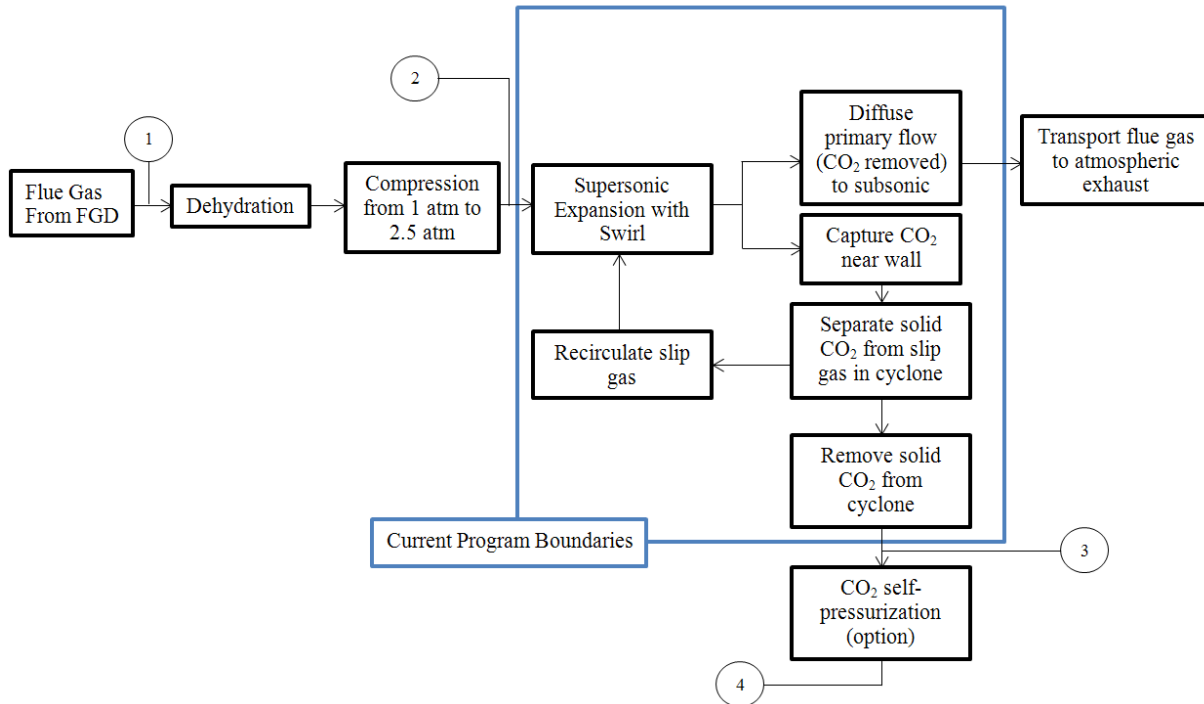
Flows critical to the design of equipment and interface between WorleyParsons and ATK are indicated in Exhibit 2-5. The characteristics of these gas flows, where available, are provided in Exhibit 2-6. The gas composition downstream from the wet FGD, location 1, is the same as that for Case 12, Stream 18 in Exhibit 4-46 of the Bituminous Baseline report. The flow rate at this location will be determined from the power plant modeling incorporating the ICES system. The characteristics of stream 4 in Exhibit 2-5, downstream of the CO_2 self-pressurization, are taken from the pipeline specifications provided in Exhibit 2-4.

Exhibit 2-6 Process Streams to and from ICES Equipment

Location	1	2	3	4
Temperature	136°F	<27°C	TBD	35°C/95°F
Pressure	14.90 psia	36.7 psia	TBD	15.3 MPa / 2,215 psia
Flow Rate	TBD	TBD	TBD	TBD
CO_2	13.50 mol%	TBD	TBD	-
H_2O	15.37 mol%	Less than saturation at 27°C	TBD	< 150 ppmv
O_2	2.38 mol%	TBD	TBD	< 40 ppmv
N_2	67.93 mol%	TBD	TBD	< 300 ppmv
SO_2	0.81 mol%	TBD	TBD	-
Ar	0.81 mol%	TBD	TBD	<10 ppmv

2.2.2   ICES Projected Performance

A CFD model was developed by ATK for a single ICES unit inside the boundary limits shown Exhibit 2-5. Exhibit 2-7 illustrates the model input and output streams Exhibit 2-8 presents the results. These results have been used for WorleyParsons' modeling which incorporated the ICES into a generation power plant to determine the impact on the plant operation and the scale and energy consumption of the equipment. Note, the input gas composition for the modeling presented in Exhibit 2-7 is not consistent with flue gas composition in the Bituminous Baseline report. For comparative purposes, the flue gas composition, adjusted to the same moisture in ICES model, from the wet FGD to the CO_2 capture system from Case 12 of the Bituminous Baseline report, are included in this table. The partitioning of the gas species by the ICES technology, as described by this Exhibit, were used to develop the conceptual plant process.

Exhibit 2-7 Input and Exit Streams from ICES CFD Model
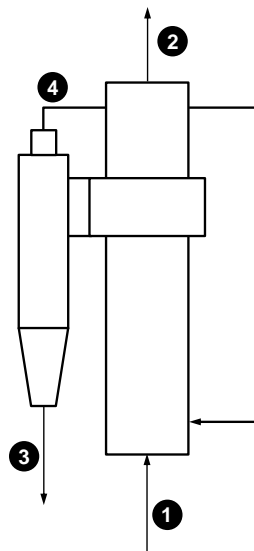
Exhibit 2-8 ICES CFD Results

Location	Flue Gas	BB Report	Flue Gas	Solid CO_2	Slip Gas

	Inlet (1)	FGD Exit	Outlet (2)	Exit (3)	Recirculation (4)
Temperature	≤80°F (≤27°C)		296°F (147°C)	-150°F (-101°C)	-150°F (-101°C)
Pressure (psia)	36.7 psia (2.53 bar)		14.7+	3.67 psia (0.253 bar)	3.67 psia (0.253 bar)
Flow Rate (lb/s)	1.836$^{(*)}$		1.363	0.381	0.092
CO_2 (mol%)	14.418	15.40	1.836	80.528	–
H_2O (mol%)	3.483$^{(**)}$	3.48	0.443	19.453	–
O_2 (mol%)	3.874	2.71	4.611	–	4.718
N_2 (mol%)	77.253	77.48	91.957	–	94.102
SO_2 (mol%)	0.003	0.00	0	0.019	–
Ar (mol%)	0.968	0.92	1.153	–	1.18

(*) Flow Rate through the current ICES unit.

(**)Equilibrium water concentration at the assumed temperature and normal pressure, lower water concentration is desirable.

2.2.3   Dehydration of Flue Gas/CO_2 Product

The CO_2 to the pipeline must be dried to an H_2O concentration of <150 ppmv, as specified in Exhibit 2-4. In the initial concept, illustrated in Exhibit 2-5, the dehydration of the CO_2 will occur upstream of the dry ice formation and CO_2 separation. The water content of the gas upstream of the CO_2 capture step will need to be adjusted such that the water content meets the pipeline specification after the CO_2 separation step. Note, since water is separated with CO_2 in the ICES process, the water content in the gas stream upstream of the ICES process needs to be significantly less than the pipeline specification. Discussion of the dehydration methods considered are provided in section 3.1.1.

2.2.4   Particulate Specification

Particulate may have a significant impact on the ICES system and the formation of the dry ice particulate. In this process, typically referred to heterogeneous nucleation, the particulate may provide nucleation sites for the dry ice crystals leading to the formation of potentially few, but larger crystals. Without the presence of particulate, homogeneous nucleation is assumed to occur, which leads to fine particles which can be difficult to separate from the gas stream.

In the coal combustion process, flyash will result in particulate in the gas stream to the ICES system. The amount of flyash in the flue gas is strongly dependent on the type of coal, the boiler firing conditions and configuration. Further, coal fired boilers typically have air pollution control (APC) equipment in place to limit particulate emissions.

For the PC configurations presented in the Bituminous Baseline Report, the APC devices upstream of the CO_2 capture equipment include a fabric baghouse and wet FGD. The same configuration was assumed with regards to equipment upstream of to the ICES CO_2 capture equipment. This assumption was used to project the particulate loading of the gas stream to the ICES CO_2 capture equipment. The following provides a brief discussion of the estimate of the particulate loading and size.

The initial particle size distribution of the flyash is illustrated in Exhibit 2-9. A baghouse removes 99.5-99.8% of the particulate depending on particle size across 0.4-100 microns as illustrated in Exhibit 2-10. Based on Case 12 in the Bituminous Baseline Report, the total particulate flow to

the baghouse is distributed by particle size according to the distribution in Exhibit 2-9 as illustrated in Exhibit 2-11. Applying the baghouse capture efficiency as a function of particle size listed in this table results in the total projected particle mass flow out of the baghouse of 85.81 (lb/hr) with the listed particle size distribution. The baghouse capture efficiencies in this table were estimated from Exhibit 2-10 for particle sizes less than 10 microns. For particle sizes greater the 10 microns, a standard 99.65% collection efficiency was used. The efficiencies were adjusted so that the total particulate loading after the baghouse match the 0.013 lb/MBtu reported in the Bituminous Baseline Report.

Exhibit 2-9 Flyash particle-size distribution in pulverized coal fired boilers.[7]
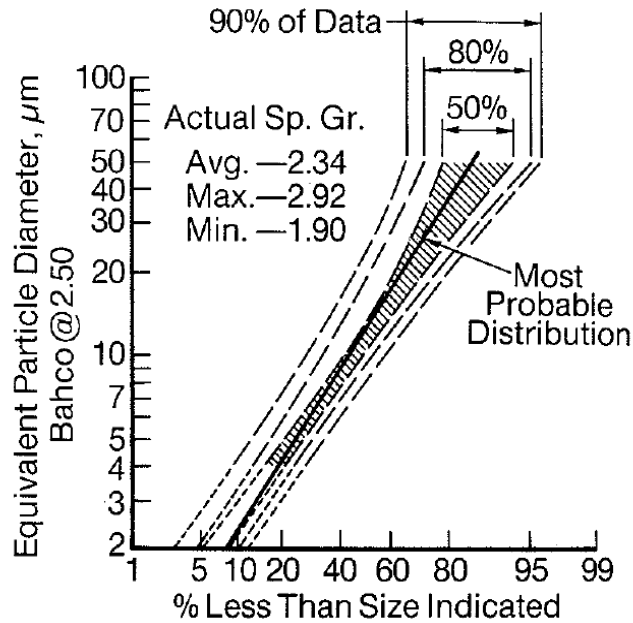
Exhibit 2-10 Particle Penetration of Fabric Filters as a Function of Particle Size.[8]
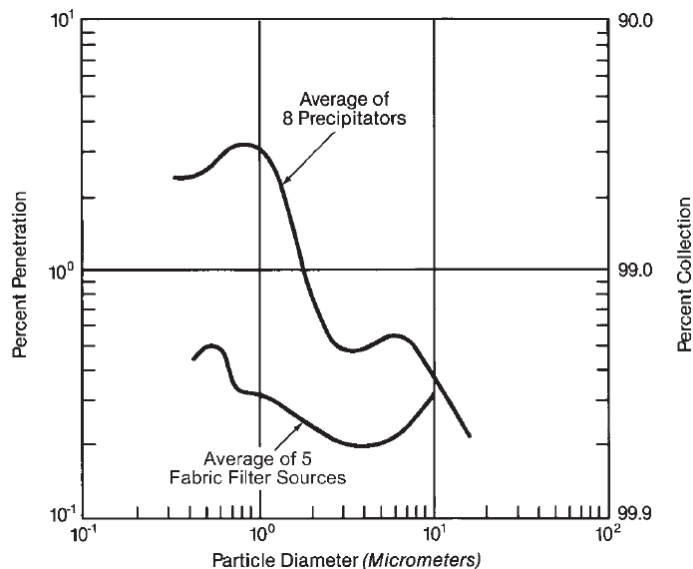
Exhibit 2-11 Projected Particle Mass Flow Rate Based on Collection Efficiencies

Particle Distribution		Flow to Baghouse	Baghouse Capture Efficiency	Post-BH/Pre-FGD	FGD Capture Efficiency	Post FGD
Size (µm)	Percentage (%)	(lb/hr)	(%)	(lb/hr)	(lb/hr)	(lb/hr)
<1	3%	1,304	99.60%	3.90	92%	0.312
1-3	10%	4,345	99.75%	6.47	93%	0.453
3-5	19%	8,256	99.80%	8.16	97%	0.245
5-10	18%	7,822	99.73%	13.21	100%	0.000
10-44	42%	18,251	99.65%	45.43	100%	0.000
44-100	8%	3,476	99.65%	8.65	100%	0.000

The typical collection efficiency of the wet FGD as a function of particle size is illustrated in Exhibit 2-12. This figure indicates that essentially all of the particulate greater than 5 microns and ~90% of the particulate in the size range of 0.1 to 1.5 micron will be removed from the gas stream. The total projected particle mass flow out of the FDG is calculated to be 1.01 (lb/hr) with a particle size less than 5 micron. The resulting particulate loading downstream of the FGD to the CO_2 capture equipment would be 0.116 mg/m^3.

Exhibit 2-12 Collection Efficiency of wet FGD as a Function of Particle Size[7].
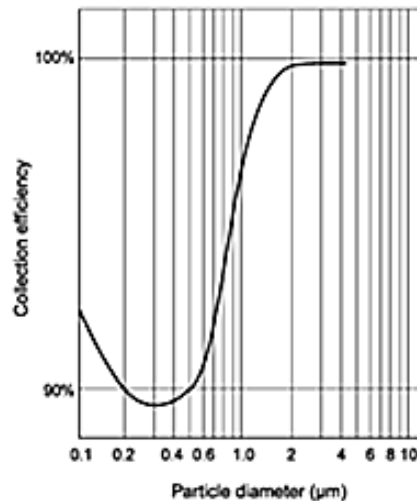
Based on discussions with air pollution control experts within WorleyParsons the total particle loading after the wet FGD is dependent of the operating conditions of the equipment and is typically in the range of 15 to 30 mg/N m^3.

For the modeling performed by WorleyParsons, the particulate present in the flue gas stream were assumed to be sufficient to lead to the nucleation and growth of sufficiently large dry ice crystals to enable separation as the gas is expanded in the system.

2.2.5 Self-Pressurization of the CO$_2$

The isochoric vaporization of the dry ice could provide the potential for achieving the sufficient pressure to produce a supercritical CO$_2$ fluid. However, the technical challenge of increasing the pressure of the dry ice from atmospheric pressure to pipeline pressure, ~2200 psig, exists. Two technical considered:

1. Auger for feeding the dry ice into the pressurized chamber to a pressure suitable for melting the CO$_2$ (~10 bara) and the subsequent pressurization to pipeline pressure through pumping.
2. Filling a tank with dry ice and heating tank to pipeline temperature, ~35°C (90°F). In a contained volume, the temperature increase is sufficient to raise the pressure to pipeline pressures.

2.3 Conceptual Industrial Scale Design

ATK has developed a conceptual design for ICES technology for industrial processes as illustrated in Exhibit 2-13. Based on information provided by ATK this unit is capable of separating approximately 100,000 lbs/hr of CO$_2$ from a flue gas stream containing approximately 13 percent CO$_2$.

In Exhibit 2-13, the compressed flue gas passes through the distribution duct on right which distributes the gas among the expansion nozzles that are in the rectangular ducts (expansion ducts) that run between the two circular ducts. The expansion nozzle is in the expansion duct near the distribution duct. The upward curve in the expansion duct causes the dry ice particles to flow along the outside of the curve where the particles are collected with a small portion of the gas stream. This combined stream is separated in the cyclone with the dry particles leaving through the bottom and the gas returning to expansion duct where it is collected in the circular duct on the left, the collection duct.

Exhibit 2-13 Conceptual Industrial Scale Design of ATK ICES CO$_2$ Capture Process

Collection Duct

CO$_2$ Free Flue Gas to Stack

Flue Gas
Expansion Duct

Collection Duct

Dry Ice Cyclone

Dry Ice

Flue Gas from Conditioning Systems
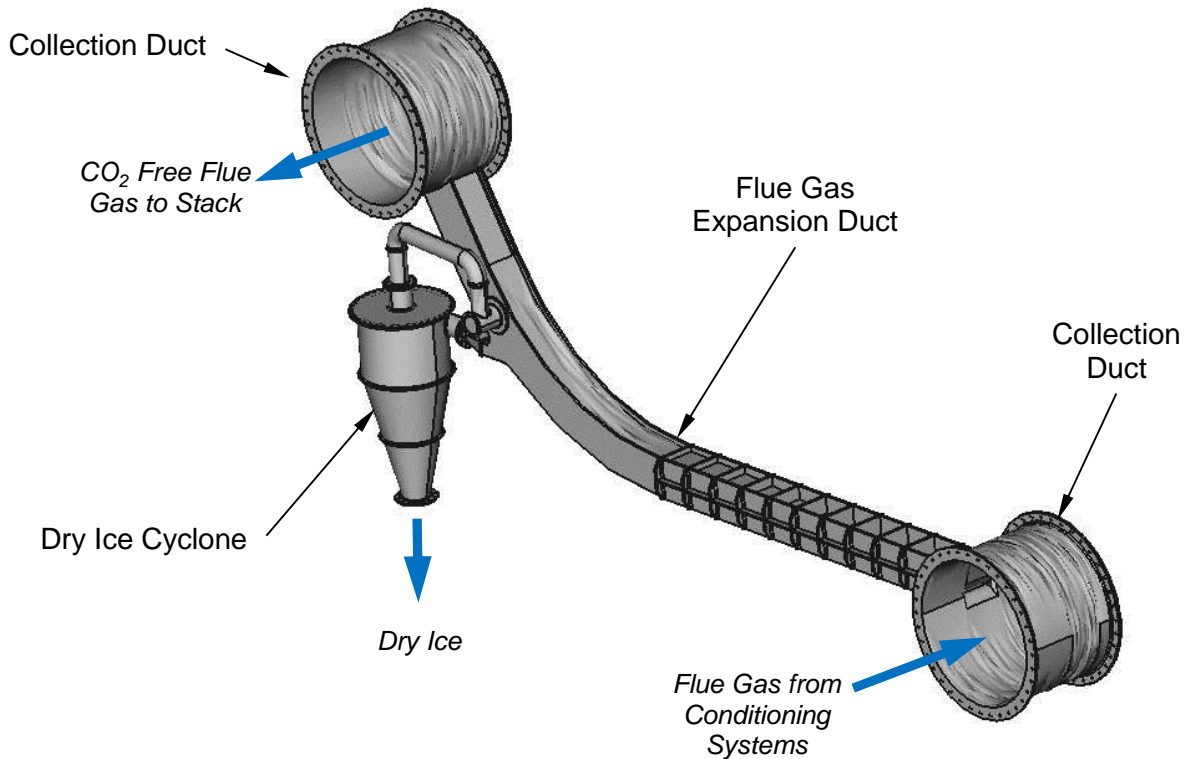
3   PC Power Plant with CO$_2$ Capture

A conceptual supercritical power plant with CO$_2$ capture design and costs were developed to compare the ATK ICES technology to state of the art CO$_2$ capture processes as presented in the Bituminous Baseline Report. In this study, the activities performed included:

- Development of supporting systems for the ATK ICES CO$_2$ capture technology
- Power plant and process performance modeling
- Equipment sizing
- Capital and O&M cost estimates
- Economic analysis

Results from the subsystem process development activities and the methodologies for the system modeling, equipment sizing, cost estimating, and economic analyses are provided in the following subsections.

3.1   ATK ICES CO$_2$ Capture Process Development

Prior to detailed process and steam cycle modeling, the systems around the ATK ICES CO$_2$ capture technology, the flue gas pretreatment and dry ice melting technologies, were assessed qualitatively to determine effective approaches for:

- Dehydrating the CO$_2$ product to a sufficiently low water content meet the pipeline specifications,
- Flue gas pretreatment prior to the ATK technology,
- Melting the dry ice, and utilizing the cold temperatures of the dry ice, and pressurizing the CO$_2$ to meet pipeline pressure specifications.

when experience counts

3.1.1 Dehydration of Flue Gas/CO_2 Product

In solvent based post-combustion technologies, the water specification for the CO_2 product is typically met by a dehydration step during the compression of the CO_2 to pipeline pressures. Initially, in this study, the assumption was made that dehydration step could be performed in the flue gas pretreatment step prior to expansion in the ATK ICES unit to produce the dry ice. Barriers to this approach are:

- The entire flue gas stream would need to be dried instead of just the CO_2
- A significantly lower water concentration in the gas stream would need to be achieved to account for the concentrating effect of the ATK ICES system on the water.

Additionally, the suitable technologies for performing this dehydration step, molecular sieves, operate more efficiently at high pressures and require a significant amount of energy for regenerating the solvent. Therefore, other approaches for removing the water from the CO_2 product were considered including:

- Dehydration of CO_2 after separation with solvents
- Separation of water ice from liquid CO_2 by physical methods including
  - Flotation
  - Cyclone
  - Separation/filtration

Exhibit 3-1 provides a summary of the approaches along with the benefits and disadvantages of the approaches. Additionally, companies that are potential providers of the technologies are included in this Exhibit. Based on this review, physical separation of the water ice from the liquid CO_2 were considered for this study.

Exhibit 3-1 Qualitative Comparison of Dehydration/Water Removal Options

Approach	Technology	Disadvantages	Benefit
Dehydration of flue gas stream prior to CO_2 separation			
Adsorption of Water	Molecular Sieve	Large equipment required to treat entire flue gas stream, high energy requirement regenerate sorbent low flue gas pressure	Uses currently available industrial equipment/technology
Expansion of flue gas stream through nozzle to produce water ice.	ATK Twister (http://twisterbv.com/)	Additional compression requirement Design for flue gas required and untested	Potential for partially expanding gas in turbo expander to offset compression energy Decrease in 2nd stage compression through reduced gas temperature and mass
Dehydration of CO_2 after separation with solvents			
Melt all dry and water ice, decompress, remove water, recompress	TEG	Energy need for recompressing and regeneration of sorbent/solvent. Potential damage to pumps from ice particles	Uses currently available industrial equipment/technology (TEG)
Melt all dry and water ice, dehydrate supercritical using glycerol solvent	Glycerol Solvent	Limited information available in literature, internal experts are not aware of this process and foresee problems with solvent contamination in CO_2 product.	Process potential applied in industry, avoids recompression of CO_2.
Separation of water ice from liquid CO_2			
Floatation	Melt CO_2 to liquid phase, temperature ~-50°C, ~10 bar, -removal of solid CO_2 from top of melting tank -Similar to desalination by freezing	-Process has not be developed for liquid CO_2 -Relies on water ice floating to top of tank -Liquid CO_2/water ice mixture properties unknown -Ability to achieve sufficient separation of water ice from liquid CO_2. -Equipment operating at ~-50°C and 10 bara.	-Low energy requirement -Potential low capital costs
Cyclone	Cyclone separators Companies: Rosedale Products	-Small particle size and density difference will not allow for cyclone separation.	-Low energy requirement -Simple equipment -Existing equipment sizes suitable

Filter	Filter Bag/Cartridge
	 Companies:
	    Norman Filters
	    Rosedale Products
		-High solids loading 6% will blind filter very quickly resulting in need for frequent filter replacement
		 -Possibly suitable for polishing filter.
			-Low energy requirement, dependent on pressure drop across filter
			 -Existing equipment sizes suitable

	Continuous Filtering
	 -Rotating drum filter
	 Companies:
	    Dürr Ecoclean
	    Russell Finex
		-Relies on filter system to continuously separate ice particles from liquid CO_2
		 -Liquid CO_2/water ice mixture properties unknown
		 -Ability to achieve sufficient separation of water ice from liquid CO_2
		 -Closest similar industry process: industrial filter systems
			-Low energy requirement
			 -Potential low capital costs
			 -Particulate filters are available for liquid CO_2,

For the separation of water ice from liquid CO_2 by physical methods, the properties of the solid ice, particularly the particle size, are of critical importance. At the time of this study, testing had not been performed to provide this data. For this study, based on the particle formation method, it was assumed that the size of the water ice particles would be in the range of 30 to 100 microns. The density difference between solid ice and liquid CO_2 (1.00 versus 1.15) and the assumed particle size would most likely limit the rate at which separation would occur by gravity separation (floatation). Thus, at this time, floatation based options, including cyclones, were not considered to viable options.

Discussions with vendors and the assumptions regarding the consistency and solids loading (greater than 1 percent) of water ice liquid CO_2 mixture indicated that a 2 step process would be required. The vendor Russell Finex offers options for solids removal options for slurries with solids contents greater than 1%. This initial step would reduce the solids content to below 1 percent. To remove the remaining material, a final filtration step with a continuous filter would be required. Illustrations of this type of equipment are provided in Exhibit 3-2. It is important to note, that this equipment has not be demonstrated for the separation and filtering of water ice from liquid CO_2, but barriers to the approach, such as available materials of construction to operate at the liquid CO_2 temperatures, were not identified. This approach for the water separation was considered in the development of the conceptual power generation facility.

Exhibit 3-2 Illustration of Potential Equipment for Separating Water Ice from Liquid CO_2.

Solid Liquids Separator [**9**]   Continuous Cleaning Filter [**10**]

3.1.2   Flue Gas Pretreatment System

Prior to introducing the flue gas stream to the ATK ICES CO_2 capture equipment, the flue gas from the FGD must be cooled from 57°C (136°F) to ≤27°C (≤80°F) and compressed to 2.53 barA (36.7 psia). Additionally, the removal of water from the flue gas at this point is beneficial to minimize the need for water separation after the CO_2 separation.

Two flue gas pretreatment options were considered in this study as illustrated in Exhibit 3-3 and Exhibit 3-4. Both options considered direct contact cooler to initially cool the flue gas and then

using the heat required for melting the dry ice as a further cooling source. The primary difference between these two options is the location where the cooling from the dry ice melting is applied. In Option 1, shown in Exhibit 3-3, the cooling from the dry ice melting is incorporated both prior to and after the compression of the flue gas. In Option 2, shown in Exhibit 3-4, this cooling is applied after the flue gas compression only.

Applying a portion of the cooling prior to the flue gas compression (Option 1), allowed for the flue gas to the compressor to be at a lower temperature and moisture content. These conditions reduced the power requirement of the compressor by ~10%. The initial estimates for the compressor load for a 550MW net power plant were on the order of 100 MW. Based on the significant size of this load, the load reduction offered by Option 1 was considered to be of great value, and therefore, Option 1 was selected for the modeling of the power generation system.

Once this option was selected, further modifications were incorporated in the concept including further heat recovery and the selection of a steam turbine drive over an electric motor for the compressor. The selection of the steam turbine drive is based on the large power requirement and the higher efficiency.

Exhibit 3-3 Flue Gas Pretreatment Option 1
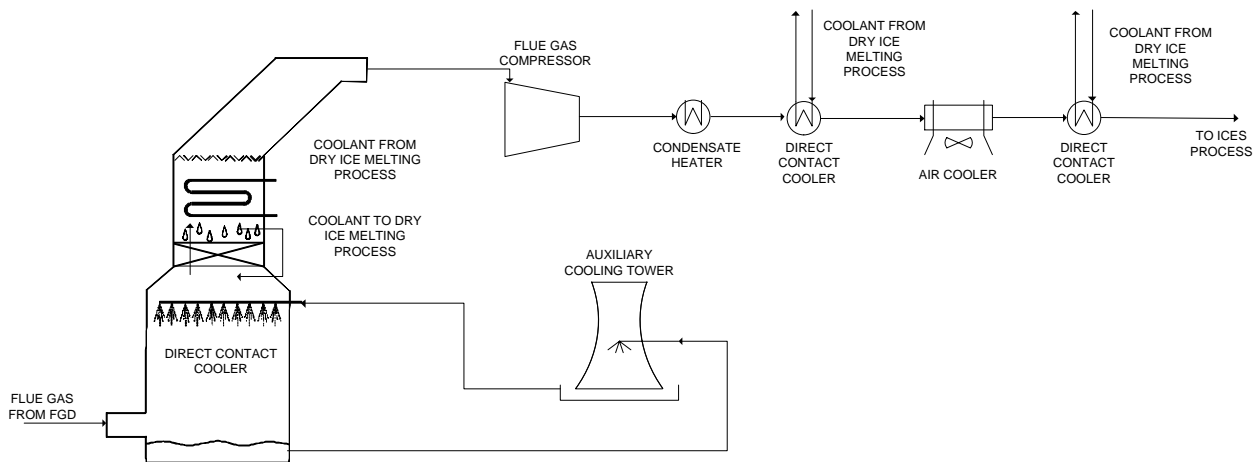
Exhibit 3-4 Flue Gas Pretreatment Option 2
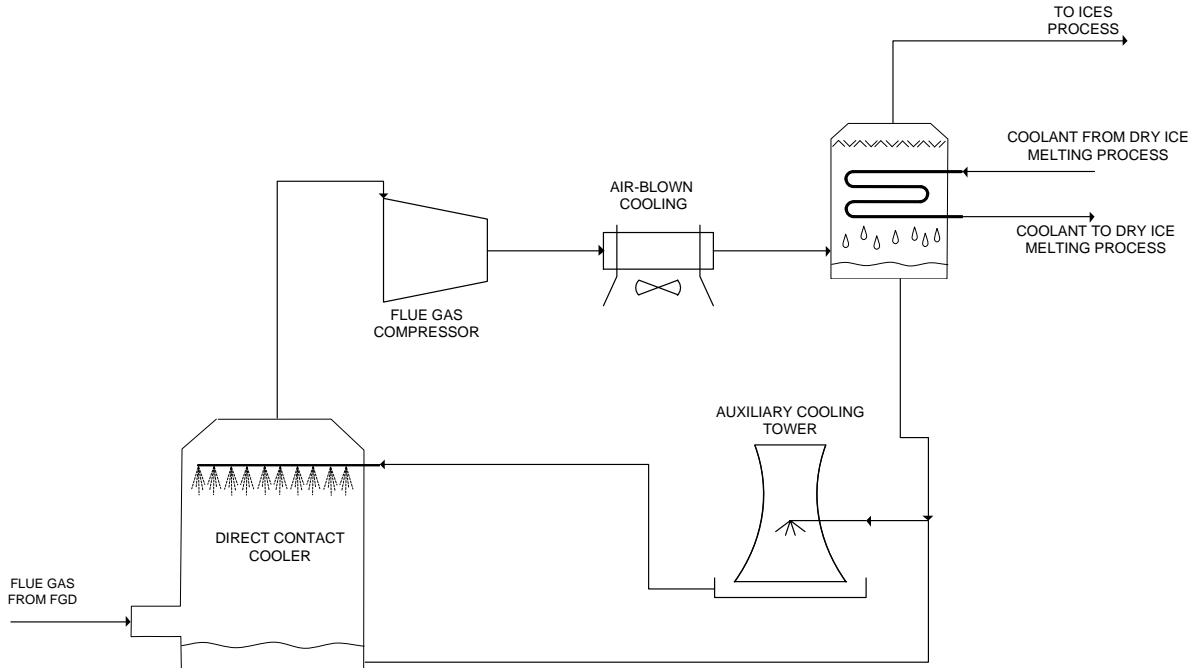
3.1.3   Dry Ice Melting and CO_2 Pressurization Systems

In the ATK ICES CO_2 capture system, the dry ice exits the bottom of the cyclone at a temperature of -150°F (-101°C) and a pressure of 0.3 bara. The dry ice is assumed to be in a fine power form with a particle size of less than 0.05 inches (1 mm). Additionally, it is expected that this CO_2 dry ice stream will contain 1 to 5 percent water. Prior to injection in to the pipeline, the CO_2 must be transformed from this solid stated to a supercritical fluid at ~35°C and a pressure of 2200 psig (151 barg) and the water content must be reduced to below 150 ppm.

A traditional route to transform the dry ice to supercritical CO_2 is to melt the dry ice at atmospheric pressure and to compress and remove the water using the methods currently employed for CO_2 capture processes. The primary disadvantage of this route is the energy required for the CO_2 compression and the resulting auxiliary load increase for the facility.

In the current study, two options were considered for the melting of the dry ice and increasing the pressure to achieve a supercritical fluid. Both of these options avoid the CO_2 in a vapor phase and the associated compression energy to achieve the supercritical state. In the first option, illustrated in Exhibit 3-5 as path 1, the dry ice is placed in a closed vessel and then heated. As the CO_2 is heated, the CO_2 will sublime and the pressure will increase following solid-vapor line and then the liquid-vapor line. Once the critical point is reached, the CO_2 in the vessel will become supercritical.   In the second option, illustrated as path 2 in Exhibit 3-5, the pressure of the dry ice is increased to ~10 bara (145 psia) which is above the triple point for CO_2. The CO_2 is then heated to produce a liquid and the pressure of the liquid is increased by pumping. In both of these options, methods for using the cold temperatures of the dry ice to reduce the cooling loads of the system were considered. A qualitative analysis was performed to select one of these options to incorporate into the conceptual facility design.

Exhibit 3-5 Comparison Methods to Convert Dry Ice to Supercritical CO_2 for Pipeline Transportation on Pressure vs. Temperature Diagram for CO_2.
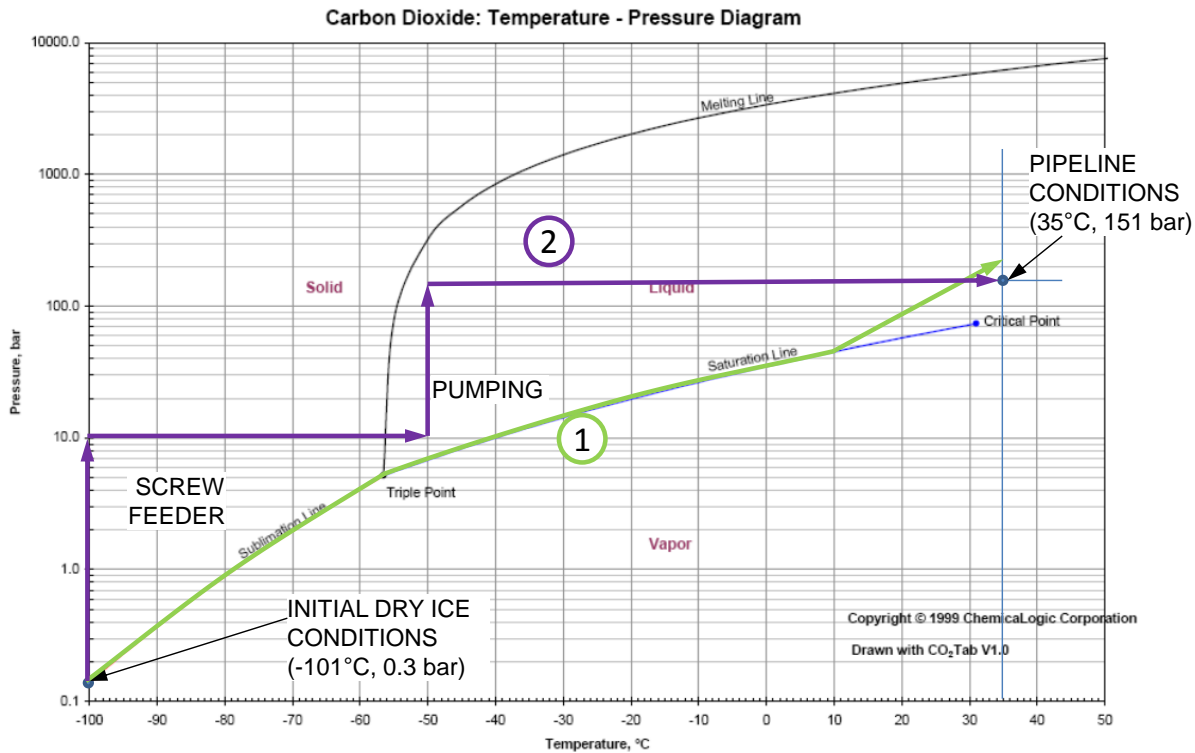
A high level illustration of the dry ice melting Option 1 equipment and process are provided in Exhibit 3-6. In developing the process, consideration was given to how the filling, melting and emptying would occur. These process steps are illustrated in Exhibit 3-6 and are as follows:

Step 1: Fill tank with dry ice

Step 2: Close valve to tank so that the pressure increases with increasing temperature

Step 3: Heat the tank to melt CO_2, required heat is obtained from cooling flue gas to ATK ICES system. During heating, the tank pressure becomes greater than the pipeline pressure.

Step 4: Open valve to pipeline so that CO_2 can flow to pipeline. Flow to the pipeline stops when the tank and pipeline pressures become equal.

Step 5: Close the valve to pipeline and open the valve to the expander and the valve to the flue gas duct downstream of the compressor. This allows for the CO_2 remaining in the tank to be depressurized to approximately 2.5 atmospheres and reintroduced into the capture system.

Step 6: Open and close valves redirect the CO_2 from expander the flue gas duct upstream of the compressor to allow the remaining CO_2 to exit the tank. The valve between the tank and the compressor is then closed and the process repeated.

Implementation of this process would require a number of tanks operating at different points in the above cycle. These tanks would be connected with a manifold to allow the control of the CO_2 from the tanks to the pipeline and the expander. Additionally, a dehydration step would

most likely be required and a suitable technology was not clearly identified. One additional item to note is that the pressure rating of the tanks would need to be greater than 152 barg (2200 psig) to handle the supercritical CO_2 at pipeline pressures.

Exhibit 3-6 Dry Ice Melting Option 1
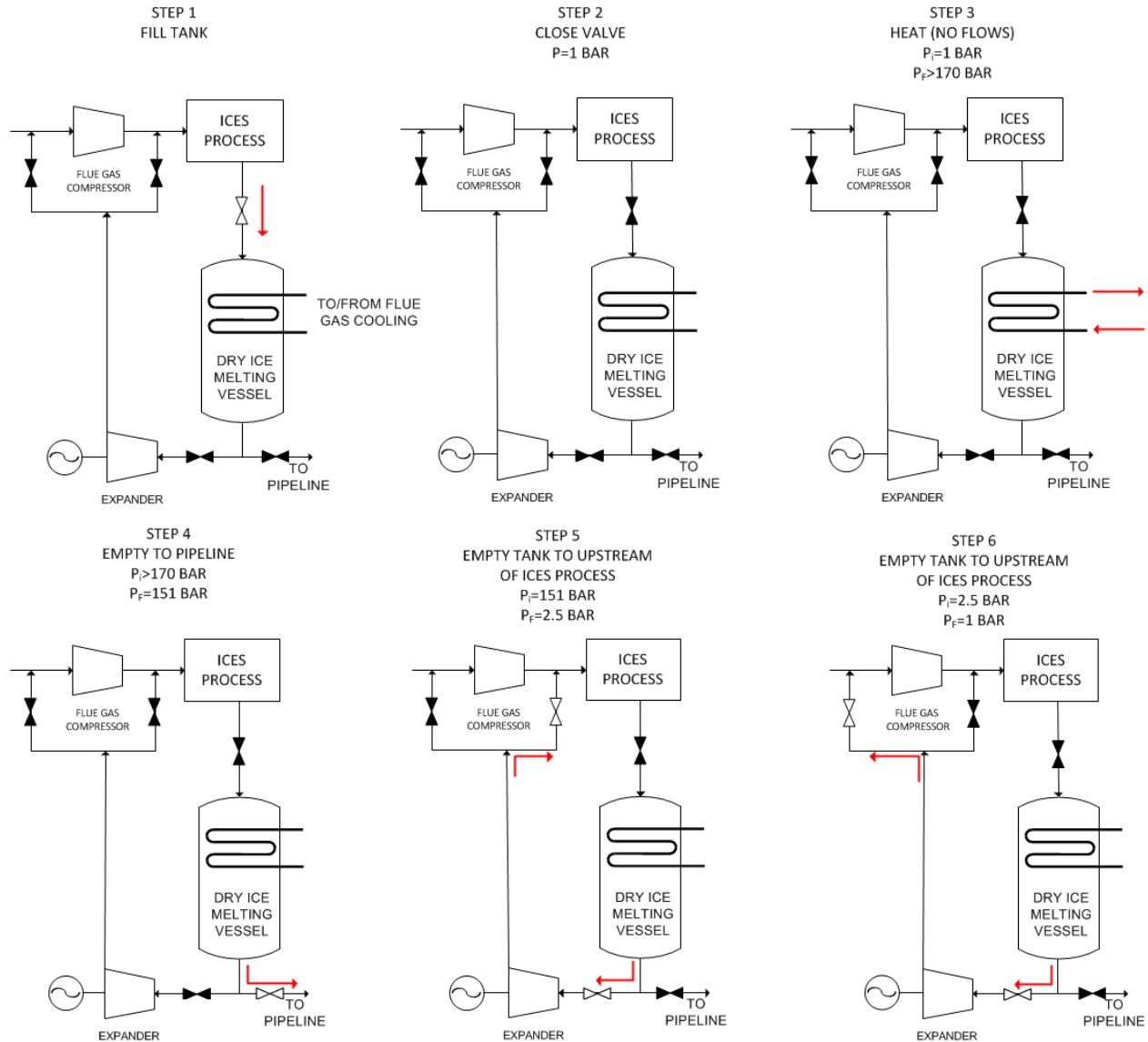
The equipment and process for the dry ice melting Option 2 are illustrated in Exhibit 3-7. This is continuous process with the dry ice being pressurized in a screw extruder to 10 bara (145 psia) where it can be melted to produce liquid CO_2. The screw extruder feeds the material into the melting vessel where heat from cooling the flue gas is used to melt the dry ice. The liquid CO_2 can then be pumped and further heated to provide supercritical CO_2 for the pipeline. One advantage of this approach is the opportunity to remove the water from the liquid CO_2 as a solid. The process in Exhibit 3-7 includes a filtration step to remove the solid water ice.

Exhibit 3-7 Dry Ice Melting Option 2
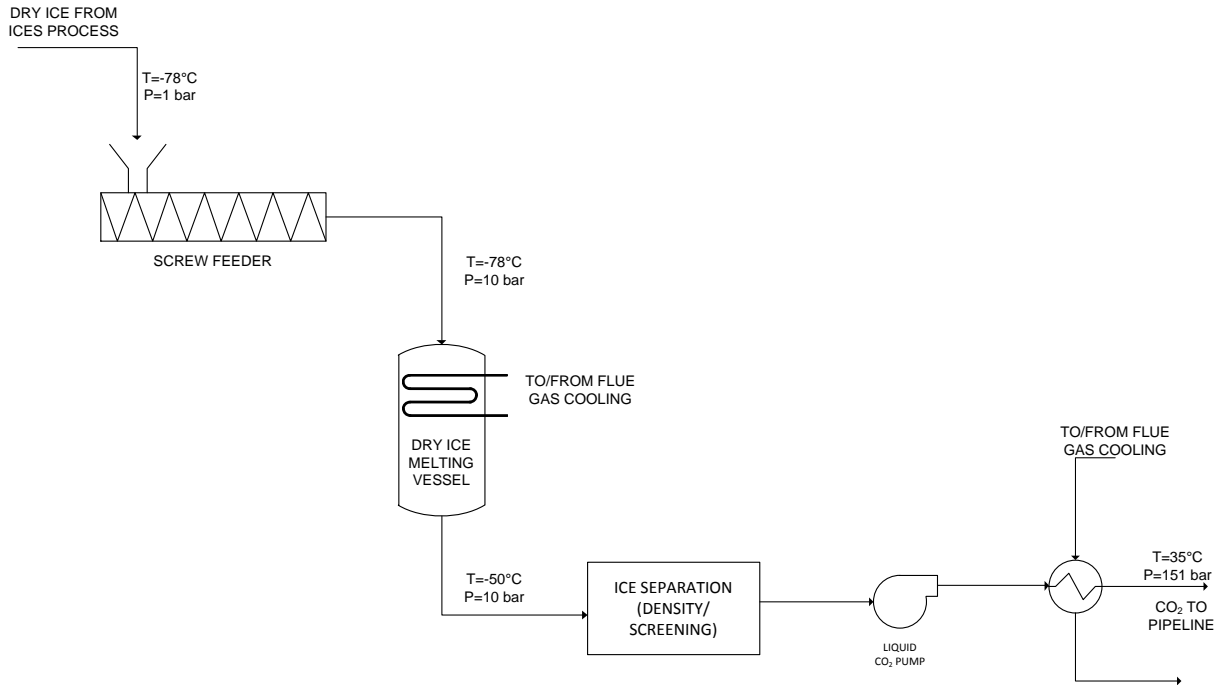
A potential hurdle associated with Option 2 is the availability of a suitable screw extruder to raise the pressure of the CO_2. While extrusion process are currently used to produce dry ice pellets, equipment operating at the scale required for the flow rates encountered with CO_2 capture from power generation (1,000,000 lbs/hr) were not identified. Available processes for dry ice operate at flow rates on the order of 1000 lbs/hr.[11] Additionally, this equipment uses a piston type pump to extrude the CO_2 powder. Commercially available screw extruders are available that can feed on the order of 200,000 lbs an hour of material, but they have not been used with dry ice. Further, the capability of this type of equipment to work with a specific material is strongly dependent on the physical properties of the material. Testing with dry ice powder from the ATK system is required to validate the suitability of this approach.

Selection of Dry Ice Melting Approach

The benefits and disadvantages of the options considered for melting the dry ice are summarized in Exhibit 3-8. The complexity and batch operating mode of Option 1 was considered to be a major deficit to this option. Additionally, the potential capital costs related the multiple tanks and high pressure requirements of the tanks were also a concern. While Option 2 requires non-typical application of existing equipment, the lower complexity and continuous operation were considered to be major benefits. Therefore, Option 2 was selected as the dry ice melting approach for this study. As mentioned, this dry ice melting requires the novel application of existing equipment. To validate the suitability of this equipment for the application will require better definition of the solid CO_2 and liquid CO_2/solid water mixture properties.

Exhibit 3-8 Comparison of Benefits and Disadvantages for Dry Ice Melting Options

	Dry Ice Melting Option 1 (self-pressurization)	Dry Ice Melting Option 2 (screw extruder)
Benefits	• Potential for energy recovery as power (20-40MW) from decompression of tanks. • Maybe used as a source of vacuum for startup (CO_2 injector)	• Continuous process • Opportunity to provide simple approach for water removal • Likely lower capital cost
Disadvantages	• Likely higher capital costs, multiple trains of melting vessels required • Potential difficulties incorporating simple water separation technology	• Low temperature energy recovery opportunity not utilized • Does not have potential to be used as a source for vacuum

3.2   Performance Modeling Methodology

The performance of the power generation unit incorporating the ATK ICES technology was determined by first modeling the CO_2 capture system and the associated heat exchangers with Aspen[TM] and then incorporating this model into a power generation plant (boiler/steam cycle) using GateCycle[TM]. Both of these software packages are commercially available and were chosen based on their suitability / modeling strengths for chemical processes and power generation.

The CO_2 capture process modeled in Aspen[TM] covers all equipment downstream of the wet FGD. Vendor's data for flue gas compressor and the information of ICES from ATK were incorporated into the model. The remaining components, primarily heat exchangers and pumps were developed based on standard engineering practices.

For modeling the power plant, a GateCycle model was first developed for the power plant steam cycle of NETL Baseline Study Case 12 – SC PC plant with amine based post-combustion CO_2 capture. The model was calibrated using the data presented in the Baseline Study Report Case 12 section. The GateCycle model was then modified to fit the study case (ATK case). The information from Aspen model, waste heat recovered from capture system for condensate heating and power requirement for turbine to drive of the flue gas compressor was used as inputs in the steam cycle model. Several iterations were performed between the steam cycle model and CO_2 capture process model to arrive to the net power generation of 550 MWe.

3.3 CO_2 Equipment Sizing Methodology

The resulting mass and energy balance data from the simulation models were used to size major pieces of equipment of the plant. For the power plant and gas conditioning equipment, sizing and sparing philosophies consistent with the Baseline Study Report were used. For CO_2 capture plant, the information from ATK and equipment vendors were used as much as possible in sizing equipment, which includes ICES system, flue gas compressor, air cooled heat exchangers cooler and flue gas ducts. The balance of the capture plant equipment was sized based on WorleyParsons in-house data.

3.4 Cost Estimate Methodology

3.4.1 Capital Cost Estimates

Capital costs were developed using a combination of commercial capital cost estimating software, factored equipment estimates, vendor information and WorleyParsons in-house parametric models supplemented by WorleyParsons' extensive in-house equipment cost database.

For process equipment costs not provided by vendors, ASPEN In-Plant Cost Estimator software was used to develop costs for most of the major equipment in the ATK ICES CO_2 removal process. This includes vessels, heat exchangers, and other specialized process equipment. The associated capital costs for bulk materials and installation were developed by applying a factor to the established equipment cost to derive a total installed cost. Factors vary by type of equipment, metallurgy, and complexity, and conform to WorleyParsons standards.

Costs for other equipment and balance of plant items were developed via scaling and/or parametric modelling based on key project and equipment parameters. These were the primary methods used to estimate the capital costs of balance of plant equipment and systems whose costs are impacted by the change in CO_2 removal process from that used in Case 12 of the DOE Bituminous Coal Baseline Study [1]. Costs not impacted by the change in CO_2 removal process, and whose performance characteristics did not change from the DOE Study remained the same as in the updated (to January 2012 dollars) costs for Case 12.

The total capital cost estimates include the cost of equipment, freight, bulk materials and labor (direct and indirect) for equipment installation and erection; materials and labor for construction of buildings, supporting structures, and site improvements; engineering, construction management, and start-up services (Professional Services); and process and project contingency. The estimate excludes owner's costs and is provided as "overnight" costs; that is, escalation to period of performance is excluded.

Home office expenses and other owner's costs were based on an allocation included in the COE analysis.

3.4.2 Operating and Maintenance Costs Estimates

The operating costs and related maintenance expenses (O&M) pertain to those charges associated with operating and maintaining the plant over its expected life. These costs include:

- Operating Labor
- Maintenance – Material and Labor
- Administrative and Labor Support
- Consumables
- Waste Disposal
- Fuel
- Co-Product or By-Products credit (that is, a negative cost for any byproducts sold)

There are two components of O&M costs; fixed O&M, which is independent of power generation, and variable O&M, which is proportional to annual power generation. The fixed operating costs do not include the cost of capital. The variable O&M cost includes an estimate of fuel cost. The annual consumables costs include accounting for the annual capacity factor (85%); that is:

Annual Cost = Hourly Consumption Rate x 8760 hours/yr x 0.85 x Unit Cost.

The operating labor cost was assumed to be the same as in the DOE Bituminous Coal Baseline study Case 12. The administrative and labor support cost is estimated based on a percentage of operating labor cost; therefore, this cost is also the same as in the DOE Study.

Maintenance material and labor is estimated as a percentage or capital cost on a system-by-system basis.

Consumables, waste disposal, and fuel costs are estimated based on a unit cost times the annual quantity consumed or disposed. The unit costs for all consumables, wastes, and fuel were assumed to be the same as in the updated (to January 2012 dollars) costs for the DOE Bituminous Coal Baseline study Case 12.

Consistent with the assumptions of the DOE Bituminous Coal Baseline study, no credit or cost of disposal was included for gypsum produced by the plant flue gas desulfurization (FGD) system.

3.4.3   Transportation Storage and Monitoring

CO_2 transport storage and monitoring costs were estimated based on the quantity of CO_2 captured and the TS&M unit cost ($ per ton of CO_2) used in the DOE Bituminous Coal Baseline study Case 12.

3.4.4   Owners' Costs

The economic analysis accounts for the owner's costs associated with the facilities. For real world projects, these costs are strongly dependent on location and the owners involved in the project. For the current study the methodology and guidance regarding the basis and rates for the owners' costs are consistent with the DOE/NETL Baseline studies and are summarized in Exhibit 3-9

Exhibit 3-9 Owners' Costs Basis

Owner's Costs	Basis
Preproduction costs	
6 Months all labor	Sum of Operating, Maintenance and Administrative Labor
1 Month maintenance materials	Annual maintenance materials @ 85% capacity
1 Month non-fuel consumables	Annual consumables @ 85% capacity
1 Month waste disposal	OPEX disposal costs @ Capacity Factor (CF)=85%
25% of 1 months fuel cost at 100% CF	Annual fuel costs @ 85% capacity
2% TPC	TPC
Inventory Capital	
60 day supply of fuel and consumables at 100% CF	OPEX fuel and consumables
Spare parts	0.5% of TPC
Land	$3,000/acre, 300 acre for PC plants
Financing Costs	2.7% of TPC

Other Owner's Costs includes:
• Preliminary feasibility studies, including Front-End Engineering Design (FEED) study
• Economic development
• Construction and/or improvement of roads and/or railroad spurs outside of site boundary
• Legal Fees
• Permitting costs
• Owner's engineering
• Owner's Contingency (Management reserve, funds to cover costs relating to delayed startup, fluctuations in equipment costs, unplanned labor incentives)
Costs not included:
  • EPC risk premium
  • Transmission interconnection-cost of connecting to grid beyond plant busbar
  • Taxes on capital costs
  • Unusual site improvements
	15% of TPC

3.5 Economic Analysis

3.5.1 Economic Analysis Metrics

The economic analysis uses the capital and O&M cost estimates along with global economic assumptions to determine the following economic metrics to compare the technologies:

- First-year COE breakdown including:

- o Capital
- o Fuel
- o Variable O&M
- o Fixed O&M
- o TS&M

- Thirty-year levelized COE (using DOE/NETL Power System Financial Model [PSFM])[12]

- Cost of CO_2 avoided

- Cost of CO_2 captured

Cost of Electricity

The COE ($/MWh) is calculated using the following equation from the BB report.

$$COE = \frac{\begin{array}{c}first\,year\\capital\,charge\end{array} + \begin{array}{c}first\,year\\fixed\,operating\\costs\end{array} + \begin{array}{c}first\,year\\variable\,operating\\costs\end{array}}{\begin{array}{c}annual\,net\,megawatt\,hours\\of\,power\,generated\end{array}}$$

$$COE = \frac{(CCF)(TOC) + OC_{FIX} + (CF)(OC_{VAR})}{(CF)(MWH)}$$

where:

COE = cost of electricity, revenue received by the generator ($/MWh) during the power plant's first year of operation (expressed in base-year dollars) assuming that the COE escalates thereafter at a nominal annual rate equal to the general inflation rate

CCF = capital charge factor based on financial structure and determined using the NETL PSFM. This factor takes into account the financial structure and construction period to distribute the costs of the plant operational life (unitless)

TOC = total overnight capital costs, expressed in base-year dollars ($)

OC_{FIX} = the sum of all fixed annual operating costs, expressed in base-year dollars ($)

OC_{VAR} = the sum of all variable operating costs (fuel and variable O&M costs), expressed in base-year dollars ($/MWh)

CF = Capacity factor (unit-less)

MWH = Total generation from facility operating for 1 year, 8760 hours (MWh).

Levelized Cost of Electricity

The LCOE ($/MWh) is determined using the following equation from the PSFM.

$$LCOE = L_{COE}COE$$

where:

L_{COE} = COE levelization factor as defined by:

$$L_{COE} = \frac{i(1+i)^n \left(1 - \frac{(1+e_{COE})^n}{(1+i)^n} \right)}{((1+i)^n - 1)(i - e_{COE})}$$

where:

n = levelization period

i = discount rate, rate of return on equity RROE

e_{COE} = COE escalation rate

Cost of CO_2 Avoided ($/tonne CO_2)

The cost of CO_2 avoided is calculated using the following equation:

$$CO_2 \ Avoided \ Cost = \frac{COE_{Capture} - COE_{NoCapture}}{CO_2 \ Emissions_{NoCapture} - CO_2 \ Emissions_{Capture}}$$

where:

$COE_{Capture}$ = COE of generation facility with CO_2 capture ($/MWh)

$COE_{No \ Capture}$ = COE of generation facility without CO_2 capture ($/MWh)

$CO_2 \ Emissions_{Capture}$ = CO_2 emissions from generation facility with CO_2 capture (tonne CO_2/MWh)

$CO_2 \ Emissions_{No \ Capture}$ = CO_2 emissions from generation facility without CO_2 capture (tonne CO_2/MWh)

Cost of CO_2 Captured

Cost of CO_2 captured ($/tonne CO_2) is calculated using the following equation:

$$CO_2 \ Capture \ Cost = \frac{COE_{Capture} - COE_{NoCapture}}{CO_2 \ Captured_{Per \ Net \ Output}}$$

where:

$CO_2 \ Captured_{Per \ Net \ Output}$ = amount of CO_2 captured per unit of generation (tonne CO_2/MWh)

3.5.2 Global Economic Assumptions and Financial Structure

The economic analysis assumptions were taken from the original DOE/NETL report. The global assumptions are summarized in Exhibit 3-10. The financial structure for low risk (no-capture) and high risk (capture) projects and the resulting factors are summarized in Exhibit 3-11.

Exhibit 3-10 Global Economic Assumptions

Parameter	Value
TAXES	
Income Tax Rate	38% (Effective: 34% Federal, 6% State)
Capital Depreciation	20 years, 150% declining balance
Investment Tax Credit	0%
Tax Holiday	0 years
CONTRACTING AND FINANCING TERMS	
Contracting Strategy	Engineering Procurement Construction Management (owner assumes project risks for performance, schedule and cost)
Type of Debt Financing	Non-Recourse (collateral that secures debt is limited to the real assets of the project)
Repayment Term of Debt	15 years
Grace Period on Debt Repayment	0 years
Debt Reserve Fund	None
ANALYSIS TIME PERIODS	
Capital Expenditure Period	5 years
Operational Period	30 years
Economic Analysis Period (used for IRROE)	35 years (capital expenditure period plus operation period)
Treatment of Capital Costs	
Capital Cost Escalation During Capital Expenditure Period (nominal annual rate)	3.6%[1]
Distribution of Total Overnight Capital over the Capital Expenditure Period (before escalation)	10%, 30%, 25%, 20%, 15%
Working Capital	Zero for all parameters
% of Total Overnight Capital that is Depreciated	100% (this assumption introduces a very small error even in a substantial amount of TOC is actually non-depreciable
ESCALATION OD OPERATING REVENUES AND COSTS	
Escalation of COE (Revenue), O&M Costs, and Fuel Costs (nominal annual rate)	3%[2]

Notes:
1. The nominal average rate of 3.6 percent is assumed for escalation of capital costs during construction. This rate is equivalent to the nominal average annual escalation rate for process plant construction costs between 1947 and 2008 according to the *Chemical Engineering* Plant Cost Index.
2. An average annual inflation of 3.0% is assumed. This rate is equivalent to the average annual escalation rated between 1947 and 2008 for the US Department of Labor's Producer Price Index for Finished Goods, the so-called "headline" index of the various Producer Price Indices.

Exhibit 3-11 Financial Structure for Investor Owned Utility

Finance Structure	High Risk CO$_2$ Capture Cases		Low Risk Non – CO$_2$ Capture Cases	
	Debt	Equity	Debt	Equity
Percent of Total	45%	50%	50%	50%
Current (Nominal) Dollar Cost	5.50%	12.00%	4.50%	12.00%
Weighted Current (Nominal) Cost	2.48%	6.60%	2.25%	6.00%
Weighted Current (Nominal) Cost Combined	9.08%		8.25%	
After Tax Weighted Cost of Capital	8.13%		7.39%	
Capital Charge Factor	0.124		0.116	
Levelization Factor	1.268		1.268	

3.6 Update of DOE Baseline Cases

The capital costs, O&M costs, and the cost of electricity (COE) estimates for Case 11 and Case 12 of the DOE/NETL Bituminous Baseline Report Volume 1, Rev. 2, 2010[1] were updated from June 2007 year dollar basis to January 2012 year dollar basis using the methodology described in this section The summary and detailed updated capital costs for Case 11 are shown in the Appendix in Exhibit B-1 and Exhibit 0-2 and the O&M cost is shown in Exhibit 0-3. The summary and detailed updated capital costs for Case 12 are also shown in the Appendix in Exhibit 0-4 and Exhibit 0-5 and the O&M cost is shown in Exhibit 0-6.

Case 11 is a 550-MWe net supercritical critical pulverized coal power plant without CO$_2$ capture and utilization and sequestration (CCUS) and Case 12 is a 550-MWe net supercritical pulverized coal power plant with CCUS based on the Fluor Economine FG Plus CO$_2$ removal technology. The purpose of the cost update is to provide a basis for comparison with the cost developed for the commercial-scale pulverized coal power plant with post-combustion CO$_2$ removal based on the ATK ICES CO$_2$ removal process.

The bituminous baseline cases were escalated from a cost basis date June 2007 to a cost basis date of January 2012 using information derived from a number of sources. These include published indices such as the Chemical Engineering (CE) Plant Cost Index, recent vendor quotations for similar equipment and materials, monthly mill pricing updates for structural steel, cost trending input from vendors, published wage rate information, and WorleyParsons in-house cost data base. In general, the CE index tends to trend slightly lower than costs developed using other sources. This can be due to several reasons including specific equipment design/sizing parameters and market conditions. In particular, the index value for construction labor and engineering services was not used because it almost always trends at a much lower rate than other sources employed.

Equipment accounts that do not follow the general cost escalation trend include consumables, that generally are escalated using the index for producer prices for industrial chemicals (per HIS Global Insight, Inc. and reported in Chemical Engineering), and CO$_2$ compressor and main power transformer costs that were re-calibrated using more recent quotes in additional to the general cost of escalation.

The coal price was estimated based on the National Energy Technology Laboratory Quality Guidelines for Energy System Studies[13].

Plant specific inputs, both technical and cost, are listed in Exhibit 3-12. The operational parameters for Case 11 and Case 12 are taken from the DOE/NETL report. The cost data for Case 11 and Case 12 from were escalated from 2007$ to 2012$ for this study.

Exhibit 3-12 Plant Specific Operational and Cost Inputs

	Case 11	Case 12
OPERATING PARAMETERS		
Net Plant Output	550.0	550.0
Net Plant Heat Rate, Btu/kWh (kJ/kWh)	8,686 ()	12,002 ()
CO_2 Captured, lb/MWh (kg/MWh)	0 (0)	2,200 (998)
CO_2 Emitted, lb/MWh net (kg/MWh net)	1,768 (802)	244 (111)
COSTS		
Total Plant Costs (2012$)	2,033	3,651
Total Overnight Cost (2012$/kw)	2,513	4,496
Bare Erected Cost	1,665	2,815
Home Office Expenses	151	256
Project Contingency	217	456
Process contingency	0	124
Owners Costs	480	844
Total Overnight Cost (2012$x1,000)	1,382,286	2,472,362
Total As Spent Capital (2012$)	2850	5125
Annual Fixed Operating Costs ($/yr)	39,826,084	65,958,457
Variable Operating Costs ($/MWh)	7.24	12.39
Fuel		
Coal Price ($/ton)	69.00	

3.6.1 Results for Update of DOE Base Cases

Economic metrics determined during this analysis are listed in Exhibit 3-13. The percent increase in the COE for Case 12 compared to the non-capture configuration in Case 11 is 77%. The COE and a breakdown of the COE are graphically compared in Exhibit 3-14.

Exhibit 3-13 Table of Economic Metrics Determined for DOE Baseline Cases

	Case 11	Case 12
COE($/MWh, 2012$)	**81.81**	**144.45**
CO_2 TS&M Costs		5.60
Fuel Costs	25.69	35.49
Variable Costs	7.24	12.39
Fixed Costs	9.72	16.11
Capital Costs	39.15	74.87
LCOE (2012$/MWh)	103.73	183.17
Cost of CO_2 Captured ($/tonne CO_2)		62.79
Cost of CO_2 Avoided ($/tonne CO_2)		90.67

Exhibit 3-14 Comparison and Breakdown of COE for NETL/DOE Baseline Case 11 and Case 12
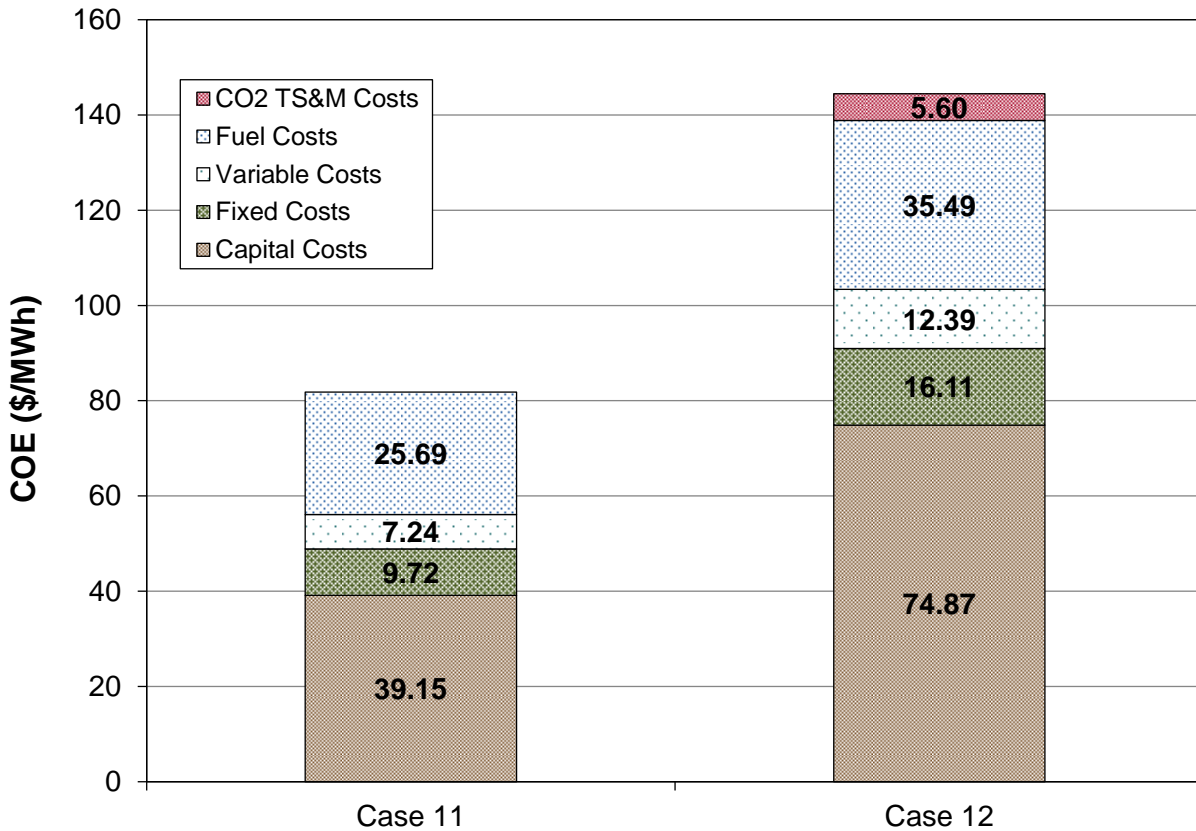
4   ICES Case

The plant configuration model for the ATK ICES CO_2 Capture incorporated into a supercritical pulverized coal plant is the same as the Bituminous Baseline Case 12 except for:

- Replacing the amine based CO_2 capture system and CO_2 compression systems with the following systems:
    - Flue gas pretreatment
    - ATK ICES CO_2 capture
    - Dry ice melting
- Increasing the pressure in the crossover duct to that in the Bituminous Baseline Case 11

A comparison of the key system assumptions are provided in Exhibit 4-1.

Exhibit 4-1 Supercritical PC Plant Study Configuration for DOE/NETL Baseline Cases 11 and 12 and the ATK ICES CO_2 Capture Case

	Case 11 w/o CO_2 Capture	Case 12 w/ CO_2 Capture	ATK ICES w/ CO_2 Capture
Steam cycle, MPa/°C/°C (psig/°F/°F)	24.1/593/593 (3500/1100/1100)	24.1/593/593 (3500/1100/1100)	24.1/593/593 (3500/1100/1100)
IP/LP turbine crossover duct steam conditions, MPa/°C (psig/°F)	0.93/364 (120/688)	0.40/556 (59/291)	0.93/363 (120/686)
Coal	Illinois No. 6	Illinois No. 6	Illinois No. 6
Condenser pressure, mm Hg (in Hg)	50.8 (2)	50.8 (2)	50.8 (2)
Boiler Efficiency, %	88	88	88
Cooling water to condenser, °C (ºF)	16 (60)	16 (60)	16 (60)
Cooling water from condenser, °C (ºF)	27 (80)	27 (80)	27 (80)
Stack temperature, °C (°F)	57 (135)	32 (89)	66 (150)
SO_2 control	Wet Limestone Forced Oxidation	Wet Limestone Forced Oxidation	Wet Limestone Forced Oxidation
FGD efficiency, % (A)	98	98 (B, C)	98
NOx control	LNB w/OFA and SCR	LNB w/OFA and SCR	LNB w/OFA and SCR
SCR efficiency, % (A)	86	86	86
Ammonia slip (end of catalyst life), ppmv	2	2	2
Particulate control	Fabric Filter	Fabric Filter	Fabric Filter
Fabric filter efficiency, % (A)	99.8	99.8	99.8
Ash distribution, Fly/Bottom	80% / 20%	80% / 20%	80% / 20%
CO_2 control	N/A	Econamine	ATK ICES
Overall CO_2 capture (A)	N/A	90.2%	90.2%
CO_2 sequestration	N/A	Off-site Saline Formation	Off-site Saline Formation

A. Removal efficiencies are based on the FG content

B. An SO_2 polishing step is included to meet more stringent SOx content limits in the FG (< 10 ppmv) to reduce formation of amine HSS during the CO_2 absorption process

C. SO_2 exiting the post-FGD polishing step is absorbed in the CO_2 capture process making stack emissions negligible

A complete process description for the Bituminous Baseline Case 12 including a block flow diagram (BFD) is available in the Bituminous Baseline Report.[1] A BFD and stream tables for the PC unit with the ATK ICES CO_2 capture system are shown in Exhibit 4-2 and Exhibit 4-3 respectively.

Exhibit 4-2 ATK ICES Case Block Flow Diagram, Supercritical Unit with CO_2 Capture

WorleyParsons
resources & energy
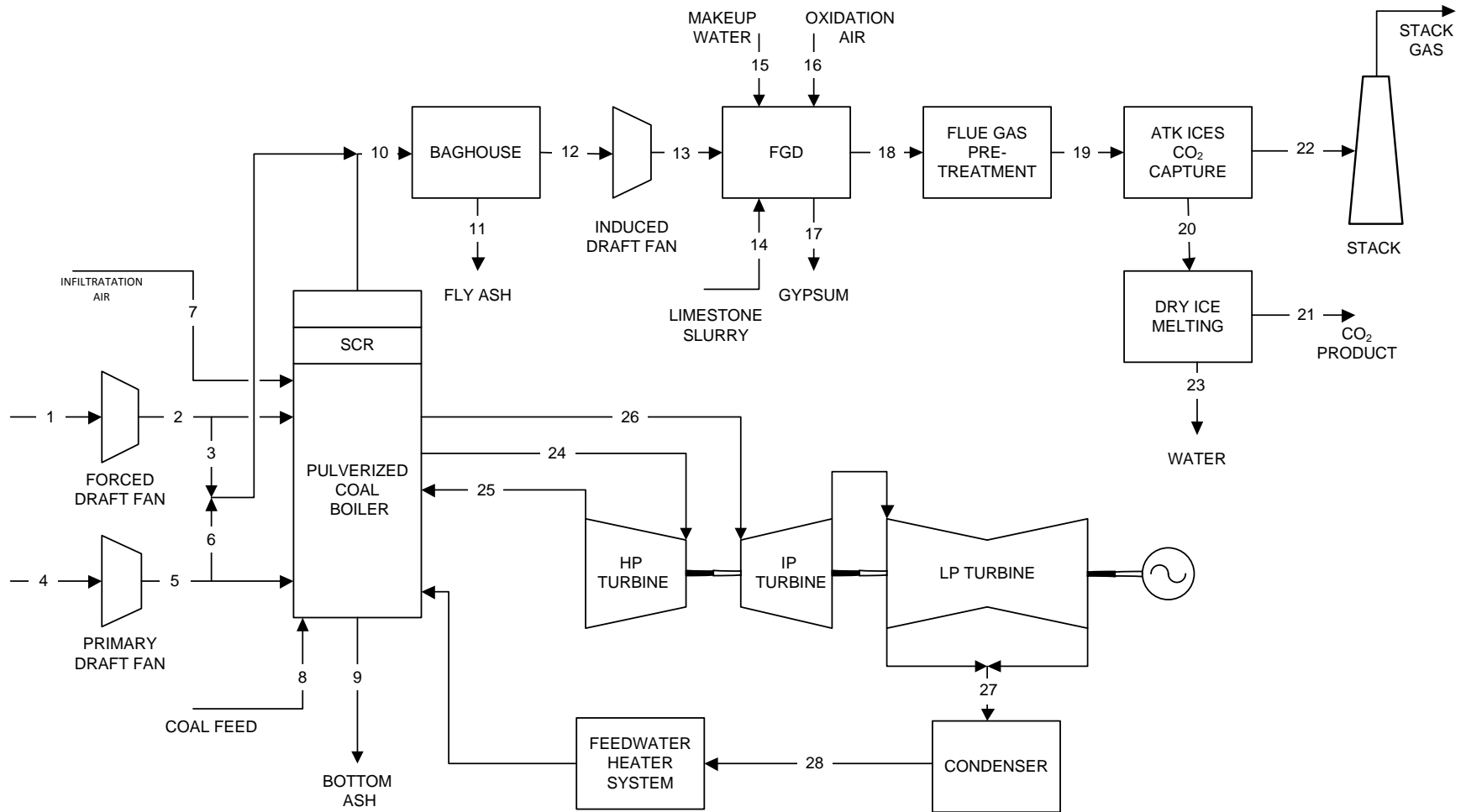
Exhibit 4-3 ATK ICES Case Stream Table, Supercritical Unit with CO_2 Capture

	1	2	3	4	5	6	7	8	9	10	11	12	13	14
V-L Mole Fraction														
Ar	0.0092	0.0092	0.0092	0.0092	0.0092	0.0092	0.0092	0.0000	0.0000	0.0087	0.0000	0.0087	0.0087	0.0000
CO_2	0.0003	0.0003	0.0003	0.0003	0.0003	0.0003	0.0003	0.0000	0.0000	0.1450	0.0000	0.1450	0.1450	0.0000
H_2	0.0000	0.0000	0.0000	0.0000	0.0000	0.0000	0.0000	0.0000	0.0000	0.0000	0.0000	0.0000	0.0000	0.0000
H_2O	0.0099	0.0099	0.0099	0.0099	0.0099	0.0099	0.0099	0.0000	0.0000	0.0870	0.0000	0.0870	0.0870	1.0000
N_2	0.7732	0.7732	0.7732	0.7732	0.7732	0.7732	0.7732	0.0000	0.0000	0.7324	0.0000	0.7324	0.7324	0.0000
O_2	0.2074	0.2074	0.2074	0.2074	0.2074	0.2074	0.2074	0.0000	0.0000	0.0247	0.0000	0.0247	0.0247	0.0000
SO_2	0.0000	0.0000	0.0000	0.0000	0.0000	0.0000	0.0000	0.0000	0.0000	0.0021	0.0000	0.0021	0.0021	0.0000
Total	1.0000	1.0000	1.0000	1.0000	1.0000	1.0000	1.0000	0.0000	0.0000	1.0000	0.0000	1.0000	1.0000	1.0000
V-L Flowrate (kg mol /hr)	66,876	66,876	1,990	20,544	20,544	2,818	1,546	0	0	94,107	0	94,107	94,107	3,385
V-L Flowrate (kg/hr)	1,588,354	1,588,354	47,044	487,926	487,926	67,152	36,705	0	0	2,799,052	0	2,799,052	2,799,052	60,975
Solids Flowrate (kg/hr)	0	0	0	0	0	0	0	211,193	4,096	16,383	16,383	0	0	25,966
Temperature (°C)	15	19	19	15	25	25	15	15	15	169	15	169	181	15
Pressure (MPa, abs)	0.1	0.11	0.11	0.1	0.11	0.11	0.1	0.1	0.1	0.1	0.1	0.1	0.11	0.1
Enthalpy (kJ/kg)A	30.23	34.36	34.36	30.23	40.78	40.78	30.23	---	---	327.37	---	308.94	321.02	---
Density (kg/m³)	1.2	1.2	1.2	1.2	1.3	1.3	1.2	---	---	0.8	---	0.8	0.8	---
V-L Molecular Weight	28.857	28.857	28.857	28.857	28.857	28.857	28.857	---	---	29.743	---	29.743	29.743	---
V-L Flowrate (lb mol /hr)	121,348	121,348	3,594	37,276	37,276	5,130	2,804	0	0	170,755	0	170,755	170,755	5,938
V-L Flowrate (lb/hr)	3,501,716	3,501,716	103,714	1,075,690	1,075,690	148,044	80,920	0	0	5,078,777	0	5,078,777	5,078,777	106,983
Solids Flowrate (lb/hr)	0	0	0	0	0	0	0	465,600	9,029	36,119	36,119	0	0	46,211
Temperature (°F)	59	66	66	59	78	78	59	59	59	59	59	59	59	59
Pressure (psia)	14.7	15.3	15.3	14.7	16.1	16.1	14.7	14.7	14.7	14.7	14.7	14.7	14.7	14.7
Enthalpy (Btu/lb)A	13	14.8	14.8	13	17.5	17.5	13	---	---	140.7	---	132.8	138	---
Density (lb/ft³)	0.076	0.078	0.078	0.076	0.081	0.081	0.076	---	---	0.05	---	0.049	0.052	---

Exhibit 4-3 ATK ICES Case Stream Table, Supercritical Unit with CO2 Capture (continued)

	15	16	17	18	19	20	21	22	23	24	25	26	27	28
V-L Mole Fraction														
Ar	0.0000	0.0128	0.0000	0.0081	0.0096	0.0000	0.0000	0.0000	0.0000	0.0000	0.0000	0.0000	0.0000	0.0000
CO_2	0.0000	0.0005	0.0004	0.1350	0.1571	0.9340	1.0000	0.0000	0.0110	0.0000	0.0000	0.0000	0.0000	0.0000
H_2	0.0000	0.0000	0.0000	0.0000	0.0000	0.0000	0.0000	0.0000	0.0000	0.0000	0.0000	0.0000	0.0000	0.0000
H_2O	1.0000	0.0062	0.9996	0.1537	0.0111	0.0660	0.0000	0.0000	0.9890	1.0000	1.0000	1.0000	1.0000	1.0000
N_2	0.0000	0.7506	0.0000	0.6793	0.7942	0.0000	0.0000	0.9660	0.0000	0.0000	0.0000	0.0000	0.0000	0.0000
O_2	0.0000	0.2300	0.0000	0.0238	0.0280	0.0000	0.0000	0.0340	0.0000	0.0000	0.0000	0.0000	0.0000	0.0000
SO_2	0.0000	0.0000	0.0000	0.0000	0.0000	0.0000	0.0000	0.0000	0.0000	0.0000	0.0000	0.0000	0.0000	0.0000
Total	1.0000	1.0000	1.0000	1.0000	1.0000	1.0000	1.0000	1.0000	1.0000	1.0000	1.0000	1.0000	1.0000	1.0000
V-L Flowrate (kg mol /hr)	13,485	975	250	102,548	72,198	10,929	10,217	55,499	721	103,260	87,211	87,211	45,984	79,441
V-L Flowrate (kg/hr)	242,941	28,289	4,498	2,956,531	2,212,219	0	449,661	1,562,259	13,196	1,860,231	1,571,110	1,571,110	828,397	1,431,132
Solids Flowrate (kg/hr)	0	0	40,138	0	0	462,228	0	0	0	0	0	0	0	0
Temperature (°C)	15	167	57	57	23	-101	35	66	32	593	354	593	38	39
Pressure (MPa, abs)	0.10	0.31	0.10	0.10	0.25	0.25	15.27	0.11	1.00	24.23	4.90	4.52	0.01	1.72
Enthalpy (kJ/kg)A	-46.8	177.65	---	298	-2109	-9258	-9143	41.9	-15667	3481	3082	3655	2346	163
Density (kg/m³)	1003.1	2.5	---	1.1	3.153074	8.51241	720.945	1.137322	545.777	69.18434	18.67769	11.56543	0.064074	993.2975
V-L Molecular Weight	18.015	29.029	---	28.855	30.64116	42.29436	44.0098	28.14918	18.30154	18.015	18.015	18.015	18.015	18.015
V-L Flowrate (lb mol /hr)	24,055	1,820	440	185,708	159,168	0	22,525	122,355	1,590	227,649	192,268	192,268	101,377	175,137
V-L Flowrate (lb/hr)	433,364	52,827	7,941	5,358,549	4,877,099	0	991,331	3,444,185	29,091	4,101,100	3,463,700	3,463,700	1,826,300	3,155,100
Solids Flowrate (lb/hr)	0	0	71,920	0	0	1,019,037	0	0	0	0	0	0	0	0
Temperature (°F)	59	333	136	136	74	-150	95	150	90	1100	669	1100	101	101
Pressure (psia)	14.7	45	14.9	14.9	36.7	36.7	2215	16.5	145	3515	711	656	0.982	250
Enthalpy (Btu/lb)A	-20.1	76.4	---	130	-907	-3980	-3931	18.0	-6736	1497	1325	1572	1008	70
Density (lb/ft³)	62.62	0.154	---	0.067	0.197	0.531	45.01	0.071	34.07	4.32	1.166	0.722	0.004	62.01

when experience counts

4.1   Performance Results

The PC unit with the ATK ICES CO_2 capture system produces 550 MW at a net plant efficiency of 34.5%(HHV basis). This represents an improvement over the efficiency of the Bituminous Baseline Study Supercritical Plant with CO_2 capture (Case 12) of 28.4%. The overall plant performance is summarized in Exhibit 4-4, which includes auxiliary power requirements. The relatively low auxiliary electric loads related to the ATK ICES CO_2 capture system are, due to:

- Performing the flue gas compression with as steam turbine instead of an electric motor.
- Pressurizing the CO_2 as a liquid instead of a gas

A heat and mass balance diagram is shown for the ATK ICES CO_2 capture case PC boiler, the FGD unit and the ATK ICES and supporting systems are shown in Exhibit 4-5. Details of the heat and mass balance for the flue gas pretreatment and dry ice melting equipment are provided in Exhibit 4-6 and Exhibit 4-7. The steam cycle for the power plant incorporating the ATK ICES CO_2 capture technology is provided in Exhibit 4-8.

.

Exhibit 4-4 ATK ICES Case Performance Summary

POWER SUMMARY (Gross Power at Generator Terminals kWe)	
Steam Turbine Power	590,170
TOTAL (STEAM TURBINE) POWER, kWe	590,170
AUXILIARY LOAD SUMMARY, kWe	
Coal handling	470
Sorbent handling and Reagent Preparation	1,030
Pulverizer	3,170
Condensate Pump	840
Miscellaneous Balance of Base Plant	2,000
PA Fan	1,480
FD Fan	1,890
ID Fan	8,530
Wet FGD	3,390
SCR	60
Baghouse	80
Glycol Pump	1,000
CO_2 Pressurization	1,850
Miscellaneous Aux Load for ATK Process	400
STG Auxiliary Load	400
Circulating Water Pumps	6,800
Ground Water Pumps	640
Cooling Tower Fan	3,520
Ash Handling	610
Transformer losses	2,040
Total Aux Load	**40,200**
NET POWER, kWe	549,970
Net Plant Efficiency (HHV)	34.5%
Net Plant Heat Rate, kJ/kWh HHV (Btu/kWh)	10,440 (9,896)
Net Plant Efficiency (LHV)	35.8%
Net Plant Heat Rate, kJ/kWh LHV (Btu/kWh)	10,070 (9,544)
CONSUMABLES	
As-Received Coal Feed, lb/hr (kg/hr)	465,610 (211,257)
Limestone Sorbent Feed, lb/hr (kg/hr)	47,083 (21,363)

Exhibit 4-5 ATK ICES Case Heat and Mass Balance, Supercritical PC Boiler with CO_2 Capture

LEGEND

- ——— AIR
- —×—×— COAL/ASH
- ·········· STEAM
- - - - - - FLUE GAS

P   ABSOLUTE PRESSURE, PSIA
T   TEMPERATURE, °F
W   FLOWRATE, LBM/HR
H   ENTHALPY BTU/LBM

NOTES:
1. ENTHALPY REFERENCE POINT IS NATURAL STATE AT 32°F AND 0.089 PSIA.

MAKE-UP WATER
(15)
433,364 W
59.0 T
14.7 P

OXIDATION AIR
(16)
52,827 W
333.0 T
45.0 P
76.4 H

BAGHOUSE

(12)
5,078,777 W
59.0 T
14.7 P
132.8 H

(13)
5,078,777 W
59.0 T
14.7 P
138.0 H

FGD

(11) ASH
36,119 W

(14)
153,194 W
59.0 T
15.0 P

LIMESTONE SLURRY

(17)
79,862 W
136.0 T
14.9 P

GYPSUM

(18)
5,358,549 W
136.0 T
14.9 P
129.6 H

FLUE GAS COMPRESSOR

COOLANT FROM DRY ICE MELTING PROCESS

CONDENSATE HEATER

DIRECT CONTACT COOLER

AIR COOLER

DIRECT CONTACT COOLER

COOLANT FROM DRY ICE MELTING PROCESS

COOLANT TO DRY ICE MELTING PROCESS

DIRECT CONTACT COOLER

AUXILIARY COOLING TOWER

(10)
5,114,896 W
59.0 T
14.7 P
140.7 H

(24)
5,024,628 W
1,100.0 T
3,514.7 P
1,494.7 H
THROTTLE STEAM TO HP TURBINE

(26)
4,100,215 W
1,100.0 T
655.8 P
1,570.2 H
SINGLE REHEAT TO IP TURBINE

AMMONIA

(19)
4,877,099 W
74.0 T
36.5 P
-906.7 H

(25)
4,100,215 W
668.0 T
710.8 P
1,324.9 H
SINGLE REHEAT EXTRACTION FROM HP TURBINE

(7)
80,920 W
59.0 T
14.7 P
13.0 H

(3)
3,501,716 W
66.0 T
15.3 P
14.8 H

PULVERIZED COAL BOILER

(22)
3,444,185 W
150.0 T
16.5 P
18.0 H
STACK

CONDENSATE HEATER
3,444,185 lb/hr
296.0 °F
16.7 psia

(1) **AIR**
3,501,716 W
59.0 T
14.7 P
13.0 H

(2)

(3)

(6)

(4) **AIR**
1,075,690 W
59.0 T
14.7 P
13.0 H

(5)
1,075,690 W
78.0 T
16.1 P
17.5 H

(8) **COAL**
465,600 W
59.0 T
14.7 P

5,024,529 W
545.5 T
4,185.0 P
539.3 H
FROM FEEDWATER HEATERS

ICES CO_2 CAPTURE PROCESS

(20)
1,019,037 W
-150.0 T
4.4 P
-3,980.4 H

DRY ICE MELTING PROCESS

WATER FROM CO_2
(23)
29,091 W
90.0 T
144.9 P
-6,735.6 H

CO_2 PRODUCT TO PIPELINE
(21)
991,331 W
95.0 T
2,214.6 P
-3,931.0 H

PLANT PERFORMANCE SUMMARY

GROSS PLANT POWER:	590 MWe
AUXILIARY LOAD:	40 MWe
NET PLANT POWER:	550 MWe
NET PLANT EFFICIENCY, HHV:	34.5%
NET PLANT HEAT RATE, HHV:	9896 BTU/kW

WorleyParsons
resources & energy

PROJECT: ATK ICES

HEAT AND MATERIAL FLOW DIAGRAM

ATK ICES CO_2 CAPTURE CASE PULVERIZED COAL BOILER AND GAS CLEANUP SYSTEMS

DRAWING NUMBER: PAGE

Exhibit 4-6 Heat and Mass Balance Details for Flue Gas Pretreatment Equipment

COOLANT FROM
DRY ICE MELTING
PROCESS

COOLANT FROM
DRY ICE MELTING
PROCESS

4,877,099 lb/hr
46.3 °F
14.2 psia

4,877,099 lb/hr
223.1 °F
36.7 psia

4,877,099 lb/hr
150.0 °F
36.7 psia

4,877,099 lb/hr
143.7 °F
36.7 psia

4,877,099 lb/hr
110.0 °F
36.5 psia

4,877,099 lb/hr
74.0 °F
36.5 psia

FLUE GAS
COMPRESSOR

CONDENSATE
HEATER

HEAT
EXCHANGER

AIR COOLER

HEAT
EXCHANGER

TO ICES PROCESS

COOLANT FROM DRY
ICE MELTING PROCESS

COOLANT TO DRY ICE
MELTING PROCESS

4,966,893 lb/hr
84.6 °F
14.5 psia

89,794 lb/hr
46.3 °F

AUXILIARY COOLING
TOWER

25,399,520 lb/hr
66.0 °F
15.0 psia

DIRECT CONTACT
COOLER

5,358,549 lb/hr
136.0 °F
14.9 psia
129.6 MMBtu/hr

25,880,970 lb/hr
84.6 °F
14.5 psia

Exhibit 4-7 Heat and Mass Balance Details for Dry Ice Melting Equipment

DRY ICE FROM
ICES PROCESS

1,019,037 lb/hr
-150.0 °F
4.4 psia

SCREW
EXTRUDER

1,019,037 lb/hr
-150.0 °F
145.0 psia

TO/FROM FLUE
GAS COOLING

DRY ICE
MELTING
VESSEL

1,019,037 lb/hr
-58.0 °F
145.0 psia

WATER ICE
SEPARATION

WATER ICE
FILTER

991,331 lb/hr
-50.0 °F
145.0 psia

991,331 lb/hr
-38.9 °F
2,214.7 psia

TO/FROM FLUE
GAS COOLING

991,331 lb/hr
95.0 °F
2,214.6 psia

CO_2 TO
PIPELINE

24,727 lb/hr
-50.0 °F
145.0 psia

4,364 lb/hr
-50.0 °F
145.0 psia

29,091 lb/hr
90.0 °F
144.9 psia

WATER FROM CO_2
DEHYDRATION

TO/FROM FLUE
GAS COOLING

Exhibit 4-8 ATK ICES Case, Supercritical Steam Cycle

4.2 Major Equipment List

The major equipment list for the ATK ICES case is provided in the Exhibit 4-9A through Exhibit 4-9L broken down into the following sub-systems of the plant:

- Fuel and Sorbent Handling

- Coal and Sorbent Preparation and Feed

- Feedwater and Miscellaneous Systems and Equipment

- Boiler And Accessories

- Flue Gas Cleanup

- CO_2 Capture (high-level)

- HRSG, Ducting, and Stack

- Steam Turbine Generator and Auxiliaries

- Cooling Water System

- Ash/Spent Sorbent Recovery and Handling

- Accessory Electric Plant

- Instrumentation and Control

In each table, a label for the piece of equipment is given, a brief description, the type if applicable, the design condition for it, the quantity used in the plant, and the number of spares, if any.

Exhibit 4-9A. Account 1 - Fuel and Sorbent Handling Equipment List

Equipment No.	Description	Type	Design Condition	Operating Quantity	Spares
1	Bottom Trestle Dumper and Receiving Hopper	N/A	200 ton	2	0
2	Feeder	Belt	520 tph	2	0
3	Conveyer No. 1	Belt	1,030 tph	1	0
4	Transfer Tower No.1	Enclosed	N/A	1	0
5	Conveyer No. 2	Belt	1,030 tph	1	0
6	As-Received Coal Sampling System	Two-stage	N/A	1	0
7	Stacker/Reclaimer	Traveling, linear	1,030 tph	1	0
8	Reclaimer Hopper	N/A	50 ton	2	1
9	Feeder	Vibratory	190 tph	2	1
10	Conveyer No. 3	Belt w/ tripper	390 tph	1	0
11	Crusher Tower	N/A	N/A	1	0

Equipment No.	Description	Type	Design Condition	Operating Quantity	Spares
12	Coal Surge Bin with Vent Filter	Dual Outlet	190 ton	2	0
13	Crusher	Impactor Reduction	3" X 0-1-1/4" X 0)	2	0
14	As-Fired Coal Sampling System	Swing hammer	N/A	1	1
15	Conveyer No. 4	Belt w/ tripper	390 tph	1	1
16	Transfer Tower No.2	Enclosed	N/A	1	0
17	Conveyer No. 5	Belt w/ tripper	390 tph	1	0
18	Coal Silo w/ Vent Filter and Slide Gates	Field erected	1,000 tons/each	3	0
19	Limestone Truck Unloading Hopper	N/A	33 ton	1	0
20	Limestone Feeder	Belt	100 tph	1	0
21	Limestone Conveyer No. L1	Belt	100 tph	1	0
22	Limestone Reclaimer Hopper	N/A	20 ton	1	0
23	Limestone Reclaimer Feeder	Belter	80 ton	1	0
24	Limestone Conveyer No. L2	Belt	80 tph	1	0
25	Limestone Day Bin	w/ actuator	320 ton	2	0

Exhibit 4-9B. Account 2 - Coal and Sorbent Preparation and Feed Equipment List

Equipment No.	Description	Type	Design Condition	Operating Quantity	Spares
1	Coal Feeder	Gravimetric	42 tph	6	0
2	Coal Pulverizer	Ball type or equivalent	42 tph	6	0
3	Limestone Weigh Feeder	Gravimetric	26 tph	1	1
4	Limestone Ball Mill	Rotary	26 tph	1	1
5	Limestone Mill Slurry Tank w/ Agitator	N/A	24,000 gal	1	1
6	Limestone Mill Recycle Pumps	Horizontal, Centrifugal	410 gpm @ 40 ft H_2O	1	1
7	Hydro-cyclone Classifier	4 active cyclones in a cyclone bank	100 gpm per cyclone	1	1

Equipment No.	Description	Type	Design Condition	Operating Quantity	Spares
8	Distribution Box	2-way	N/A	1	1
9	Limestone Slurry Storage Tank w/ Agitator	Field erected	135,000 gal	1	1
10	Limestone Slurry Feed Pumps	Horizontal, Centrifugal	280 gpm @ 30 ft H_2O	1	1

Exhibit 4-9C. Account 3 - Feedwater and Miscellaneous Systems and Equipment List

Equipment No.	Description	Type	Design Condition	Operating Quantity	Spares
1	Demineralized Water Storage Tank	Vertical, cylindrical, outdoor	326,000 GAL	2	0
2	Condensate Pump / Motor Driven	Vertical canned	3,600 gpm @ 700 ft H_2O	1	1
3	Deaerator and Storage Tank	Horizontal spray type	4,517,000 lb/hr 5 min. tank	1	0
4	Main Boiler Feed Pump / Turbine Driven	Horizontal, barrel type, multistage, centrifugal	9,100 gpm @ 11,500 ft H_2O	1	1
5	Startup Boiler Feed Pump / Motor Driven	Horizontal, barrel type, multistage, centrifugal	2,700 gpm @ 11,500 ft H_2O	1	0
6	LP Heater 1A/1B	Horizontal U-Tube	348,000 lb/hr	2	0
7	LP Heater 2A/2B	Horizontal U-Tube	348,000 lb/hr	2	0
8	LP Heater 3A/3B	Horizontal U-Tube	1,736,000 lb/hr	2	0
9	LP Heater 4A/4B	Horizontal U-Tube	1,736,000 lb/hr	2	0
10	HP Heater 6	Horizontal U-Tube	4,520,000 lb/hr	1	0
11	HP Heater 7	Horizontal U-Tube	4,520,000 lb/hr	1	0
12	HP Heater 8	Horizontal U-Tube	4,520,000 lb/hr	1	0
13	Auxiliary Boiler	Shop fabricated, water tube	33,000 lb/hr, 400 psig, 650 °F	1	
14	Fuel Oil System	No. 2 fuel oil for light off	250,000 gal	1	0
15	Service Air Compressor	Flooded screw	1,000 scfm @ 100 psig	2	1
16	Instrument Air Drier	Duplex, regenerative	1,000 scfm	2	1
17	Close Cooling Water Heat Exchanger	Shell and Tube	50 mmbtu/hr each	2	0
18	Close Cooling Water Pump	Horizontal, centrifugal	5,500 gpm @ 100 ft H_2O	2	1

Equipment No.	Description	Type	Design Condition	Operating Quantity	Spares
19	Diesel Engine Driven Fire Water Pump	Vertical, turbine	1,000 gpm @ 290 ft H_2O	1	1
20	Fire Service Booster Pump	Two-stage horizontal, centrifugal	700 gpm @ 210 ft H_2O	1	1
21	Raw Water Supply Pump	Stainless steel, single suction	1,970 gpm @ 60 ft	2	1
22	Ground Water Pump	Stainless steel, single suction	790 gpm @ 880 ft	5	1
23	Filtered Water Pump	Stainless steel, single suction	490 gpm @ 160 ft	2	1
24	Filtered Water Tank	Vertical Cylindrical	467,000 gal	1	0
25	Makeup Water Demineralizer	Multi-media filter, cartridge filter, RO membrane assembly and electrodeionization	220 gpm	1	1
26	Waste Water Treatment System		10 years, 24-hour storm	1	0

Exhibit 4-9D. Account 4 - Boiler and Accessories Equipment List

Equipment No.	Description	Type	Design Condition	Operating Quantity	Spares
1	Boiler	Supercritical, drum, wall-fired, low NOx burners, over-fire air	3,700 psig / 1,115 F / 1,115 F 4,520,000 lb/hr	1	0
2	Primary Air Fan	Centrifugal	592,000 lb/hr, 129,000 acfm @ 48 in WG	2	0
3	Forced Draft Fan	Centrifugal	1,919,000 lb/hr, 421,000 acfm @ 19 in WG	2	0
4	Induced Draft Fan	Axial	2,783,000 lb/hr, 944,000 acfm @ 41 in WG	2	0
5	SCR Reactor Vessel	Space for spar layer	5,588,000 lb/hr	2	0
6	SCR Catalyst			3	0
7	Dilution Air Blower	Centrifugal	5,400 acfm @ 42 in WG	2	1
8	Ammonia Storgae	Horizontal Tank	44,000 gal	5	0
9	Aqueous Ammonia Feed Pump	Centrifugal	9 gpm @ 300 ft H_2O	2	1

Exhibit 4-9E. Account 5 - Flue Gas Cleanup Equipment List

Equipment No.	Description	Type	Design Condition	Operating Quantity	Spares
1	Fabric Filter	Single stage, high ratio with pulse-jet online cleaning system	2,774,000 lb/hr 99.8% efficiency	2	0
2	Absorber Module	Counter-current open spray	1,777,000 acfm	1	0
3	Recirculation Pumps	Horizontal, Centrifugal	47,000 gpm @ 210 ft H_2O	5	1
4	Bleed Pumps	Horizontal, Centrifugal	1,210 gpm @ 20% weight solids	2	1
5	Oxidation Air Blowers	Centrifugal	3,140 acfm @ 37 psia	2	1
6	Agitators	Side entering	40 hp	5	1
7	Dewatering cyclones	Radial assembly, 5 units each	310 gpm per cyclone	2	0
8	Vacuum Filter Belt	Horizontal belt	41 tph of 50% slurry	2	1
9	Filtrate Water Return Pump	Horizontal, Centrifugal	180 gpm @ 40 ft H_2O	1	1
10	Filtrate Water Return Storage Tank	Vertical, lined	130,000 gal	1	0
11	Process Makeup Water Pump	Horizontal, Centrifugal	970 gpm @ 70 ft H_2O	1	1

Exhibit 4-9F. Account 5B - Flue Gas Pretreatment, CO_2 Capture, and Dry Ice Melting Equipment List

Equipment No.	Description	Type	Design Condition	Operating Quantity	Spares
1	Direct Contact Cooler	Vertical, CS/SS	Flow: 5,351,000 lb/hr 15 psia / 136 F	1	0
2	Flue Gas Cooler 1 (Dry Ice Cooler 1)	Shell and tube, 304SS	Gas Side (Shell): Flow: 5,351,000 lb/hr 15 psia/85F Cold Side (Tube): 100 psia/70 F Duty: 141 mmbtu/hr	1	0
3	Flue Gas Compressor / Turbine	By vendor, complete with driving turbine and required ancillaries	Inlet: 1,624,000 lb/hr (each) 14.5 psia/46F Outlet: 37 psia	3	0
4	Flue Gas Cooler 2 (Condensate Heater 1)	Tube and shell, 304SS	86 mmbtu/hr Shell side: 37psia/223 F Tube side: 245 psia/168 F	1	0

Equipment No.	Description	Type	Design Condition	Operating Quantity	Spares
5	Flue Gas Cooler 3 (Dry Ice Cooler 3)	Shell and tube, 304SS	Flow: 4,870,000 lb/hr Hot Side: 37 psia/150F Cold Side: 100 psia/150F Duty: 7 mmbtu/hr	1	0
6	Air Cooler	Fin fan cooler	39 mmbtu/hr Hot in (gas): 150F/37psia	1	0
7	Flue Gas Cooler 4 (Dry Ice Cooler 2)	Shell and tube, 304SS	Flow: 4,870,000 lb/hr Hot Side: 37 psia/110F Cold Side: 100 psia/110F Duty: 42 mmbtu/hr	1	0
8	ICES System	Complete system	Inlet Flow: 4,870,000 lb/hr, 37 psia/74F 90% CO_2 capture eff.	1	0
9	Screw Feeder	By vendor	170,000 lb/hr (each) 150 psia/-150F	6	0
10	Dry Ice Melting Vessel	Complete with internal heat exchanger, water ice filter and other required ancillaries Stainless Steel, ID/L: 8 FT/14 FT (or by vendor)	Inlet: 255,000 lb/hr (each) 150 psia/-150F Outlet: 150 psia/-50F Internal HX duty: 48 mmbtu/hr (each)	4	0
11	ICES Exhaust Cooler (Condensate Heater 2)	Shell and tube, 304SS	Gas Side (Shell): Flow: 3,441,000 lb/hr 17 psia/296F Cold Side (Tube): 245 psia/206F Duty: 125 mmbtu/hr	1	0
12	CO_2 Pump	By vendor	245,000 lb/hr Inlet 145 psia/-50F Outlet: 2,215 psia/-39 F	4	0
13	CO2 Product Heater	Shell and tube, 304SS	67 mmbtu/hr Shell side: 100 psia/150 F Tube side: 2215 psia/-39 F	1	0
14	Glycol Pump	Centrifugal	Flow: 5,880,000 lb/hr (each) Inlet: 15 psia/70F Outlet: 100 psia	2	0

Exhibit 4-9G. Account 7 - HRSG, Ducting, and Stack Equipment List

Equipment No.	Description	Type	Design Condition	Operating Quantity	Spares
1	Stack	Reinforced concrete chimney equipped with a FRP flue and Continuous Emissions Monitoring System (CEMS)	500' height, 18 ft diameter	1	0

Exhibit 4-9H. Account 8 - Steam Turbine Generator and Auxiliaries Equipment List

Equipment No.	Description	Type	Design Condition	Operating Quantity	Spares
1	Steam Turbine	Commercially available advanced turbine	620 MWe 3,500 psig / 1,100°F / 1,100°F	1	0
2	Steam Turbine Generator	Hydrogen cooled, static excitation	690 MVA @0.9 p.f. 24 Kv, 60Hz, 3 phase	1	0
3	Surface Condenser	single pass, divided waterbox including vacuum pumps	2,720 MMBtu/hr 20 °F temp. rise Hotwell storage – 5 min	1	0

Exhibit 4-9I. Account 9 - Cooling Water System Equipment List

Equipment No.	Description	Type	Design Condition	Operating Quantity	Spares
1	Circulating Water Pumps	Vertical wet pit, electric motor driven	181,000 gpm @ 100 ft	2	1
2	Cooling Tower	Evaporative, mechanical draft, multi-cell	51.5 °F WB/ 60 °F CWT/ 80 °F HWT 3,610 MMBtu/hr	1	0

Exhibit 4-9J. Account 10 - Ash/Spent Sorbent Recovery and Handling Equipment List

Equipment No.	Description	Type	Design Condition	Operating Quantity	Spares
1	Economizer Hopper	Boiler vendor supply scope		4	0
2	Bottom Ash Hopper	Boiler vendor supply scope		2	0
3	Clinker Grinder		5 tph	1	1
4	Pyrites Hopper	Boiler vendor supply scope		6	0
5	Hydro-ejectors			12	0

Equipment No.	Description	Type	Design Condition	Operating Quantity	Spares
6	Economizer/Pyrites Transfer Tank			1	0
7	Ash Sluice Pumps	Vertical wet pit, electric motor driven	50 gpm @ 56 ft	1	1
8	Ash Seal Water Pumps	Vertical wet pit, electric motor driven	1,700 gpm @ 28 ft	1	1
9	Hydro-bins		50 gpm	1	1
10	Baghouse Hopper	Baghouse vendor supply scope		24	0
11	Air Heater Hopper	Boiler vendor supply scope		10	0
12	Air Blower	Centrifugal	590 scfm @ 24 psia	1	1
13	Fly Ash Silo	Reinforced concrete	1,200 ton	2	0
14	Slide Gate Valves			2	0
15	Unloader			1	0
16	Telescoping Unloading Chute		120 tph	1	0

Exhibit 4-9K. Account 11 - Accessory Electric Plant Equipment List

Equipment No.	Description	Type	Design Condition	Operating Quantity	Spares
1	STG Step-up Transformer	Oil-filled	24 kV / 345 kV, 650 MVA 3-ph, 60 Hz	1	0
2	Auxiliary Transformer	Oil-filled	24 kV/ 4.16 kV, 42 MVA, 3-ph, 60 Hz	1	1
3	Low Voltage Transformer	Dry Ventilated	4.16 kV/ 480 V, 16 MVA, 3-ph, 60 Hz	1	1
4	STG Isolated Phase Bus Duct and Tap Bus	Aluminum, Self-cooled	24 kV, 3-ph, 60 Hz	1	0
5	Medium Voltage Switchgear	Metal clad	4.16 kV, 3-ph, 60 Hz	1	1
6	Low Voltage Switchgear	Metal enclosed	480 V, 3-ph, 60 Hz	1	0
7	Emergency Diesel Engine Generator Set	Sized for emergency shutdown	750 kW 480V, 3-ph, 60 Hz	1	0

Exhibit 4-9L. Account 12 - Instrumentation and Control Equipment List

Equipment No.	Description	Type	Design Condition	Operating Quantity	Spares
1	DCS - Main Control	Monitor/keyboard; Operator printer; Eng. Printer	Operator stations/printers and engineering station/printers	1	0
2	DCS - Processor	Microprocessor with Redundant Input/Output	N/A	1	0
3	DCS - Data Highway	Fiber optic	Fully redundant, 25% spare	1	0

4.3   Cost Estimate

The cost estimating methodology used to determine the capital costs and operating costs were previously described in Section 3.4. Exhibit 4-10 provides the total plant capital cost summary organized by cost account and Exhibit 4-11 provides a more detailed breakdown. The development of the Bare Erected Costs for the ATK ICES CO_2 capture system including the flue gas pretreatment equipment, the ICES CO_2 capture equipment and the dry ice melting system is provided in Exhibit 4-12. The equipment costs for the expansion duct were developed based on weights and instrumentation details (sensors and controls) as provided by ATK. Exhibit 4-13 provides the operating and maintenance costs for the supercritical facility with the ATK ICES CO_2 capture system.

WorleyParsons
resources & energy

Exhibit 4-10 ATK ICES Case Total Plant Cost Summary

Client:	ATK						Report Date:	2012-Dec-19	
Project:	ATK Post Combustion CO2 Capture								

TOTAL PLANT COST SUMMARY

Case:	ATK Case - 1x550 Mwnet SCPC w/ CO2 capture								
Plant Size:	550.0 MW,net		Estimate Type: Conceptual				Cost Base (Jan) 2012	($x1000)	

Acct No.	Item/Description	Equipment Cost	Material Cost	Labor Direct	Labor Indirect	Sales Tax	Bare Erected Cost $	Eng'g CM H.O.& Fee	Contingencies Process	Contingencies Project	TOTAL PLANT COST $	TOTAL PLANT COST $/kW
1	COAL & SORBENT HANDLING	$21,916	$5,568	$13,040	$0	$0	$40,524	$3,556	$0	$6,612	$50,691	$92
2	COAL & SORBENT PREP & FEED	$14,818	$825	$3,743	$0	$0	$19,386	$1,650	$0	$3,155	$24,192	$44
3	FEEDWATER & MISC. BOP SYSTEMS	$58,179	$0	$26,854	$0	$0	$85,033	$7,476	$0	$15,077	$107,587	$196
4	PC BOILER											
4.1	PC Boiler & Accessories	$208,167	$0	$116,889	$0	$0	$325,056	$30,821	$0	$35,588	$391,465	$712
4.2	SCR (w/4.1)	$0	$0	$0	$0	$0	$0	$0	$0	$0	$0	$0
4.3	Open	$0	$0	$0	$0	$0	$0	$0	$0	$0	$0	$0
4.4-4.9	Boiler BoP (w/ ID Fans)	$0	$0	$0	$0	$0	$0	$0	$0	$0	$0	$0
	SUBTOTAL 4	$208,167	$0	$116,889	$0	$0	$325,056	$30,821	$0	$35,588	$391,465	$712
5	FLUE GAS CLEANUP	$108,400	$0	$36,301	$0	$0	$144,701	$13,322	$0	$15,802	$173,826	$316
5B	CO2 REMOVAL	$161,338	$0	$90,965	$0	$0	$252,303	$23,402	$47,864	$64,714	$388,282	$706
6	COMBUSTION TURBINE/ACCESSORIES											
6.1	Combustion Turbine Generator	N/A	$0	N/A	$0	$0	$0	$0	$0	$0	$0	$0
6.2-6.9	Combustion Turbine Other	$0	$0	$0	$0	$0	$0	$0	$0	$0	$0	$0
	SUBTOTAL 6	$0	$0	$0	$0	$0	$0	$0	$0	$0	$0	$0
7	HRSG, DUCTING & STACK											
7.1	Heat Recovery Steam Generator	N/A	$0	N/A	$0	$0	$0	$0	$0	$0	$0	$0
7.2-7.9	HRSG Accessories, Ductwork and Stack	$18,458	$950	$12,409	$0	$0	$31,816	$2,830	$0	$4,546	$39,193	$71
	SUBTOTAL 7	$18,458	$950	$12,409	$0	$0	$31,816	$2,830	$0	$4,546	$39,193	$71
8	STEAM TURBINE GENERATOR											
8.1	Steam TG & Accessories	$69,548	$0	$8,496	$0	$0	$78,044	$6,805	$0	$8,485	$93,334	$170
8.2-8.9	Turbine Plant Auxiliaries and Steam Piping	$35,433	$1,276	$16,587	$0	$0	$53,297	$4,284	$0	$8,127	$65,708	$119
	SUBTOTAL 8	$104,981	$1,276	$25,084	$0	$0	$131,341	$11,089	$0	$16,612	$159,041	$289
9	COOLING WATER SYSTEM	$19,510	$9,872	$17,605	$0	$0	$46,987	$4,265	$0	$6,928	$58,181	$106
10	ASH/SPENT SORBENT HANDLING SYS	$6,019	$175	$7,753	$0	$0	$13,947	$1,286	$0	$1,566	$16,799	$31
11	ACCESSORY ELECTRIC PLANT	$22,032	$8,921	$23,809	$0	$0	$54,762	$4,709	$0	$7,418	$66,889	$122
12	INSTRUMENTATION & CONTROL	$12,165	$0	$12,303	$0	$0	$24,469	$2,158	$1,223	$3,436	$31,285	$57
13	IMPROVEMENTS TO SITE	$3,601	$2,070	$7,748	$0	$0	$13,419	$1,326	$0	$2,949	$17,694	$32
14	BUILDINGS & STRUCTURES	$0	$27,843	$26,869	$0	$0	$54,711	$4,845	$0	$8,933	$68,490	$125
	TOTAL COST	$759,583	$57,500	$421,372	$0	$0	$1,238,455	$112,735	$49,087	$193,337	$1,593,614	$2,898

WorleyParsons
resources & energy

Exhibit 4-11 ATK ICES Case Total Plant Cost Details

Client:	ATK						Report Date:	2012-Dec-19	
Project:	ATK Post Combustion CO2 Capture								

TOTAL PLANT COST SUMMARY

Case:	ATK Case - 1x550 Mwnet SCPC w/ CO2 capture								
Plant Size:	550.0 MW,net		Estimate Type: Conceptual				Cost Base (Jan) 2012	($x1000)	

Acct No.	Item/Description	Equipment Cost	Material Cost	Labor Direct	Labor Indirect	Sales Tax	Bare Erected Cost $	Eng'g CM H.O.& Fee	Contingencies Process	Contingencies Project	TOTAL PLANT COST $	TOTAL PLANT COST $/kW
1	COAL & SORBENT HANDLING											
1.1	Coal Receive & Unload	$4,491	$0	$2,040	$0	$0	$6,531	$566	$0	$1,065	$8,162	$15
1.2	Coal Stackout & Reclaim	$5,804	$0	$1,308	$0	$0	$7,112	$603	$0	$1,157	$8,872	$16
1.3	Coal Conveyors	$5,396	$0	$1,294	$0	$0	$6,690	$568	$0	$1,089	$8,347	$15
1.4	Other Coal Handling	$1,412	$0	$299	$0	$0	$1,711	$145	$0	$278	$2,135	$4
1.5	Sorbent Receive & Unload	$182	$0	$55	$0	$0	$237	$20	$0	$39	$296	$1
1.6	Sorbent Stackout & Reclaim	$2,945	$0	$537	$0	$0	$3,482	$294	$0	$566	$4,342	$8
1.7	Sorbent Conveyors	$1,051	$226	$256	$0	$0	$1,533	$129	$0	$249	$1,911	$3
1.8	Other Sorbent Handling	$635	$148	$331	$0	$0	$1,114	$96	$0	$181	$1,391	$3
1.9	Coal & Sorbent Hnd.Foundations	$0	$5,194	$6,920	$0	$0	$12,114	$1,135	$0	$1,987	$15,236	$28
	SUBTOTAL 1.	$21,916	$5,568	$13,040	$0	$0	$40,524	$3,556	$0	$6,612	$50,691	$92
2	COAL & SORBENT PREP & FEED											
2.1	Coal Crushing & Drying	$2,585	$0	$501	$0	$0	$3,087	$261	$0	$502	$3,849	$7
2.2	Coal Conveyor to Storage	$6,620	$0	$1,437	$0	$0	$8,057	$683	$0	$1,311	$10,050	$18
2.3	Coal Injection System	$0	$0	$0	$0	$0	$0	$0	$0	$0	$0	$0
2.4	Misc.Coal Prep & Feed	$0	$0	$0	$0	$0	$0	$0	$0	$0	$0	$0
2.5	Sorbent Prep Equipment	$5,009	$215	$1,035	$0	$0	$6,258	$528	$0	$1,018	$7,804	$14
2.6	Sorbent Storage & Feed	$603	$0	$230	$0	$0	$833	$72	$0	$136	$1,041	$2
2.7	Sorbent Injection System	$0	$0	$0	$0	$0	$0	$0	$0	$0	$0	$0
2.8	Booster Air Supply System	$0	$0	$0	$0	$0	$0	$0	$0	$0	$0	$0
2.9	Coal & Sorbent Feed Foundation	$0	$610	$541	$0	$0	$1,151	$107	$0	$189	$1,446	$3
	SUBTOTAL 2.	$14,818	$825	$3,743	$0	$0	$19,386	$1,650	$0	$3,155	$24,192	$44
3	FEEDWATER & MISC. BOP SYSTEMS											
3.1	Feedwater System	$24,664	$0	$7,925	$0	$0	$32,589	$2,762	$0	$5,303	$40,654	$74
3.2	Water Makeup & Pretreating	$6,654	$0	$2,083	$0	$0	$8,737	$788	$0	$1,905	$11,430	$21
3.3	Other Feedwater Subsystems	$7,830	$0	$3,174	$0	$0	$11,004	$932	$0	$1,790	$13,727	$25
3.4	Service Water Systems	$1,329	$0	$690	$0	$0	$2,019	$179	$0	$440	$2,638	$5
3.5	Other Boiler Plant Systems	$9,653	$0	$9,063	$0	$0	$18,716	$1,688	$0	$3,061	$23,464	$43
3.6	FO Supply Sys & Nat Gas	$339	$0	$394	$0	$0	$733	$65	$0	$120	$918	$2
3.7	Waste Treatment Equipment	$4,385	$0	$2,501	$0	$0	$6,886	$653	$0	$1,508	$9,047	$16
3.8	Misc. Equip.(cranes,AirComp.,Comm.)	$3,326	$0	$1,022	$0	$0	$4,349	$409	$0	$952	$5,709	$10
	SUBTOTAL 3.	$58,179	$0	$26,854	$0	$0	$85,033	$7,476	$0	$15,077	$107,587	$196
4	PC BOILER											
4.1	PC Boiler & Accessories	$208,167	$0	$116,889	$0	$0	$325,056	$30,821	$0	$35,588	$391,465	$712
4.2	SCR (w/4.1)	$0	$0	$0	$0	$0	$0	$0	$0	$0	$0	$0
4.3	Open	$0	$0	$0	$0	$0	$0	$0	$0	$0	$0	$0
4.4	Boiler BoP (w/ ID Fans)	$0	$0	$0	$0	$0	$0	$0	$0	$0	$0	$0
4.5	Primary Air System	w/4.1	$0	w/4.1	$0	$0	$0	$0	$0	$0	$0	$0
4.6	Secondary Air System	w/4.1	$0	w/4.1	$0	$0	$0	$0	$0	$0	$0	$0
4.8	Major Component Rigging	$0	w/4.1	w/4.1	$0	$0	$0	$0	$0	$0	$0	$0
4.9	Boiler Foundations	$0	w/14.1	w/14.1	$0	$0	$0	$0	$0	$0	$0	$0
	SUBTOTAL 4.	$208,167	$0	$116,889	$0	$0	$325,056	$30,821	$0	$35,588	$391,465	$712

| Client: | ATK | | | | | | Report Date: | 2012-Dec-19 | | |
| Project: | ATK Post Combustion CO2 Capture | | | | | | | | | |

TOTAL PLANT COST SUMMARY

| Case: | ATK Case - 1x550 Mwnet SCPC w/ CO2 capture | | | | | | | | | |
| Plant Size: | 550.0 MW,net | | | Estimate Type: Conceptual | | | Cost Base (Jan) | 2012 | ($x1000) | |

Acct No.	Item/Description	Equipment Cost	Material Cost	Labor Direct	Labor Indirect	Sales Tax	Bare Erected Cost $	Eng'g CM H.O.& Fee	Contingencies Process	Contingencies Project	TOTAL PLANT COST $	TOTAL PLANT COST $/kW
	5 FLUE GAS CLEANUP											
5.1	Absorber Vessels & Accessories	$75,330	$0	$15,952	$0	$0	$91,282	$8,361	$0	$9,964	$109,607	$199
5.2	Other FGD	$3,931	$0	$4,382	$0	$0	$8,313	$780	$0	$909	$10,002	$18
5.3	Bag House & Accessories	$21,462	$0	$13,398	$0	$0	$34,861	$3,239	$0	$3,810	$41,909	$76
5.4	Other Particulate Removal Materials	$1,452	$0	$1,529	$0	$0	$2,981	$279	$0	$326	$3,587	$7
5.5	Gypsum Dewatering System	$6,224	$0	$1,040	$0	$0	$7,264	$664	$0	$793	$8,721	$16
5.6	Mercury Removal System	$0	$0	$0	$0	$0	$0	$0	$0	$0	$0	$0
5.9	Open	$0	$0	$0	$0	$0	$0	$0	$0	$0	$0	$0
	SUBTOTAL 5.	$108,400	$0	$36,301	$0	$0	$144,701	$13,322	$0	$15,802	$173,826	$316
	5B CO2 REMOVAL											
5B.1	CO2 Removal System	$154,477	$0	$84,842	$0	$0	$239,319	$22,188	$47,864	$61,874	$371,246	$675
5B.2	CO2 Product Pumping	$6,861	$0	$6,123	$0	$0	$12,984	$1,213	$0	$2,839	$17,036	$31
	SUBTOTAL 5.	$161,338	$0	$90,965	$0	$0	$252,303	$23,402	$47,864	$64,714	$388,282	$706
	6 COMBUSTION TURBINE/ACCESSORIES											
6.1	Combustion Turbine Generator	N/A	$0	N/A	$0	$0	$0	$0	$0	$0	$0	$0
6.2	Open	$0	$0	$0	$0	$0	$0	$0	$0	$0	$0	$0
6.3	Compressed Air Piping	$0	$0	$0	$0	$0	$0	$0	$0	$0	$0	$0
6.9	Combustion Turbine Foundations	$0	$0	$0	$0	$0	$0	$0	$0	$0	$0	$0
	SUBTOTAL 6.	$0	$0	$0	$0	$0	$0	$0	$0	$0	$0	$0
	7 HRSG, DUCTING & STACK											
7.1	Heat Recovery Steam Generator	N/A	$0	N/A	$0	$0	$0	$0	$0	$0	$0	$0
7.2	HRSG Accessories	$0	$0	$0	$0	$0	$0	$0	$0	$0	$0	$0
7.3	Ductwork	$9,565	$0	$6,150	$0	$0	$15,715	$1,335	$0	$2,558	$19,608	$36
7.4	Stack	$8,893	$0	$5,119	$0	$0	$14,011	$1,300	$0	$1,531	$16,842	$31
7.9	Duct & Stack Foundations	$0	$950	$1,140	$0	$0	$2,090	$195	$0	$457	$2,743	$5
	SUBTOTAL 7.	$18,458	$950	$12,409	$0	$0	$31,816	$2,830	$0	$4,546	$39,193	$71
	8 STEAM TURBINE GENERATOR											
8.1	Steam TG & Accessories	$69,548	$0	$8,496	$0	$0	$78,044	$6,805	$0	$8,485	$93,334	$170
8.2	Turbine Plant Auxiliaries	$437	$0	$920	$0	$0	$1,357	$129	$0	$149	$1,634	$3
8.3	Condenser & Auxiliaries	$9,122	$0	$2,281	$0	$0	$11,403	$1,046	$0	$1,245	$13,694	$25
8.4	Steam Piping	$25,874	$0	$11,257	$0	$0	$37,131	$2,789	$0	$5,988	$45,907	$83
8.9	TG Foundations	$0	$1,276	$2,130	$0	$0	$3,406	$320	$0	$745	$4,472	$8
	SUBTOTAL 8.	$104,981	$1,276	$25,084	$0	$0	$131,341	$11,089	$0	$16,612	$159,041	$289
	9 COOLING WATER SYSTEM											
9.1	Cooling Towers	$14,588	$0	$4,469	$0	$0	$19,057	$1,753	$0	$2,081	$22,890	$42
9.2	Circulating Water Pumps	$2,871	$0	$204	$0	$0	$3,075	$262	$0	$334	$3,671	$7
9.3	Circ.Water System Auxiliaries	$773	$0	$101	$0	$0	$875	$80	$0	$95	$1,050	$2
9.4	Circ.Water Piping	$0	$6,489	$5,846	$0	$0	$12,334	$1,083	$0	$2,013	$15,430	$28
9.5	Make-up Water System	$649	$0	$828	$0	$0	$1,476	$135	$0	$242	$1,853	$3
9.6	Component Cooling Water Sys	$629	$0	$479	$0	$0	$1,109	$100	$0	$181	$1,390	$3
9.9	Circ.Water System Foundations & Structures	$0	$3,384	$5,678	$0	$0	$9,061	$852	$0	$1,983	$11,896	$22
	SUBTOTAL 9.	$19,510	$9,872	$17,605	$0	$0	$46,987	$4,265	$0	$6,928	$58,181	$106

Client:	ATK						Report Date:	2012-Dec-19		
Project:	ATK Post Combustion CO2 Capture									

TOTAL PLANT COST SUMMARY

Case:	ATK Case - 1x550 Mwnet SCPC w/ CO2 capture									
Plant Size:	550.0 MW,net			Estimate Type: Conceptual			Cost Base (Jan)	2012	($x1000)	

Acct No.	Item/Description	Equipment Cost	Material Cost	Labor Direct	Labor Indirect	Sales Tax	Bare Erected Cost $	Eng'g CM H.O.& Fee	Contingencies Process	Contingencies Project	TOTAL PLANT COST $	TOTAL PLANT COST $/kW
10	ASH/SPENT SORBENT HANDLING SYS											
10.1	Ash Coolers	N/A	$0	N/A	$0	$0	$0	$0	$0	$0	$0	$0
10.2	Cyclone Ash Letdown	N/A	$0	N/A	$0	$0	$0	$0	$0	$0	$0	$0
10.3	HGCU Ash Letdown	N/A	$0	N/A	$0	$0	$0	$0	$0	$0	$0	$0
10.4	High Temperature Ash Piping	N/A	$0	N/A	$0	$0	$0	$0	$0	$0	$0	$0
10.5	Other Ash Recovery Equipment	N/A	$0	N/A	$0	$0	$0	$0	$0	$0	$0	$0
10.6	Ash Storage Silos	$789	$0	$2,391	$0	$0	$3,180	$303	$0	$348	$3,831	$7
10.7	Ash Transport & Feed Equipment	$5,230	$0	$5,145	$0	$0	$10,376	$947	$0	$1,132	$12,455	$23
10.8	Misc. Ash Handling Equipment	$0	$0	$0	$0	$0	$0	$0	$0	$0	$0	$0
10.9	Ash/Spent Sorbent Foundation	$0	$175	$217	$0	$0	$392	$37	$0	$86	$514	$1
	SUBTOTAL 10.	**$6,019**	**$175**	**$7,753**	**$0**	**$0**	**$13,947**	**$1,286**	**$0**	**$1,566**	**$16,799**	**$31**
11	ACCESSORY ELECTRIC PLANT											
11.1	Generator Equipment	$1,978	$0	$320	$0	$0	$2,299	$207	$0	$188	$2,694	$5
11.2	Station Service Equipment	$3,695	$0	$1,255	$0	$0	$4,951	$462	$0	$406	$5,819	$11
11.3	Switchgear & Motor Control	$4,241	$0	$747	$0	$0	$4,988	$464	$0	$545	$5,997	$11
11.4	Conduit & Cable Tray	$0	$2,963	$9,523	$0	$0	$12,485	$1,157	$0	$2,046	$15,689	$29
11.5	Wire & Cable	$0	$5,591	$10,032	$0	$0	$15,623	$1,249	$0	$2,531	$19,404	$35
11.6	Protective Equipment	$210	$0	$739	$0	$0	$949	$91	$0	$104	$1,144	$2
11.7	Standby Equipment	$1,523	$0	$36	$0	$0	$1,559	$144	$0	$170	$1,873	$3
11.8	Main Power Transformers	$10,384	$0	$213	$0	$0	$10,597	$811	$0	$1,141	$12,548	$23
11.9	Electrical Foundations	$0	$367	$944	$0	$0	$1,311	$124	$0	$287	$1,721	$3
	SUBTOTAL 11.	**$22,032**	**$8,921**	**$23,809**	**$0**	**$0**	**$54,762**	**$4,709**	**$0**	**$7,418**	**$66,889**	**$122**
12	INSTRUMENTATION & CONTROL											
12.1	PC Control Equipment	w/12.7	$0	w/12.7	$0	$0	$0	$0	$0	$0	$0	$0
12.2	Combustion Turbine Control	N/A	$0	N/A	$0	$0	$0	$0	$0	$0	$0	$0
12.3	Steam Turbine Control	w/8.1	$0	w/8.1	$0	$0	$0	$0	$0	$0	$0	$0
12.4	Other Major Component Control	$0	$0	$0	$0	$0	$0	$0	$0	$0	$0	$0
12.5	Signal Processing Equipment	w/12.7	$0	w/12.7	$0	$0	$0	$0	$0	$0	$0	$0
12.6	Control Boards,Panels & Racks	$604	$0	$374	$0	$0	$978	$92	$49	$168	$1,287	$2
12.7	Distributed Control System Equipment	$6,100	$0	$1,102	$0	$0	$7,202	$669	$360	$823	$9,054	$16
12.8	Instrument Wiring & Tubing	$3,738	$0	$6,782	$0	$0	$10,520	$847	$526	$1,784	$13,677	$25
12.9	Other I & C Equipment	$1,724	$0	$4,044	$0	$0	$5,768	$550	$288	$661	$7,267	$13
	SUBTOTAL 12.	**$12,165**	**$0**	**$12,303**	**$0**	**$0**	**$24,469**	**$2,158**	**$1,223**	**$3,436**	**$31,285**	**$57**
13	IMPROVEMENTS TO SITE											
13.1	Site Preparation	$0	$61	$1,292	$0	$0	$1,353	$131	$0	$297	$1,781	$3
13.2	Site Improvements	$0	$2,010	$2,664	$0	$0	$4,674	$462	$0	$1,027	$6,163	$11
13.3	Site Facilities	$3,601	$0	$3,791	$0	$0	$7,392	$733	$0	$1,625	$9,750	$18
	SUBTOTAL 13.	**$3,601**	**$2,070**	**$7,748**	**$0**	**$0**	**$13,419**	**$1,326**	**$0**	**$2,949**	**$17,694**	**$32**
14	BUILDINGS & STRUCTURES											
14.1	Boiler Building	$0	$10,057	$8,983	$0	$0	$19,041	$1,680	$0	$3,108	$23,829	$43
14.2	Turbine Building	$0	$14,385	$13,617	$0	$0	$28,002	$2,478	$0	$4,572	$35,052	$64
14.3	Administration Building	$0	$746	$801	$0	$0	$1,547	$138	$0	$253	$1,938	$4
14.4	Circulation Water Pumphouse	$0	$204	$164	$0	$0	$368	$32	$0	$60	$460	$1
14.5	Water Treatment Buildings	$0	$808	$749	$0	$0	$1,557	$138	$0	$254	$1,949	$4
14.6	Machine Shop	$0	$499	$340	$0	$0	$839	$73	$0	$137	$1,049	$2
14.7	Warehouse	$0	$338	$344	$0	$0	$683	$61	$0	$111	$855	$2
14.8	Other Buildings & Structures	$0	$276	$239	$0	$0	$515	$45	$0	$84	$645	$1
14.9	Waste Treating Building & Str.	$0	$529	$1,630	$0	$0	$2,159	$200	$0	$354	$2,714	$5
	SUBTOTAL 14.	**$0**	**$27,843**	**$26,869**	**$0**	**$0**	**$54,711**	**$4,845**	**$0**	**$8,933**	**$68,490**	**$125**
	TOTAL COST	**$759,583**	**$57,500**	**$421,372**	**$0**	**$0**	**$1,238,455**	**$112,735**	**$49,087**	**$193,337**	**$1,593,614**	**$2,898**

when experience counts

Exhibit 4-12 Buildup of ATK ICES CO$_2$ Capture System and Supporting Systems Bare Erected Cost

Item No.	Item Description	Equipment Cost (Total)	Material Cost	Labor Cost	Bare Erected Cost $
1	Direct Contact Cooler	$6,490,260	$2,379,762	$4,997,500	$13,867,522
2	Flue Gas Cooler 1	$22,705,800	$9,839,180	$20,662,278	$53,207,258
3	Flue Gas Compressor /	$32,118,564	$6,423,713	$13,489,797	$52,032,074
4	Flue Gas Cooler 2	$1,469,250	$636,675	$1,337,018	$3,442,943
5	Flue Gas Cooler 3	$129,000	$55,900	$117,390	$302,290
6	Air Cooler	$1,270,000	$508,000	$1,066,800	$2,844,800
7	Flue Gas Cooler 4	$1,989,450	$862,095	$1,810,400	$4,661,945
8	ICES System				
	Distribution Duct	$960,000	$320,000	$672,000	$1,952,000
	Expansion Duct	$7,200,000	$2,400,000	$5,040,000	$14,640,000
	Dry Ice Cyclone	$6,646,596	$4,431,064	$9,305,234	$20,382,894
	Collection Duct	$960,000	$320,000	$672,000	$1,952,000
9	Screw Feeder	$18,000,000	$6,000,000	$12,600,000	$36,600,000
10	Dry Ice Melting Vessel	$1,983,720	$1,267,180	$2,661,078	$5,911,978
10.1	Separation Equipment	$128,000	$42,667	$89,600	$260,267
10.2	Filtration Equipment	$144,000	$48,000	$100,800	$292,800
11	ICES Exhaust Cooler	$4,858,350	$2,105,285	$4,421,099	$11,384,734
12	CO2 Pump	$2,128,800	$2,128,800	$4,470,480	$8,728,080
13	CO2 Product Heater	$1,816,050	$786,955	$1,652,606	$4,255,611
14	Glycol pump	$1,142,400	$1,142,400	$2,399,040	$4,683,840
	Ductwork, incl. foundations and supports		$7,500,000	$3,400,000	$10,900,000
	Total	**$112,140,240**	**$49,197,676**	**$90,965,119**	**$252,303,034**

Exhibit 4-13 ATK ICES Case Initial and Annual Operating and Maintenance Costs

INITIAL & ANNUAL O&M EXPENSES					Cost Base (Jan):	2012
ATK Case - 1x550 Mwnet SCPC w/ CO2 capture					Heat Rate-net (Btu/kWh):	9,877
					MWe-net:	550
					Capacity Factor (%):	85

OPERATING & MAINTENANCE LABOR

Operating Labor				
Operating Labor Rate (base):	40.50	$/hour		
Operating Labor Burden:	30.00	% of base		
Labor O-H Charge Rate:	25.00	% of labor		

		Total		
Skilled Operator	2.0	2.0		
Operator	11.3	11.3		
Foreman	1.0	1.0		
Lab Tech's, etc.	2.0	2.0		
TOTAL-O.J.'s	16.3	16.3		

		Annual Cost $	Annual Unit Cost $/kW-net
Annual Operating Labor Cost		$7,533,008	$13.698
Maintenance Labor Cost		$10,519,185	$19.128
Administrative & Support Labor		$4,513,048	$8.206
Property Taxes and Insurance		$31,872,282	$57.955
TOTAL FIXED OPERATING COSTS		**$54,437,524**	**$98.986**

VARIABLE OPERATING COSTS						$/kWh-net
Maintenance Material Cost					**$15,778,778**	**$0.00385**

Consumables	Consumption Initial Fill	/Day	Unit Cost	Initial Fill Cost		
Water(/1000 gallons)	0	4,932	1.48	$0	$2,272,125	$0.00055
Chemicals						
MU & WT Chem.(lbs)	0	23,874	0.24	$0	$1,759,766	$0.00043
Limestone (ton)	0	565	29.70	$0	$5,205,801	$0.00127
Carbon (Mercury Removal) lb	0	0	1.44	$0	$0	$0.00000
MEA Solvent (ton)	0	0.00	3,088.59	$0	$0	$0.00000
NaOH (tons)	0	0.00	595.34	$0	$0	$0.00000
H2SO4 (tons)	0	0.00	190.51	$0	$0	$0.00000
Corrosion Inhibitor	0	0	0.00	$0	$0	$0.00000
Activated Carbon (lb)	0	0	1.44	$0	$0	$0.00000
Ammonia (19% NH3) ton	0	84	292.72	$0	$7,628,662	$0.00186
Subtotal Chemicals				$0	**$14,594,229**	**$0.00356**
Other						
Supplemental Fuel (MBtu)	0	0	0.00	$0	$0	$0.00000
SCR Catalyst (m3)	w/equip.	0.35	7,929.08	$0	$860,999	$0.00021
Emission Penalties	0	0	0.00	$0	$0	$0.00000
Subtotal Other				$0	**$860,999**	**$0.00021**
Waste Disposal						
Fly Ash (ton)	0	433	22.27	$0	$2,995,141	$0.00073
Bottom Ash (ton)	0	108	22.27	$0	$748,806	$0.00018
Subtotal-Waste Disposal				$0	**$3,743,947**	**$0.00091**
By-products & Emissions						
Gypsum (tons)	0	873	0.00	$0	$0	$0.00000
Subtotal By-Products				$0	**$0**	**$0.00000**
TOTAL VARIABLE OPERATING COSTS				$0	**$37,250,078**	**$0.00910**
Fuel (ton)	0	5,587	68.60	$0	**$118,915,770**	**$0.02904**

4.4 Economic Analysis

Plant specific inputs, both technical and cost, for the power plant with the ATK ICES CO_2 capture system are listed in Exhibit 4-14. This exhibit compares the results to those for the DOE/NETL Case 11 and Case 12.

Exhibit 4-14 Comparison of Operating Parameters and Costs between the DOE/NETL Baseline Cases and the ATK ICES Case

	Case 11	Case 12	ATK ICES
OPERATING PARAMETERS			
Net Plant Output, MWe	550.0	550.0	550.0
Net Plant Heat Rate, Btu/kWh HHV (kJ/kWh)	8,686 (9,165)	12,002 (12,663)	9,896 (10,441)
CO_2 Captured, lb/MWh (kg/MWh)	-	2,200 (998)	1,813 (822)
CO_2 Emitted, lb/MWh net (kg/MWh net)	1768 (802)	244 (111)	201 (91)
COSTS			
Risk	Low	High	High
Total Plant Costs (2012$)	2,033	3,651	2,897
Total Overnight Cost (2012$/kW)	2,513	4,496	3,565
Bare Erected Cost	1,665	2,815	2,252
Home Office Expenses	151	256	205
Project Contingency	217	456	352
Process contingency	0	124	89
Owners Costs	480	844	668
Total Overnight Cost (2012$x1,000)	1,382,286	2,472,362	1,960,975
Total As Spent Capital (2012$)	2,850	5,125	4,065
Annual Fixed Operating Costs ($/yr)	39,826,084	65,958,457	56,039,860
Variable Operating Costs ($/MWh)	7.24	12.39	9.23
Fuel			
Coal Price ($/ton)		69.00	

The comparison in LCOE between the DOE Case 11 and 12 and the ATK ICES case is shown in Exhibit 4-15. The ATK ICES case has the following key advantages compared to DOE/NETL Case 12, which also has CCS:

- A lower COE by $28/MWh, a 20% reduction
- A lower LCOE by $36/MWh, also a 20% reduction
- A lower cost of CO_2 captured by $21.0/tonne CO_2, a 33% reduction
- A lower cost of CO_2 avoided by $42.3/tonne CO_2, a 46% reduction

The increases in COE from the non-capture, Case 11, are 77% and 42% for the DOE/NETL Case 12 and the ATK IES case respectively.

Exhibit 4-15 Comparison of the Economic Analysis Results between the DOE/NETL Cases and the ATK ICES Case

	Case 11	Case 12	ATK ICES
COE ($/MWh, 2012$)	**81.81**	**144.45**	**116.17**
CO_2 TS&M Costs		5.60	4.61
Fuel Costs	25.69	35.49	29.27
Variable Costs	7.24	12.39	9.23
Fixed Costs	9.72	16.11	13.68
Capital Costs	39.15	74.87	59.38
LCOE (2012$/MWh)	103.73	183.17	147.30
Cost of CO_2 Captured ($/tonne CO_2)		62.79	41.79
Cost of CO_2 Avoided ($/tonne CO_2)		90.67	48.36

Exhibit 4-16 Comparison and Breakdown of COE for the DOE/NETL Baseline Cases and the ATK ICES Case
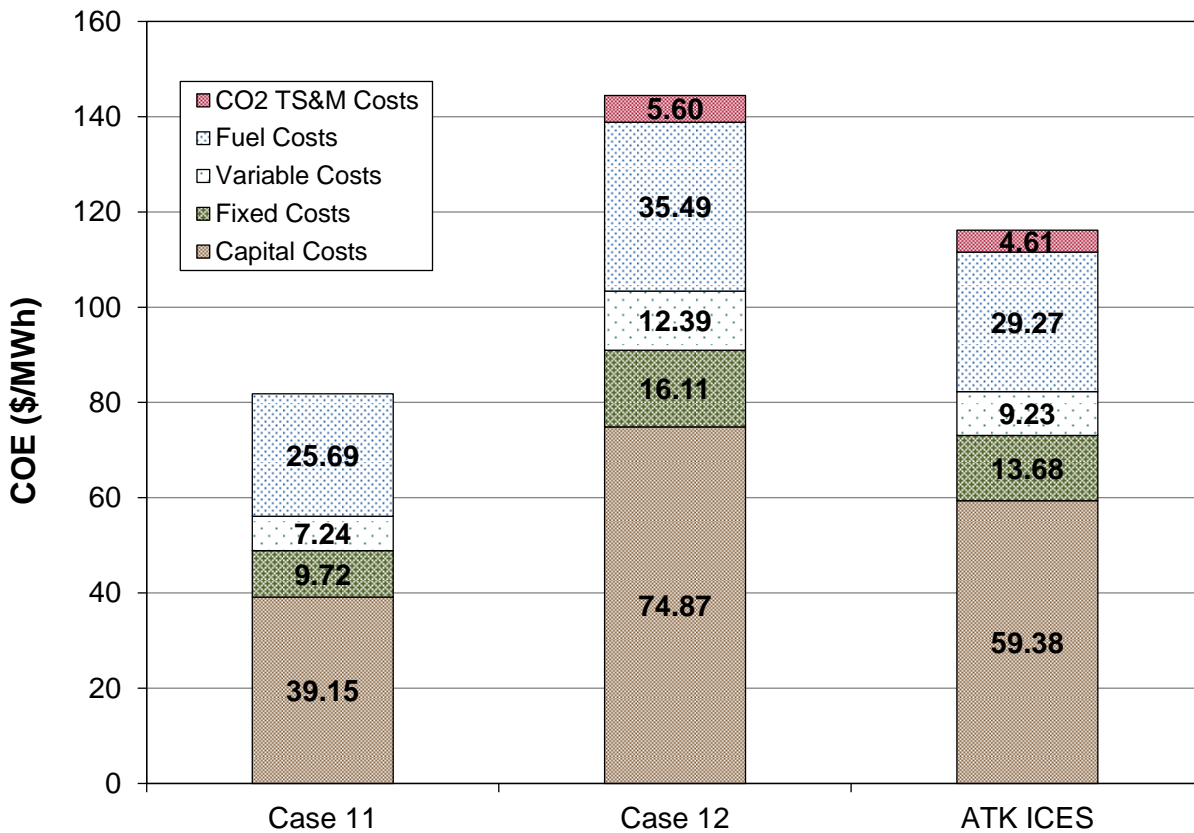
4.5 Facility Layout and Rendering

Based on the design of the ATK ICES CO_2 capture equipment provided by ATK, a plant layout illustrating the arrangement of the capture equipment and the supporting systems was developed. The objects of developing these layouts were to:

a. Illustrate how the ATK ICES CO_2 capture technology would be incorporated into a plant design
b. Determine a footprint of the ATK ICES CO_2 capture technology for comparison to MEA and other solvent based post-combustion capture technologies.

ATK provided the basic design of a commercial sized unit as previously illustrated in Exhibit 2-13. For a 550 MW power plant, 12 of the units would be required and can be configured as illustrated in Exhibit 4-17. Additionally, in the layout of the equipment, the ability to bypass the CO_2 capture system was included. When the CO_2 capture system is bypassed, the flue gas from the FGD is vented directly to the stack. This option allows for power generation to continue in the case of equipment failure in the CO_2 capture system or shut down of the CO_2 transportation or storage facilities.

Exhibit 4-17 Configuration on ATK ICES CO_2 Capture Units for 550 MW net Coal Fired Power Plant.
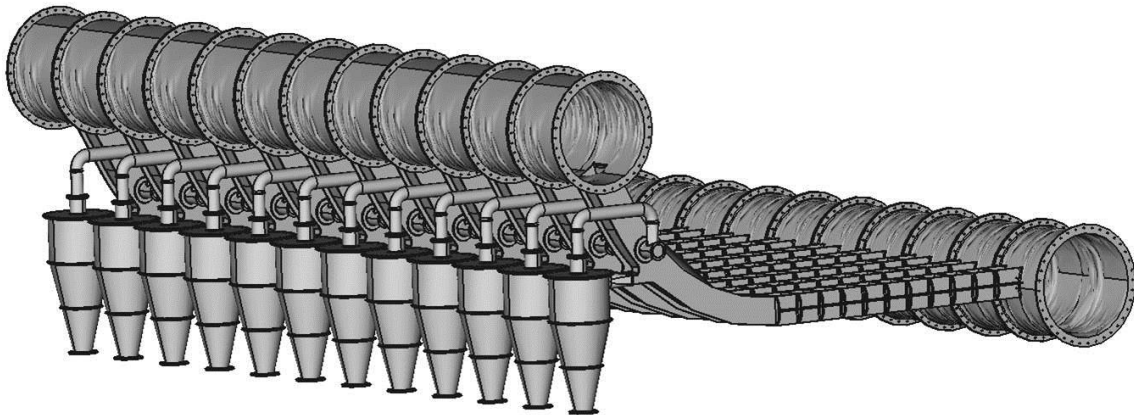
In the development of the plant, consideration was given to minimizing the ATK ICES footprint without significantly modifying the configuration of the equipment or increasing the capital costs. This assumption is suitable for a typical greenfield site in the United States, where land and space are not a premium consideration. For retrofit case, where the equipment must fit into a predefined area, or locations in other countries such as parts of Europe and Asia, where land is a premium, further options for reducing the footprint can be considered. These include:

1. Stacking the direct contact cooler on top of the FGD
2. Stacking the ICES units (6 units on top of 6)
3. Placing the ICES units over the flue gas conditioning equipment
4. Orienting the expansion ducts at an angle or vertically

These optional configurations will add both cost and complexity to the system and layout. Based on the conceptual level of the current study and no fixed space constraints for the facility, these optional configurations were not considered.

Exhibit 4-18 illustrates the ATK ICES CO_2 capture system incorporated into a typical power plant with a net capacity of 500 MW.

Exhibit 4-18 Layout of ATK ICES Capture and Related Equipment (marked by red box) Incorporated in Supercritical PC Generation Unit
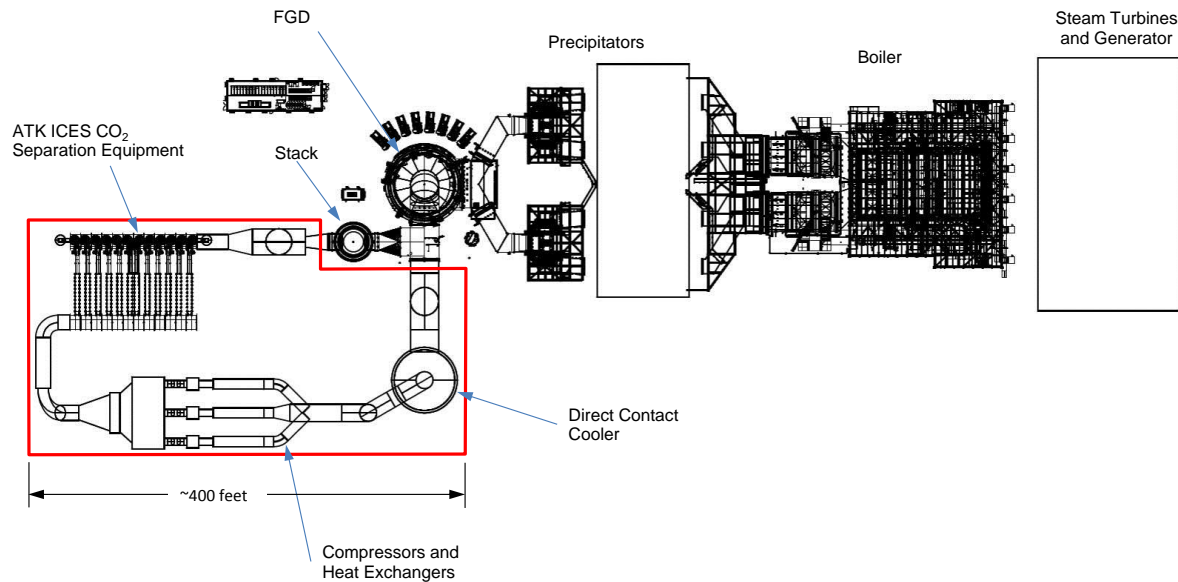
The area of the ATK ICES CO_2 capture system outline by the red box in Exhibit 4-18 is on the order of 8000 m^2. Based on a quick review of the literature of conceptual and proposed post green-field post combustion facilities of a similar size, the area of the capture equipment is on the order of 20,000 to 30,000 m^2. Therefore, the footprint of the ATK ICES CO_2 capture system is on the order of one half to one third of proposed MEA systems.[2-4]

The conceptual layout in Exhibit 4-18 was used to prepare a 3D modeling of the power plant with the ATK ICES CO_2 capture system. A rendering of the complete plant from this model is provided in Exhibit 4-19. Exhibit 4-20 provides detailed rendering of the capture equipment.

Exhibit 4-19 Rendering of ATK ICES Capture and Related Equipment Incorporated in Supercritical PC Generation Unit
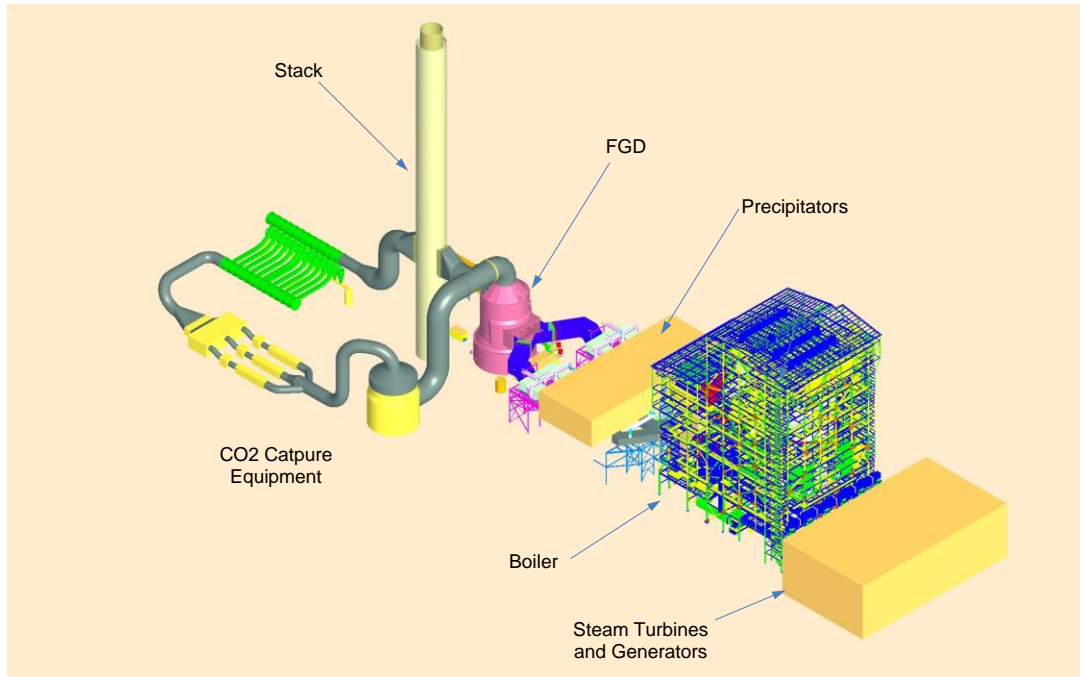
Exhibit 4-20 Rendering of ATK ICES Capture and Related Equipment
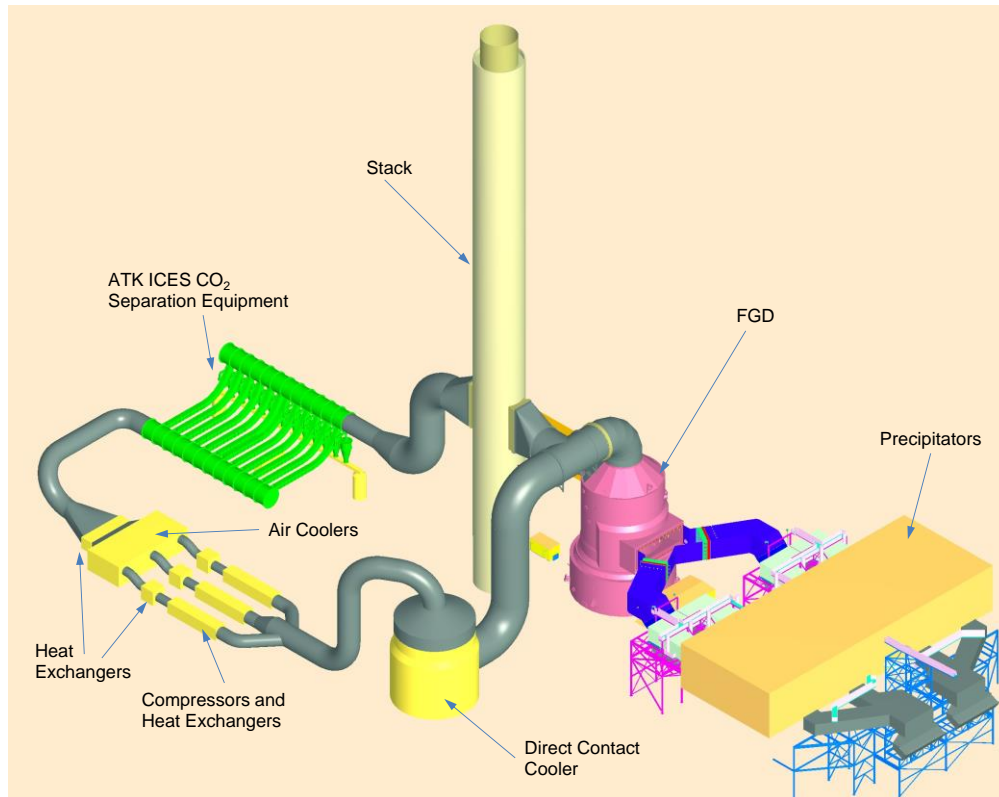
5 Findings

5.1 Performance and Cost Summaries

The current study developed a conceptual supercritical pulverized coal fired unit that incorporated the ATK ICES CO_2 capture technology. As part of this study, systems for pretreating the flue gas prior to the CO_2 capture technology and melting the dry ice after separation were developed. Reducing the auxiliary loads through minimizing the compression energy and utilizing the cooling potential of the dry ice were considered to improve the plant efficiency. A summary of the plant performance, the capital costs, and economic results are provided in Exhibit 5-1.

Exhibit 5-1 Summary of Plant Performance, Capital Costs, and Economic Results.

	Case 11	Case 12	ATK ICES
PLANT DESCRIPTION			
Steam Cycle	Supercritical	Supercritical	Supercritical
CO_2 Capture	No	Yes	Yes
OPERATING PARAMETERS			
Net Plant Output, MWe	550.0	550.0	550.0
Net Plant Heat Rate, Btu/kWh HHV (kJ/kWh)	8,686 (9,165)	12,002 (12,663)	9,896 (10,441)
Net Plant Efficiency, HHV	39.3%	28.4%	34.5%
CO_2 Captured, lb/MWh (kg/MWh)	-	2,200 (998)	1,813 (822)
CO_2 Emitted, lb/MWh net (kg/MWh net)	1768 (802)	244 (111)	201 (91)
CAPITAL AND OPERATING COSTS			
Total Overnight Cost (2012$/kW)	2,513	4,496	3,565
Variable Operating and Maintenance ($/MWh)	7.24	12.39	9.23
Fixed Operating and Maintenance ($/yr)	39,826,084	65,958,457	56,039,860
ECONOMIC METRICS			
COE ($/MWh, 2012$)	81.81	144.45	116.17
Cost of CO_2 Captured ($/tonne CO_2)	NA	62.79	41.79
Cost of CO_2 Avoided ($/tonne CO_2)	NA	90.67	48.36

The implementation of carbon capture to power generation increases capital costs, operating and maintenance costs. Compared to the cost increases incurred with the adding the Fluor Econamine technology to a supercritical power plant as illustrated by Cases 11 and 12 in the Bituminous Baseline report ATK ICES CO_2 capture technology offers several advantages. The reduction in cost increases are:

- Capital costs: 47%
- Variable Operating and Maintenance Costs: 61%
- Fixed Operating Costs: 38%

Additionally, the improvement in the plant efficiency decrease the additional fuel costs by 63% compared to the Bituminous Baseline Report capture case (Case 12).

The increase in the cost of electricity for the facility with the ATK ICES CO_2 capture technology is 42%. This compares 77% for the supercritical CO_2 capture case in the Bituminous Baseline report. This relatively lower increase of the cost of electricity for the ATK ICES technology is a result of the lower capital and O&M costs and improvements in the overall plant efficiency.

5.2 Footprint Compared to MEA Capture Systems

A layout for a 550 MW net generation facility with the ATK ICES CO_2 capture equipment was developed to illustrate the arrangement of the equipment and determine the footprint of the capture system. The footprint for the ATK ICES CO_2 capture equipment was determined to be on the order of 8,000 m^2 which compares to 20,000 to 30,000 m^2 for amine capture systems plants with similar net capacities. [2-4]

5.3 Potential Technology Hurdles

During the process development work two potential technical hurdles were identified:

3. The pressurization of the dry ice from atmospheric pressure to ~10 bar to allow the melting to result in liquid CO_2.
4. The future use of the filtration method to remove the solid water ice from the liquid CO_2.

These potential hurdles are a result of the unique material characteristics of the flow streams that are encountered in the ATK ICES CO_2 capture technology. While a review of the literature and discussions with equipment vendors provided insight to solutions that would work, the approach to developing the solution, selection of appropriate equipment and sizing of the equipment, requires testing with the actual materials to be process or at minimum a better understanding of their properties. For the pressurization of the dry ice, the particle size and the resulting behavior in an auger need to be investigated. For the separation of the water ice from the liquid CO_2, characteristics of the water ice particles in the liquid CO_2 are important.

Appendix A Evaluation Basis Document

1   Project Description & Objectives

ATK has requested WorleyParsons' support in evaluation of a conceptual CO_2 capture plant based on ATK's Inertial CO_2 Extraction System (ICES). As part of ATK's ARPA-E Phase 2 project, WorleyParsons' support will focus on:

5. Refinement of specific system components, specifically:

    g) Dehydration and compression of the flue case prior to the ICES

    h) Creation of vacuum to initiate the ICES

    i) Transfer of the dry ice/CO_2 from the ICES to pipeline as supercritical CO_2

    j) Use of dry ice as a cooling source.

6. Integration of the capture system into a supercritical pulverized coal (PC) power plant.

7. Preparation of a preliminary economic assessment.

This Evaluation Basis Document (EBD) will specify the evaluation criteria that will form the basis of the subsequent engineering and cost estimating efforts. As such, this document is an important communication tool to ensure the project basis is properly defined and understood by all the parties involved. The EBD will maximize project efficiency and minimize rework.

Note: Throughout the EBD, reference will be made to the National Energy Technology Laboratory's (NETL) report titled "Cost and Performance Baseline for Fossil Energy Plants – Volume 1: Bituminous Coal and Natural Gas to Electricity" [1], from here on referred to as the "Bituminous Baseline Report" or simply "BB Report".

2   Engineering/Technical Design Specifications

The technical design specifications to be used in this study will be the same as those used in the pulverized coal plants in the BB report [1].   The following sections will highlight specific aspects of importance to the ATK process.

2.1   Site Conditions

The power plant to be used in the study is based on a site in Midwestern United States. A specific location is chosen as the reference site, in order that the performance and cost will be developed on a consistent and realistic basis.   These conditions are described completely in the BB report.   Process modeling work will be based on ISO ambient conditions summarized in Exhibit 2-1.

Exhibit 2-1 Site Ambient Conditions Based ISO

Parameter	ISO Value
Elevation, m (ft) (above MSL)	0 (0)
Barometric Pressure, psia	14.696
Dry Bulb Temperature, °C (°F)	15 (59)
Wet Bulb Temperature, °C (°F)	11 (51.5)
Relative Humidity, %	60

Site characteristics are presented in Exhibit 2-2.

Exhibit 2-2 Site Characteristics

Parameter	Value
Cost Basis	Greenfield, Midwestern USA
Topography	Level

The following evaluation considerations are site-specific, and will not be quantified for this study.   Allowances for normal conditions and construction will be included in the cost estimates. Typically the considerations of these factors do not have a significant impact on the cost unless the site specific situation is unusual or extreme.

> Flood plain considerations.
> Existing soil/site conditions.
> Rainfall/snowfall criteria.
> Seismic design.
> Buildings/enclosures.
> Wind loading
> Fire protection.
> Local code height requirements.
> Noise regulations – Impact on site and surrounding area.

2.2 Coal Characteristics

The particulate remaining from the coal ash after bag house and FGD may have a significant impact on the ICES in that it may lead to wear of components in the C/D nozzle and swirl vanes of the ICES system and nucleation of the dry ice. The 2010 version of the BB report does not provide information regarding the ash composition. Based on other sources [5], the mineral analysis and ash properties for this coal are provided in Exhibit 2-3.

Exhibit 2-3 Typical Illinois #6 Ash Mineral Analysis and Fusion Properties

Typical Ash Mineral Analysis		Weight Percent
Silica	SiO_2	45.0%
Aluminum Oxide	Al_2O_3	18.0%
Titanium Dioxide	TiO_2	1.0%
Iron Oxide	Fe_2O_3	20.0%
Calcium Oxide	CaO	7.0%
Magnesium Oxide	MgO	1.0%
Sodium Oxide	Na_2O	0.6%
Potassium Oxide	K_2O	1.9%
Phosphorus Pentoxide	P_2O_5	0.2%
Sulfur Trioxide	SO_3	3.5%
Undetermined		1.8%
Total		**100.0%**

2.3 Product Carbon Dioxide

The CO_2 is to be transported and injected as a supercritical fluid in order to avoid two-phase flow and to reach maximum efficiency [6]. CO_2 is supplied to the pipeline at the plant fence line at a pressure of 15.3 MPa (2,215 psia). The CO_2 product gas composition varies, but is expected to meet the specification described in Exhibit 2-4. A glycol dryer located near the mid-point of the compression train is used to meet the moisture specification.

Exhibit 2-4 CO$_2$ Pipeline Specification

Parameter	Units	Value
Inlet Pressure	MPa (psia)	15.3 (2,215)
Outlet Pressure	MPa (psia)	10.4 (1,515)
Inlet Temperature	°C (°F)	35 (95)
N$_2$ Concentration	ppmv	< 300
O$_2$ Concentration	ppmv	< 40
Ar Concentration	ppmv	< 10
H$_2$O Concentration	ppmv	< 150

3 ICES Technology Description

3.1 ICES Process Overview

The current evaluation is based on boundaries set by ATK; this boundary is shown in the process flow diagram (PFD) in Exhibit 3-1. The focus of the design basis will concentrate on the pre and post processes. Key pre-processes will include the dehydration and compression of the flue gas post the desulfurization unit. Post process design will concentrate on the movement of the solid CO_2 from the cyclone to pipeline.

Exhibit 3-1 ICES Process Flow Diagram
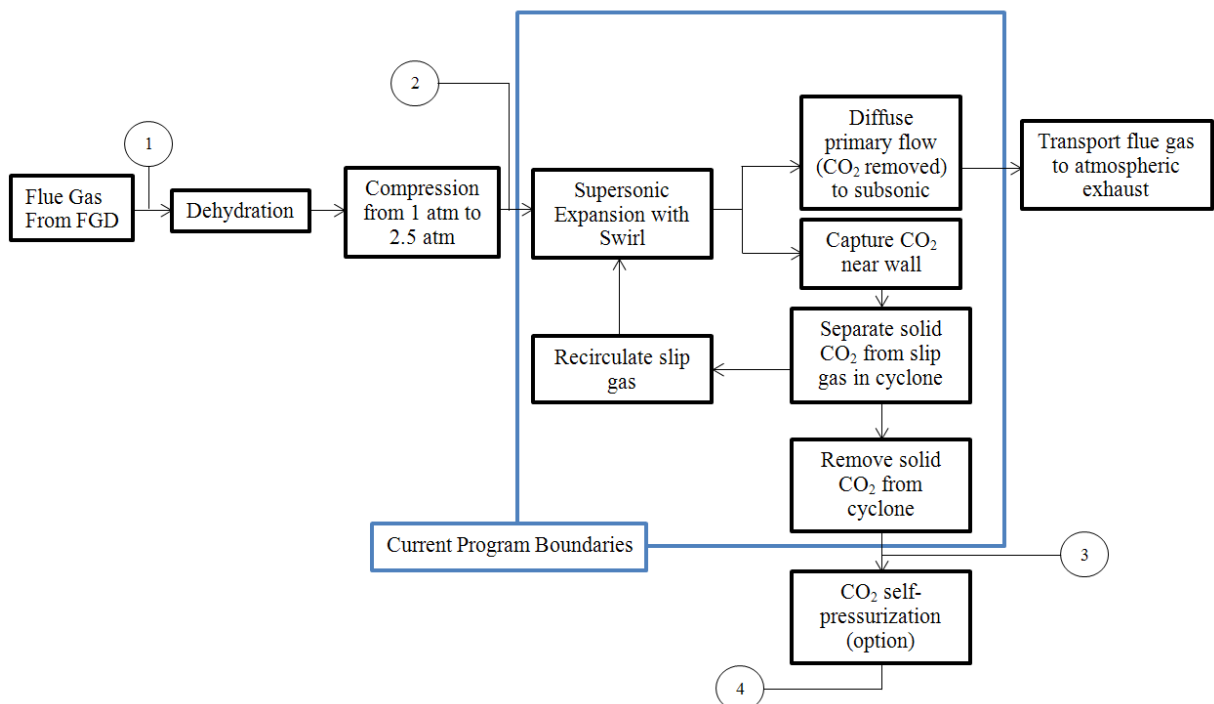
Flows critical to the design of equipment and interface between WorleyParsons and ATK are indicated in Exhibit 3-1. The characteristics of these gas flows, where available, are provided in Exhibit 3-2. The gas composition downstream from the wet FGD, location 1, is the same as that for Case 12, Stream 18 in Exhibit 4-46 of the Bituminous Baseline report. The flow rate at this location will be determined from the power plant modeling incorporating the ICES system. The characteristics of stream 4 in Exhibit 3-1, downstream of the CO_2 self-pressurization, are taken from the pipeline specifications provided in Exhibit 2-4.

Exhibit 3-2 Process Streams to and from ICES Equipment

Location	1	2	3	4
Temperature	136°F	TBD	TBD	35°C/95°F
Pressure	14.90	TBD	TBD	15.3 MPa / 2,215 psia
Flow Rate	TBD	TBD	TBD	TBD
CO_2	13.50 mol%	TBD	TBD	-
H_2O	15.37 mol%	TBD	TBD	< 150 ppmv
O_2	2.38 mol%	TBD	TBD	< 40 ppmv
N_2	67.93 mol%	TBD	TBD	< 300 ppmv
SO_2	0.81 mol%	TBD	TBD	-
Ar	0.81 mol%	TBD	TBD	<10 ppmv

[Note:, gas temperature upstream from compressor not to exceed 300K (the lower the better). Moisture content not to exceed saturation point at 300K (the lower the better)

3.2   ICES Projected Performance

A CFD model was developed by ATK for a single ICES unit inside the boundary limits shown Exhibit 3-1. Exhibit 3-3 illustrates the model input and output streams while Exhibit 3-4 presents the results. These results will be used for WorleyParsons' modeling which will incorporate the ICES into a generation power plant to determine the impact on the plant operation and the scale and energy consumption of the equipment. Note, the input gas composition for the modeling presented in Exhibit 3-4 is not consistent with flue gas composition in the Bituminous Baseline report. For comparative purposes, the flue gas composition, adjusted to the same moisture in ICES model, from the wet FGD to the CO_2 capture system from Cases 10 and 12 of the Bituminous Baseline report, are included in this table. Cases 10 and 12 of the Bituminous Baseline report are the pulverized coal-fired boiler configuration with CO_2 capture. Note, there are some slight differences in the gas streams between Bituminous Baseline study and the work performed by ATK. Additionally, the following items were identified in the review of the information provided:

1. The input and output flows of this model do not match, the following should be true:

     Stream 1= Stream 2+ Stream 3.

Exhibit 3-3 Input and Exit Streams to ICES CFD Model
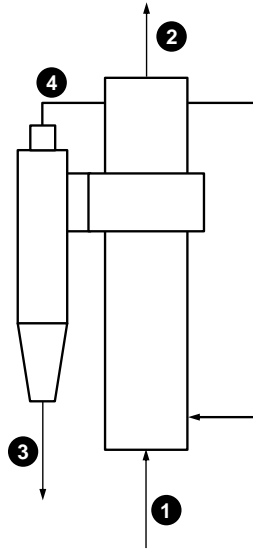
Exhibit 3-4 ICES CFD Results

Location	Flue Gas Inlet (1)	BB Report FGD Exit	Flue Gas Outlet (2)	Solid CO_2 Exit (3)	Slip Gas Recirculation (4)
Temperature	≤80°F (≤27°C)		296°F (147°C)	-150°F (-101°C)	-150°F (-101°C)
Pressure (psia)	36.7 psia (2.53 bar)		14.7+	3.67 psia (0.253 bar)	3.67 psia (0.253 bar)
Flow Rate (lb/s)	1.836[*]		1.363	0.381	0.092
CO_2 (mol%)	14.418	15.40	1.836	80.528	–
H_2O (mol%)	3.483[**]	3.48	0.443	19.453	–
O_2 (mol%)	3.874	2.71	4.611	–	4.718
N_2 (mol%)	77.253	77.48	91.957	–	94.102
SO_2 (mol%)	0.003	0.00	0	0.019	–
Ar (mol%)	0.968	0.92	1.153	–	1.18

(*) Flow Rate through the current ICES unit.

(**)Equilibrium water concentration at the assumed temperature and normal pressure, lower water concentration is desirable.

Two modifications to this modeling will be considered in the assumptions used for developing the Flue Gas Inlet conditions to the ICES equipment:

1. The removal of water upstream of the CO_2 capture system as illustrated in Exhibit 3-1.

2. The specification for particulate in the gas stream.

3.2.1 Dehydration of Flue Gas

The CO_2 to the pipeline must be dried to an H_2O concentration of <150 ppmv, as specified in Exhibit 2-4. In the initial concept, illustrate in Exhibit 3-1, the dehydration of the CO_2 will occur upstream of the dry ice formation and CO_2 separation. The water content of the gas upstream of the CO_2 capture step will need to be adjusted such that the water content meets the pipeline specification after the CO_2 separation step. Note, since water is separated with CO_2 in the ICES process, the water content in the gas stream upstream of the ICES process will be significantly less than the pipeline specification.

At this stage, the dehydration is envisioned to occur by chilling the flue gas flow (Stream 1) or other technology such as membranes, upstream of compressor before the ICES equipment. The final approach to meet the H_2O pipeline specification will be determined through the study work performed by WorleyParsons.

A second approach would be to remove the water from the superfluid CO_2 after the compression step, location 4 in Exhibit 3-1. Advantages of this approach include handling a smaller volume of fluid and a decrease in the dryness that must be achieved by the equipment. One additional advantage maybe that during the expansion, cooling of the gas, and subsequent dry ice formation; the water in the flue gas will precipitate before the CO_2 and form water ice particles. These water particles may then act as nucli for the formation of larger dry ice particles.

3.2.2 Particulate Specification

Particulate may have a significant impact on the ICES system and the formation of the dry ice particulate. In this process, typically referred to heterogeneous nucleation, the particulate may provide nucleation sites for the dry ice crystals leading to the formation of potentially few, but larger crystals. Without the presence of particulate, homogeneous nucleation is assumed to occur, which leads to fine particles which can be difficult to separate from the gas stream.

In the coal combustion process, flyash will result in particulate in the gas stream to the ICES system.. The amount of flyash in the flue gas is strongly dependent on the type of coal, the boiler firing conditions and configuration. Further, coal fired boilers typically have air pollution control (APC) equipment in place to limit particulate emissions.

For the PC configurations presented in the Bituminous Baseline report, the APC devices upstream of the CO_2 capture equipment include a fabric baghouse and wet FGD. The same configuration will be assumed with regards to equipment upstream of to the ICES CO_2 capture equipment. This assumption will be used to project the particulate loading of the gas stream to the ICES CO_2 capture equipment. The following provides a brief discussion of the estimate of the particulate loading and size.

The initial particle size distribution of the flyash is illustrated in Exhibit 3-5. A baghouse removes 99.5-99.8% of the particulate depending on particle size across 0.4-100 microns as illustrated in Exhibit 3-6. Based on Case 12 in the bituminous baseline, the total particulate flow to the baghouse is distributed by particle size according to the distribution in Exhibit 3-5 as illustrated in Exhibit 3-7. Applying the baghouse capture efficiency as a function of particle size listed in this table results in the total projected particle mass flow out of the baghouse of 85.81 (lb/hr) with the listed particle size distribution. The baghouse capture efficiencies in this table were estimated from Exhibit 3-6 for particle sizes less than 10

microns. For particle sizes greater the 10 microns, a standard 99.65% collection efficiency was used. The efficiencies were adjusted so that the total particulate loading after the baghouse match the 0.013 lb/MBtu reported in the Bituminous Baseline report.

Exhibit 3-5 Flyash particle-size distribution in pulverized coal fired boilers.[7]
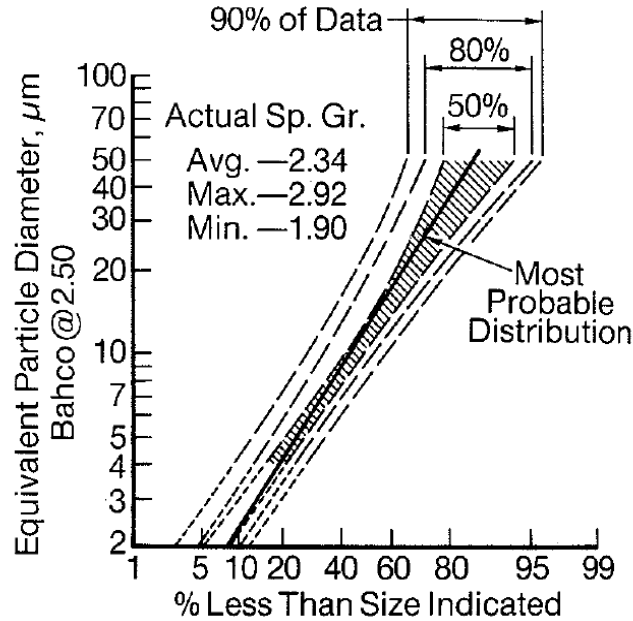
Exhibit 3-6 Particle Penetration of Fabric Filters as a Function of Particle Size.[8]
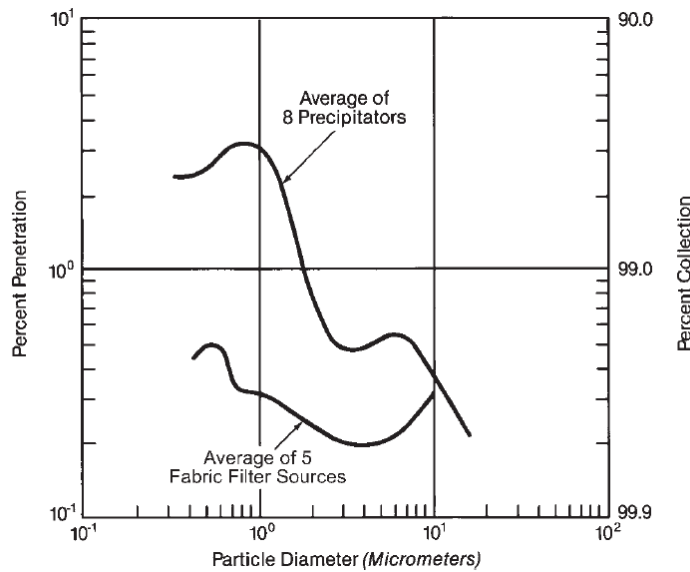
Exhibit 3-7 Projected Particle Mass Flow Rate Based on Collection Efficiencies

Particle Distribution		Flow to Baghouse	Baghouse Capture Efficiency	Post-BH/Pre-FGD	FGD Capture Efficiency	Post FGD
Size (µm)	Percentage (%)	(lb/hr)	(%)	(lb/hr)	(lb/hr)	(lb/hr)
<1	3%	1,304	99.60%	3.90	92%	0.312
1-3	10%	4,345	99.75%	6.47	93%	0.453
3-5	19%	8,256	99.80%	8.16	97%	0.245
5-10	18%	7,822	99.73%	13.21	100%	0.000
10-44	42%	18,251	99.65%	45.43	100%	0.000
44-100	8%	3,476	99.65%	8.65	100%	0.000

The typical collection efficiency of the wet FGD as a function of particle size is illustrated in Exhibit 3-8. This figure indicates that essentially all of the particulate greater than 5 microns and ~90% of the particulate in the size range of 0.1 to 1.5 micron will be removed from the gas stream. The total projected particle mass flow out of the FDG is calculated to be 1.01 (lb/hr) with a particle size less than 5 micron. The resulting particulate loading downstream of the FGD to the CO_2 capture equipment would be 0.116 mg/m^3.

Exhibit 3-8 Collection Efficiency of wet FGD as a Function of Particle Size [7]
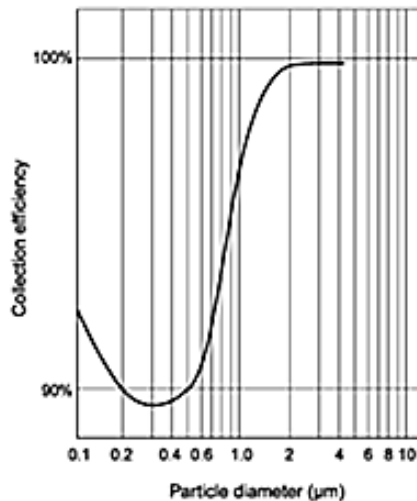
Based on discussions with air pollution control experts within WorleyParsons the total particle loading after the wet FGD is dependent of the operating conditions of the equipment and is typically in the range of 15 to 30 mg/N m^3.

For the modeling to be performed by WorleyParsons, the particulate present in the flue gas stream are assumed to be sufficient to lead to the nucleation and growth of sufficiently large dry ice crystals as the gas is expanded in the system.

3.3 Self-Pressurization of the CO_2

The vaporization of the dry ice will provide the potential to provide the sufficient pressure to produce a supercritical CO_2 fluid. However, the technical challenge of increasing the pressure of the dry ice from atmospheric pressure to pipeline pressure, ~2200 psig, exists. Two technical options to be considered will include:

3. Auger for feeding the dry ice into the pressurized chamber
4. Lock-hopper design similar to that currently used to feed solids into gasifiers

Appendidx B - Update of DOE/NETL Baseline Cases 11 and Case 12

Exhibit B-1 Summary of Updated Capital Costs for DOE/NETL Bituminous Coal Baseline Case 11.

| Client: | ATK | Report Date: | 2012-Dec-14 |
| Project: | Bituminous Baseline Study | | |

TOTAL PLANT COST SUMMARY

| Case: | Case 11 - 1x550 MWnet SuperCritical PC | | | |
| Plant Size: | 550.0 MW,net | Estimate Type: | Conceptual | Cost Base (Jan) 2012 ($x1000) |

Acct No.	Item/Description	Equipment Cost	Material Cost	Labor Direct	Labor Indirect	Sales Tax	Bare Erected Cost $	Eng'g CM H.O.& Fee	Contingencies Process	Contingencies Project	TOTAL PLANT COST $	TOTAL PLANT COST $/kW
1	COAL & SORBENT HANDLING	$20,174	$5,137	$12,027	$0	$0	$37,337	$3,276	$0	$6,092	$46,706	$85
2	COAL & SORBENT PREP & FEED	$13,557	$749	$3,421	$0	$0	$17,727	$1,509	$0	$2,885	$22,122	$40
3	FEEDWATER & MISC. BOP SYSTEMS	$53,048	$0	$24,407	$0	$0	$77,455	$6,805	$0	$13,688	$97,947	$178
4	PC BOILER											
4.1	PC Boiler & Accessories	$192,465	$0	$108,071	$0	$0	$300,536	$28,496	$0	$32,903	$361,935	$658
4.2	SCR (w/4.1)	$0	$0	$0	$0	$0	$0	$0	$0	$0	$0	$0
4.3	Open	$0	$0	$0	$0	$0	$0	$0	$0	$0	$0	$0
4.4-4.9	Boiler BoP (w/ ID Fans)	$0	$0	$0	$0	$0	$0	$0	$0	$0	$0	$0
	SUBTOTAL 4	$192,465	$0	$108,071	$0	$0	$300,536	$28,496	$0	$32,903	$361,935	$658
5	FLUE GAS CLEANUP	$99,166	$0	$33,129	$0	$0	$132,295	$12,180	$0	$14,447	$158,922	$289
5B	CO2 REMOVAL & COMPRESSION	$0	$0	$0	$0	$0	$0	$0	$0	$0	$0	$0
6	COMBUSTION TURBINE/ACCESSORIES											
6.1	Combustion Turbine Generator	N/A	$0	N/A	$0	$0	$0	$0	$0	$0	$0	$0
6.2-6.9	Combustion Turbine Accessories	$0	$0	$0	$0	$0	$0	$0	$0	$0	$0	$0
	SUBTOTAL 6	$0	$0	$0	$0	$0	$0	$0	$0	$0	$0	$0
7	HRSG, DUCTING & STACK											
7.1	Heat Recovery Steam Generator	N/A	$0	N/A	$0	$0	$0	$0	$0	$0	$0	$0
7.2-7.9	HRSG Accessories, Ductwork and Stack	$21,477	$1,160	$14,470	$0	$0	$37,107	$3,308	$0	$5,267	$45,682	$83
	SUBTOTAL 7	$21,477	$1,160	$14,470	$0	$0	$37,107	$3,308	$0	$5,267	$45,682	$83
8	STEAM TURBINE GENERATOR											
8.1	Steam TG & Accessories	$68,265	$0	$8,410	$0	$0	$76,675	$6,686	$0	$8,336	$91,697	$167
8.2-8.9	Turbine Plant Auxiliaries and Steam Piping	$30,854	$1,263	$15,420	$0	$0	$47,538	$3,850	$0	$7,210	$58,597	$107
	SUBTOTAL 8	$99,119	$1,263	$23,830	$0	$0	$124,213	$10,536	$0	$15,546	$150,295	$273
9	COOLING WATER SYSTEM	$15,218	$7,926	$14,044	$0	$0	$37,188	$3,375	$0	$5,510	$46,073	$84
10	ASH/SPENT SORBENT HANDLING SYS	$5,605	$163	$7,220	$0	$0	$12,988	$1,198	$0	$1,458	$15,644	$28
11	ACCESSORY ELECTRIC PLANT	$20,880	$8,107	$22,100	$0	$0	$51,086	$4,396	$0	$6,887	$62,369	$113
12	INSTRUMENTATION & CONTROL	$10,733	$0	$10,854	$0	$0	$21,587	$1,904	$0	$2,898	$26,388	$48
13	IMPROVEMENTS TO SITE	$3,407	$1,958	$7,329	$0	$0	$12,694	$1,254	$0	$2,790	$16,738	$30
14	BUILDINGS & STRUCTURES	$0	$27,398	$26,397	$0	$0	$53,796	$4,764	$0	$8,784	$67,343	$122
	TOTAL COST	$554,848	$53,861	$307,300	$0	$0	$916,009	$83,001	$0	$119,155	$1,118,165	$2,033

Exhibit 0-2 Details of Updated Capital Costs for DOE/NETL Bituminous Coal Baseline Case 11.

Client:	ATK					Report Date:	2012-Dec-14
Project:	Bituminous Baseline Study						
	TOTAL PLANT COST SUMMARY						
Case:	Case 11 - 1x550 MWnet SuperCritical PC						
Plant Size:	550.0 MW,net	Estimate Type:	Conceptual		Cost Base (Jan)	2012	($x1000)

Acct No.	Item/Description	Equipment Cost	Material Cost	Labor Direct	Labor Indirect	Sales Tax	Bare Erected Cost $	Eng'g CM H.O.& Fee	Contingencies Process	Contingencies Project	TOTAL PLANT COST $	TOTAL PLANT COST $/kW
1	COAL & SORBENT HANDLING											
1.1	Coal Receive & Unload	$4,147	$0	$1,884	$0	$0	$6,031	$523	$0	$983	$7,538	$14
1.2	Coal Stackout & Reclaim	$5,360	$0	$1,208	$0	$0	$6,568	$557	$0	$1,069	$8,194	$15
1.3	Coal Conveyors	$4,983	$0	$1,195	$0	$0	$6,178	$525	$0	$1,006	$7,709	$14
1.4	Other Coal Handling	$1,304	$0	$277	$0	$0	$1,580	$134	$0	$257	$1,971	$4
1.5	Sorbent Receive & Unload	$166	$0	$50	$0	$0	$216	$18	$0	$35	$269	$0
1.6	Sorbent Stackout & Reclaim	$2,679	$0	$488	$0	$0	$3,168	$267	$0	$515	$3,950	$7
1.7	Sorbent Conveyors	$956	$206	$233	$0	$0	$1,395	$117	$0	$227	$1,739	$3
1.8	Other Sorbent Handling	$577	$135	$301	$0	$0	$1,013	$87	$0	$165	$1,265	$2
1.9	Coal & Sorbent Hnd.Foundations	$0	$4,797	$6,391	$0	$0	$11,188	$1,048	$0	$1,835	$14,071	$26
	SUBTOTAL 1.	$20,174	$5,137	$12,027	$0	$0	$37,337	$3,276	$0	$6,092	$46,706	$85
2	COAL & SORBENT PREP & FEED											
2.1	Coal Crushing & Drying	$2,375	$0	$460	$0	$0	$2,836	$240	$0	$461	$3,537	$6
2.2	Coal Conveyor to Storage	$6,082	$0	$1,320	$0	$0	$7,402	$627	$0	$1,204	$9,234	$17
2.3	Coal Injection System	$0	$0	$0	$0	$0	$0	$0	$0	$0	$0	$0
2.4	Misc.Coal Prep & Feed	$0	$0	$0	$0	$0	$0	$0	$0	$0	$0	$0
2.5	Sorbent Prep Equipment	$4,551	$195	$940	$0	$0	$5,686	$480	$0	$925	$7,091	$13
2.6	Sorbent Storage & Feed	$548	$0	$209	$0	$0	$757	$65	$0	$123	$946	$2
2.7	Sorbent Injection System	$0	$0	$0	$0	$0	$0	$0	$0	$0	$0	$0
2.8	Booster Air Supply System	$0	$0	$0	$0	$0	$0	$0	$0	$0	$0	$0
2.9	Coal & Sorbent Feed Foundation	$0	$554	$491	$0	$0	$1,046	$97	$0	$171	$1,314	$2
	SUBTOTAL 2.	$13,557	$749	$3,421	$0	$0	$17,727	$1,509	$0	$2,885	$22,122	$40
3	FEEDWATER & MISC. BOP SYSTEMS											
3.1	Feedwater System	$22,930	$0	$7,368	$0	$0	$30,298	$2,568	$0	$4,930	$37,795	$69
3.2	Water Makeup & Pretreating	$5,615	$0	$1,758	$0	$0	$7,374	$665	$0	$1,608	$9,646	$18
3.3	Other Feedwater Subsystems	$7,279	$0	$2,951	$0	$0	$10,230	$867	$0	$1,665	$12,762	$23
3.4	Service Water Systems	$1,121	$0	$583	$0	$0	$1,704	$151	$0	$371	$2,226	$4
3.5	Other Boiler Plant Systems	$8,767	$0	$8,232	$0	$0	$16,999	$1,533	$0	$2,780	$21,311	$39
3.6	FO Supply Sys & Nat Gas	$336	$0	$391	$0	$0	$727	$65	$0	$119	$910	$2
3.7	Waste Treatment Equipment	$3,701	$0	$2,111	$0	$0	$5,812	$551	$0	$1,273	$7,635	$14
3.8	Misc. Equip.(cranes,AirComp.,Comm.)	$3,299	$0	$1,014	$0	$0	$4,312	$406	$0	$944	$5,661	$10
	SUBTOTAL 3.	$53,048	$0	$24,407	$0	$0	$77,455	$6,805	$0	$13,688	$97,947	$178
4	PC BOILER											
4.1	PC Boiler & Accessories	$192,465	$0	$108,071	$0	$0	$300,536	$28,496	$0	$32,903	$361,935	$658
4.2	SCR (w/4.1)	$0	$0	$0	$0	$0	$0	$0	$0	$0	$0	$0
4.3	Open	$0	$0	$0	$0	$0	$0	$0	$0	$0	$0	$0
4.4	Boiler BoP (w/ ID Fans)	$0	$0	$0	$0	$0	$0	$0	$0	$0	$0	$0
4.5	Primary Air System	w/4.1	$0	w/4.1	$0	$0	$0	$0	$0	$0	$0	$0
4.6	Secondary Air System	w/4.1	$0	w/4.1	$0	$0	$0	$0	$0	$0	$0	$0
4.8	Major Component Rigging	$0	w/4.1	w/4.1	$0	$0	$0	$0	$0	$0	$0	$0
4.9	Boiler Foundations	$0	w/14.1	w/14.1	$0	$0	$0	$0	$0	$0	$0	$0
	SUBTOTAL 4.	$192,465	$0	$108,071	$0	$0	$300,536	$28,496	$0	$32,903	$361,935	$658

| Client: | ATK | | | Report Date: | 2012-Dec-14 |
| Project: | Bituminous Baseline Study | | | | |

TOTAL PLANT COST SUMMARY

| Case: | Case 11 - 1x550 MWnet SuperCritical PC | | | | |
| Plant Size: | 550.0 MW,net | Estimate Type: | Conceptual | Cost Base (Jan) | 2012 ($x1000) |

Acct No.	Item/Description	Equipment Cost	Material Cost	Labor Direct	Labor Indirect	Sales Tax	Bare Erected Cost $	Eng'g CM H.O.& Fee	Contingencies Process	Contingencies Project	TOTAL PLANT COST $	TOTAL PLANT COST $/kW
	5 FLUE GAS CLEANUP											
5.1	Absorber Vessels & Accessories	$69,069	$0	$14,626	$0	$0	$83,695	$7,666	$0	$9,136	$100,497	$183
5.2	Other FGD	$3,604	$0	$4,018	$0	$0	$7,622	$715	$0	$834	$9,171	$17
5.3	Bag House & Accessories	$19,452	$0	$12,143	$0	$0	$31,595	$2,935	$0	$3,453	$37,983	$69
5.4	Other Particulate Removal Materials	$1,316	$0	$1,386	$0	$0	$2,702	$253	$0	$296	$3,251	$6
5.5	Gypsum Dewatering System	$5,725	$0	$956	$0	$0	$6,681	$611	$0	$729	$8,021	$15
5.6	Mercury Removal System	$0	$0	$0	$0	$0	$0	$0	$0	$0	$0	$0
5.9	Open	$0	$0	$0	$0	$0	$0	$0	$0	$0	$0	$0
	SUBTOTAL 5.	**$99,166**	**$0**	**$33,129**	**$0**	**$0**	**$132,295**	**$12,180**	**$0**	**$14,447**	**$158,922**	**$289**
	5B CO2 REMOVAL & COMPRESSION											
5B.1	CO2 Removal System	$0	$0	$0	$0	$0	$0	$0	$0	$0	$0	$0
5B.2	CO2 Compression & Drying	$0	$0	$0	$0	$0	$0	$0	$0	$0	$0	$0
	SUBTOTAL 5.	**$0**	**$0**	**$0**	**$0**	**$0**	**$0**	**$0**	**$0**	**$0**	**$0**	**$0**
	6 COMBUSTION TURBINE/ACCESSORIES											
6.1	Combustion Turbine Generator	N/A	$0	N/A	$0	$0	$0	$0	$0	$0	$0	$0
6.2	Open	$0	$0	$0	$0	$0	$0	$0	$0	$0	$0	$0
6.3	Compressed Air Piping	$0	$0	$0	$0	$0	$0	$0	$0	$0	$0	$0
6.9	Combustion Turbine Foundations	$0	$0	$0	$0	$0	$0	$0	$0	$0	$0	$0
	SUBTOTAL 6.	**$0**	**$0**	**$0**	**$0**	**$0**	**$0**	**$0**	**$0**	**$0**	**$0**	**$0**
	7 HRSG, DUCTING & STACK											
7.1	Heat Recovery Steam Generator	N/A	$0	N/A	$0	$0	$0	$0	$0	$0	$0	$0
7.2	HRSG Accessories	$0	$0	$0	$0	$0	$0	$0	$0	$0	$0	$0
7.3	Ductwork	$10,618	$0	$6,827	$0	$0	$17,445	$1,482	$0	$2,839	$21,766	$40
7.4	Stack	$10,859	$0	$6,250	$0	$0	$17,109	$1,587	$0	$1,870	$20,566	$37
7.9	Duct & Stack Foundations	$0	$1,160	$1,392	$0	$0	$2,552	$239	$0	$558	$3,349	$6
	SUBTOTAL 7.	**$21,477**	**$1,160**	**$14,470**	**$0**	**$0**	**$37,107**	**$3,308**	**$0**	**$5,267**	**$45,682**	**$83**
	8 STEAM TURBINE GENERATOR											
8.1	Steam TG & Accessories	$68,265	$0	$8,410	$0	$0	$76,675	$6,686	$0	$8,336	$91,697	$167
8.2	Turbine Plant Auxiliaries	$432	$0	$911	$0	$0	$1,343	$127	$0	$147	$1,617	$3
8.3	Condenser & Auxiliaries	$8,357	$0	$2,803	$0	$0	$11,160	$1,027	$0	$1,219	$13,406	$24
8.4	Steam Piping	$22,065	$0	$9,599	$0	$0	$31,664	$2,378	$0	$5,106	$39,148	$71
8.9	TG Foundations	$0	$1,263	$2,108	$0	$0	$3,371	$317	$0	$738	$4,426	$8
	SUBTOTAL 8.	**$99,119**	**$1,263**	**$23,830**	**$0**	**$0**	**$124,213**	**$10,536**	**$0**	**$15,546**	**$150,295**	**$273**
	9 COOLING WATER SYSTEM											
9.1	Cooling Towers	$11,311	$0	$3,465	$0	$0	$14,776	$1,359	$0	$1,614	$17,749	$32
9.2	Circulating Water Pumps	$2,220	$0	$142	$0	$0	$2,361	$201	$0	$256	$2,819	$5
9.3	Circ.Water System Auxiliaries	$620	$0	$81	$0	$0	$702	$64	$0	$77	$842	$2
9.4	Circ.Water Piping	$0	$5,205	$4,689	$0	$0	$9,894	$869	$0	$1,614	$12,377	$23
9.5	Make-up Water System	$562	$0	$717	$0	$0	$1,279	$117	$0	$209	$1,606	$3
9.6	Component Cooling Water Sys	$505	$0	$385	$0	$0	$889	$80	$0	$145	$1,115	$2
9.9	Circ.Water System Foundations& Structures	$0	$2,721	$4,565	$0	$0	$7,286	$685	$0	$1,594	$9,566	$17
	SUBTOTAL 9.	**$15,218**	**$7,926**	**$14,044**	**$0**	**$0**	**$37,188**	**$3,375**	**$0**	**$5,510**	**$46,073**	**$84**

Client:		ATK								**Report Date:**	2012-Dec-14	
Project:		Bituminous Baseline Study										

TOTAL PLANT COST SUMMARY

Case:		Case 11 - 1x550 MWnet SuperCritical PC										
Plant Size:		550.0 MW,net		**Estimate Type:**	Conceptual			**Cost Base (Jan)**	2012	($x1000)		

Acct No.	Item/Description	Equipment Cost	Material Cost	Labor Direct	Labor Indirect	Sales Tax	Bare Erected Cost $	Eng'g CM H.O.& Fee	Contingencies Process	Contingencies Project	TOTAL PLANT COST $	TOTAL PLANT COST $/kW
10	ASH/SPENT SORBENT HANDLING SYS											
10.1	Ash Coolers	N/A	$0	N/A	$0	$0	$0	$0	$0	$0	$0	$0
10.2	Cyclone Ash Letdown	N/A	$0	N/A	$0	$0	$0	$0	$0	$0	$0	$0
10.3	HGCU Ash Letdown	N/A	$0	N/A	$0	$0	$0	$0	$0	$0	$0	$0
10.4	High Temperature Ash Piping	N/A	$0	N/A	$0	$0	$0	$0	$0	$0	$0	$0
10.5	Other Ash Recovery Equipment	N/A	$0	N/A	$0	$0	$0	$0	$0	$0	$0	$0
10.6	Ash Storage Silos	$735	$0	$2,226	$0	$0	$2,961	$282	$0	$324	$3,567	$6
10.7	Ash Transport & Feed Equipment	$4,871	$0	$4,792	$0	$0	$9,662	$882	$0	$1,054	$11,598	$21
10.8	Misc. Ash Handling Equipment	$0	$0	$0	$0	$0	$0	$0	$0	$0	$0	$0
10.9	Ash/Spent Sorbent Foundation	$0	$163	$202	$0	$0	$365	$34	$0	$80	$479	$1
	SUBTOTAL 10.	$5,605	$163	$7,220	$0	$0	$12,988	$1,198	$0	$1,458	$15,644	$28
11	ACCESSORY ELECTRIC PLANT											
11.1	Generator Equipment	$1,962	$0	$318	$0	$0	$2,280	$205	$0	$186	$2,672	$5
11.2	Station Service Equipment	$3,345	$0	$1,136	$0	$0	$4,482	$418	$0	$367	$5,267	$10
11.3	Switchgear & Motor Control	$3,840	$0	$676	$0	$0	$4,515	$420	$0	$494	$5,429	$10
11.4	Conduit & Cable Tray	$0	$2,682	$8,620	$0	$0	$11,302	$1,048	$0	$1,852	$14,202	$26
11.5	Wire & Cable	$0	$5,062	$9,081	$0	$0	$14,143	$1,131	$0	$2,291	$17,565	$32
11.6	Protective Equipment	$309	$0	$1,088	$0	$0	$1,397	$134	$0	$153	$1,684	$3
11.7	Standby Equipment	$1,513	$0	$36	$0	$0	$1,548	$143	$0	$169	$1,860	$3
11.8	Main Power Transformers	$9,911	$0	$211	$0	$0	$10,122	$774	$0	$1,090	$11,986	$22
11.9	Electrical Foundations	$0	$363	$934	$0	$0	$1,298	$122	$0	$284	$1,704	$3
	SUBTOTAL 11.	$20,880	$8,107	$22,100	$0	$0	$51,086	$4,396	$0	$6,887	$62,369	$113
12	INSTRUMENTATION & CONTROL											
12.1	PC Control Equipment	w/12.7	$0	w/12.7	$0	$0	$0	$0	$0	$0	$0	$0
12.2	Combustion Turbine Control	N/A	$0	N/A	$0	$0	$0	$0	$0	$0	$0	$0
12.3	Steam Turbine Control	w/8.1	$0	w/8.1	$0	$0	$0	$0	$0	$0	$0	$0
12.4	Other Major Component Control	$0	$0	$0	$0	$0	$0	$0	$0	$0	$0	$0
12.5	Signal Processing Equipment	w/12.7	$0	w/12.7	$0	$0	$0	$0	$0	$0	$0	$0
12.6	Control Boards,Panels & Racks	$533	$0	$330	$0	$0	$863	$81	$0	$142	$1,086	$2
12.7	Distributed Control System Equipment	$5,381	$0	$972	$0	$0	$6,354	$590	$0	$694	$7,638	$14
12.8	Instrument Wiring & Tubing	$3,297	$0	$5,984	$0	$0	$9,281	$747	$0	$1,504	$11,532	$21
12.9	Other I & C Equipment	$1,521	$0	$3,568	$0	$0	$5,089	$485	$0	$557	$6,132	$11
	SUBTOTAL 12.	$10,733	$0	$10,854	$0	$0	$21,587	$1,904	$0	$2,898	$26,388	$48
13	IMPROVEMENTS TO SITE											
13.1	Site Preparation	$0	$57	$1,222	$0	$0	$1,280	$124	$0	$281	$1,685	$3
13.2	Site Improvements	$0	$1,901	$2,520	$0	$0	$4,421	$437	$0	$972	$5,830	$11
13.3	Site Facilities	$3,407	$0	$3,586	$0	$0	$6,993	$693	$0	$1,537	$9,223	$17
	SUBTOTAL 13.	$3,407	$1,958	$7,329	$0	$0	$12,694	$1,254	$0	$2,790	$16,738	$30
14	BUILDINGS & STRUCTURES											
14.1	Boiler Building	$0	$9,986	$8,920	$0	$0	$18,906	$1,668	$0	$3,086	$23,661	$43
14.2	Turbine Building	$0	$14,263	$13,502	$0	$0	$27,765	$2,457	$0	$4,533	$34,755	$63
14.3	Administration Building	$0	$707	$759	$0	$0	$1,467	$131	$0	$240	$1,837	$3
14.4	Circulation Water Pumphouse	$0	$203	$164	$0	$0	$366	$32	$0	$60	$458	$1
14.5	Water Treatment Buildings	$0	$682	$632	$0	$0	$1,314	$116	$0	$214	$1,644	$3
14.6	Machine Shop	$0	$473	$323	$0	$0	$796	$69	$0	$130	$995	$2
14.7	Warehouse	$0	$321	$327	$0	$0	$647	$57	$0	$106	$810	$1
14.8	Other Buildings & Structures	$0	$262	$226	$0	$0	$488	$43	$0	$80	$611	$1
14.9	Waste Treating Building & Str.	$0	$501	$1,545	$0	$0	$2,047	$190	$0	$336	$2,572	$5
	SUBTOTAL 14.	$0	$27,398	$26,397	$0	$0	$53,796	$4,764	$0	$8,784	$67,343	$122
	TOTAL COST	$554,848	$53,861	$307,300	$0	$0	$916,009	$83,001	$0	$119,155	$1,118,165	$2,033

Exhibit 0-3 Updated O&M Costs for DOE/NETL Bituminous Coal Baseline 11

INITIAL & ANNUAL O&M EXPENSES					Cost Base (Jan):	2012
Case 11 - 1x550 MWnet SuperCritical PC					Heat Rate-net (Btu/kWh):	8,686
					MWe-net:	550
					Capacity Factor (%):	85

OPERATING & MAINTENANCE LABOR

Operating Labor
Operating Labor Rate (base): 40.50 $/hour
Operating Labor Burden: 30.00 % of base
Labor O-H Charge Rate: 25.00 % of labor

		Total
Skilled Operator	2.0	2.0
Operator	9.0	9.0
Foreman	1.0	1.0
Lab Tech's, etc.	2.0	2.0
TOTAL-O.J.'s	14.0	14.0

	Annual Cost $	Annual Unit Cost $/kW-net
Annual Operating Labor Cost	$6,456,996	$11.740
Maintenance Labor Cost	$7,513,236	$13.660
Administrative & Support Labor	$3,492,558	$6.350
Property Taxes and Insurance	$22,363,295	$40.659
TOTAL FIXED OPERATING COSTS	**$39,826,084**	**$72.408**

VARIABLE OPERATING COSTS

						$/kWh-net
Maintenance Material Cost					$11,269,853	$0.00275

Consumables	Consumption		Unit	Initial Fill		
	Initial Fill	/Day	Cost	Cost		
Water (/1000 gallons)	0	3,884	1.48	$0	$1,789,174	$0.00044
Chemicals						
MU & WT Chem.(lbs)	0	18,799	0.24	$0	$1,385,719	$0.00034
Limestone (ton)	0	488	29.70	$0	$4,494,017	$0.00110
Carbon (Mercury Removal) (lb)	0	0	1.44	$0	$0	$0.00000
MEA Solvent (ton)	0	0	3,088.59	$0	$0	$0.00000
NaOH (tons)	0	0	595.34	$0	$0	$0.00000
H2SO4 (tons)	0	0	190.51	$0	$0	$0.00000
Corrosion Inhibitor	0	0	0.00	$0	$0	$0.00000
Activated Carbon (lb)	0	0	1.44	$0	$0	$0.00000
Ammonia (19% NH3) ton	0	74	292.72	$0	$6,677,259	$0.00163
Subtotal Chemicals				$0	**$12,556,995**	$0.00307
Other						
Supplemental Fuel (MBtu)	0	0	0.00	$0	$0	$0.00000
SCR Catalyst (m3)	w/equip.	0.31	7,929.08	$0	$760,242	$0.00019
Emission Penalties	0	0	0.00	$0	$0	$0.00000
Subtotal Other				$0	**$760,242**	$0.00019
Waste Disposal						
Fly Ash (ton)	0	381	22.27	$0	$2,634,412	$0.00064
Bottom Ash (ton)	0	95	22.27	$0	$658,603	$0.00016
Subtotal-Waste Disposal				$0	**$3,293,016**	$0.00080
By-products & Emissions						
Gypsum (tons)	0	759	0.00	$0	$0	$0.00000
Subtotal By-Products				$0	**$0**	$0.00000
TOTAL VARIABLE OPERATING COSTS				$0	**$29,669,280**	$0.00724
Fuel (ton)	0	4,914	68.60	$0	$104,590,800	$0.02554

WorleyParsons
resources & energy

Exhibit 0-4 Summary of Updated Capital Costs for DOE/NETL Bituminous Coal Baseline Case 12

	Client:	ATK						Report Date:	2012-Dec-14	
	Project:	Bituminous Baseline Study								

TOTAL PLANT COST SUMMARY

	Case:	Case 12 - 1x550 MWnet Super-Critical PC w/ CO2 Capture								
	Plant Size:	550.0 MW,net		Estimate Type: Conceptual				Cost Base (Jan)	2012 ($x1000)	

Acct No.	Item/Description	Equipment Cost	Material Cost	Labor Direct	Labor Indirect	Sales Tax	Bare Erected Cost $	Eng'g CM H.O.& Fee	Contingencies Process	Contingencies Project	TOTAL PLANT COST $	$/kW
1	COAL & SORBENT HANDLING	$24,752	$6,285	$14,720	$0	$0	$45,757	$4,015	$0	$7,466	$57,238	$104
2	COAL & SORBENT PREP & FEED	$16,840	$936	$4,253	$0	$0	$22,029	$1,875	$0	$3,586	$27,490	$50
3	FEEDWATER & MISC. BOP SYSTEMS	$68,560	$0	$31,660	$0	$0	$100,221	$8,823	$0	$17,887	$126,931	$231
4	PC BOILER											
4.1	PC Boiler & Accessories	$239,767	$0	$134,633	$0	$0	$374,399	$35,500	$0	$40,990	$450,889	$820
4.2	SCR (w/4.1)	$0	$0	$0	$0	$0	$0	$0	$0	$0	$0	$0
4.3	Open	$0	$0	$0	$0	$0	$0	$0	$0	$0	$0	$0
4.4-4.9	Boiler BoP (w/ ID Fans)	$0	$0	$0	$0	$0	$0	$0	$0	$0	$0	$0
	SUBTOTAL 4	$239,767	$0	$134,633	$0	$0	$374,399	$35,500	$0	$40,990	$450,889	$820
5	FLUE GAS CLEANUP	$125,791	$0	$42,244	$0	$0	$168,034	$15,471	$0	$18,351	$201,856	$367
5B	CO2 REMOVAL & COMPRESSION	$305,338	$0	$95,769	$0	$0	$401,107	$36,898	$67,206	$101,042	$606,253	$1,102
6	COMBUSTION TURBINE/ACCESSORIES											
6.1	Combustion Turbine Generator	N/A	$0	N/A	$0	$0	$0	$0	$0	$0	$0	$0
6.2-6.9	Combustion Turbine Other	$0	$0	$0	$0	$0	$0	$0	$0	$0	$0	$0
	SUBTOTAL 6	$0	$0	$0	$0	$0	$0	$0	$0	$0	$0	$0
7	HRSG, DUCTING & STACK											
7.1	Heat Recovery Steam Generator	N/A	$0	N/A	$0	$0	$0	$0	$0	$0	$0	$0
7.2-7.9	HRSG Accessories, Ductwork and Stack	$21,647	$1,114	$14,553	$0	$0	$37,314	$3,319	$0	$5,331	$45,964	$84
	SUBTOTAL 7	$21,647	$1,114	$14,553	$0	$0	$37,314	$3,319	$0	$5,331	$45,964	$84
8	STEAM TURBINE GENERATOR											
8.1	Steam TG & Accessories	$75,100	$0	$9,231	$0	$0	$84,331	$7,354	$0	$9,169	$100,854	$183
8.2-8.9	Turbine Plant Auxiliaries and Steam Piping	$37,137	$1,392	$18,778	$0	$0	$57,307	$4,563	$0	$8,892	$70,763	$129
	SUBTOTAL 8	$112,238	$1,392	$28,009	$0	$0	$141,639	$11,917	$0	$18,061	$171,616	$312
9	COOLING WATER SYSTEM	$25,624	$12,514	$22,589	$0	$0	$60,728	$5,513	$0	$8,910	$75,151	$137
10	ASH/SPENT SORBENT HANDLING SYS	$6,707	$195	$8,639	$0	$0	$15,541	$1,433	$0	$1,745	$18,719	$34
11	ACCESSORY ELECTRIC PLANT	$32,550	$13,990	$36,978	$0	$0	$83,518	$7,170	$0	$11,367	$102,055	$186
12	INSTRUMENTATION & CONTROL	$12,301	$0	$12,440	$0	$0	$24,742	$2,182	$1,237	$3,474	$31,634	$58
13	IMPROVEMENTS TO SITE	$3,810	$2,190	$8,197	$0	$0	$14,196	$1,403	$0	$3,120	$18,719	$34
14	BUILDINGS & STRUCTURES	$0	$29,885	$28,806	$0	$0	$58,691	$5,197	$0	$9,583	$73,471	$134
	TOTAL COST	$995,923	$68,501	$483,491	$0	$0	$1,547,915	$140,716	$68,443	$250,912	$2,007,986	$3,651

Exhibit 0-5 Details of Updated Capital Costs for DOE/NETL Bituminous Coal Baseline Case 12

Client:	ATK								**Report Date:**	2012-Dec-14	
Project:	Bituminous Baseline Study										

TOTAL PLANT COST SUMMARY

Case: Case 12 - 1x550 MWnet Super-Critical PC w/ CO2 Capture
Plant Size: 550.0 MW,net   **Estimate Type:** Conceptual   Cost Base (Jan) 2012 ($x1000)

Acct No.	Item/Description	Equipment Cost	Material Cost	Labor Direct	Labor Indirect	Sales Tax	Bare Erected Cost $	Eng'g CM H.O.& Fee	Contingencies Process	Contingencies Project	TOTAL PLANT COST $	TOTAL PLANT COST $/kW
1	COAL & SORBENT HANDLING											
1.1	Coal Receive & Unload	$5,068	$0	$2,302	$0	$0	$7,370	$639	$0	$1,201	$9,210	$17
1.2	Coal Stackout & Reclaim	$6,550	$0	$1,476	$0	$0	$8,025	$681	$0	$1,306	$10,012	$18
1.3	Coal Conveyors	$6,089	$0	$1,460	$0	$0	$7,550	$641	$0	$1,229	$9,420	$17
1.4	Other Coal Handling	$1,593	$0	$338	$0	$0	$1,931	$164	$0	$314	$2,409	$4
1.5	Sorbent Receive & Unload	$207	$0	$62	$0	$0	$268	$23	$0	$44	$335	$1
1.6	Sorbent Stackout & Reclaim	$3,336	$0	$608	$0	$0	$3,944	$333	$0	$642	$4,918	$9
1.7	Sorbent Conveyors	$1,190	$256	$290	$0	$0	$1,737	$146	$0	$282	$2,165	$4
1.8	Other Sorbent Handling	$719	$167	$375	$0	$0	$1,262	$108	$0	$205	$1,575	$3
1.9	Coal & Sorbent Hnd.Foundations	$0	$5,861	$7,809	$31	$0	$13,670	$1,280	$0	$2,243	$17,194	$31
	SUBTOTAL 1.	$24,752	$6,285	$14,720	$0	$0	$45,757	$4,015	$0	$7,466	$57,238	$104
2	COAL & SORBENT PREP & FEED											
2.1	Coal Crushing & Drying	$2,940	$0	$570	$0	$0	$3,510	$297	$0	$571	$4,378	$8
2.2	Coal Conveyor to Storage	$7,529	$0	$1,634	$0	$0	$9,163	$776	$0	$1,491	$11,430	$21
2.3	Coal Injection System	$0	$0	$0	$0	$0	$0	$0	$0	$0	$0	$0
2.4	Misc.Coal Prep & Feed	$0	$0	$0	$0	$0	$0	$0	$0	$0	$0	$0
2.5	Sorbent Prep Equipment	$5,685	$244	$1,174	$0	$0	$7,104	$599	$0	$1,155	$8,858	$16
2.6	Sorbent Storage & Feed	$685	$0	$261	$0	$0	$946	$82	$0	$154	$1,182	$2
2.7	Sorbent Injection System	$0	$0	$0	$0	$0	$0	$0	$0	$0	$0	$0
2.8	Booster Air Supply System	$0	$0	$0	$0	$0	$0	$0	$0	$0	$0	$0
2.9	Coal & Sorbent Feed Foundation	$0	$692	$614	$0	$0	$1,306	$121	$0	$214	$1,642	$3
	SUBTOTAL 2.	$16,840	$936	$4,253	$0	$0	$22,029	$1,875	$0	$3,586	$27,490	$50
3	FEEDWATER & MISC. BOP SYSTEMS											
3.1	Feedwater System	$28,146	$0	$9,044	$0	$0	$37,190	$3,152	$0	$6,051	$46,394	$84
3.2	Water Makeup & Pretreating	$8,810	$0	$2,759	$0	$0	$11,569	$1,043	$0	$2,522	$15,134	$28
3.3	Other Feedwater Subsystems	$8,935	$0	$3,623	$0	$0	$12,558	$1,064	$0	$2,043	$15,665	$28
3.4	Service Water Systems	$1,759	$0	$914	$0	$0	$2,673	$238	$0	$582	$3,493	$6
3.5	Other Boiler Plant Systems	$11,172	$0	$10,490	$0	$0	$21,662	$1,953	$0	$3,542	$27,158	$49
3.6	FO Supply Sys & Nat Gas	$364	$0	$422	$0	$0	$786	$70	$0	$128	$984	$2
3.7	Waste Treatment Equipment	$5,806	$0	$3,312	$0	$0	$9,118	$865	$0	$1,997	$11,979	$22
3.8	Misc. Equip.(cranes,AirComp.,Comm.)	$3,568	$0	$1,096	$0	$0	$4,664	$439	$0	$1,020	$6,123	$11
	SUBTOTAL 3.	$68,560	$0	$31,660	$0	$0	$100,221	$8,823	$0	$17,887	$126,931	$231
4	PC BOILER											
4.1	PC Boiler & Accessories	$239,767	$0	$134,633	$0	$0	$374,399	$35,500	$0	$40,990	$450,889	$820
4.2	SCR (w/4.1)	$0	$0	$0	$0	$0	$0	$0	$0	$0	$0	$0
4.3	Open	$0	$0	$0	$0	$0	$0	$0	$0	$0	$0	$0
4.4	Boiler BoP (w/ ID Fans)	$0	$0	$0	$0	$0	$0	$0	$0	$0	$0	$0
4.5	Primary Air System	w/4.1	$0	w/4.1	$0	$0	$0	$0	$0	$0	$0	$0
4.6	Secondary Air System	w/4.1	$0	w/4.1	$0	$0	$0	$0	$0	$0	$0	$0
4.8	Major Component Rigging	$0	w/4.1	w/4.1	$0	$0	$0	$0	$0	$0	$0	$0
4.9	Boiler Foundations	$0	w/14.1	w/14.1	$0	$0	$0	$0	$0	$0	$0	$0
	SUBTOTAL 4.	$239,767	$0	$134,633	$0	$0	$374,399	$35,500	$0	$40,990	$450,889	$820

WorleyParsons
resources & energy

Client:	ATK	Report Date:	2012-Dec-14
Project:	Bituminous Baseline Study		

TOTAL PLANT COST SUMMARY

Case:	Case 12 - 1x550 MWnet Super-Critical PC w/ CO2 Capture	
Plant Size:	550.0 MW,net	Estimate Type: Conceptual

Cost Base (Jan)   2012   ($x1000)

Acct No.	Item/Description	Equipment Cost	Material Cost	Labor Direct	Labor Indirect	Sales Tax	Bare Erected Cost $	Eng'g CM H.O.& Fee	Contingencies Process	Contingencies Project	TOTAL PLANT COST $	TOTAL PLANT COST $/kW
5	FLUE GAS CLEANUP											
5.1	Absorber Vessels & Accessories	$87,389	$0	$18,506	$0	$0	$105,895	$9,699	$0	$11,559	$127,153	$231
5.2	Other FGD	$4,560	$0	$5,084	$0	$0	$9,644	$905	$0	$1,055	$11,603	$21
5.3	Bag House & Accessories	$25,139	$0	$15,693	$0	$0	$40,832	$3,793	$0	$4,463	$49,088	$89
5.4	Other Particulate Removal Materials	$1,701	$0	$1,791	$0	$0	$3,492	$327	$0	$382	$4,201	$8
5.5	Gypsum Dewatering System	$7,002	$0	$1,170	$0	$0	$8,172	$747	$0	$892	$9,810	$18
5.6	Mercury Removal System	$0	$0	$0	$0	$0	$0	$0	$0	$0	$0	$0
5.9	Open	$0	$0	$0	$0	$0	$0	$0	$0	$0	$0	$0
	SUBTOTAL 5.	$125,791	$0	$42,244	$0	$0	$168,034	$15,471	$0	$18,351	$201,856	$367
5B	CO2 REMOVAL & COMPRESSION											
5B.1	CO2 Removal System	$258,746	$0	$77,282	$0	$0	$336,028	$30,893	$67,206	$86,825	$520,952	$947
5B.2	CO2 Compression & Drying	$46,592	$0	$18,487	$0	$0	$65,079	$6,005	$0	$14,217	$85,301	$155
	SUBTOTAL 5.	$305,338	$0	$95,769	$0	$0	$401,107	$36,898	$67,206	$101,042	$606,253	$1,102
6	COMBUSTION TURBINE/ACCESSORIES											
6.1	Combustion Turbine Generator	N/A	$0	N/A	$0	$0	$0	$0	$0	$0	$0	$0
6.2	Open	$0	$0	$0	$0	$0	$0	$0	$0	$0	$0	$0
6.3	Compressed Air Piping	$0	$0	$0	$0	$0	$0	$0	$0	$0	$0	$0
6.9	Combustion Turbine Foundations	$0	$0	$0	$0	$0	$0	$0	$0	$0	$0	$0
	SUBTOTAL 6.	$0	$0	$0	$0	$0	$0	$0	$0	$0	$0	$0
7	HRSG, DUCTING & STACK											
7.1	Heat Recovery Steam Generator	N/A	$0	N/A	$0	$0	$0	$0	$0	$0	$0	$0
7.2	HRSG Accessories	$0	$0	$0	$0	$0	$0	$0	$0	$0	$0	$0
7.3	Ductwork	$11,218	$0	$7,213	$0	$0	$18,430	$1,566	$0	$2,999	$22,995	$42
7.4	Stack	$10,429	$0	$6,003	$0	$0	$16,432	$1,525	$0	$1,796	$19,752	$36
7.9	Duct & Stack Foundations	$0	$1,114	$1,337	$0	$0	$2,451	$229	$0	$536	$3,217	$6
	SUBTOTAL 7.	$21,647	$1,114	$14,553	$0	$0	$37,314	$3,319	$0	$5,331	$45,964	$84
8	STEAM TURBINE GENERATOR											
8.1	Steam TG & Accessories	$75,100	$0	$9,231	$0	$0	$84,331	$7,354	$0	$9,169	$100,854	$183
8.2	Turbine Plant Auxiliaries	$476	$0	$1,003	$0	$0	$1,480	$140	$0	$162	$1,782	$3
8.3	Condenser & Auxiliaries	$6,859	$0	$2,487	$0	$0	$9,346	$861	$0	$1,021	$11,229	$20
8.4	Steam Piping	$29,802	$0	$12,965	$0	$0	$42,767	$3,212	$0	$6,897	$52,876	$96
8.9	TG Foundations	$0	$1,392	$2,322	$0	$0	$3,714	$349	$0	$813	$4,876	$9
	SUBTOTAL 8.	$112,238	$1,392	$28,009	$0	$0	$141,639	$11,917	$0	$18,061	$171,616	$312
9	COOLING WATER SYSTEM											
9.1	Cooling Towers	$19,238	$0	$5,893	$0	$0	$25,131	$2,311	$0	$2,744	$30,186	$55
9.2	Circulating Water Pumps	$3,785	$0	$303	$0	$0	$4,089	$349	$0	$444	$4,882	$9
9.3	Circ.Water System Auxiliaries	$980	$0	$129	$0	$0	$1,109	$101	$0	$121	$1,331	$2
9.4	Circ.Water Piping	$0	$8,225	$7,410	$0	$0	$15,635	$1,373	$0	$2,551	$19,559	$36
9.5	Make-up Water System	$822	$0	$1,049	$0	$0	$1,872	$171	$0	$306	$2,349	$4
9.6	Component Cooling Water Sys	$798	$0	$608	$0	$0	$1,406	$127	$0	$230	$1,762	$3
9.9	Circ.Water System Foundations & Structure	$0	$4,289	$7,197	$0	$0	$11,486	$1,080	$0	$2,513	$15,080	$27
	SUBTOTAL 9.	$25,624	$12,514	$22,589	$0	$0	$60,728	$5,513	$0	$8,910	$75,151	$137

WorleyParsons
resources & energy

Client:	ATK	Report Date: 2012-Dec-14
Project:	Bituminous Baseline Study	

TOTAL PLANT COST SUMMARY

Case:	Case 12 - 1x550 MWnet Super-Critical PC w/ CO2 Capture	
Plant Size:	550.0 MW,net Estimate Type: Conceptual	Cost Base (Jan) 2012 ($x1000)

Acct No.	Item/Description	Equipment Cost	Material Cost	Labor Direct	Labor Indirect	Sales Tax	Bare Erected Cost $	Eng'g CM H.O.& Fee	Contingencies Process	Contingencies Project	TOTAL PLANT COST $	TOTAL PLANT COST $/kW
10	ASH/SPENT SORBENT HANDLING SYS											
10.1	Ash Coolers	N/A	$0	N/A	$0	$0	$0	$0	$0	$0	$0	$0
10.2	Cyclone Ash Letdown	N/A	$0	N/A	$0	$0	$0	$0	$0	$0	$0	$0
10.3	HGCU Ash Letdown	N/A	$0	N/A	$0	$0	$0	$0	$0	$0	$0	$0
10.4	High Temperature Ash Piping	N/A	$0	N/A	$0	$0	$0	$0	$0	$0	$0	$0
10.5	Other Ash Recovery Equipment	N/A	$0	N/A	$0	$0	$0	$0	$0	$0	$0	$0
10.6	Ash Storage Silos	$879	$0	$2,664	$0	$0	$3,543	$337	$0	$388	$4,268	$8
10.7	Ash Transport & Feed Equipment	$5,828	$0	$5,733	$0	$0	$11,561	$1,055	$0	$1,262	$13,878	$25
10.8	Misc. Ash Handling Equipment	$0	$0	$0	$0	$0	$0	$0	$0	$0	$0	$0
10.9	Ash/Spent Sorbent Foundation	$0	$195	$242	$0	$0	$436	$41	$0	$95	$573	$1
	SUBTOTAL 10.	$6,707	$195	$8,639	$0	$0	$15,541	$1,433	$0	$1,745	$18,719	$34
11	ACCESSORY ELECTRIC PLANT											
11.1	Generator Equipment	$2,120	$0	$344	$0	$0	$2,464	$222	$0	$201	$2,887	$5
11.2	Station Service Equipment	$5,872	$0	$1,995	$0	$0	$7,866	$734	$0	$645	$9,246	$17
11.3	Switchgear & Motor Control	$6,739	$0	$1,186	$0	$0	$7,926	$737	$0	$866	$9,529	$17
11.4	Conduit & Cable Tray	$0	$4,707	$15,131	$0	$0	$19,838	$1,839	$0	$3,252	$24,929	$45
11.5	Wire & Cable	$0	$8,885	$15,940	$0	$0	$24,825	$1,985	$0	$4,021	$30,831	$56
11.6	Protective Equipment	$309	$0	$1,088	$0	$0	$1,397	$134	$0	$153	$1,684	$3
11.7	Standby Equipment	$1,611	$0	$38	$0	$0	$1,649	$152	$0	$180	$1,981	$4
11.8	Main Power Transformers	$15,898	$0	$231	$0	$0	$16,129	$1,232	$0	$1,736	$19,097	$35
11.9	Electrical Foundations	$0	$398	$1,025	$0	$0	$1,424	$134	$0	$312	$1,870	$3
	SUBTOTAL 11.	$32,550	$13,990	$36,978	$0	$0	$83,518	$7,170	$0	$11,367	$102,055	$186
12	INSTRUMENTATION & CONTROL											
12.1	PC Control Equipment	w/12.7	$0	w/12.7	$0	$0	$0	$0	$0	$0	$0	$0
12.2	Combustion Turbine Control	N/A	$0	N/A	$0	$0	$0	$0	$0	$0	$0	$0
12.3	Steam Turbine Control	w/8.1	$0	w/8.1	$0	$0	$0	$0	$0	$0	$0	$0
12.4	Other Major Component Control	$0	$0	$0	$0	$0	$0	$0	$0	$0	$0	$0
12.5	Signal Processing Equipment	w/12.7	$0	w/12.7	$0	$0	$0	$0	$0	$0	$0	$0
12.6	Control Boards,Panels & Racks	$611	$0	$378	$0	$0	$989	$93	$49	$170	$1,302	$2
12.7	Distributed Control System Equipment	$6,168	$0	$1,115	$0	$0	$7,282	$676	$364	$832	$9,155	$17
12.8	Instrument Wiring & Tubing	$3,779	$0	$6,858	$0	$0	$10,637	$856	$532	$1,804	$13,829	$25
12.9	Other I & C Equipment	$1,743	$0	$4,089	$0	$0	$5,832	$556	$292	$668	$7,348	$13
	SUBTOTAL 12.	$12,301	$0	$12,440	$0	$0	$24,742	$2,182	$1,237	$3,474	$31,634	$58
13	IMPROVEMENTS TO SITE											
13.1	Site Preparation	$0	$64	$1,367	$0	$0	$1,431	$139	$0	$314	$1,884	$3
13.2	Site Improvements	$0	$2,126	$2,819	$0	$0	$4,945	$489	$0	$1,087	$6,520	$12
13.3	Site Facilities	$3,810	$0	$4,011	$0	$0	$7,820	$775	$0	$1,719	$10,315	$19
	SUBTOTAL 13.	$3,810	$2,190	$8,197	$0	$0	$14,196	$1,403	$0	$3,120	$18,719	$34
14	BUILDINGS & STRUCTURES											
14.1	Boiler Building	$0	$10,674	$9,534	$0	$0	$20,207	$1,783	$0	$3,299	$25,289	$46
14.2	Turbine Building	$0	$15,446	$14,621	$0	$0	$30,067	$2,660	$0	$4,909	$37,637	$68
14.3	Administration Building	$0	$776	$833	$0	$0	$1,609	$143	$0	$263	$2,015	$4
14.4	Circulation Water Pumphouse	$0	$212	$171	$0	$0	$382	$34	$0	$62	$479	$1
14.5	Water Treatment Buildings	$0	$1,070	$991	$0	$0	$2,061	$182	$0	$337	$2,580	$5
14.6	Machine Shop	$0	$519	$354	$0	$0	$873	$76	$0	$142	$1,091	$2
14.7	Warehouse	$0	$352	$358	$0	$0	$710	$63	$0	$116	$889	$2
14.8	Other Buildings & Structures	$0	$287	$248	$0	$0	$536	$47	$0	$87	$670	$1
14.9	Waste Treating Building & Str.	$0	$550	$1,695	$0	$0	$2,246	$208	$0	$368	$2,822	$5
	SUBTOTAL 14.	$0	$29,885	$28,806	$0	$0	$58,691	$5,197	$0	$9,583	$73,471	$134
	TOTAL COST	$995,923	$68,501	$483,491	$0	$0	$1,547,915	$140,716	$68,443	$250,912	$2,007,986	$3,651

Exhibit 0-6 Updated O&M Costs for DOE/NETL Bituminous Coal Baseline 12

INITIAL & ANNUAL O&M EXPENSES						
Case 12 - 1x550 MWnet Super-Critical PC w/ CO2 Capture				Cost Base (Jan):		2012
				Heat Rate-net (Btu/kWh):		12,002
				MWe-net:		550
				Capacity Factor (%):		85

OPERATING & MAINTENANCE LABOR

Operating Labor		
Operating Labor Rate (base):	40.50	$/hour
Operating Labor Burden:	30.00	% of base
Labor O-H Charge Rate:	25.00	% of labor

		Total
Skilled Operator	2.0	2.0
Operator	11.3	11.3
Foreman	1.0	1.0
Lab Tech's, etc.	2.0	2.0
TOTAL-O.J.'s	16.3	16.3

	Annual Cost $	Annual Unit Cost $/kW-net
Annual Operating Labor Cost	$7,533,008	$13.697
Maintenance Labor Cost	$13,105,985	$23.831
Administrative & Support Labor	$5,159,748	$9.382
Property Taxes and Insurance	$40,159,715	$73.023
TOTAL FIXED OPERATING COSTS	**$65,958,457**	**$119.933**

VARIABLE OPERATING COSTS

						$/kWh-net
Maintenance Material Cost					$19,658,977	$0.00480

Consumables	Consumption Initial Fill	/Day	Unit Cost	Initial Fill Cost		
Water(/1000 gallons)	0	7,324	1.48	$0	$3,374,022	$0.00082
Chemicals						
MU & WT Chem.(lbs)	0	35,452	0.24	$0	$2,613,188	$0.00064
Limestone (ton)	0	687	29.70	$0	$6,329,310	$0.00155
Carbon (Mercury Removal) lb	0	0	1.44	$0	$0	$0.00000
MEA Solvent (ton)	1,028	1.46	3,088.59	$3,174,284	$1,396,341	$0.00034
NaOH (tons)	73	7.26	595.34	$43,220	$1,340,914	$0.00033
H2SO4 (tons)	69	6.93	190.51	$13,199	$409,490	$0.00010
Corrosion Inhibitor	0	0	0.00	$142,156	$6,769	$0.00000
Activated Carbon (lb)	0	1,741	1.44	$0	$778,563	$0.00019
Ammonia (19% NH3) ton	0	102	292.72	$0	$9,225,565	$0.00225
Subtotal Chemicals				**$3,372,860**	**$22,100,141**	**$0.00540**
Other						
Supplemental Fuel (MBtu)	0	0	0.00	$0	$0	$0.00000
SCR Catalyst (m3)	w/equip.	0.43	7,929.08	$0	$1,050,182	$0.00026
Emission Penalties	0	0	0.00	$0	$0	$0.00000
Subtotal Other				**$0**	**$1,050,182**	**$0.00026**
Waste Disposal						
Fly Ash (ton)	0	527	22.27	$0	$3,639,809	$0.00089
Bottom Ash (ton)	0	132	22.27	$0	$909,952	$0.00022
Subtotal-Waste Disposal				**$0**	**$4,549,761**	**$0.00111**
By-products & Emissions						
Gypsum (tons)	0	1,062	0.00	$0	$0	$0.00000
Subtotal By-Products				**$0**	**$0**	**$0.00000**
TOTAL VARIABLE OPERATING COSTS				**$3,372,860**	**$50,733,084**	**$0.01239**
Fuel (ton)	0	6,790	68.60	$0	**$144,504,012**	**$0.03529**

References

1. United States Department of Energy (DOE), National Energy Technology Laboratory (NETL). (2010). Cost and Performance Baseline for Fossil Energy Plants Volume 1: Bituminous Coal and Natural Gas to Electricity Rev. 2. (DOE/NETL-2010/1397).Pittsburgh, Pennsylvania: U.S. DOE.

2. Jockenhövel, T., "Development of and Economic Post-Combustion Carbon Capture Process," GHGT-9 Conference, Washington D.C., November 18, 2008. Retrived on December 10, 2012 from http://www.energy.siemens.com/us/pool/hq/power-generation/power-plants/carbon-capture-solutions/post-combustion-carbon-capture/proprietary-post-combustion-capture-process/development-of-an-economic-post-combustion-carbon-capture-processl.pdf.

3. "Carbon Capture Plant Layout Optimization with a New Coal Fired Power Generating Facility," Report to Global CCS Institute, February 2011

4. e.on," Kingsnorth Carbon Capture & Storage Project, Carbon Capture Readiness Report," KCP-EEN-CON-REP-001. Retrieved on December 10, 2012 from http://www.decc.gov.uk/assets/decc/11/ccs/chapter9/9.21-carbon-capture-readiness-report.pdf

5. Coal Specifications for Quality Guidelines, Prepared for The United States Department of Energy National Energy Technology Laboratory, prepared by WorleyParsons, RDS SUBTASK 41817.305.01.02.059, Draft report, Rev. 0, May 2005

6. Smith, Lawrence A., Gupta, Neeraj, Sass, Bruce M. and Mubenik, Thomas A., "Engineering and Economic Assessment of Carbon Dioxide Sequestration in Saline Formations," Battelle Memorial Institute, 2001

7. Singer, Joseph G., "Combustion Fossil Power," ABB/Combustion Engineering Inc., Connecticut, USA, 1991, Fourth Edition

8. W.R. Lane and A. Khosla, "Comparison of Baghouse and Electrostatic Precipitator Fine Particulate, Trace Element and Total Emissions," ASME-IEEE Joint Power Conference, Indianapolis, IN, September 27, 1983.

9. Russell Finex website, "Liquid Solid Separators," http://www.russellfinex.com/separators/liquid-solid-separators.html, accessed on January 3, 2013.

10. Russell Finex, "High Capacity Filtration with the New Russell Finex Eco 900 Series," http://www.russellfinex.com/self-cleaning-filters/industrial-filters.html, accessed on January 3, 2013

11. Cold Jet Website, Dry Ice Production Equipment, http://www.coldjet.com/en/products/dry-ice-production/, accessed on December 21, 2012.

12. Worhach, P. , "Power Systems Financial Model Version 6.6," DOE/NETL-2011/1492, May 2011, available from http://www.netl.doe.gov/energy-analyses/refshelf/PubDetails.aspx?Action=View&PubId=382

13. U. S. Department of Energy National Energy Technology Laboratory (NETL), Quality Guideline for Energy System Studies: Fuel Prices for Selected Feedstocks in NETL Studies, DOE/NETL-341/121211, August 2011.